The spatial distribution of root water uptake rates in drying soils

Inaugural-Dissertation

zur Erlangung des Doktorgrades der

Mathematisch-Naturwissenschaftlichen Fakultät der

Heinrich-Heine-Universität Düsseldorf

vorgelegt von

Yannik Müllers

aus Traben-Trarbach

Düsseldorf, Januar 2023

Aus dem
Institut für Pflanzenwissenschaften, IBG-2
des Forschungszentrum Jülich

Gedruckt mit der Genehmigung der
Mathematisch-naturwissenschaftlichen Fakultät der
Heinrich-Heine-Universität Düsseldorf

Berichterstatter:

1. Prof. Dr. Ulrich Schurr

2. Prof. Dr. Georg Groth

Tag der mündlichen Prüfung: 28.11.2023

Eidesstattliche Erklärung

Ich versichere an Eides statt, dass die Dissertation von mir selbstständig und ohne unzulässige fremde Hilfe unter Beachtung der „Grundsätze guter wissenschaftlicher Praxis an der Heinrich-Heine-Universität Düsseldorf“ erstellt worden ist.

Die Dissertation habe ich in dieser oder ähnlicher Form noch bei keiner anderen Fakultät vorgelegt.

Ich habe bisher keine erfolglosen Promotionsversuch vorgenommen.

Düsseldorf, 26.01.2023

Table of Contents

Summary

There is growing evidence that changes in below-ground hydraulic traits are crucial determinants of the extent of plant water stress at a given soil water deficit. However, this relation heavily depends on the spatial distribution of root hydraulic conductance relatively to remaining water resources. Since these distributions are largely unknown due to limitations of existing measurement technologies, there is a missing link between soil drying and the resulting plant water stress. Novel opportunity to address this issue is provided by a recently developed highly precise soil water sensor, called soil water profiler (SWaP). By establishing an experimental design combining the SWaP with shoot hydraulic measurements and root system imaging, the aim of the present thesis was to analyze how soil drying affects the hydraulic conductance of the root system, its spatial distribution relatively to remaining soil water resources, and the resulting consequences for water flow regulation in the shoot. I started with measuring to what extent root length distributions determine water uptake profiles in well-watered soil. Then, I analyzed the effect of soil drying on the total conductance of the root system and its interaction with stomatal regulation. Lastly, I investigated how changes in root conductance were distributed over depth and how this affected the overall plant water balance.

In well-watered soil, shallow roots not only were more abundant but also had a greater intrinsic conductivity than deeper roots. Consequently, water was largely taken up from upper soil layers. When irrigation was restricted, this resulted in an enhanced vertical gradient in soil water potential with relatively drier layers in the top and relatively wetter layers in the bottom. At a local soil water potential, far from the permanent wilting point, the conductance of roots in the top 10 cm declined exponentially which was the primary reason for plant water stress in form of a reduced plant water potential and stomatal closure. Maize, with a lower exponential decline rate, could maintain higher stomatal conductance compared to faba bean. This was partly due to local increases in root conductance in deeper, relatively wet soil layers in maize, but not in faba bean. Consequently, maize could mitigate water stress by a facilitated deep-water uptake which considerably improved the overall water balance. The analysis presented in this thesis emphasizes that alterations of the root conductance are the principal factors determining the plant water balance under drought. Plants can reduce water stress by adjusting the distribution of root conductance to the vertical soil water gradient.

Introduction

A continuous flow of water from soil through plants towards the atmosphere is vital for most terrestrial plants. Besides a relatively small fraction used for plant growth, usually less than 5% of total water uptake (McElrone et al., 2013), the flow itself is essential as it regulates plant temperature (Gates, 1968) and transports macronutrients such as K^+, Ca^{2+}, NO^{3-}, PO_4^{3-} (Malone et al., 2002), amino acids (Fischer et al., 1998), and stress hormones (Jackson, 1997). Sustaining a continuous water flow at a certain rate requires a negative water pressure in the plant, called plant water potential, which depends on the soil water availability: When the soil is kept moist by regular rainfall or irrigation, soil water is easy to extract, and only a moderately negative plant water potential is required. When soil water becomes scarce, which, in recent years, has been the case for 39% (and rising) of croplands world-wide (Liu et al., 2022), the plant water potential drops to more negative values to sustain a certain water flow rate. A proceeding reduction in plant water potential comes with impairments for various essential plant functions including water and nutrient transport (H. Cochard & Tyree, 1990; Sevanto, 2014; Urli et al., 2013), CO_2 acquisition (McDowell, 2011), and various metabolic processes (Bartlett et al., 2012; Lawlor & Cornic, 2002). Regulation of the water flow from leaves to atmosphere via stomata plays an important role for the water stress level of the plant, and has been intensively studied to better understand and improve plant tolerance to soil drying (Atkinson et al., 2000; Cominelli et al., 2005; González et al., 1999; Khan et al., 2007; Medrano et al., 2002; Qu et al., 2016; Sirichandra et al., 2009). However, there is growing evidence that changes in the hydraulic properties of the soil-root system are equally important, and might even drive water flow regulation in the shoot (Bourbia et al., 2021; Carminati & Javaux, 2020; Martínez-Vilalta & Garcia-Forner, 2017; Rodriguez-Dominguez & Brodribb, 2020; Saliendra & Meinzer, 1989). A wide range of mechanisms at different scales, with partly counteracting effects have been investigated in this context: Processes like severe water depletion in the soil around the roots (Cai et al., 2022; Carminati & Javaux, 2020; Hayat et al., 2020), root shrinkage (Carminati et al., 2009; Duddek et al., 2022; Koebernick et al., 2018; North & Nobel, 1997), increased root suberization (Cruz et al., 1992; North & Nobel, 1991), and a reduced amount of active aquaporins (P. Martre, 2001; Rodríguez-Gamir et al., 2019) decreased the hydraulic conductance of the soil-root system under drought, and thus hampered root water uptake.

In contrast, root mucilage exudation (Mutez A. Ahmed et al., 2014; Carminati et al., 2016), increased aquaporin activity (Grondin et al., 2016; Johnson et al., 2014; Lian et al., 2004), or directed root growth (Alsina et al., 2011; Asseng et al., 1998; Dubrovsky et al., 1998; Rodrigues et al., 1995; Sharp & Davies, 1985) could increase the soil-root hydraulic conductance and thus facilitate water uptake under drought. All these different mechanism not only can change the total conductance of the root system, but may also change the distribution of root hydraulic properties relatively to remaining soil water resources. According to the theoretical work from Couvreur et al. (2012), this spatial relation is a major factor determining the water stress level of a plant. Thus, it might account for varying responses to soil drying among plants and could be a key target towards improved drought tolerance. However, how roots and their hydraulic properties are distributed, and how this distribution is affected by soil drying is unknown, mainly due to limitations of existing measurement technologies. In this context, the development of a highly precise, non-invasive soil water sensor, called soil water profiler (SWaP), which measures water uptake profiles of entire root systems (van Dusschoten et al., 2020) has been a crucial step forward. Based on this methods, the goal of the present thesis was to analyze how soil drying affects the conductance of the root system, its spatial distribution relatively to remaining soil water resources, and the resulting consequences for the water stress level of the plant. To this end, I first determined how root water uptake rates are distributed relatively to root length in well-watered soil by combining SWaP measurements with measurements of root length distribution using MRI and scanning of harvested roots (Manuscript I). Second, I established an experimental setup to simultaneously perform SWaP measurements, leaf water potential measurements, and leaf gas exchange measurements. Using this setup, I quantified the effect of soil drying on the total conductance of the root system, and the resulting consequences for stomatal regulation and compared it between different species (Manuscript II). Third, I analyzed how changes in the total root system conductance were distributed over depth, relatively to remaining water resources, and how this influenced the overall plant water balance (Manuscript III). To narrow down the causes for the observed change, I included modeling of the water potential at the root surface.

Water flow from soil through plants to atmosphere

The water source for most terrestrial plants is soil water, which is taken up radially by roots, flows, mostly vertically, from roots towards the leaves inside xylem vessels, and evaporates from the leaf interior into the atmosphere. According to the commonly accepted cohesion-tension theory (Dixon & Joly, 1895), the main mechanism driving water flow in plants is as follows: At the sites of evaporation inside leaves, water in liquid phase is in contact with air spaces and forms menisci. In a process called transpiration, water from these menisci evaporates into air spaces inside the leaves and then diffuses through pores, called stomata, into the atmosphere. The inherent tensile force of the menisci pulls water towards the surface to replace evaporated molecules. Due to the cohesive nature of water, the tensile force propagates into the adjacent xylem vessels in the leaf veins and, along the water column in the xylem vessels, towards the roots. This process persists as long as water evaporates in the leaves, resulting in a continuous lift of the water column inside the xylem vessels, which is supplied by soil water.

For quantification, water flow along the hydraulic pathway from soil through plant to the atmosphere can be described by an analogue to Ohm's law, similarly to the flow of electrons in an electrical circuit (van den Honert, 1948): For any part of the pathway, the water flow rate (Q) is determined as the product of the hydraulic conductance (K) and the gradient in water potential (Ψ) across that part:

$$Q = K \cdot \Delta\Psi \quad (1)$$

The gradient in water potential is the driving force for water flow. Water potential is a measure for the ability of a certain part of the hydraulic pathway to take up additional water. The local water potential depends on different parameters, with varying importance along the hydraulic pathway, which is elaborated below. Water potential is measured in units of pressure and has negative values by convention. Water flow is directed from less negative towards more negative water potential and thus, water flow from soil through plants towards atmosphere requires $\Psi_{atmosphere} < \Psi_{plant} < \Psi_{soil}$. Typical values for $\Psi_{atmosphere}$ are of the order of -100 MPa, and, in well-watered conditions, between -0.1 and -0.8 MPa for Ψ_{plant} and close to zero for Ψ_{soil} (McElrone et al., 2013). The hydraulic conductance (inverse of a resistance) describes the ease with which the hydraulic pathway conducts water. The greater the conductance, the greater the water flow rate at a given water potential difference, or the lower the water potential difference at a given water flow rate. The hydraulic conductance is determined by two factors 1) the intrinsic conductivity, depending on the water permeability of the conducting material, and 2) an extensive scaling factor depending on size. Generally, eq. 1, in partly modified form, applies to each part of the hydraulic pathway from soil through the plant towards the atmosphere: the transpiration (T) from leaves to the bulk air through stomata, the axial water flow (Q_X) from the roots to the leaves through xylem vessels, and the radial water flow from soil into the root xylem across different cell layers, called total root water uptake (U_{tot}). Using the conductance between leaf and atmosphere, (K_{LA}), the vapor pressure in the leaf (e_{leaf}) and in the air (e_{air}), atmospheric pressure (P), the axial xylem conductance (K_X), the water potential in root (Ψ_{root}) and leaf (Ψ_{leaf}), the radial root conductance (K_{root}), and the soil water potential (Ψ_{soil}), the water flow equations write:

$$T = K_{LA} \cdot \frac{(e_{leaf} - e_{air})}{P} \qquad (2)$$

$$Q_X = K_X \cdot (\Psi_{root} - \Psi_{leaf}) \qquad (3)$$

$$U_{tot} = K_{root} \cdot (\Psi_{soil} - \Psi_{root}) \qquad (4)$$

In the following, the hydraulic conductance and water potential gradients in each part of the hydraulic pathways are explained in detail, starting with the transpiration from leaves as the origin of water flow.

Transpiration from leaf to atmosphere

Since transpiration is not a flow of water in liquid phase but in gas phase, the driving force is not a gradient in water potential but in water vapor pressure between the evaporating cell in the leaf and the bulk air around the leaf, normalized by the atmospheric pressure (Farquhar & Sharkey, 1982). Following the approach of Gaastra (1959), it is assumed that the intercellular air spaces inside leaves are fully saturated with water, and thus, e_{leaf} equals the saturated vapor pressure at leaf temperature. Although this assumption is questioned by studies indicating that under conditions of low (more negative) leaf water potential, vapor pressure in leaves is considerably below saturation (Cernusak et al., 2018; Jarvis & Slatyer, 1970; Vesala et al., 2017), Kramer & Boyer (1995) point out that the consequent reduction in e_{leaf} usually is negligible compared to the difference between e_{leaf} and e_{air}. This ongoing controversy is closely linked to the discussion about the principal locations of evaporation inside leaves and their resistances (Buckley et al., 2017). Nevertheless, compared to the leaf interior, vapor pressure of the bulk air around the leaf can deviate much stronger from saturation, and e_{air} increases with increasing relative humidity. Additionally, e_{air} increases with increasing temperature of the bulk air. However, the air temperature also influences the leaf temperature. Since the vapor pressure in the leaf is close to saturation, it increases much stronger with temperature than that the vapor pressure in the air (Kramer & Boyer, 1995). To conclude, the vapor pressure difference between leaf and bulk air, and thus the driving force for transpiration not only increases with decreasing relative humidity, but also with increasing ambient temperature.

The interface between the leaf epidermis and the bulk air is formed by the leaf cuticle, a membrane largely impermeable for water. The cuticle is perforated by pores in the epidermis called stomata, each formed by two guard cells. Stomata are the primary sites for gas exchange between plant and atmosphere, which mainly involves CO_2 uptake and water release. Transpiration of water from the leaf into the atmosphere almost exclusively occurs through stomata (Bange, 1953). Only a minor fraction of water transport is realized via the so-called cuticular permeance (Kerstiens, 1996), directly through the cuticle matrix past the stomata. Therefore, the hydraulic conductance from leaf to air is largely determined by the stomatal conductance (g_s). Stomatal conductance, which is usually given in units normalized by leaf area, depends on the stomatal density and stomatal aperture. The stomatal aperture is regulated by guard cell turgor which in turn is responsive to atmospheric conditions, such as photosynthetically active radiation, humidity, temperature or CO_2 concentration (Lawson & Morison, 2004). By this regulation mechanism, plants are able to quickly adjust the stomatal conductance, transpiration rate, and thus their water demand in response to changing atmospheric conditions. For instance, in response to an increased light intensity the increase in stomatal conductance peaked 5 to 60 min, depending on species, after the light stimulus (McAusland et al., 2016). As explained in more detail below, stomata not only respond to atmospheric conditions but also to the plant water status. In addition to the stomatal conductance, which is in control of the plant, the conductance of the air boundary layer adjacent to the leaf surface, which is largely determined by wind velocity and leaf geometry also contributes to K_{LA} (Kramer & Boyer, 1995).

Axial water flow from roots to leaves

Water flows from roots towards leaves through the vessels of the xylem tissue. These vessels are formed by individual, longitudinally interconnected cells called vessel elements. Vessel elements differentiate from stem cells from the procambium and cambium (Růžička et al., 2015): Primary xylem is derived from cells from the procambium, and consists of earlier formed protoxylem with narrow vessel elements and later formed metaxylem with wider vessel elements. In a second, lateral growth process in dicots but not monocots, cells from the vascular cambium differentiate into secondary xylem. Both primary and secondary xylem undergo a maturation process called xylogenesis, which is characterized by cell elongation, secondary cell wall formation and lignification, and ultimately cell death (Samuels et al., 2006). Fully mature vessel elements are dead, hollow cells without any cell organs. With proceeding differentiation and maturation, the resistance for water flow through the vessel elements gradually decreases (Heo et al., 2017).

The water potential gradient along the xylem vessels between root and leaf is generated by transpiration which reduces the leaf water potential and thus drives xylem water flow. Therefore, the water potential gradient is under control of the plant via stomatal regulation, and, for a given transpiration rate, depends on the axial hydraulic conductance of the xylem vessels. A common, straightforward approach to analyze K_X is interpreting the xylem vessels as ideal hollow cylinders, and calculating K_X according to Poiseuille's law (Wind, 1955). Following this model, K_X increases with the number of conducting vessels and the fourth power of their diameter, while it decreases linearly with vessel length. However, the model of xylem vessels as ideal, long cylinders is incomplete. This is especially due to perforation plates between interconnected vessel elements, and pits in the vessel walls, which considerably reduce the axial conductance (Choat et al., 2006; Schulte et al., 2015; Schulte & Castle, 1993). If the Poiseuille-model takes into account the reduced conductance caused by these structures, it reliably predicts measured values (Schulte et al., 1987; Sperry et al., 2005; Zwieniecki et al., 2001). However, this model only works for fully mature xylem vessels. Due to the induced anatomical changes, the axial conductance usually increases with proceeding development and maturation of xylem vessels (Knipfer & Fricke, 2011; Pierre Martre et al., 2000). This is especially relevant in young, growing roots. There is a broad consensus about K_X generally increasing with increasing distance from the root tip, the youngest and least developed part of the root (Aubin et al., 1986; Clément et al., 2022; Frensch & Steudle, 1989; B Huang & Nobel, 1993; McCully, 1994, 1995; Melchior & Steudle, 1993; Meunier et al., 2018; Peterson & Steudle, 1993; Pierret et al., 2006; Sanderson et al., 1988; Watt et al., 2008). The extent of variation in K_X and its relevance for water transport, however, is controversially debated. While some authors suggest that water flow is limited due to a low K_X in non-mature xylem up to 20-50 cm behind the root tip (Aubin et al., 1986; McCully, 1995; Pierret et al., 2006; Sanderson et al., 1988), others argue that K_X is limiting only within the 5 apical centimeter without fully developed early metaxylem, while beyond this region, K_X is much greater than the radial root conductance, and thus variation in K_X is negligible (Frensch & Steudle, 1989; Melchior & Steudle, 1993; Steudle & Peterson, 1998). In any case, as K_X decreases with path length, its influence on water uptake generally increases with increasing distance from the plant collar.

Radial root water uptake

Radial root water uptake is driven by the difference in water potential between soil and root xylem. The soil water potential is mainly composed of the matric potential, depending on soil water content, and furthermore of osmotic potential, and gravity (Or et al., 2005). The water potential in the root xylem is primarily set by the transpiration rate and additionally depends on the soil water potential and the radial root conductance (K_{root}). In contrast to the axial water flow through xylem vessels, radial water flow must cross several cell layers, namely the epidermis with root hairs which are in physical contact with the soil, followed by the exodermis, the root cortex, the endodermis, and the xylem vessel walls. According to the composite transport model (Steudle, 1994), three different pathways of radial root water flow are realized simultaneously: Two pathways from cell to cell by either crossing cell membranes (transcellular pathway) or within plasmodesmata (symplastic pathway), and one pathway around protoplasts (apoplastic pathway). Water transport across the transcellular pathway of the cell-to-cell pathway is facilitated by water channels in cell membranes called aquaporins. As summarized by Javot & Maurel (2002), different studies on a wide range of species showed that aquaporin inhibition using mercury caused a 32 – 90% reduction in K_{root}. Studies using different inhibitors such as azide or hydroxy radicals found similar values, ranging from 50-85% (Grondin et al., 2016; Rodríguez-Gamir et al., 2019). Although these numbers should be carefully interpreted due to the potential side-effects of the inhibitors, they indicate that root aquaporins play an important role for radial root water uptake. By regulating the gene expression of aquaporins and their posttranslational modification, plants are able to adjust K_{root} in response to external stimuli or diurnal patterns within timescales of minutes (Meng et al., 2016; Sakurai-Ishikawa et al., 2011; Vandeleur et al., 2014). In contrast to the facilitating role of aquaporins in the transcellular path, hydrophobic suberin structures in hypodermal and endodermal cell walls function as partial barrier of the apoplastic pathway (Schreiber et al., 1999). Accordingly, the presence of cell layers containing suberin structures was shown to considerably reduce the hydraulic conductance (Steudle & Peterson, 1998; Zimmermann & Steudle, 1998). A major factor determining the level of suberization is root maturity: The abundance of suberin structures usually is greater in more developed, basal root parts while a small apical zone of several centimeter at the root tip is not suberized (Gambetta et al., 2013; Melchior & Steudle, 1993; Ranathunge et al., 2017). Two other factors associated with a reduced radial conductance are cortical senescence (Schneider et al., 2017) and an increased radial path length (Bingru Huang & Eissenstat, 2000; Rieger & Litvin, 1999), resulting, for example, from secondary thickening in dicots. Therefore, K_{root} decreases during maturation of the root system. As discussed above, beyond five centimeters from the root tip, K_{root} usually becomes much lower than K_X, and thus, limiting for water uptake.

The effect of soil drying on soil and plant hydraulic properties

Soil drying is a continuous reduction of the soil water content (θ). Soil water is depleted due to root water uptake, evaporation from the top soil, and water drainage towards deeper layers (Ritchie, 1998). In absence of irrigation, these processes gradually lead to soil drying. θ is a crucial determinant of the matric potential, and thus Ψ_{soil}, which becomes more negative with decreasing θ. The exact relation between Ψ_{soil} and θ depends on additional soil parameters, mainly pore size distribution, and thus varies among different soil types. Generally, at a given θ, sandy soils have the least negative Ψ_{soil}, followed by silty soils, while clay soils have the most negative Ψ_{soil} (Schelle et al., 2013). The curve describing the relation $\Psi_{soil}(\theta)$ is called water retention curve which, especially in the dry regime, is highly non-linear: small changes in water content cause great changes in water potential. The water retention curve needs to be derived for each specific soil type by measuring Ψ_{soil} at varying θ and fitting the measured data using a model (e.g. those developed by van Genuchten (1980) or Brooks & Corey (1964)).

However, not only Ψ_{soil} but also the hydraulic conductance between soil and leaf (K_{SL}) can be reduced: 1) in the soil around the roots, due to a severe soil water depletion zone (Abdalla et al., 2022; Cai et al., 2022; Carminati & Javaux, 2020; Hayat et al., 2020), 2) at the root surface, due to root shrinkage and a decrease in soil-root contact (Carminati et al., 2009; Duddek et al., 2022; Koebernick et al., 2018; North & Nobel, 1997), 3) in the roots due to a modified gene expression or activity of aquaporins (Johnson et al., 2014; P. Martre et al., 2001; Rodríguez-Gamir et al., 2019), suberization of different cell layers in the radial root pathway (Cruz et al., 1992; North & Nobel, 1991), or hydraulic failure of fine roots (Cuneo et al., 2016), and 4) in shoot and leaves due to xylem embolisms (Hervé Cochard, 2006; Ryu et al., 2016).

The plant water balance in drying soils

Assuming that the total root water uptake rate, the total axial flow rate, and the transpiration rate are equal (i.e. neglecting the capacitive function of the plant), a simplified model of the plant water balance can be derived from eq. 2-4:

$$\Psi_{leaf} = \Psi_{soil} - \frac{U_{tot}}{K_{SL}} \qquad (5)$$

U_{tot} is set by the transpiration rate, and therefore is primarily determined by temperature, relative humidity, leaf area, and stomatal conductance (eq. 2). The leaf water potential, generated for a given U_{tot}, depends on the soil water potential and the hydraulic conductance between soil and leaf (eq. 5). As described above, soil drying comes with a reduction in Ψ_{soil} and K_{SL}. As long as the transpiration rate is sustained, this causes an according reduction in the plant water potential, measured as Ψ_{leaf} (eq. 5). A too negative plant water potential can lead to xylem embolism, especially in larger vessels (H. Cochard & Tyree, 1990), and subsequently to hydraulic failure (Urli et al., 2013), restricted phloem transport (Sevanto, 2014), and a general impairment of enzymatic reactions due to cell turgor loss (Bartlett et al., 2012). To prevent a severe drop of the plant water potential, stomata partly close which reduces the water flow rate across the plant, and thus the required water potential gradient. Since not only evaporation of water but also CO_2 uptake occurs via stomata, reducing stomatal conductance comes with the drawback of a reduced CO_2 uptake rate, up to carbon starvation (McDowell, 2011). How drought stress is distributed between reduced plant water potential and reduced CO_2 uptake depends on the sensitivity of the stomata to water stress, which varies among plant species (Tardieu & Simmoneau, 1998). This variation in stomatal sensitivity led to the classification of plant species into two ideotypes: Isohydric species keep their leaf water potential constant at a certain threshold by gradually closing stomata. Anisohydric species keep their transpiration rate constant, which leads to a gradually reduced plant water potential. However, this binary classification is deprecated and it has been shown that species can rather be arranged on a continuous scale ranging from more isohydric to more anisohydric (Klein, 2014). The exact mechanism leading to stomatal closure under water deficit is still under debate: In a recent review, hydraulic signaling via leaf water potential was identified as the main cause for stomatal regulation (Buckley, 2019). Nevertheless, there are also studies suggesting a direct signaling cascade from roots to leaves involving hormones such as abscisic acid (Liang et al., 1997), cytokinin (Blackman & Davies, 1985), or stringolactone (Visentin et al., 2016). In any case, the demand for stomatal regulation strongly depends on how the hydraulic pathway upstream towards the stomata, so from soil to leaf is affected by soil drying. A greater reduction in Ψ_{soil} and K_{SL} requires a greater water potential gradient between soil and leaf to achieve a similar water flow rate compared to well-watered conditions. This causes water stress in form of a drop in 1) plant water potential (eq. 5) and/or 2) transpiration rate and thus CO_2 uptake rate, depending on stomatal regulation.

Hydraulic model of spatially varying soil and root hydraulic traits

In well-watered soil, the vertical gradient in Ψ_{soil} is mainly determined by gravity, and thus is of the order of 0.01 MPa m^{-1}. For cops with rooting depths of several meters, this vertical gradient is small compared to the radial water potential gradient between soil and root xylem. Under these conditions, root placement and the distribution of root conductance are of minor importance for the water balance of a plant (Lobet et al., 2014). This changes when soil is drying and significant gradients in soil water potential arise. Since upper soil layers usually contain more roots, they dry faster than deeper layers. Therefore, there typically is a vertical gradient in soil water potential with more negative values in shallow than in deeper layers during droughts (Hillel et al., 1976; Kondo et al., 2000; Markesteijn et al., 2010). Under these circumstances, a spatial component of water uptake by roots is required for an appropriate quantification of the plant water balance. This requirement is emphasized by eq. 5 describing the plant water balance: Which is the right soil water potential to consider when it is non-uniformly distributed along the root system? A solution for this issue can be obtained using the hydraulic architecture approach which considers the spatial arrangement of root hydraulic properties: Based on the quantitative description of water flow into single roots (Landsberg & Fowkes, 1978), Alm et al. (1992) developed a finite element model, separating individual roots into segments, each with specific radial, and axial conductivities and water potential gradient between soil and root xylem. Doussan et al. (1998) scaled up this approach to the root system level by interpreting the root system as a hierarchical tree made of nodes (radial water uptake) and edges (axial water transport) and derived a set of linear equations describing the water flow into each root node. Using a similar approach, Couvreur et al. (2012) were able to derive macroscopic parameters which consider the spatial distribution of root hydraulic properties, and allow for a quantitative description of water flow into the root system by only two equations. One crucial macroscopic parameter is the normalized distribution of root water uptake rates along the root system under conditions of a uniform soil water potential. Since this distribution only depends on the spatial arrangement of root hydraulic traits, it is called here normalized plant-driven root water uptake distribution ($\widehat{U}_P$). Using $\widehat{U}_P$, the equivalent soil water potential (Ψ_{seq}) can be derived which considers the distribution of root hydraulic conductance relative to the distribution of soil water potential with depth z:

$$\Psi_{seq} = \sum_z \widehat{U}_P(z) \cdot \Psi_{soil}(z) \qquad (6)$$

Due to the normalization of $\widehat{U}_P$ ($\sum_z \widehat{U}_P(z) = 1$) Ψ_{seq} is equal to Ψ_{soil} at each depth under conditions of a uniformly distributed Ψ_{soil}. When Ψ_{soil} is non-uniformly distributed, Ψ_{soil} in layers with greater root conductance, and thus greater $\widehat{U}_P$, is weighted stronger than in layers with smaller $\widehat{U}_P$. In layers without any roots, $\widehat{U}_P$ is zero, and thus, the local Ψ_{soil} does not affect Ψ_{seq}. Using Ψ_{seq}, eq. 5 can be extended such that it describes the plant water balance under conditions of non-uniform soil water potential:

$$\Psi_{leaf} = \Psi_{seq} - \frac{U_{tot}}{K_{SL}} \qquad (7)$$

More detailed descriptions of the hydraulic model and the resulting water flow equations are provided in the single chapters of this thesis.

The need and challenges of analyzing root water uptake distributions

The main factor influencing how a plant is affected by soil drying is the extent of water stress in form of a reduced plant water potential, measured as Ψ_{leaf} and reduced water flow rate, measured as U_{tot}. For a given soil water deficit, i.e. a reduction in soil water content compared to a reference value, the extent of water stress depends on 1) the resulting drop in the equivalent soil water potential, and thus on the distribution of root hydraulic conductance, measured as $\widehat{U}_P$, relatively to remaining soil water resources, measured as Ψ_{soil} (eq. 6-7), and 2) the resulting change in total conductance between soil and leaf, measured as K_{SL} (eq. 7). Variation in $\widehat{U}_P$, Ψ_{soil}, and K_{SL} might explain variation in the water stress level at a given soil water deficit among different soil-plant systems, and thus account for varying drought tolerance. However, theses parameters and their responses to soil drying are poorly investigated, or, in case of $\widehat{U}_P$ not known at all.

This is because $\widehat{U}_P$ is challenging to measure, and some of these challenges cannot be overcome by existing experimental methods: The root hydraulic conductance can be directly measured using invasive pressure chamber or flow-meter techniques on entire root systems (Lo Gullo et al., 1998; Martínez-Ballesta et al., 2003; Tyree et al., 1995). However, obtaining spatial information with these techniques is difficult and requires excavating and measuring root samples from different sites of the root system (Johnson et al., 2014; McLean et al., 2011; Mu et al., 2006). This method can be used to detect local differences in root conductance but is not suitable to derive the spatial distribution across entire root system. A better suited approach is non-invasively measuring the distribution of root water uptake rates and infer the distribution of root conductance. However, since the distribution of water uptake rates is not only determined by the distribution of root hydraulic conductance, but also by the distribution of soil water potential, the influences of these two factors need to be separated. This comes with several key requirements for the measurement of root water uptake rates. Previous studies have used neutron meters (Coelho & Or, 1999; Green & Clothier, 1995) or time domain reflectometry (TDR) (Ehlers et al., 1991; Shein & Pachepsky, 1995) to measure root water uptake rates. However, the spatial resolution of these techniques is limited as it requires one measuring device (neutron meter or TDR) at each depth. This makes it almost impossible to achieve measurements which are continuous in space, and thus, to obtain the total water uptake rate of the root system. Additionally, the ability to detect small local changes in root water uptake rates is limited with TDR due to an insufficient sensitivity (van Dusschoten et al., 2020). As explained below, both, high sensitivity, and the continuous character of water uptake measurements are crucial requirements for the determination of $\widehat{U}_P$. A more advanced technique is imaging of the soil-root zone using neutron radiography (NR). With NR, the spatial distribution of soil water within a sample can be imaged at different time points to calculate root water uptake rates (Dara et al., 2015; Esser et al., 2010). In combination with injection of deuterated water, NR allows for direct tracing of water transport from soil into roots (Ahmed et al., 2016, 2018; Zarebanadkouki et al., 2013, 2014). However, this approach requires expensive equipment for imaging, which is rarely available. Additionally, the injection of deuterated water changes the local environment of the roots (increased soil water potential) which makes it difficult to generalize and scale up observations to the root system level.

Recently, a measurement technology called soil water profiler (SWaP) (van Dusschoten et al., 2020) has been developed, which overcomes the existing challenges and, for the first time, allows for determination of $\widehat{U}_P$. This is mainly due to the precision of the SWaP sensors, which is about a factor 10 higher compared to TDR (van Dusschoten et al., 2020). Additionally, the measurements are continuous in space, and thus the total root water uptake rate can be straightforwardly calculated. These features, in combination with an alternating light intensity, allow for separating water flow patterns driven by the distribution of root hydraulic conductance and those, driven by the distribution of soil water potential. This way, $\widehat{U}_P$ of entire root systems can be determined non-invasively, at a vertical resolution of 1 cm. The next chapter provides a more detailed explanation on the measurement principle of the SWaP, the associated theory, and some example measurements. Additionally, the establishment of an experimental workflow that combines SWaP measurements with leaf water potential measurements, leaf gas exchange measurements, and measurements of root length distributions, will be described, which was required to answer the central questions addressed in this thesis.

Aims of the thesis

The extent of plant water stress in form of reduced soil water potential and transpiration rate depends on how the hydraulic conductance of the root system, and its distribution relatively to remaining water resources are affected by soil drying. This effect is unknown due to limitations of previous technologies for measuring root water uptake profiles. The aim of this thesis was to establish an experimental setup, which combines a novel soil water sensor technology with hydraulic measurements of the shoot and non-invasive determination of root distributions to answer the following questions:

1) Which parameters determine the distribution of root water uptake rates and the underlying conductance in well-watered conditions?
2) How relevant are soil drying induced changes in the total root system conductance for the plant water balance and water flow regulation in the shoot?
3) How are these changes distributed across the root system, relatively to the remaining soil water resources, and thus affect water uptake?

References

Abdalla, M., Ahmed, M. A., Cai, G., Wankmüller, F., Schwartz, N., Litig, O., Javaux, M., & Carminati, A. (2022). Stomatal closure during water deficit is controlled by below-ground hydraulics. *Annals of Botany*, *129*(2), 161–170. https://doi.org/10.1093/aob/mcab141

Ahmed, Mutez A., Kroener, E., Holz, M., Zarebanadkouki, M., & Carminati, A. (2014). Mucilage exudation facilitates root water uptake in dry soils. *Functional Plant Biology*, *41*(11), 1129–1137. https://doi.org/10.1071/FP13330

Ahmed, Mutez Ali, Zarebanadkouki, M., Kaestner, A., & Carminati, A. (2016). Measurements of water uptake of maize roots: the key function of lateral roots. *Plant and Soil*, *398*(1–2), 59–77. https://doi.org/10.1007/s11104-015-2639-6

Ahmed, Mutez Ali, Zarebanadkouki, M., Meunier, F., Javaux, M., Kaestner, A., & Carminati, A. (2018). Root type matters: Measurement of water uptake by seminal, crown, and lateral roots in maize. *Journal of Experimental Botany*, *69*(5), 1199–1206. https://doi.org/10.1093/jxb/erx439

Alm, D. J., Cavelier, J., & Nobel, P. S. (1992). A finite-element model of radial and axial conductivities for individual roots: Development and validation for two desert succulents. *Annals of Botany*, *69*(1), 87–92.

Alsina, M. M., Smart, D. R., Bauerle, T., De Herralde, F., Biel, C., Stockert, C., Negron, C., & Save, R. (2011). Seasonal changes of whole root system conductance by a drought-tolerant grape root system. *Journal of Experimental Botany*, *62*(1), 99–109. https://doi.org/10.1093/jxb/erq247

Asseng, S., Ritchie, J. T., Smucker, A. J. M., & Robertson, M. J. (1998). Root growth and water uptake during water deficit and recovering in wheat. *Plant and Soil*, *201*(2), 265–273. https://doi.org/10.1023/A:1004317523264

Atkinson, C. J., Policarpo, M., Webster, A. D., & Kingswell, G. (2000). Drought tolerance of clonal Malus determined from measurements of stomatal conductance and leaf water potential. *Tree Physiology*, *20*(8), 557–563. https://doi.org/10.1093/treephys/20.8.557

Aubin, G. S., Canny, M. J., & Mccully, M. E. (1986). Living vessel elements in the late metaxylem of sheathed maize roots. *Annals of Botany*, *58*(4), 577–588. https://doi.org/10.1093/annbot/58.4.577

Bange, G. G. J. . (1953). ON THE QUANTITATIVE EXPLANATION OF STOMATAL TRANSPIRATION. *ACTA BOTANICA NEERLANDICA, 2*(3), 255–297.

Baroni, G., Facchi, A., Gandolfi, C., Ortuani, B., Horeschi, D., & Van Dam, J. C. (2010). Uncertainty in the determination of soil hydraulic parameters and its influence on the performance of two hydrological models of different complexity. *Hydrology and Earth System Sciences*, *14*(2), 251–270. https://doi.org/10.5194/hess-14-251-2010

Bartlett, M. K., Scoffoni, C., & Sack, L. (2012). The determinants of leaf turgor loss point and prediction of drought tolerance of species and biomes: A global meta-analysis. *Ecology Letters*, *15*(5), 393–405. https://doi.org/10.1111/j.1461-0248.2012.01751.x

Blackman, P. G., & Davies, W. J. (1985). Root to shoot communication in maize plants of the effects of soil drying. *Journal of Experimental Botany*, *36*(1), 39–48. https://doi.org/10.1093/jxb/36.1.39

Bourbia, I., Pritzkow, C., & Brodribb, T. J. (2021). Herb and conifer roots show similar high sensitivity to water deficit. *Plant Physiol*, *186*(4), 1908–1918. https://doi.org/10.1093/PLPHYS/KIAB207

Brooks, R. H., & Corey, A. T. (1964). Hydraulic properties of porous media. *Hydrology Papers*, *27*(3), 293–296.

Buckley, T. N. (2019). How do stomata respond to water status? *New Phytologist*, *224*(1), 21–36. https://doi.org/10.1111/nph.15899

Buckley, T. N., John, G. P., Scoffoni, C., & Sack, L. (2017). The sites of evaporation within leaves. *Plant Physiology*, *173*(3), 1763–1782. https://doi.org/10.1104/pp.16.01605

Cai, G., Ahmed, M. A., Abdalla, M., & Carminati, A. (2022). Root hydraulic phenotypes impacting water uptake in drying soils. *Plant, Cell & Environment*, 0–3. https://doi.org/10.1111/pce.14259

Carminati, A., & Javaux, M. (2020). Soil Rather Than Xylem Vulnerability Controls Stomatal Response to Drought. *Trends in Plant Science*, *xx*(xx), 1–13. https://doi.org/10.1016/j.tplants.2020.04.003

Carminati, A., Kroener, E., Ahmed, M. A., Zarebanadkouki, M., Holz, M., & Ghezzehei, T. (2016). Water for Carbon, Carbon for Water. *Vadose Zone Journal*, *15*(2), vzj2015.04.0060. https://doi.org/10.2136/vzj2015.04.0060

Carminati, A., Vetterlein, D., Weller, U., Vogel, H.-J., & Oswald, S. E. (2009). When Roots Lose Contact. *Vadose Zone Journal*, *8*(3), 805–809. https://doi.org/10.2136/vzj2008.0147

Cernusak, L. A., Ubierna, N., Jenkins, M. W., Garrity, S. R., Rahn, T., Powers, H. H., Hanson, D. T., Sevanto, S., Wong, S. C., McDowell, N. G., & Farquhar, G. D. (2018). Unsaturation of vapour pressure inside leaves of two conifer species. *Scientific Reports*, *8*(1), 1–7. https://doi.org/10.1038/s41598-018-25838-2

Choat, B., Brodie, T. W., Cobb, A. R., Zwieniecki, M. A., & Holbrook, N. M. (2006). Direct measurements of intervessel pit membrane hydraulic resistance in two angiosperm tree species. *American Journal of Botany*, *93*(7), 993–1000. https://doi.org/10.3732/ajb.93.7.993

Clément, C., Schneider, H. M., Dresbøll, D. B., Lynch, J. P., & Thorup-Kristensen, K. (2022). Root and xylem anatomy varies with root length, root order, soil depth and environment in intermediate wheatgrass (Kernza®) and alfalfa. *Annals of Botany*, 1–16. https://doi.org/10.1093/aob/mcac058

Cochard, H., & Tyree, M. T. (1990). Xylem dysfunction in Quercus: vessel sizes, tyloses, cavitation and seasonal changes in embolism. *Tree Physiology*, *6*(4), 393–407. https://doi.org/10.1093/treephys/6.4.393

Cochard, Hervé. (2006). Cavitation in trees. *Comptes Rendus Physique*, *7*(9–10), 1018–1026. https://doi.org/10.1016/j.crhy.2006.10.012

Coelho, E. F., & Or, D. (1999). Root distribution and water uptake patterns of corn under surface and subsurface drip irrigation. *Plant and Soil*, *206*, 123–136. https://doi.org/10.1023/A:1004325219804

Cominelli, E., Galbiati, M., Vavasseur, A., Conti, L., Sala, T., Vuylsteke, M., Leonhardt, N., Dellaporta, S. L., & Tonelli, C. (2005). A guard-cell-specific MYB transcription factor regulates stomatal movements and plant drought tolerance. *Current Biology*, *15*(13), 1196–1200. https://doi.org/10.1016/j.cub.2005.05.048

Couvreur, V., Vanderborght, J., & Javaux, M. (2012). A simple three-dimensional macroscopic root water uptake model based on the hydraulic architecture approach. *Hydrology and Earth System Sciences*, *16*(8), 2957–2971. https://doi.org/10.5194/hess-16-2957-2012

Cruz, R. T., Jordan, W. R., & Drew, M. C. (1992). Structural changes and associated reduction of hydraulic conductance in roots of Sorghum bicolor L. following exposure to water deficit. *Plant Physiology*, *99*(1), 203–212. https://doi.org/10.1104/pp.99.1.203

Cuneo, I. F., Knipfer, T., Brodersen, C. R., & McElrone, A. J. (2016). Mechanical failure of fine root cortical cells initiates plant hydraulic decline during drought. *Plant Physiology*, *172*(3), 1669–1678. https://doi.org/10.1104/pp.16.00923

Dara, A., Moradi, B. A., Vontobel, P., & Oswald, S. E. (2015). Mapping compensating root water uptake in heterogeneous soil conditions via neutron radiography. *Plant and Soil*, *397*(1–2), 273–287. https://doi.org/10.1007/s11104-015-2613-3

Dixon, H. H., & Joly, J. (1895). On the Ascent of Sap. *Ann. Botany*, *8*, 468–470.

Doussan, C., Pages, L., & Vercambre, G. (1998). Modelling of the Hydraulic Architecture of Root Systems : An Integrated Approach to Water Absorption — Model Description. *Annals of Botany*, *81*, 213–223.

Dubrovsky, J. G., North, G. B., & Nobel, P. S. (1998). Root growth, developmental changes in the apex, and hydraulic conductivity for Opuntia ficus-indica during drought. *New Phytologist*, *138*(1), 75–82. https://doi.org/10.1046/j.1469-8137.1998.00884.x

Duddek, P., Carminati, A., Koebernick, N., Ohmann, L., Lovric, G., Delzon, S., Rodriguez-Dominguez, C. M., King, A., & Ahmed, M. A. (2022). The impact of drought-induced root and root hair shrinkage on root–soil contact. *Plant Physiology*, 1232–1236. https://doi.org/10.1093/plphys/kiac144

Ehlers, W., Hamblin, A. P., Tennant, D., & van der Ploeg, R. R. (1991). Root system parameters determinig water uptake of field crops. *Irrigation Science*, *12*, 115–124.

Farquhar, G. D., & Sharkey, T. D. (1982). Stomatal Conductance and Photosynthesis. *Annual Review of Plant Physiology*, *33*(1), 317–345. https://doi.org/10.1146/annurev.pp.33.060182.001533

Fischer, W. N., André, B., Rentsch, D., Krolkiewicz, S., Tegeder, M., Breitkreuz, K., &

Frommer, W. B. (1998). Amino acid transport in plants. *Trends in Plant Science*, *3*(5), 188–195. https://doi.org/10.1016/S1360-1385(98)01231-X

Frensch, J., & Steudle, E. (1989). Axial and Radial Hydraulic Resistance to Roots of Maize (Zea mays L.). *Plant Physiology*, *91*(2), 719–726. https://doi.org/10.1104/pp.91.2.719

Gaastra, P. (1959). PHOTOSYNTHESIS OF CROP PLANTS AS INFLUENCED BY LIGHT, CARBON DIOXIDE, TEMPERATURE, AND STOMATAL DIFFUSION RESISTANCE. In *Meded. Landbouwhogeschool, Wageningen* (Vol. 59). https://doi.org/10.1111/j.1432-1033.1975.tb02169.x

Gambetta, G. A., Fei, J., Rost, T. L., Knipfer, T., Matthews, M. A., Shackel, K. A., Andrew Walker, M., & McElrone, A. J. (2013). Water uptake along the length of grapevine fine roots: Developmental anatomy, tissue-specific aquaporin expression, and pathways of water transport. *Plant Physiology*, *163*(3), 1254–1265. https://doi.org/10.1104/pp.113.221283

Gates, D. M. (1968). Transpiration and Leaf Temperature. *Annual Review of Plant Physiology*, *19*(1), 211–238. https://doi.org/10.1146/annurev.pp.19.060168.001235

González, A., Martín, I., & Ayerbe, L. (1999). Barley yield in water-stress conditions. *Field Crops Research*, *62*(1), 23–34. https://doi.org/10.1016/s0378-4290(99)00002-7

Green, S. R., & Clothier, B. E. (1995). Root water uptake by kiwifruit vines following partial wetting of the root zone. *Plant and Soil*, *173*(2), 317–328. https://doi.org/10.1007/BF00011470

Grondin, A., Mauleon, R., Vadez, V., & Henry, A. (2016). Root aquaporins contribute to whole plant water fluxes under drought stress in rice (Oryza sativa L.). *Plant Cell and Environment*, *39*(2), 347–365. https://doi.org/10.1111/pce.12616

Hayat, F., Ahmed, M. A., Zarebanadkouki, M., Javaux, M., Cai, G., & Carminati, A. (2020). Transpiration Reduction in Maize (Zea mays L) in Response to Soil Drying. *Frontiers in Plant Science*, *10*(January), 1–8. https://doi.org/10.3389/fpls.2019.01695

Heo, J. ok, Blob, B., & Helariutta, Y. (2017). Differentiation of conductive cells: a matter of life and death. *Current Opinion in Plant Biology*, *35*, 23–29. https://doi.org/10.1016/j.pbi.2016.10.007

Hillel, D., Talpaz, H., & van Keulen, H. (1976). A macroscopic-scale model of water uptake by a nonuniform root system and of water and salt movement in the soil profile. *Soil Science*, *121*(4).

Huang, B, & Nobel, P. S. (1993). Hydraulic conductivity and anatomy along lateral roots of cacti: changes with soil water status. *New Phytol.*, *123*, 499–507.

Huang, Bingru, & Eissenstat, D. M. (2000). Linking Hydraulic Conductivity to Anatomy in Plants that Vary in Specific Root Length. *Journal of the American Society for Horticultural Science*, *125*(2), 260–264.

Jackson, M. (1997). Hormones from roots as signals for the shoots of stressed plants. *Trends in Plant Science*, *2*(1), 22–28. https://doi.org/10.1016/s1360-1385(96)10050-9

Jarvis, P. G., & Slatyer, R. O. (1970). The role of the mesophyll cell wall in leaf transpiration. *Planta*, *90*(4), 303–322. https://doi.org/10.1007/BF00386383

Javot, H., & Maurel, C. (2002). The role of aquaporins in root water uptake. *Annals of Botany*, *90*(3), 301–313. https://doi.org/10.1093/aob/mcf199

Johnson, D. M., Sherrard, M. E., Domec, J. C., & Jackson, R. B. (2014). Role of aquaporin activity in regulating deep and shallow root hydraulic conductance during extreme drought. *Trees - Structure and Function*, *28*(5), 1323–1331. https://doi.org/10.1007/s00468-014-1036-8

Kerstiens, G. (1996). Cuticular water permeability and its physiological significance. *Journal of Experimental Botany*, *47*(305), 1813–1832. https://doi.org/10.1093/jxb/47.12.1813

Khan, H. U. R., Link, W., Hocking, T. J., & Stoddard, F. L. (2007). Evaluation of physiological traits for improving drought tolerance in faba bean (Vicia faba L.). *Plant and Soil*, *292*(1–2), 205–217. https://doi.org/10.1007/s11104-007-9217-5

Klein, T. (2014). The variability of stomatal sensitivity to leaf water potential across tree species indicates a continuum between isohydric and anisohydric behaviours. *Functional Ecology*, *28*(6), 1313–1320. https://doi.org/10.1111/1365-2435.12289

Knipfer, T., & Fricke, W. (2011). Water uptake by seminal and adventitious roots in relation to whole-plant water flow in barley (Hordeum vulgare L.). *Journal of Experimental Botany*, *62*(2), 717–733. https://doi.org/10.1093/jxb/erq312

Koebernick, N., Schlüter, S., Blaser, S. R. G. A., & Vetterlein, D. (2018). Root-soil contact dynamics of Vicia faba in sand. *Plant and Soil Soil*, *431*, 417–431.

Kondo, M., Murty, M. V. R., & Aragones, D. V. (2000). Characteristics of root growth and water uptake from soil in upland rice and maize under water stress. *Soil Science and Plant Nutrition*, *46*(3), 721–732. https://doi.org/10.1080/00380768.2000.10409137

Kramer, P. J., & Boyer, J. S. (1995). Transpiration and the Ascent of Sap. In *Water Relations of Plants and Soil* (p. 514). http://books.google.com/books?id=7kuQvPOd7AUC

Landsberg, J. J., & Fowkes, N. D. (1978). Water Movement Through Plant Roots. *Ann. Botany*, *42*(August), 493–508. https://doi.org/10.1093/oxfordjournals.aob.a085488

Lawlor, D. W., & Cornic, G. (2002). Photosynthetic carbon assimilation and associated metabolism in relation to water deficits in higher plants. *Regulation*, *44*(Evans 1998), 275–294. https://doi.org/10.1046/j.0016-8025.2001.00814.x

Lawson, T., & Morison, J. I. L. (2004). Stomatal function and physiology. *The Evolution of Plant Physiology*, 217–242. https://doi.org/10.1016/B978-012339552-8/50013-5

Lian, H. L., Yu, X., Ye, Q., Ding, X. S., Kitagawa, Y., Kwak, S. S., Su, W. A., & Tang, Z. C. (2004). The role of aquaporin RWC3 in drought avoidance in rice. *Plant and Cell Physiology*, *45*(4), 481–489. https://doi.org/10.1093/pcp/pch058

Liang, J., Zhang, J., & Wong, M. H. (1997). How do roots control xylem sap ABA concentration in response to soil drying? *Plant and Cell Physiology*, *38*(1), 10–16. https://doi.org/10.1093/oxfordjournals.pcp.a029078

Liu, X., Liu, W., Tang, Q., Liu, B., Wada, Y., & Yang, H. (2022). Global Agricultural Water Scarcity Assessment Incorporating Blue and Green Water Availability Under Future Climate Change. *Earth's Future*, *10*(4). https://doi.org/10.1029/2021EF002567

Lo Gullo, M. A., Nardini, A., Salleo, S., & Tyree, M. T. (1998). Changes in root hydraulic conductance (K(R)) of Olea oleaster seedlings following drought stress and irrigation. *New Phytologist*, *140*(1), 25–31. https://doi.org/10.1046/j.1469-8137.1998.00258.x

Lobet, G., Couvreur, V., Meunier, F., Javaux, M., & Draye, X. (2014). Plant Water Uptake in Drying Soils. *Plant Physiology*, *164*(4), 1619–1627. https://doi.org/10.1104/pp.113.233486

Malone, M., Herron, M., & Morales, M. A. (2002). Continuous measurement of macronutrient ions in the transpiration stream of intact plants using the meadow spittlebug coupled with ion chromatography. *Plant Physiology*, *130*(3), 1436–1442. https://doi.org/10.1104/pp.007740

Markesteijn, L., Iraipi, J., Bongers, F., & Poorter, L. (2010). Seasonal variation in soil and plant water potentials in a Bolivian tropical moist and dry forest. *Journal of Tropical Ecology*, *26*(5), 497–508. https://doi.org/10.1017/S0266467410000271

Martínez-Ballesta, M. C., Aparicio, F., Pallás, V., Martínez, V., & Carvajal, M. (2003). Influence of saline stress on root hydraulic conductance and PIP expression in Arabidopsis. *Journal of Plant Physiology*, *160*(6), 689–697. https://doi.org/10.1078/0176-1617-00861

Martínez-Vilalta, J., & Garcia-Forner, N. (2017). Water potential regulation, stomatal behaviour and hydraulic transport under drought: deconstructing the iso/anisohydric concept. *Plant Cell and Environment*, *40*(6), 962–976. https://doi.org/10.1111/pce.12846

Martre, P. (2001). Hydraulic Conductance and Mercury-Sensitive Water Transport for Roots of Opuntia acanthocarpa in Relation to Soil Drying and Rewetting. *Plant Physiology*, *126*(1), 352–362. https://doi.org/10.1104/pp.126.1.352

Martre, P., North, G. B., & Nobel, P. S. (2001). Hydraulic conductance and mercury-sensitive water transport for roots of Opuntia acanthocarpa in relation to soil drying and rewetting. *Plant Physiology*, *126*(1), 352–362. https://doi.org/10.1104/pp.126.1.352

Martre, Pierre, Durand, J. L., & Cochard, H. (2000). Changes in axial hydraulic conductivity along elongating leaf blades in relation to xylem maturation in tall fescue. *New Phytologist*, *146*(2), 235–247. https://doi.org/10.1046/j.1469-8137.2000.00641.x

McAusland, L., Vialet-Chabrand, S., Davey, P., Baker, N. R., Brendel, O., & Lawson, T. (2016). Effects of kinetics of light-induced stomatal responses on photosynthesis and water-use efficiency. *The New Phytologist*, *211*(4), 1209–1220. https://doi.org/10.1111/nph.14000

McCully, M. E. (1994). Accumulation of high levels of potassium in the developing xylem elements in roots of soybean and some other dicotyledons. *Protoplasma*, *183*(1–4), 116–125. https://doi.org/10.1007/BF01276819

McCully, M. E. (1995). How Do Real Roots Work? Some new Views of Root Structure. *Plant Physiol*, *109*, 1–6. https://doi.org/10.1104/pp.109.1.1

McDowell, N. G. (2011). Mechanisms linking drought, hydraulics, carbon metabolism, and vegetation mortality. *Plant Physiology*, *155*(3), 1051–1059. https://doi.org/10.1104/pp.110.170704

McElrone, A. J., Choat, B., Gambetta, G. A., & Brodersen, C. R. (2013). Water Uptake and Transport in Vascular Plants. *Nature Education Knowledge*, *4*(5). https://doi.org/10.1149/ma2012-02/13/1483

McLean, E. H., Ludwig, M., & Grierson, P. F. (2011). Root hydraulic conductance and aquaporin abundance respond rapidly to partial root-zone drying events in a riparian Melaleuca species. *New Phytologist*, *192*(3), 664–675. https://doi.org/10.1111/j.1469-8137.2011.03834.x

Medrano, H., Escalona, J. M., Bota, J., Gulías, J., & Flexas, J. (2002). Regulation of photosynthesis of C3 plants in response to progressive drought: Stomatal conductance as a reference parameter. *Annals of Botany*, *89*, 895–905. https://doi.org/10.1093/aob/mcf079

Melchior, W., & Steudle, E. (1993). Water transport in onion (Allium cepa L.) roots: Changes of axial and radial hydraulic conductivities during root development. *Plant Physiology*, *101*(4), 1305–1315. https://doi.org/10.1104/pp.101.4.1305

Meng, D., Walsh, M., & Fricke, W. (2016). Rapid changes in root hydraulic conductivity and aquaporin expression in rice (Oryza sativa l.) in response to shoot removal – Xylem tension as a possible signal. *Annals of Botany*, *118*(4), 809–819. https://doi.org/10.1093/aob/mcw150

Meunier, F., Zarebanadkouki, M., Ahmed, M. A., Carminati, A., Couvreur, V., & Javaux, M. (2018). Hydraulic conductivity of soil-grown lupine and maize unbranched roots and maize root-shoot junctions. *Journal of Plant Physiology*, *227*(December 2017), 31–44. https://doi.org/10.1016/j.jplph.2017.12.019

Mu, Z., Zhang, S., Zhang, L., Liang, A., & Liang, Z. (2006). Hydraulic conductivity of whole root system is better than hydraulic conductivity of single root in correlation with the leaf water status of maize. *Botanical Studies*, *47*(2), 145–151.

North, G. B., & Nobel, P. S. (1991). CHANGES IN HYDRAULIC CONDUCTIVITY AND ANATOMY CAUSED BY DRYING AND REWETTING ROOTS OF AGAVE DESERTI (AGAVACEAE). *American Journal of Botany*, *78*(7), 906–915.

North, G. B., & Nobel, P. S. (1997). Drought-induced changes in soil contact and hydraulic conductivity for roots of Opuntia ficus-indica with and without rhizosheaths. *Plant and Soil*, *191*(2), 249–258. https://doi.org/10.1023/A:1004213728734

Or, D., Tuller, M., & Wraith, J. M. (2005). SOIL WATER POTENTIAL. *Encyclopedia of Soils in the Environment*, *3*, 270–277.

Peterson, C. A., & Steudle, E. (1993). Lateral hydraulic conductivity of early metaxylem vessels in Zea mays L. roots. *Planta*, *189*(2), 288–297. https://doi.org/10.1007/BF00195088

Pierret, A., Doussan, C., & Pagès, L. (2006). Spatio-temporal variations in axial conductance of primary and first-order lateral roots of a maize crop as predicted by a model of the hydraulic architecture of root systems. *Plant and Soil*, *282*(1–2), 117–126. https://doi.org/10.1007/s11104-005-5373-7

Qu, M., Hamdani, S., Li, W., Wang, S., Tang, J., Chen, Z., Song, Q., Li, M., Zhao, H., Chang, T., Chu, C., & Zhu, X. (2016). Rapid stomatal response to fluctuating light: An under-explored mechanism to improve drought tolerance in rice. *Functional Plant Biology*, *43*(8), 727–738. https://doi.org/10.1071/FP15348

Ranathunge, K., Kim, Y. X., Wassmann, F., Kreszies, T., Zeisler, V., & Schreiber, L. (2017). The composite water and solute transport of barley (Hordeum vulgare) roots: effect of suberized barriers. *Annals of Botany*, *119*(4), 629–643. https://doi.org/10.1093/aob/mcw252

Rieger, M., & Litvin, P. (1999). Root system hydraulic conductivity in species with contrasting root anatomy. *Journal of Experimental Botany*, *50*(331), 201–209. https://doi.org/10.1093/jxb/50.331.201

Ritchie, J. T. (1998). *Soil water balance and plant water stress*. *October*, 41–54. https://doi.org/10.1007/978-94-017-3624-4_3

Rodrigues, M. L., Pacheco, C. M. A., & Chaves, M. M. (1995). Soil-plant water relations, root distribution and biomass partitioning in Lupinus albus L. under drought conditions. *Journal of Experimental Botany*, *46*(8), 947–956. https://doi.org/10.1093/jxb/46.8.947

Rodriguez-Dominguez, C. M., & Brodribb, T. J. (2020). Declining root water transport drives stomatal closure in olive under moderate water stress. *New Phytologist*, *225*(1), 126–134. https://doi.org/10.1111/nph.16177

Rodríguez-Gamir, J., Xue, J., Clearwater, M. J., Meason, D. F., Clinton, P. W., & Domec, J. C. (2019). Aquaporin regulation in roots controls plant hydraulic conductance, stomatal conductance, and leaf water potential in Pinus radiata under water stress. *Plant Cell and Environment*, *42*(2), 717–729. https://doi.org/10.1111/pce.13460

Růžička, K., Ursache, R., Hejátko, J., & Helariutta, Y. (2015). Xylem development - from the cradle to the grave. *New Phytologist*, *207*(3), 519–535. https://doi.org/10.1111/nph.13383

Ryu, J., Hwang, B. G., Kim, Y. X., & Lee, S. J. (2016). Direct observation of local xylem embolisms induced by soil drying in intact Zea mays leaves. *Journal of Experimental Botany*, *67*(9), 2617–2626. https://doi.org/10.1093/jxb/erw087

Sakurai-Ishikawa, J., Murai-Hatano, M., Hayashi, H., Ahamed, A., Fukushi, K., Matsumoto, T., & Kitagawa, Y. (2011). Transpiration from shoots triggers diurnal changes in root aquaporin expression. *Plant, Cell and Environment*, *34*(7), 1150–1163. https://doi.org/10.1111/j.1365-3040.2011.02313.x

Saliendra, N. Z., & Meinzer, F. C. (1989). Relationship between root/soil hydraulic properties and stomatal behavior in sugarcane. *Australian Journal of Plant Physiology*, *16*(3), 241–250. https://doi.org/10.1071/PP9890241

Samuels, A. L., Kaneda, M., & Rensing, K. H. (2006). The cell biology of wood formation: From cambial divisions to mature secondary xylem. *Canadian Journal of Botany*, *84*(4), 631–639. https://doi.org/10.1139/B06-065

Sanderson, J., Whitbread, F. C., & Clarkson, D. T. (1988). Persistent xylem cross-walls reduce the axial hydraulic conductivity in the apical 20 cm of barley seminal root axes: implications for the driving force for water movement. *Plant, Cell & Environment*, *11*(4), 247–256. https://doi.org/10.1111/j.1365-3040.1988.tb01143.x

Schelle, H., Heise, L., Jänicke, K., & Durner, W. (2013). Water retention characteristics of soils over the whole moisture range: A comparison of laboratory methods. *European Journal of Soil Science*, *64*(6), 814–821. https://doi.org/10.1111/ejss.12108

Schneider, H. M., Wojciechowski, T., Postma, J. A., Brown, K. M., Lücke, A., Zeisler, V., Schreiber, L., & Lynch, J. P. (2017). Root cortical senescence decreases root respiration, nutrient content and radial water and nutrient transport in barley. *Plant Cell and Environment*, *40*(8), 1392–1408. https://doi.org/10.1111/pce.12933

Schreiber, L., Hartmann, K., Skrabs, M., & Zeier, J. (1999). Apoplastic barriers in roots: Chemical composition of endodermal and hypodermal cell walls. *Journal of Experimental Botany*, *50*(337), 1267–1280. https://doi.org/10.1093/jxb/50.337.1267

Schulte, P. J., & Castle, A. L. (1993). Water flow through vessel perforation plates - a fluid mechanical approach. *Journal of Experimental Botany*, *44*(7), 1135–1142. https://doi.org/10.1093/jxb/44.7.1135

Schulte, P. J., Gibson, A. C., & Nobel, P. S. (1987). Xylem Anatomy and Hydraulic Conductance of Psilotum nudum. *American Journal of Botany*, *74*(9), 1438. https://doi.org/10.2307/2444320

Schulte, P. J., Hacke, U. G., & Schoonmaker, A. L. (2015). Pit membrane structure is highly variable and accounts for a major resistance to water flow through tracheid pits in stems and roots of two boreal conifer species. *New Phytologist*, *208*(1), 102–113. https://doi.org/10.1111/nph.13437

Sevanto, S. (2014). Phloem transport and drought. *Journal of Experimental Botany*, *65*(7), 1751–1759. https://doi.org/10.1093/jxb/ert467

Sharp, R. E., & Davies, W. J. (1985). Root growth and water uptake by maize plants in drying soil. *Journal of Experimental Botany*, *36*(9), 1441–1456. https://doi.org/10.1093/jxb/36.9.1441

Shein, E. V., & Pachepsky, Y. A. (1995). Influence of root density on the critical soil water potential. *Plant and Soil*, *171*(2), 351–357. https://doi.org/10.1007/BF00010291

Sirichandra, C., Wasilewska, A., Vlad, F., Valon, C., & Leung, J. (2009). The guard cell as a single-cell model towards understanding drought tolerance and abscisic acid action. *Journal of Experimental Botany*, *60*(5), 1439–1463. https://doi.org/10.1093/jxb/ern340

Sperry, J. S., Hacke, U. G., & Wheeler, J. K. (2005). Comparative analysis of end wall resistivity in xylem conduits. *Plant, Cell and Environment*, *28*(4), 456–465. https://doi.org/10.1111/j.1365-3040.2005.01287.x

Steudle, E. (1994). Water transport across roots. *Plant and Soil*, *167*(1), 79–90. https://doi.org/10.1007/BF01587602

Steudle, E., & Peterson, C. A. (1998). How does water get through roots? *Journal of Experimental Botany*, *49*(322), 775–788. https://doi.org/10.1093/jexbot/49.322.775

Tardieu, F., & Simmoneau, T. (1998). Variability among species of stomatal control under fluctuating soil water status and evaporative demand: Modelling isohydric and anisohydric behaviours. *Journal of Experimental Botany*, *49*(Special Issue), 443–452. https://doi.org/10.1093/jexbot/49.suppl

Tyree, M. T., Patiño, S., Bennink, J., & Alexander, J. (1995). Dynamic measurements of roots hydraulic conductance using a high-pressure flowmeter in the laboratory and field. *Journal of Experimental Botany*, *46*(1), 83–94. https://doi.org/10.1093/jxb/46.1.83

Urli, M., Porté, A. J., Cochard, H., Guengant, Y., Burlett, R., & Delzon, S. (2013). Xylem embolism threshold for catastrophic hydraulic failure in angiosperm trees. *Tree Physiology*, *33*(7), 672–683. https://doi.org/10.1093/treephys/tpt030

van den Honert, T. H. (1948). Water transport as a catenary process. *Discussions of the Faraday Society*, *3*, 146–153. https://doi.org/10.1039/DF9480300146

van Dusschoten, D., Kochs, J., Kuppe, C. W., Sydoruk, V. A., Couvreur, V., Pflugfelder, D., & Postma, J. A. (2020). Spatially resolved root water uptake determination using a precise soil water sensor. *Plant Physiology*, *184*(3), 1221–1235. https://doi.org/10.1104/pp.20.00488

van Dusschoten, D., Metzner, R., Kochs, J., Postma, J. A., Pflugfelder, D., Buehler, J., Schurr, U., & Jahnke, S. (2016). Quantitative 3D Analysis of Plant Roots growing in Soil using Magnetic Resonance Imaging. *Plant Physiology*, *170*(March), pp.01388.2015. https://doi.org/10.1104/pp.15.01388 van Genuchten, M. T. (1980). A Closed-form Equation for Predicting the Hydraulic Conductivity of Unsaturated Soils. *Soil Science Society of America Journal*, *44*(5), 892–898. https://doi.org/10.2136/sssaj1980.03615995004400050002x

Vandeleur, R. K., Sullivan, W., Athman, A., Jordans, C., Gilliham, M., Kaiser, B. N., & Tyerman, S. D. (2014). Rapid shoot-to-root signalling regulates root hydraulic conductance via aquaporins. *Plant, Cell and Environment*, *37*(2), 520–538. https://doi.org/10.1111/pce.12175

Vesala, T., Sevanto, S., Grönholm, T., Salmon, Y., Nikinmaa, E., Hari, P., & Hölttä, T. (2017). Effect of leaf water potential on internal humidity and CO2 dissolution: Reverse transpiration and improved water use efficiency under negative pressure. *Frontiers in Plant Science*, *8*(FEBRUARY), 1–10. https://doi.org/10.3389/fpls.2017.00054

Visentin, I., Vitali, M., Ferrero, M., Zhang, Y., Ruyter-Spira, C., Novák, O., Strnad, M., Lovisolo, C., Schubert, A., & Cardinale, F. (2016). Low levels of strigolactones in roots as a component of the systemic signal of drought stress in tomato. *New Phytologist*, *212*(4), 954–963. https://doi.org/10.1111/nph.14190

Watt, M., Magee, L. J., & McCully, M. E. (2008). Types, structure and potential for axial water flow in the deepest roots of field-grown cereals. *New Phytologist*, *178*(3), 690. https://doi.org/10.1111/j.1469-8137.2008.02434.x

Wind, G. P. (1955). Flow of water through plant roots. *Netherlands Journal of Agricultural Science*, *3*(4), 259–264. https://doi.org/10.18174/njas.v3i4.17804

Zarebanadkouki, M., Kim, Y. X., & Carminati, A. (2013). Where do roots take up water? Neutron radiography of water flow into the roots of transpiring plants growing in soil. *New Phytologist*, *199*(4), 1034–1044. https://doi.org/10.1111/nph.12330

Zarebanadkouki, M., Kroener, E., Kaestner, A., & Carminati, A. (2014). Visualization of Root Water Uptake: Quantification of Deuterated Water Transport in Roots Using Neutron Radiography and Numerical Modeling. *Plant Physiology*, *166*(2), 487–499. https://doi.org/10.1104/pp.114.243212

Zimmermann, H. M., & Steudle, E. (1998). Apoplastic transport across young maize roots: effect of the exodermis. *Planta*, *206*, 7–19.

Zwieniecki, M. A., Melcher, P. J., & Holbrook, N. M. (2001). Hydraulic properties of individual xylem vessels of Fraxinus americana. *Journal of Experimental Botany*, *52*(355), 257–264. https://doi.org/10.1093/jxb/52.355.257

Abbreviations

term	meaning	unit
e_{air}	vapor pressure in the bulk air	MPa
e_{leaf}	vapor pressure in the leaf	MPa
g_s	stomatal conductance	ml h^{-1} m^{-2}
K	hydraulic conductance	ml h^{-1} MPa^{-1}
K_{LA}	hydraulic conductance between leaf and atmosphere	ml h^{-1} MPa^{-1}
K_{root}	radial root conductance	ml h^{-1} MPa^{-1}
K_{SL}	hydraulic conductance between soil and leaf	ml h^{-1} MPa^{-1}
K_X	axial xylem conductance	ml h^{-1} MPa^{-1}
NR	neutron radiography	
P	atmospheric pressure	MPa
Q	water flow rate	ml h^{-1}
Q_X	axial water flow rate from roots to leaves	ml h^{-1}
RWU	root water uptake rate	ml h^{-1}
SWaP	soil water profiler	
T	transpiration rate	ml h^{-1}
TDR	time domain reflectometry	
$\widehat{U}_P$	normalized plant-driven root water uptake distribution with depth	
U_{tot}	total root water uptake rate	ml h^{-1}
z	depth	cm
θ	volumetric soil water content	ml cm^{-3}
Ψ	water potential	MPa
Ψ_{leaf}	leaf water potential	MPa
Ψ_{seq}	equivalent soil water potential	MPa
Ψ_{soil}	soil water potential	MPa
Ψ_{root}	root water potential	MPa

Theory and practice of measurements with the soil water profiler

Recently, a highly precise soil water sensor, called soil water profiler (SWaP), has been developed that can be used to non-invasively measure root water uptake profiles (van Dusschoten et al., 2020). These measurements are fundamental for the analysis of the main question addressed in this thesis: How does soil drying affect the hydraulic conductance of the root system and its spatial distribution relatively to remaining water resources? Such an analysis had not been done before, and part of this work was to develop a suitable experimental design based on the SWaP. In principle, this involved: rebuilding and recalibrating measurement hardware, adaptations of SWaP data processing, correction of MRI-measured root length, establishing simultaneous measurements of root water uptake profiles, plant water potential, and leaf gas exchange, refining data analysis. In this chapter, descriptions from the Materials and Methods sections of the single manuscripts are expanded, supported with additional data, and set into a larger methodological context, to provide a comprehensive explanation on the SWaP measurements, the associated theory, and the adaptations made during this project.

Measurement principle and basic data processing

The basis of the SWaP sensors is a resonant circuit, consisting of two opposing copper plates forming a capacitor, connected to a coil. This resonant circuit is inductively coupled to a vector network analyzer (VNWA), which allows for determination of the resonance frequency. The two copper plates are glued on the inside of two hollow, 12 cm high PVC cylinders, which are shielded by an aluminum frame. The inner diameter of the PVC cylinders is slightly greater than the outer diameter of the pots used for plant growth, such that the pots can be placed into the SWaP sensors (Fig. 1A). When a soil-filled pot is placed into the SWaP sensors, the permittivity between the copper plates, and thus the resonance frequency, is a function of the soil water content (θ, %). Therefore, with all other parameters kept constant, the resonance frequency is a measure for the soil water content. Relating the measured resonance frequency to a certain soil water content requires calibration of the sensors.

Attrition, mostly due to friction with the PVC pots, can gradually change the condition of the sensors, especially of the copper plates. Therefore, one of the first steps of this work was to rebuild SWaP sensors. Since these were hand-made, some characteristics, such as the size of the copper plates, or the distance between the coils used for inductive coupling, are subject to variation, and so is the resulting resonance frequency. Thus, the newly build sensors were recalibrated. For this, the soil substrate used was homogeneously mixed with a defined amount of water, filled into 12 cm high pots at a given dry density, and sealed to avoid evaporation. Then pots with soil were placed into the SWaP to measure the resonance frequency. This procedure was repeated for varying defined soil water content, ranging from 2 to 30 % in 2 % steps. The measured data were fitted using a second order polynomial (Online Resource 2 of the first manuscript of this thesis). The fitting parameters obtained for a specific soil type at a specific dry density were used to convert measured resonance frequencies into volumetric soil water content.

The SWaP is equipped with a stepper motor enabling automatic vertical movement of the sensors along pots in 1 cm steps. At every step, the local resonance frequency, and thus the local soil water content is determined. A complete scan gives the vertical profile of soil water content. However, the local measurements of the resonance frequency are not only influenced by the local water content of the 1 cm high soil layer at the center of the sensor, but also by the water content of the adjacent layers. This is because the electrical field between the copper plates is distributed across the entire 12 cm height of the sensor. Thus, the measured resonance frequency is a convolution of the profile of electrical field strength, and the resonance frequency of the 12 layers enclosed by the sensor. This especially becomes important at the borders of the soil columns, where a sharp transition in permittivity takes place. Using a deconvolution, the actual resonance frequency in each layer can be determined from the measured, convolved signal. This requires the profile of electric field strength, and the exact resonance frequency beyond the pot borders to be known. Here, the pots were placed onto sockets, filled with watered soil. Five vials containing water were put on top of the soil columns. The resonance frequency of both, the sockets, and a pot containing the water-filled vessels, were measured. With this information, a numerical deconvolution of the measured soil water profile can be performed. In a previous protocol, this was done with a model-constrained deconvolution using a 7th order polynomial for approximation. Here, a novel method was established, not relying on model constraints but using a regularization term which avoids overfitting, and thus reduces fluctuations of the deconvolved profiles. Fig. 1B shows an example of a measured profile of soil water content with, and without deconvolution. Especially at the edges of the soil columns, correcting the measured, convolved signal is essential.

Redistributive water flow in a soil column

For the setup used in this project (four parallel moving sensors with interlaced measurements), a full vertical scan of 45 cm high soil columns took around twelve minutes. For reasons of synchronization with a modulated light intensity, the scans were started every 15 minutes. Based on consecutively measured soil water profiles, the change in soil water content over time, called soil water depletion rate ($\frac{\partial \theta}{\partial t}$, ml cm^{-3} h^{-1}), in each layer can be determined. As shown in the following example measurement, this approach is, for instance, suitable to analyze redistributive soil water flow (rSWF, ml cm^{-3} h^{-1}) within a soil column. The soil substrate used for this measurement was 80% (v) of a loamy sand collected at Kaldenkirchen, Germany (Pohlmeier et al., 2009) with additional 20% coarse sand. Addition of coarse sand was required to avoid contraction of the soil column which the SWaP measurement is sensitive for. A fixed amount of this soil substrate, yielding a dry bulk density of 1.47 kg/l, was mixed with water and filled into the pots under gentle shaking. For this measurement, four soil columns with a varying soil water content (5, 9, 14, and 20 %(v)) were prepared. The pots were placed into the SWaP and the soil water profiles were continuously scanned for two days. Fig 2A shows the vertical profiles of soil water content at the start, and after 40 h of measuring. In general, there is a similar trend among the four different soil columns: The soil water content decreases in upper soil layers, while it increases in deeper layers over time. Besides evaporation (of the order of 0.02 ml cm^{-3} h^{-1}), these dynamics are caused by redistributive soil water flow along a vertical gradient in soil water potential. For the setup used here, the two most important factors affecting the soil water potential are 1) gravity, and 2) the matric potential depending on soil water content. At the start, when the soil water was almost homogeneously distributed, the matric potential was close to uniform, and the vertical gradient in soil water potential is dominated by gravity. With ongoing water flow from upper towards deeper layers, the matric potential decreases (becomes more negative) in upper soil layers and increases (becomes less negative) in deeper layers. Thus, a vertical gradient in matric potential is established in opposite direction to gravity. The vertical redistribution of soil water lasts until the gradient in matric potential compensates gravity. At the end of the measurement, the extent of the vertical gradient is greater in soil columns with greater average soil water content. This is because the water retention curve of the soil is non-linear: In the dry regime, a certain difference in soil water content causes a greater difference in soil water potential compared to the wet regime. Additionally, as shown in Fig. 2B, the rate of the vertical soil water flow at the start of the measurement is greater for soil columns with greater water content. These differences are caused by the soil water conductivity which increases with increasing soil water content. A greater conductivity results in a greater water flow rate at a given water potential gradient. Compared to the start of the measurement, the water depletion rates at the end of the measurement decreased in all four soil columns. As explained above, this is because the redistribution of soil water gradually reduced the vertical gradient in soil water potential, and thus, the driving force for water flow. Fig. 2C shows the local soil water content at different depths for each soil column over time. The soil water content decreases in upper layers, due to evaporation and rSWF, while it is almost constant in the middle of the pot and increases in deeper layers due to rSWF. The rate of soil water redistribution and the resulting differences in local soil water content among layers at different depths increases with increasing average soil water content.

Plant- and soil-driven water uptake distributions

The principal purpose of the SWaP measurements in this project is to determine the vertical distribution of root water uptake rates and the underlying distribution of root hydraulic conductance. Two factors basically determine the distribution of root water uptake rates (RWU, ml h^{-1}) over depth: 1) the distribution of soil water potential and 2) the distribution of root hydraulic conductance. Local root water uptake rates increase with increasing radial water potential gradient (and thus less negative soil water potential at a given water potential in the root xylem) and increasing radial root conductance. These two factors must be separated from each other to obtain vertical profiles of root hydraulic conductance from SWaP measurements. One option would be to measure root water uptake rates in soils with a homogeneous vertical distribution of soil water potential. The resulting water uptake profile would be fully determined by the distribution of root hydraulic conductance, and thus represent an inherent plant characteristic that is independent of the soil water distribution. This water uptake profile is called here plant-driven distribution of root water uptake rates (U_P, ml h^{-1}). However, generating and maintaining conditions of uniform soil water potential in soil columns containing transpiring plants is almost impossible. Thus, root water uptake profiles usually deviate from U_P. The difference between the actual root water uptake profile and U_P is determined by the distribution of soil water potential and is called here soil driven root water uptake redistribution (U_S, ml h^{-1}).

The meaning of U_P and U_S can be illustrated by the following hypothetical scenario: Two identical plants with identical distribution of root hydraulic traits, and identical total root water uptake rates are exposed to two different soil water conditions: 1) a soil with uniformly distributed soil water potential and 2) a soil with non-uniformly distributed soil water potential but the same average water potential as in the uniform case. In the uniform soil, U_S is zero in all layers and RWU is equal to U_P. In the non-uniform soil, root water uptake rates in soil layers with a water potential below (more negative) the average water potential are lower than in the uniform soil. The local U_S is negative and thus, RWU is smaller than U_P. In contrast, in soil layers with a water potential above (less negative) average, water uptake rates are greater than in uniform soil. The local U_S is positive and RWU is greater than U_P. Across the whole pot, U_P always sums up to the total root water uptake rate (U_{tot}, ml h^{-1}), whereas U_S sums up to zero: Compared to uniformly wet soil, the increase in water uptake rates from relatively wet soil layers is equal to the decrease in water uptake rates from relatively dry layers.

Mathematically, the separation of RWU into U_P and U_S can be derived using a simplified form of the hydraulic network model developed by Couvreur et al. (2012). The 45 cm high soil columns used here are interpreted as 45 vertically stacked layers of 1 cm height. Layers are numbered with i= 1,…, 45 from top to bottom. The upper boundary of each layer is at depth z_i = 0,…, 45 cm. The entirety of roots in a layer has a specific radial conductance ($K_R(z_i)$, ml h^{-1} MPa^{-1}) , axial conductance ($K_X(z_i)$, ml h^{-1} MPa^{-1}), and xylem water potential ($\Psi_X(z_i)$, MPa). Additionally, each layer has a specific soil water potential ($\Psi_{soil}(z_i)$, MPa). The local root water uptake rate ($RWU(z_i)$, m h^{-1}) is determined by the radial root conductance times the water potential gradient between root xylem and soil (Alm et al., 1992):

$$RWU(z_i) = K_R(z_i) \cdot (\Psi_{soil}(z_i) - \Psi_X(z_i)) \qquad [1]$$

Ψ_X can be approximated by the water potential at the plant collar (Ψ_{collar}, MPa) under the assumption of a much greater axial than radial root conductance. Ψ_{collar} is determined by the total root water uptake rate (U_{tot}, ml h^{-1}), total root conductance (K_{tot} ml h^{-1} MPa^{-1}), and the equivalent soil water potential (Ψ_{seq}, MPa) (Couvreur et al., 2012):

$$\Psi_{collar} = \Psi_{seq} - \frac{U_{tot}}{K_{tot}} \qquad [2]$$

Approximating Ψ_X in eq. 1 by the expression for Ψ_{collar} in eq. 2 gives:

$$RWU(z_i) = K_R(z_i) \cdot \frac{U_{tot}}{K_{tot}} + K_R(z_i) \cdot (\Psi_{soil}(z_i) - \Psi_{seq}) \qquad [3]$$

Eq. 3 shows that the distribution of root water uptake rates can be separated into the two terms introduced above: 1) the plant-driven root water uptake distribution, $U_P(z_i) = K_R(z_i) \cdot \frac{U_{tot}}{K_{tot}}$ and 2) the soil-driven root water uptake redistribution $U_S(z_i) = K_R(z_i) \cdot (\Psi_{soil}(z_i) - \Psi_{seq})$.

With these definitions, eq. 3 writes:

$$RWU(z_i) = U_P(z_i) + U_S(z_i) \qquad [4]$$

The distribution of U_P along the 45 soil layers only depends on the distribution of root conductance. Dividing U_P by the total water uptake rate gives the normalized distribution of plant-driven root water uptake rates ($\widehat{U}_P$):

$$\widehat{U}_P(z_i) = \frac{U_P(z_i)}{U_{tot}} = \frac{K_R(z_i)}{K_{tot}} \qquad [5]$$

Alternating light intensity to separate water flow patterns

The SWaP in combination with an alternating light intensity offers an option to determine $\widehat{U}_P$ without depending on conditions of uniform soil water potential. The basic principle of this approach is that a light-induced change in the transpiration rate causes a fast change in the local soil water depletion rate in each layer which is directly proportional to the fraction of root conductance in that layer. This requires assuming that on short time scales changes in U_S and redistributive soil water flow (rSWF) are independent of changes in the transpiration rate. To achieve this, changes in light intensity must be modulated at a sufficiently high frequency. Additionally, the amplitude of the changes must be sufficiently high to induce detectable changes of local soil water depletion rates. For the setup used here, a photosynthetically active radiation alternating between 500 µmol m^{-2} s^{-1} and 1000 µmol m^{-2} s^{-1} in periods of 2 h was applied. The following example illustrates the approach using an alternating light pattern to derive $\widehat{U}_P$ (Table 1): Assuming two halves (top and bottom) of a soil column, with the top half at a soil water potential of -0.2 MPa and the bottom half at -0.1 MPa respectively. The root conductance in the top half is 2 ml h^{-1} MPa^{-1}, and 1 ml h^{-1} MPa^{-1} in the bottom half. At low light intensity, the transpiration would generate a water potential of, for instance, -0.5 MPa in the root xylem. According to eq. 1, this would result in a RWU of 0.6 ml h^{-1} in the top half, and 0.4 ml h^{-1} in the bottom half. At high light intensity, the transpiration rate increases, and thus Ψ_X decreases to, for instance, -1.0 MPa. Following eq.1, this would result in a RWU of 1.6 ml h^{-1} in the top half and 0.9 ml h^{-1} in the bottom half. Table 1 shows that the change in the local root water uptake rate in relation to the change in total root water uptake rate, caused by the change in light intensity, is equal to the ratio of the local and total root conductance. Therefore, the relation between local and total changes in water uptake rates reflect the distribution of root hydraulic conductance, and thus $\widehat{U}_P$ (eq. 5).

Table 1: Hypothetical example on how light induced changes of the local root water uptake rates relate to the local fraction of root conductance. In this example the upper half (top) and lower half (bottom) of a soil column are treated separately. Given values of the soil water potential (Ψ_{soil}), radial root conductance (K_R), and the xylem water potential (Ψ_X) are arbitrary. The resulting root water uptake rates (RWU) were calculated using eq. 1. The goal of this procedure is to determine how the conductance in top and bottom half relate to each other using measured values on the local RWU and the total root water uptake rate (U_{tot}).

			Low light with Ψ_X = -0.5 MPa	High light with Ψ_X = -1.0 MPa		
	Ψ_{soil} (MPa)	K_R (ml h^{-1} MPa^{-1})	RWU (ml h^{-1})	RWU (ml h^{-1})	$\frac{\Delta RWU}{\Delta U_{tot}}$	$\widehat{U}_P = \frac{K_R}{K_{tot}}$
top	-0.2	2	0.6	1.6	$\frac{1.0}{1.5} = \frac{2}{3}$	$\frac{2}{3}$
bottom	-0.1	1	0.4	0.9	$\frac{0.5}{1.5} = \frac{1}{3}$	$\frac{1}{3}$
total		3	1	2.5		

Soil water depletion rates not only depend on RWU but also on redistributive soil water flow (Fig. 2), which was neglected for the example given in Table 1. However, the principle works similarly when redistributive soil water flow is present. This becomes obvious when a constant soil water flow (e.g. 0.1 ml h^{-1}) from the wetter bottom half towards the drier top half is added in Table 1. The resulting soil water depletion rates would be 0.5 ml h^{-1} in both halves at low light intensity, and 1.5 ml h^{-1} and 1.0 ml h^{-1} respectively in top and bottom half at high light intensity. Dividing the change in local soil water depletion rate by the change in total root water uptake rate would still give $\widehat{U}_P$.

Determining plant-driven root water uptake distributions of growing plants

In practice, determination of $\widehat{U}_P$ works as follows: The soil water profiles of pots with soil columns, containing transpiring plants are continuously measured with the SWaP for 14 h under conditions of alternating light intensity (4 high light phases and 3 low light phases of 2 h each). Based on these measurements, total root water uptake rates and local soil water depletion rates ($\frac{\partial \theta(z_i,t)}{\partial t}$, ml cm^{-3} h^{-1}) are determined. $\frac{\partial \theta}{\partial t}$ is the sum of local root water uptake rates (U_P+U_S) and redistributive soil water flow:

$$\frac{\partial \theta(z_i,t)}{\partial t} = \frac{U_P(z_i)+U_S(z_i)}{V} + rSWF(z_i) \qquad [6]$$

Division by the pot volume is required here to obtain the same units for $\frac{\partial \theta}{\partial t}$ and RWU. Writing U_P according to eq. 5, and summarizing U_S and rSWF as redistributive water flow through soil and roots (S_R, ml cm^{-3} h^{-1}) gives:

$$\frac{\partial \theta(z_i,t)}{\partial t} = \widehat{U}_P(z_i) \cdot \frac{U_{tot}\,(t)}{V} + S_R(z_i,t) \qquad [7]$$

The continuously measured data on $\frac{\partial \theta(z_i,t)}{\partial t}$ and U_{tot} show variation due to the alternating light conditions. According to eq. 7, $\widehat{U}_P$ in each layer can be determined using a linear regression between $\frac{\partial \theta(z_i,t)}{\partial t}$ and U_{tot}. Supplemental Fig. 2 of the second manuscript of this thesis illustrates the data processing of SWaP measurements used to determine $\widehat{U}_P$. As pointed out above, one requirement for this approach is that the changes in U_{tot} and in U_S and rSWF are independent. This is achieved by the comparably fast alterations of the light intensity, such that the fast, light-induced effect on the local soil water depletion rates always dominates the comparably slow effect of a gradually changing soil water distribution which alter U_S and rSWF. Additionally, the high precision of the SWaP sensor is a crucial factor for this approach, since for younger plants, the local changes in soil water depletion rate can be of the order of 0.1 ml h^{-1} and below. As pointed out by van Dusschoten et al. (2020), if the precision of the SWaP was 10 times lower, which would be still high compared to other methods, the approach described here would not work.

Fig. 3A shows $\widehat{U}_P$ profiles, of a maize plant at an age of two, three, and four weeks, measured with the SWaP. With increasing plant age, the $\widehat{U}_P$ profile shifted towards deeper layers. Since $\widehat{U}_P$ is a measure for the normalized distribution of root conductance, this shift indicates that the hydraulic conductance in deeper layers increases relatively to the hydraulic conductance in upper layers. One major factor influencing root conductance is root length, and thus, changes in the distribution of roots can cause changes in $\widehat{U}_P$. Therefore, data on root length distribution are required to interpret data on $\widehat{U}_P$. For the example shown here, and any other measurement over time, root length distribution must be determined non-invasively. This can be achieved using magnetic resonance imaging (MRI) (van Dusschoten et al., 2016). Fig. 3B shows MRI images of the root system of the measured maize plant at an age of two, three, and four weeks. Compared to the age of two weeks, additional roots predominantly grew in deeper layers during the third and fourth week. This additional root growth caused an increase in root conductance in deeper layers. If this increase is greater than the increase in upper layers, it causes a shift in $\widehat{U}_P$ towards deeper layers as shown in Fig. 3A. Dividing $\widehat{U}_P$ by the distribution of root length gives the distribution of intrinsic root hydraulic conductivity. In principle, vertical distribution of root length can be directly determined based on MRI images using NMRooting software (van Dusschoten et al., 2016). However, root detection with the MRI setup used was limited to roots with diameter > 200-300 µm (van Dusschoten et al., 2016). Part of this work was to correct for the missing fine root fraction by comparative measurements of vertical root length distributions using MRI and scanning of harvested roots. For this, plants of four different species, barley, maize, faba bean, and zucchini were grown in soil filled pots and root systems were imaged with MRI. Then, shoots were cut off, the soil columns with roots were removed from the pots, and cut into 5 layers, each of 9 cm height. Roots of each part of the soil column were separately harvested and scanned using WinRHIZO software (Regents Instruments). Using both, MRI and destructively measured root length, correction factors were calculated, to correct for the missing fine root fraction of MRI measurements.

Simultaneously measuring hydraulic parameters at soil, root, and shoot level

The example shown in Fig. 3 highlights, that $\widehat{U}_P$ is a measure for how the root hydraulic conductance is distributed along the root system but does not provide information about the absolute root hydraulic conductance. This requires additional data on the total conductance of the root system (eq. 5). Furthermore, as this project aimed at analyzing the interaction between below-ground hydraulic traits and water flow regulation at the shoot, measurements of the stomatal conductance were needed. One possibility to determine the total conductance of the root system is simultaneously measuring the total root water uptake rate and the water potential gradient between soil and plant (eq. 2). Using the SWaP, the total root water uptake rate can be measured. Additionally, if the water retention curve of the soil is known, the soil water potential can be calculated from measurements of the soil water content. However, one major drawback of the SWaP compared to an imaging technique such as neutron radiography is, that the measurement is only one-dimensional. This could become relevant during soil drying, due to the emergence of a severe water depletion zone around the roots (Carminati et al., 2020). In such a scenario, the water potential sensed at the root surface could differ considerably from the bulk soil water potential as measured with the SWaP. Thus, part of this work was to correct for this water depletion zone by modeling the water potential at the root surface following the approach from Carminati et al. (2020). How this was done is described in Supplemental Method S1 of Manuscript II.

With this correction, the SWaP measurement allows for determination of the root system conductance when the plant water potential is known. Thus, one crucial part of this project was to establish combined SWaP and leaf water potential measurements using psychrometers (ICT International). Psychrometer measurements work as follows: after carefully abrading the leaf cuticle, the small chamber of the psychrometer, containing two thermocouples, was attached to the water conducting tissue of the leaf and sealed. The vapor pressure in the chamber, equilibrates with the vapor pressure of the conducting tissue, which depends on the local water potential. Then, a cooling pulse is applied to one of the thermocouples, causing water condensation, which then evaporates again. The change in temperature, sensed by the thermocouple during evaporation, depends on the evaporation rate, which is a function of the vapor pressure in the chamber, and thus, of leaf water potential. The second thermocouple is used to correct for temperature gradients. Using a calibration curve, obtained by psychrometer readings of filter paper soaked in salt solution with varying, defined water potential, the leaf water potential can be determined. Both, SWaP and psychrometer measurements are non-invasive, and thus suitable to detect changes in living plants during soil drying. Dividing the total root water uptake rate by the gradient between the equivalent soil water potential and leaf water potential gives the hydraulic conductance between soil and leaf (K_{SL}), which is mainly determined by root conductance (Corso et al., 2020; Frensch & Steudle, 1989; Reid & Hutchison, 1986; Rodríguez-Gamir et al., 2019). As explained in more detail in the second manuscript, the dynamics of soil drying-induced changes in K_{SL} could be characterized using a single parameter, which is related to the drought robustness of the plant. To analyze how changes in the hydraulic parameters below-ground interact with regulation of water flow in the shoot, data on stomatal conductance are needed. Here, we performed leaf gas exchange measurements using a portable LiCor 6400 photosynthesis system. These three measurement technologies, SWaP, leaf psychrometer, and LICOR do not interfere with each other and thus can be performed at the same plant simultaneously (Fig. 4). The drawback of this approach is its low throughput: The SWaP setup used here can measure four plants simultaneously, which can be scaled up comparably easily. However, leaf water potential and gas exchange measurement require one measurement device per plant, and especially the LiCOR systems are relatively expensive. In this work, one LiCOR 6400 was used to measure multiple plants in parallel, which is not ideal, since the SWaP measurement is sensitive to vibrations in the climate chamber. Additionally, repetitively interchanging the LiCOR between plants is comparably time-consuming regarding an otherwise fully automated measurement setup. Nevertheless, this experimental setup covers the complete hydraulic pathway from soil to plant and atmosphere, and allows for determining a unique data set, consisting of the following parameters: the vertical distribution of soil water content and soil water potential, the normalized distribution of plant-driven water uptake rates, the total root water uptake rate, the total conductance of the root system, the vertical distribution of root hydraulic conductance, the leaf water potential, and stomatal conductance. Using this setup, the central questions addressed in this thesis were analyzed.

References

Alm, D. J., Cavelier, J., & Nobel, P. S. (1992). A finite-element model of radial and axial conductivities for individual roots: Development and validation for two desert succulents. *Annals of Botany*, *69*(1), 87–92.

Carminati, A., Ahmed, M. A., Zarebanadkouki, M., Cai, G., Lovric, G., & Javaux, M. (2020). Stomatal closure prevents the drop in soil water potential around roots. *New Phytologist*, *226*(6), 1541–1543. https://doi.org/10.1111/nph.16451

Corso, D., Delzon, S., Lamarque, L. J., Cochard, H., Torres-Ruiz, J. M., King, A., & Brodribb, T. (2020). Neither xylem collapse, cavitation, or changing leaf conductance drive stomatal closure in wheat. *Plant Cell and Environment*, *43*(4), 854–865. https://doi.org/10.1111/pce.13722

Couvreur, V., Vanderborght, J., & Javaux, M. (2012). A simple three-dimensional macroscopic root water uptake model based on the hydraulic architecture approach. *Hydrology and Earth System Sciences*, *16*(8), 2957–2971. https://doi.org/10.5194/hess-16-2957-2012

Frensch, J., & Steudle, E. (1989). Axial and Radial Hydraulic Resistance to Roots of Maize (Zea mays L.). *Plant Physiology*, *91*(2), 719–726. https://doi.org/10.1104/pp.91.2.719

Pohlmeier, A., Haber-Pohlmeier, S., & Stapf, S. (2009). A Fast Field Cycling Nuclear Magnetic Resonance Relaxometry Study of Natural Soils. *Vadose Zone Journal*, *8*(3), 735–742. https://doi.org/10.2136/vzj2008.0030

Reid, J. B., & Hutchison, B. (1986). Soil and plant resistances to water uptake by Vicia faba L. *Plant and Soil*, *92*(3), 431–441. https://doi.org/10.1007/BF02372491

Rodríguez-Gamir, J., Xue, J., Clearwater, M. J., Meason, D. F., Clinton, P. W., & Domec, J. C. (2019). Aquaporin regulation in roots controls plant hydraulic conductance, stomatal conductance, and leaf water potential in Pinus radiata under water stress. *Plant Cell and Environment*, *42*(2), 717–729. https://doi.org/10.1111/pce.13460

van Dusschoten, D., Kochs, J., Kuppe, C. W., Sydoruk, V. A., Couvreur, V., Pflugfelder, D., & Postma, J. A. (2020). Spatially resolved root water uptake determination using a precise soil water sensor. *Plant Physiology*, *184*(3), 1221–1235. https://doi.org/10.1104/pp.20.00488 van Dusschoten, D., Metzner, R., Kochs, J., Postma, J. A., Pflugfelder, D., Buehler, J., Schurr, U., & Jahnke, S. (2016). Quantitative 3D Analysis of Plant Roots growing in Soil using Magnetic Resonance Imaging. *Plant Physiology*, *170*(March), pp.01388.2015. https://doi.org/10.1104/pp.15.01388

Figures

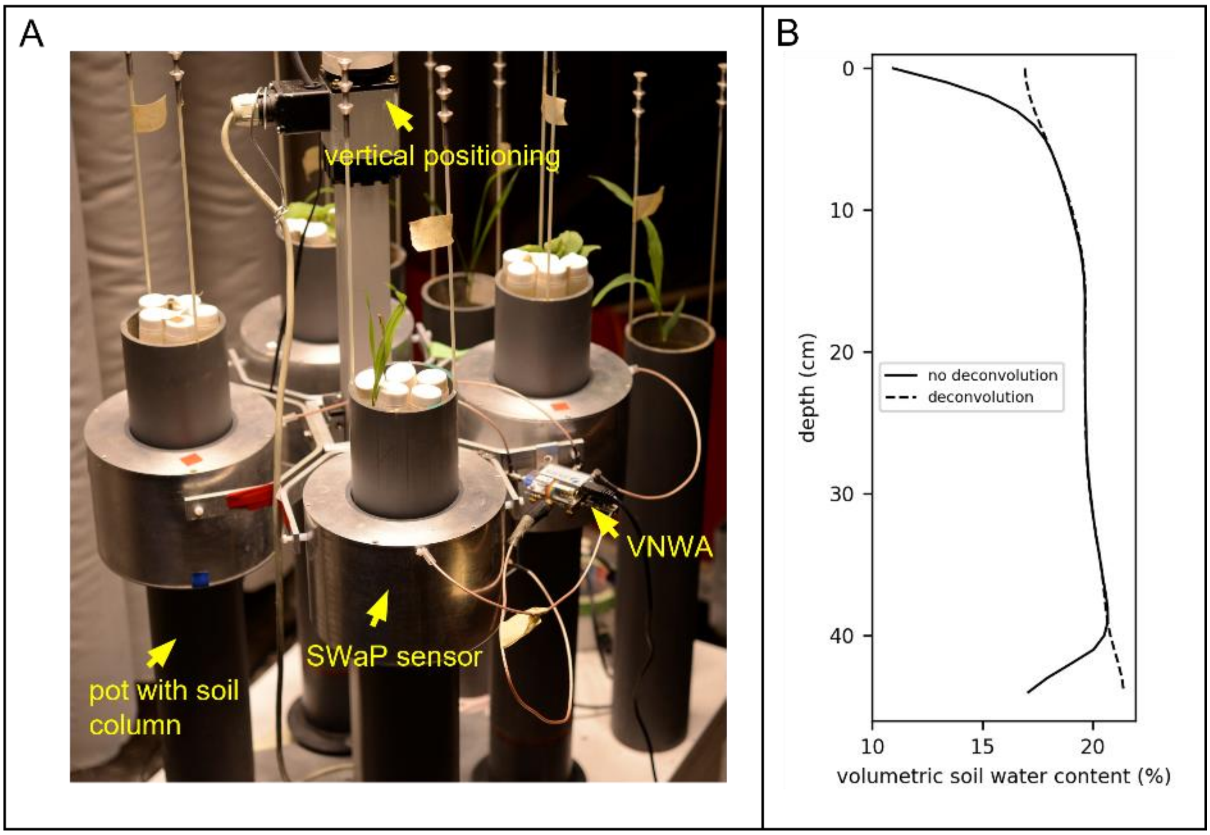

Fig. 1 (A) Sensors of the soil water profiler (SWaP) measuring the water uptake profiles of soil-filled pots with plants. The resonance frequency of the sensors is measured using a vector network analyzer (VNWA) and provides information about the local soil water content. A stepper motor is used to automatically move the sensors along the pots. (B) Vertical profiles of soil water content measured with the SWaP. To derive the actual distribution of soil water content (dotted line), a deconvolution of the measured profile (solid line) must be performed. Especially at the pot border with huge permittivity jumps, the convolved and deconvolved data deviate strongly.

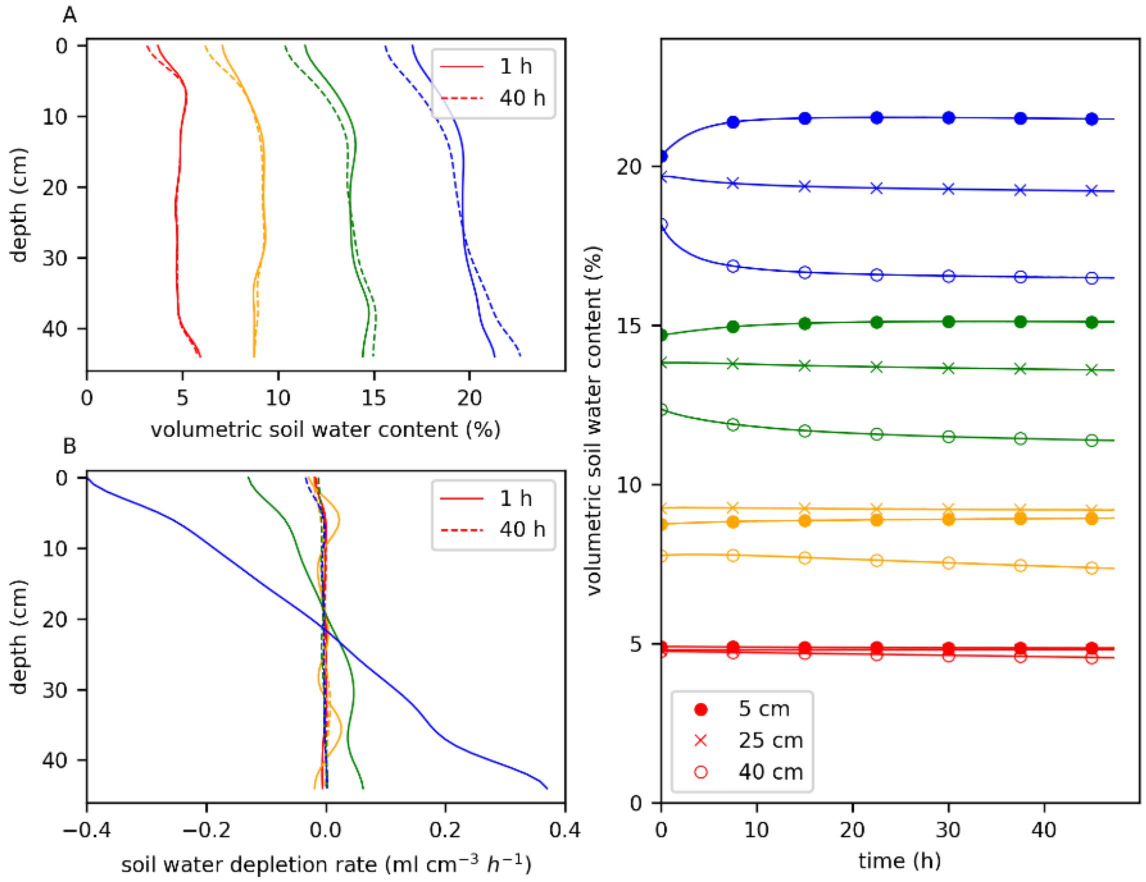

Fig. 2 Soil water dynamics in four pots filled with soil at varying water content, as indicated by the different colors. (A) Vertical profiles of volumetric soil water content at the start (solid line), and 40 h after the start of the measurement (dotted line). (B) Vertical profiles of soil water depletion rates at the start (solid line), and 40 h after the start of the measurement (dotted line). (C) Volumetric soil water content over time in selected soil layers at different depths, as indicated by different symbols.

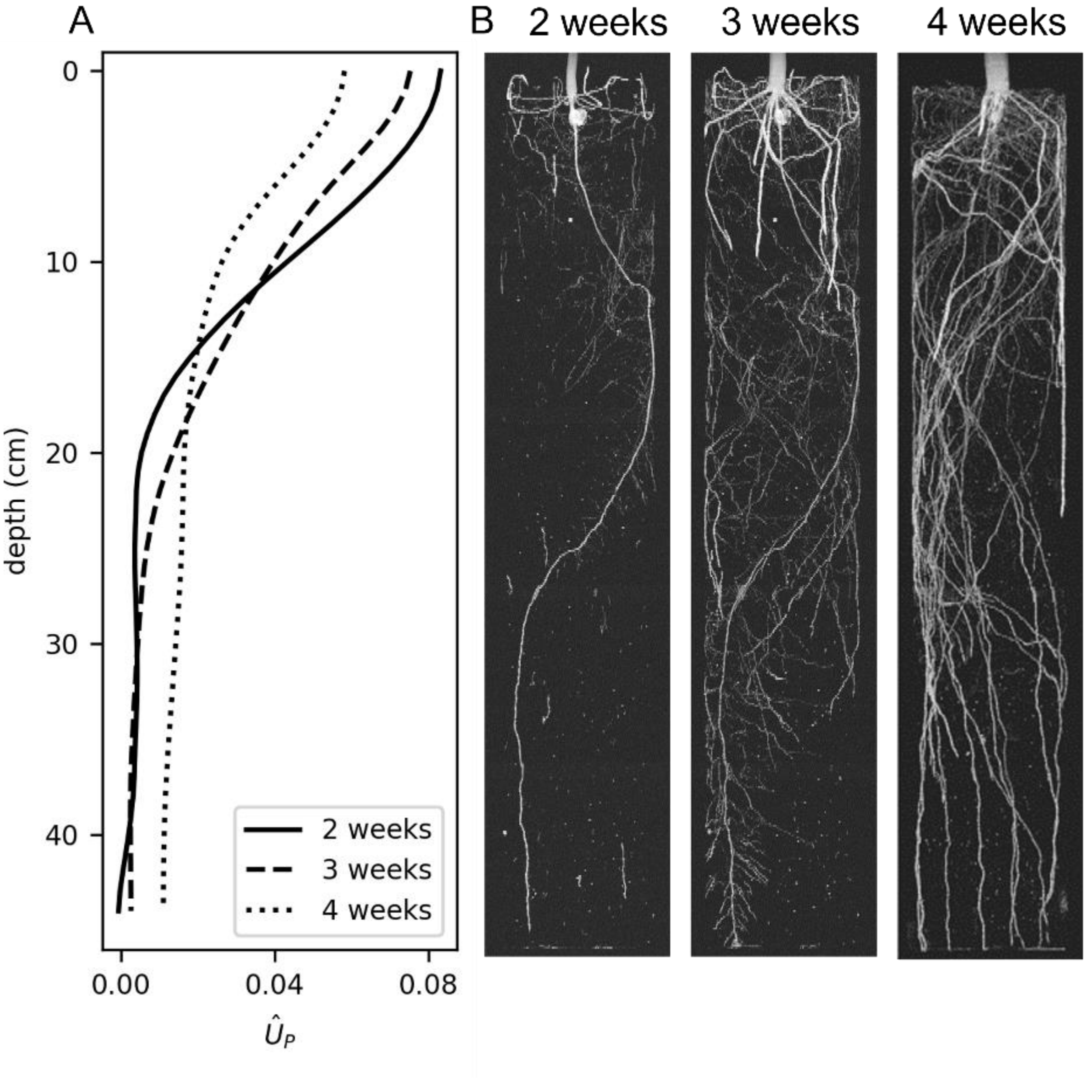

Fig. 3 The distribution of roots and their hydraulic properties of a maize plant at different time points after germination. (A) Normalized plant-driven root water uptake distribution over depth ($\widehat{U}_P$) measured with the SWaP in combination with an alternating light pattern. (C) Images of the root system of the maize plant, measured with MRI at three different time points. MRI measurements and the equipment used are described in the materials and methods sections of the manuscripts presented below.

Fig. 4 Experimental setup established in this thesis. SWaP-, psychrometer, and LICOR measurements were performed simultaneously on the same plant under controlled environmental conditions in a climate chamber. The SWaP in combination with the leaf psychrometer allows for determination of the hydraulic conductance of the root system and its spatial distribution. Since both measurements are non-invasive, they are suitable to observe changes in these parameters over time, e.g. in response to soil drying. By adding the LICOR measurements of stomatal conductance, potential changes in the hydraulic traits below-ground can be related to water flow regulation at the shoot. Using this setup, measurements were performed on maize (A) and faba bean (B).

Abbreviations

term	meaning	unit
K_R	radial root conductance	ml h^{-1} MPa^{-1}
K_{SL}	hydraulic conductance between soil and leaf	ml h^{-1} MPa^{-1}
K_{tot}	total root sytem conductance	ml h^{-1} MPa^{-1}
K_X	axial xylem conductance	ml h^{-1} MPa^{-1}
MRI	magnetic resonance imaging	
rSWF	redistributive soil water flow	ml cm^{-3} h^{-1}
RWU	root water uptake distribution	ml h^{-1}
S_R	Redistributive water flow through soil and roots	ml cm^{-3} h^{-1}
SWaP	soil water profiler	
U_P	plant-driven root water uptake distribution	ml h^{-1}
$\widehat{U}_P$	normalized plant-driven root water uptake distribution	
U_S	soil-driven root water uptake redistribution	ml h^{-1}
U_{tot}	total root water uptake rate	ml h^{-1}
VNWA	vector network analyzer	
z	depth	cm
θ	volumetric soil water content	ml cm^{-3}
$\frac{\partial \theta}{\partial t}$	soil water depletion rate	ml cm^{-3} h^{-1}
Ψ_{collar}	water potential at plant collar	MPa
Ψ_{leaf}	leaf water potential	MPa
Ψ_{seq}	equivalent soil water potential	MPa
Ψ_{soil}	soil water potential	MPa
Ψ_X	root xylem water potential	MPa

Manuscript I

Müllers, Y., Postma, J. A., Poorter, H., Kochs, J., Pflugfelder, D., Schurr, U., & van Dusschoten, D. (2022). Shallow roots of different crops have greater water uptake rates per unit length than deep roots in well-watered soil. *Plant and Soil*, 481, 475–493 (2022). https://doi.org/10.1007/s11104-022-05650-8

Own contribution: Design of the study (together with JP, HP, DvD, and US), Conductance of the experiments (with contributions from DvD), Data analysis (with contributions from DvD and DP), Drafting the manuscript, Revision and editing of the manuscript (with contributions from all authors)

Plant Soil (2022) 481:475–493
https://doi.org/10.1007/s11104-022-05650-8

RESEARCH ARTICLE

Shallow roots of different crops have greater water uptake rates per unit length than deep roots in well-watered soil

Yannik Müllers · Johannes A. Postma · Hendrik Poorter · Johannes Kochs · Daniel Pflugfelder · Ulrich Schurr · Dagmar van Dusschoten

Received: 30 May 2022 / Accepted: 4 August 2022

Abstract
Purpose Commonly, root length distributions are used as a first approximation of root water uptake profiles. In this study we want to test the underlying hypothesis of a constant water uptake rate per unit root length over depth.
Methods Root water uptake profiles were measured using a novel sensor technology. Root length was measured with MRI and by scanning harvested roots. Experiments were performed with pot-grown barley (*Hordeum vulgare*), maize (*Zea mays*), faba bean (*Vicia faba*), and zucchini (*Cucurbita pepo*).
Results For barley, maize, and faba bean, we found that roots in the top 15 cm had significantly greater water uptake rates per unit length than roots in the bottom 30 cm. For zucchini, the trend was similar but not significant. Therefore, variation of root water uptake rates with depth could be explained only partly (61–71%) by a variation of root length with depth.
Conclusion The common approximation of root water uptake profiles by root length distributions relies on constant water uptake rates per unit root length. This hypothesis does not hold in our study, as we found significantly greater water uptake rates per unit length in shallower than in deeper roots. This trend was consistent among species, despite the partly strong variation in physiological parameters. We suggest that this is caused by a decreasing axial transport conductance with depth. This might result in a general underestimation of water uptake rates in shallow soil layers when they are approximated by the root length distribution.

Keywords Root water uptake profiles · Root length distribution · Uniform soil water potential · Root hydraulic conductance · Soil water profiler · MRI

Abbreviations

A	Water uptake rate per unit root length (ml h^{-1} m^{-1})
K_R	Local radial root conductance (cm^3 h^{-1} MPa^{-1})
K_{tot}	Total root conductance (cm^3 h^{-1} MPa^{-1})
L	Root length distribution (m)
$\hat{L}$	Normalized root length distribution
MRI	Magnetic resonance imaging
nMAE	Normalized mean absolute error

Responsible Editor: Hans Lambers.

Supplementary Information The online version contains supplementary material available at https://doi.org/10.1007/s11104-022-05650-8.

Y. Müllers · J. A. Postma · H. Poorter · J. Kochs · D. Pflugfelder · U. Schurr · D. van Dusschoten (✉)
Plant Sciences, IBG-2, Forschungszentrum Jülich, Jülich, Germany
e-mail: d.van.dusschoten@fz-juelich.de

H. Poorter
Department of Biological Sciences, Macquarie University, North Ryde, Australia

rSWF	Redistributive soil water flow ($cm^3\ cm^{-3}\ h^{-1}$)
RWU	Root water uptake rate ($cm^3\ cm^{-3}\ h^{-1}$)
SWaP	Soil water profiler
U_P	Plant-driven root water uptake distribution ($cm^3\ cm^{-3}\ h^{-1}$)
$\widehat{U}_P$	Normalized plant-driven root water uptake distribution
U_S	Soil-driven root water uptake redistribution ($cm^3\ cm^{-3}\ h^{-1}$)
U_{tot}	Total root water uptake rate ($cm^3\ h^{-1}$)
z_i	Depth of soil layer i (cm)
θ	Volumetric soil water content ($cm^3\ cm^{-3}$)
$\frac{\partial\theta}{\partial t}$	Soil water depletion rate ($cm^3\ cm^{-3}\ h^{-1}$)
Ψ_{collar}	Water potential at the plant collar (MPa)
Ψ_{soil}	Local soil water potential (MPa)
Ψ_{seq}	Equivalent, or plant sensed soil water potential (MPa)

Introduction

Spatial information on root water uptake rates is often required to describe soil–plant water relations. Since root water uptake profiles are challenging to measure, they are commonly approximated by the distribution of root length with depth, especially in macroscopic water uptake models (Coppola et al. 2015, 2019; Feddes et al. 2001; Wu et al. 1999). This approximation implies constant root water uptake rates per unit root length with depth. At the single root scale, however, uptake rates per unit root length vary with root branching order (Rewald et al. 2012), root type (Ahmed et al. 2016, 2018), distance from the root tip (Ahmed et al. 2016, 2018; Meunier et al. 2018; Steudle and Peterson 1998), root cortical senescence (Schneider et al. 2017) and root age (Schneider et al. 2020). Most of these parameters are related to root age, which is usually distributed along a vertical gradient, with older roots in shallow layers and younger roots in deeper layers (Koebernick et al. 2014). Therefore, one could expect a systematic variation in water uptake rates per unit root length with depth. Nevertheless, empirical studies, operating at a vertical resolution between 10 and 20 cm, generally suggest a good correlation between profiles of water uptake rates and root length (Ehlers et al. 1991; Sharp and Davies 1985; Shein and Pachepsky 1995), which supports the common assumption in macroscopic models. It needs to be considered, however, that usually, a homogenous soil water potential distribution is a prerequisite for a reasonable comparison between root length distributions and water uptake profiles. This is highlighted by studies in which the strength of the correlation between root length and water uptake profiles varied among different soil water conditions (Dara et al. 2015; Sharp and Davies 1985; Shein and Pachepsky 1995). Since a homogeneous water potential distribution is difficult to achieve in experiments with natural soil substrates, approximating water uptake profiles by root length distributions still comes with uncertainty.

Generally local root water uptake rates (RWU) are determined by the radial root conductance (K_R) and the water potential gradient between soil (Ψ_{soil}) and the root xylem (Ψ_X). Focusing on the vertical axis with depth z, this writes:

$$\boldsymbol{RWU}(z) = \boldsymbol{K_R}(z) \cdot (\boldsymbol{\Psi_{soil}}(z) - \boldsymbol{\Psi_X}(z)) \tag{1}$$

In our study, we measure a component of the water uptake profile which is independent of Ψ_{soil}. This is achieved by measuring the short-term response of RWU to a change in light intensity which alters Ψ_X but not Ψ_{soil}, and thus, according to Eq. 1, only depends on K_R and Ψ_X. The theoretical framework for deriving a component of RWU which is independent of the soil water distribution has been developed by Couvreur et al. (2012). In their study, the authors show that local root water uptake rates (RWU) can be disentangled into two terms which we call plant-driven root water uptake distribution (U_P) and soil-driven root water uptake redistribution (U_S):

$$\boldsymbol{RWU}(z) = \boldsymbol{U_P}(z) + \boldsymbol{U_S}(z) \tag{2}$$

$U_P(z)$ is determined by the spatial arrangement of root hydraulic conductance which depends on the distribution of intrinsic hydraulic conductivities and root length. $U_P(z)$ integrates to the total root water uptake rate (U_{tot}) across the whole root system. $U_S(z)$ additionally depends on the distribution of soil water potential (Ψ_{soil}) and can be interpreted as a redistributive water flow through the root system from relatively wet soil layers into relatively dry soil layers. Across the whole root system, $U_S(z)$ integrates to zero (Fig. 1A). Using the hydraulic network presented in Online Resource 1, we show in Appendix 1 that in a simplified form (compare Couvreur et al. (2012)), U_P and U_S can be expressed as:

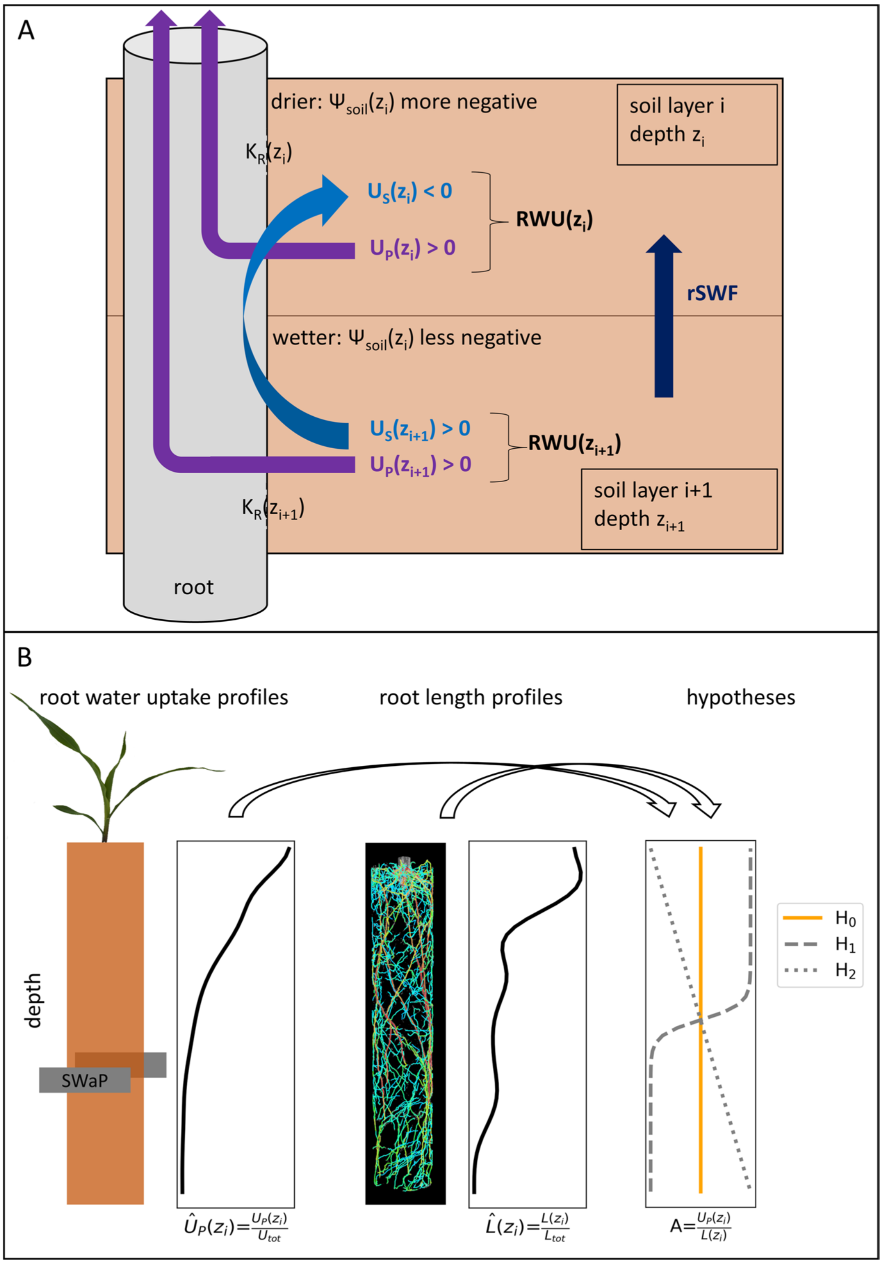

Fig. 1 **A** Scheme of different water flow patterns in the soil root system, separated into vertically stacked layers. Local root water uptake rates (RWU) are the sum of the plant driven root water uptake distribution (U_P) and the soil driven root water uptake redistribution (U_S). U_P is the local fraction of the total root water uptake rate, determined by the local root conductance (K_R). Direct water flow from wetter to drier soil layers is called redistributive soil water flow (rSWF). **B** Overview of the measured parameters and the tested hypotheses. Normalized root water uptake profiles ($\hat{U}_P$) were determined with the SWaP, normalized root length profiles ($\hat{L}$) were determined with MRI. Based on these profiles we calculated the water uptake rates per unit root length (A) over depth. We tested the null hypothesis (H_0) that A is constant over depth, and the alternative hypothesis of systematic deviations of A with depth (H_1 or H_2)

$$\boldsymbol{U_P}(z) = \boldsymbol{U_{tot}} \cdot \frac{\boldsymbol{K_R}(z)}{\boldsymbol{K_{tot}}} \text{ and } \boldsymbol{U_S}(z) = \boldsymbol{K_R}(z) \cdot (\boldsymbol{\Psi_{soil}}(z) - \boldsymbol{\Psi_{seq}}) \tag{3}$$

In Eq. 3 we used the total water uptake rate (U_{tot}), the total root conductance (K_{tot}), and the plant sensed soil water potential (Ψ_{seq}). Note that K_{tot} and Ψ_{seq} are not measured in our study but are introduced here, to describe the meaning of U_P and U_S. In case of a homogeneous distribution of soil water potential ($\Psi_{soil}(z) = \Psi_{seq}$, in all layers), U_S becomes zero throughout. Therefore, U_P reflects the distribution of water uptake rates in a soil with uniform water potential distribution (corrected for gravity). Deviations from a uniform soil water distribution are considered by U_S.

Due to its independence of the soil water distribution, U_P is better suited than RWU to analyze how well water uptake profiles can be approximated by root length distribution. Recently, a method was introduced to measure U_P without actually depending on a uniform soil water distribution, using a highly precise soil water sensor in combination with a fluctuating light intensity (van Dusschoten et al. 2020). With this technology, we test the null hypothesis that root water uptake rates per unit root length (A) are constant with depth:

$$\boldsymbol{H}_0 : \boldsymbol{A}(z) = \frac{\boldsymbol{U_P}(z)}{\boldsymbol{L}(z)} = \boldsymbol{constant} \tag{4}$$

As alternative hypothesis, we test whether water uptake rates per root length vary systematically with depth, indicating a spatial gradient of root conductivity. Figure 1B gives an overview over the analyzed parameters and the tested hypotheses. Root system architecture potentially affects our hypothesis, since a simulation study predicted less variation in water uptake rates per root length for taproot compared to fibrous root systems (Javaux et al. 2013). We therefore tested whether H_0 is true across four different crop species: two monocots with a fibrous root system, barley and maize, and two dicots with a taproot system, zucchini, and faba bean. We performed the following analysis for each of the four species: In a first step, we analyzed to what extent the variation of U_P with depth is explained by a variation of L with depth and to what extent by a variation of A with depth. In a next step, we evaluated H_0 by testing for significant differences between water uptake rates per root length in shallow (upper third of the pots) and deeper layers (lower two thirds). Potential deviations from H_0 would indicate a variation of root conductivity. Since root conductivity is closely linked to root diameter (Ahmed et al. 2016; Frensch and Steudle 1989; Huang and Eissenstat 2000), we checked in a third step, whether variations of A(z) can be explained by root diameter distributions over depth.

Material and methods

Plant growing conditions

We grew four different plant species: the monocots barley (*Hordeum vulgare*), and maize (*Zea mays*), and the dicots faba bean (*Vicia faba*), and zucchini (*Cucurbita pepo cylindrica*). Seeds were germinated for 2–3 days in the dark on moistened germination paper. Seedlings were transferred into soil-filled PVC pipes (50 cm high, Inner Diameter: 8.1 cm), suitable for both MRI and SWaP measurements. We used a sandy loam, collected in Kaldenkirchen, Germany with 73.3% sand, 23.1% silt, 3.6% clay, (Pohlmeier et al. 2009) mixed with 20% (v) coarse sand (0.7–1.4 mm). Water saturation was reached at volumetric soil water content (θ) of 40.7%. The soil type was selected because it wets easily and uniformly within half a day after rewatering. Additionally, its water retention curve is relatively flat in the wet regime, making it easier to avoid large vertical soil water potential gradients. Note that even though our measurement of U_P is independent of the soil water potential distribution, vertical soil water flows would introduce noise during the analysis process. Furthermore, the soil type used leads to a good image quality of the MRI measurements which is related to the low silt, clay, and ferromagnetic content (Pflugfelder et al. 2017). The pots were filled with soil to a height of 45 cm, resulting in a total substrate volume of 2.32 l. Pots were filled under gentle shaking to promote uniform compaction, achieving a bulk density of 1.47 kg/l. Four plants per species were grown in the prepared pots in a climate chamber providing a controlled temperature of 21.5 °C ± 0.2 °C and a VPD_{air} of 1.49 kPa. Plants were watered from the top every 2nd or 3rd day to keep them well-watered at an average θ of above 20% (v/v). Before and during water uptake measurements, plants were not watered for approximately 24 h to minimize spatial gradients of soil water potential during the measurement, as confirmed by our measurements (Fig. 3). For fertilization, NPK nutrient salt (Hakaphos Red; Compo Expert; 8% N, 12% P, 24% K), diluted in water at 0.3% (v/v) was given to the plants once a week. The total amount of fertilized water supplied to the plants depended on the actual water use and varied between 30 ml (1st week) and up to 200 ml (4th week). We used a water-cooled LED panel (3200 K, 5 × 5 LEDs á 20 W) for illumination. During the day, two levels of light intensity alternated in periods of two hours for 14 h in total (three low light periods and four high light periods) for the full growing and measurement period. Photosynthetically active radiation of the lower level was 500 µmol m^{-2} s^{-1}, that of the higher level 1000 µmol m^{-2} s^{-1}. The light intensity sums up to a daily light integral of 39.6 mol m^{-2} d^{-1}. This light fluctuation was required for the derivation of root water uptake profiles as described below. Twenty-eight days after germination, we measured the root water uptake profiles with the SWaP and the root length distribution with MRI of each individual plant. Within one day, we could measure all four replicates of one species. Below, we describe the SWaP and MRI measurements in detail.

SWaP measurement of $\widehat{U}_P\left(z_i\right)$

We measured $\widehat{U}_P$ with a recently developed soil water profiler (SWaP) (van Dusschoten et al. 2020). The sensors of the SWaP basically consist of two opposing copper plates (7×5 cm^2) in a 12 cm high PVC sleeve, shielded with aluminum. The sensors partially enclose the pots with soil columns and are movable along the z-axis. The copper plates form a capacitor which is connected to a coil, forming a resonator circuit. The resonance frequency of the circuit is a function of the electrical permittivity of the material in between the copper plates, which is largely determined by the soil water content θ. Thus, measuring the resonance frequency allows determination of θ as described below. A vector network analyzer (DG8SAQ, VNWA3, SDR-Kits, UK) was used to determine the resonance frequency of the circuit by applying a frequency sweep between 150 and 220 MHz. The sensors move vertically along the pots and measure the resonance frequency in equidistant steps of 1 cm. A complete scan of four pots with 45 cm high soil columns simultaneously took around 12 min. To synchronize with light fluctuations, scans were started every 15 min. For conversion of the resonance frequency into θ, we measured a calibration curve. To this end, we filled 12 cm high PVC pots with soil at a defined bulk density (1.47 kg/l, as used for plant growth) and a defined θ ranging from 2 to 30% and measured the resulting resonance frequency with the SWaP. The data were fitted using a second order polynomial (Online Resource 2). This procedure enabled us to measure the vertical θ profiles of our soil columns in 1-cm steps.

For our analysis, we interpreted the 45 cm high soil column as 45 stacked layers each of 1 cm height and uniform θ. The layers were indexed i = 1 (top layer),…, 45 (bottom layer) with the top of each layer at depth z_i=0 cm,…, 44 cm. Given the 12 cm height of the SWaP sensors, the measurement at each 1-cm layer is not the precise θ value in that layer, but a convolution of (1) the electrical field strength between the copper plates and (2) the 12 soil layers enclosed by the sensor. To achieve a spatial resolution of 1 cm, a deconvolution was applied. This procedure requires measuring the exact θ-values at the pot borders and the profile of the electrical field strength. Given these values we performed a numerical deconvolution. As this amplifies errors, we constrained the deconvoluted result by a regularization term which reduces fluctuations of the profile.

Given the deconvolved θ profiles over time we could, in a next step, derive the profiles of water uptake rates. For that, we calculated the rate of change in water content over time ($\frac{\partial\theta\left(z_i,t\right)}{\partial t}$) in each layer. A change in water content in layer i is caused by local RWU, redistributive soil water flow (rSWF) between adjacent layers, and evaporation in the top layer $E_s(t)$:

$$\frac{\partial\boldsymbol{\theta}\left(z_i,t\right)}{\partial\mathbf{t}} = \mathbf{RWU}\left(z_i,t\right) + \mathbf{rSWF}\left(z_i,t\right) + \begin{cases} E_s(t), & z_i = 0 \\ 0, & z_i \neq 0 \end{cases} \tag{5}$$

Using Eq. 2 we can express RWU as the sum of U_P and U_S with $U_P\left(z_i,t\right) = \frac{\widehat{U}_P\left(z_i\right)\cdot U_{tot}(t)}{V}$, total pot volume V and $U_{tot}(t) = \sum_{i=1}^{45}\frac{\partial\theta\left(z_i,t\right)}{\partial t}$. Neither U_S nor rSWF contribute to U_{tot} but sum up to zero across the whole pot. We summarize these two terms as soil water redistribution through soil and roots (S_r) and write Eq. 5 as:

$$\frac{\partial\theta\left(z_i,t\right)}{\partial t} = \widehat{U}_P\left(z_i\right)\cdot\frac{U_{tot}(t)}{V} + S_r\left(z_i,t\right) + \begin{cases} E_s(t), & z_i = 0 \\ 0, & z_i \neq 0 \end{cases} \tag{6}$$

To determine $\widehat{U}_P$ from Eq. 6, we make use of the light intensity fluctuating between a lower and a higher level at a period of two hours. The alternating light intensity induces a fast response of the transpiration rate, via stomatal regulation, and thus U_{tot}. Note that the transpiration rate and U_{tot} are almost similar, and only differ by the shoot growth rate. The response of U_P to a change of U_{tot} is much faster than the response of S_r, as it takes time to generate water potential gradients within the soil which drive both rSWF and Us. Therefore, U_P and S_r can be separated based on their response rate to fluctuating light intensity. Biologically, this can be understood as follows: A greater local root conductance leads to a greater change in the water uptake rate when the light intensity changes. Therefore, the stronger the local $\frac{\partial\theta(t)}{\partial t}$ responds to a change in light intensity, and thus in U_{tot}, the greater the local root conductance, and thus U_P. Mathematically, $\widehat{U}_P$ can be derived as slope of a linear regression between $\frac{\partial\theta(t)}{\partial t}$ and $U_{tot}(t)$ according to Eq. 6 (Online resource 3). Such a regression was performed in each layer separately, using the data acquired during a 12 h period (7.00 am to 7.00 pm) covering three high and low light intensity periods of two hours each.

Determination of soil water potential and conductance

The soil water retention curve was measured using the evaporation method (Peters and Durner 2008) with the HYPROP setup (METER Group, Munich, Germany). The characteristic parameters of the water retention curve were obtained by fitting a Brooks-Corey model (Brooks and Corey 1964) to the measured data of the pressure head h (cm) for varying θ:

$$\boldsymbol{h}(\boldsymbol{\theta}) = \boldsymbol{\alpha}^{-1}\left(\frac{\boldsymbol{\theta}-\boldsymbol{\theta}_r}{\boldsymbol{\theta}_s-\boldsymbol{\theta}_r}\right)^{-\frac{1}{\lambda}} \tag{7}$$

with saturated water content θ_s, residual water content θ_r, air entry pressure head α^{-1} (cm), and a dimensionless pore size index λ. To obtain the soil water potential Ψ_{soil}, a gravity component was added to the pressure head:

$$\Psi_{soil}(\theta(z)) = (\mathrm{h}(\theta(z)) - \mathrm{z}) \cdot 9.8 \cdot 10^{-5}\,\frac{MPa}{cm}\ \text{with depth z = 0 cm, … , 44 cm.} \tag{8}$$

MRI measurement and processing of root length

Roots were non-invasively imaged using MRI. For logistical reasons, MRI measurements were either shortly before or after the SWaP measurements. Since plants were not under controlled conditions during MRI, scanning was preferably conducted during the night. The MRI setup consisted of a 4.7 T vertical wide bore (310 mm) magnet (Magnex, Oxford, UK) and a gradient coil (ID 205 mm (MR Solutions)) providing gradients up to 400 mT/m. The MRI experiments were controlled using an MR Solutions (Guildford, UK) console. NMRooting software (van Dusschoten et al. 2016) was used to analyze MRI data and calculate root length. Data of the root system were arranged in 45 vertical layers of 1 cm height (across a pot diameter of 8.1 cm). Using NMRooting, we obtained the root length present in each layer. For a similar MRI setup (van Dusschoten et al. 2016), a detection limit for root diameters between 200 µm and 300 µm was reported.

Harvest and root scanning

To include the fine root fraction below the detection limit of MRI, roots were harvested after the MRI or SWaP measurement respectively. Since we were interested in the vertical distribution of root traits, soil columns were taken out of the pots and cut into five blocks of 9 cm height each. The roots were isolated from the soil using sieves with different mesh sizes (0.3 mm to 2.0 mm) and stored in a solution of 70% water and 30% ethanol. Roots of each block were scanned separately. We used WinRHIZO software (Regent Instruments, Ottawa, Canada) to analyze total root length and root length in 20 equidistant diameter classes ranging from 0.0 mm to 2.0 mm (last class included all roots thicker than 2.0 mm) for all 5 blocks per plant separately. Using the distribution of harvested roots, we calculated correction factors for each 9 cm high soil block. The MRI measured root distribution was corrected accordingly. Finally, we applied the same convolution and deconvolution procedure to the root length profile as to $\widehat{U}_P$ to achieve a similar degree of smoothing caused by this procedure. Normalized, corrected, and deconvolved root length profile is called $\widehat{L}$. Leaf area and shoot fresh weight were also determined at harvest.

Quantitatively explaining the variation in UP(z)

Here we use a concept which has been developed to relate how important the variation of each of two factors of a product is to explain the variation of the product (Poorter and Nagel, 2000). For that we write U_P as product of L and A:

$$\boldsymbol{U_P = L \cdot A} \tag{9}$$

and apply an ln transformation:

$$\boldsymbol{ln}(\boldsymbol{U_P}) = \boldsymbol{ln}(\mathbf{L} \cdot \mathbf{A}) \tag{10}$$

which can be written as:

$$1 = \frac{\boldsymbol{ln}(\mathrm{L})}{\boldsymbol{ln}(\boldsymbol{U_P})} + \frac{\boldsymbol{ln}(\mathrm{A})}{\boldsymbol{ln}(\boldsymbol{U_P})} \tag{11}$$

Given the U_P, L, and A profiles of a plant or species, each consisting of 45 values, we thus linearly fitted the ln of the 45 U_P values against the ln of the 45 L or A values respectively. Then the two terms on the right-hand side of Eq. 11 were determined as the slopes of the linear fits. According to Eq. 11, these two slopes add up to one, and are a measure for the relative importance of L, and A in explaining variation in U_P.

Results

Characteristic plant and soil parameters

Maize and zucchini had significantly greater shoot fresh weight than barley and faba bean (14–50 g) (Fig. 2). In barley, also the leaf area was significantly smaller than in maize and zucchini (199–576 cm^2). The total root length of faba bean (27 m) was significantly smaller than that of the other species (82–94 m). During the 12 h measurement period, zucchini took up significantly more water (95 ml) than

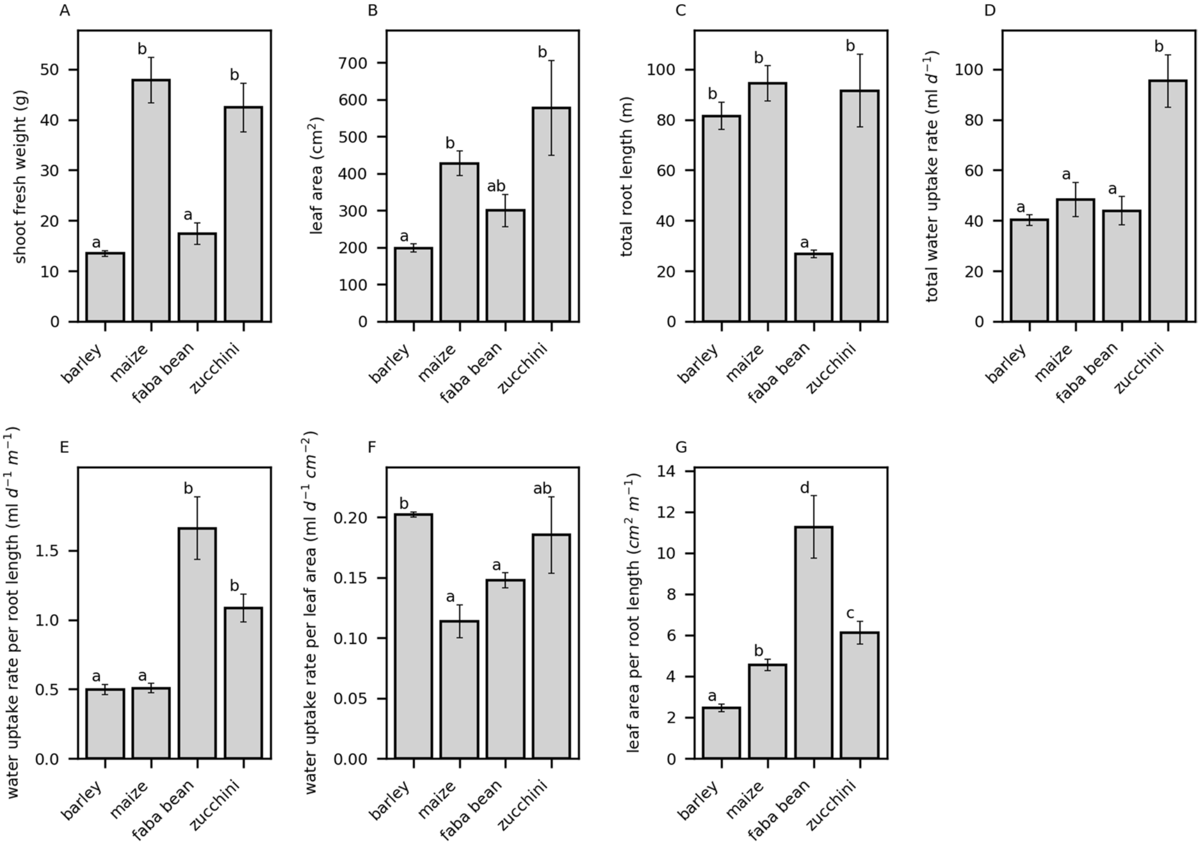

Fig. 2 Characteristic parameters of the species at the day of measurement: **A** shoot fresh weight, **B** leaf area, **C** total root length, **D** total root water uptake rate, **E** Water uptake rate per unit root length, **F** water uptake rate per leaf area, and **G** root-to-shoot ratio, expressed as leaf are per root length. Height of the bars are species averages ($n = 4$), error bars are standard errors of the mean. Differences between species were considered significant if p-values of a Student's t-test were < 0.05. Significant differences between groups are indicated by different letters

the other species (40 – 48 ml). The total water uptake rate per unit length was significantly greater in faba bean (1.7 ml d^{-1} m^{-1}) and zucchini (1.1 ml d^{-1} m^{-1}) than in barley and maize (both 0.5 ml d^{-1} m^{-1}). However, water uptake per unit leaf area was significantly greater in barley (0.20 ml d^{-1} cm^{-2}) than in maize and faba bean (0.11 – 0.15 ml d^{-1} cm^{-2}). Shoot to root ratio, expressed as leaf area per root length, was significantly different among all species. It was lowest in barley, followed by maize and zucchini and highest in faba bean (2.5 – 11.3 cm^2 m^{-1}).

For all species, we generally measured a vertical gradient in Ψ_{soil} with more negative values at the top and less negative values at the bottom (Fig. 3). This gradient was more pronounced at the end compared to the start of the measurement. At start, the average Ψ_{soil} with depth ($\overline{\Psi}_{soil}$) was similar (-9 to -11 kPa) among the four species. At the end of the measurement, $\overline{\Psi}_{soil}$ for zucchini (-21 kPa) was significantly more negative than for barley (-12 kPa) and faba bean (-13 kPa). For maize (-14 kPa), $\overline{\Psi}_{soil}$ was not significantly different from the other species. Ψ_{soil} profiles of each individual plant are shown in Online Resource 4.

Root length distribution explains 61 – 71% of variation in water uptake profiles

Due to the higher abundance of roots in shallow soil layers, water uptake profiles and root length were both generally high in top layers and declined with depth (Fig. 4). In maize, both profiles dropped rather sharply within the top 10 cm but declined smoother in barley and faba bean. In zucchini, both profiles were generally flatter compared to the other species. In barley, maize, and faba bean, $\widehat{U}_P$ was consistently

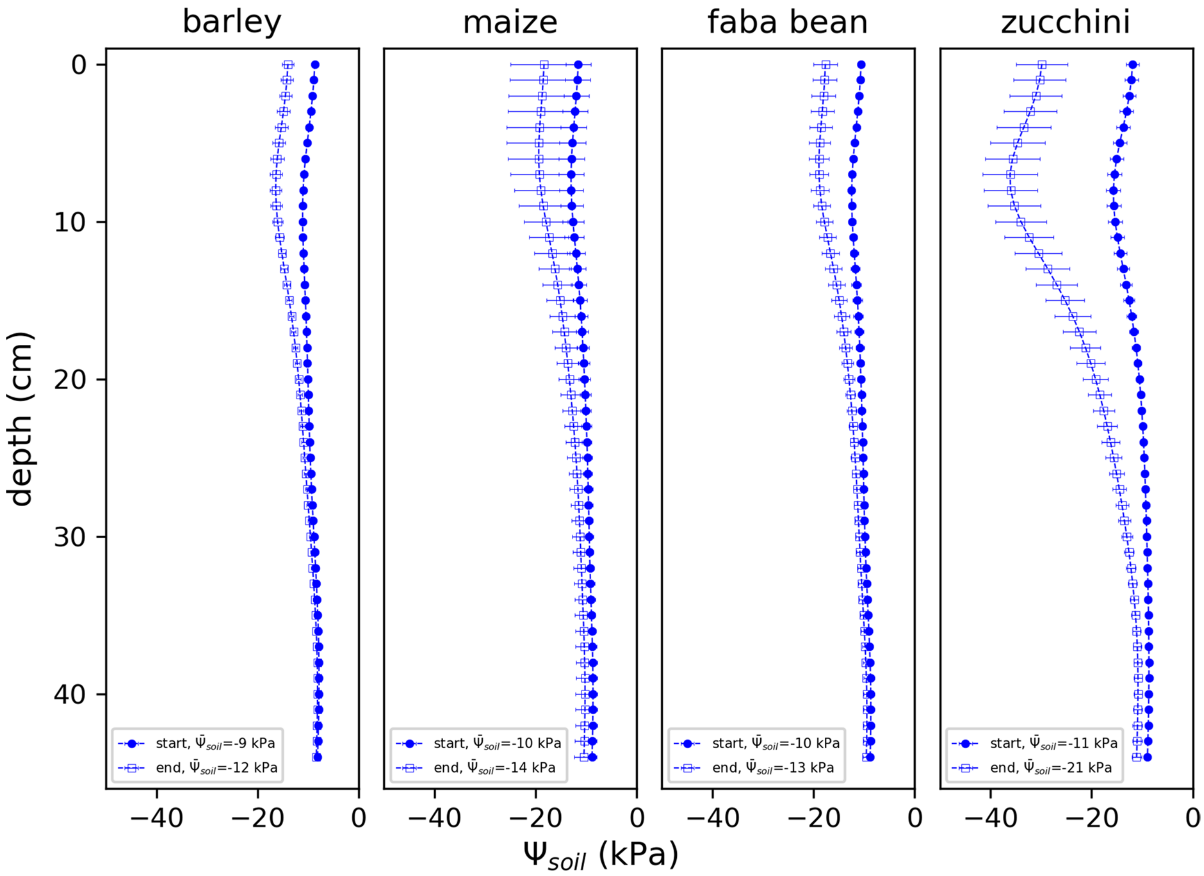

Fig. 3 Distribution of Ψ_{soil} at start (filled circles) and end (empty squares) of the SWaP measurements as species averages ($n=4$). Error bars are standard errors of the mean. Mean values over depth ($\overline{\Psi}_{soil}$) at start and end of the measurement are given in the legend

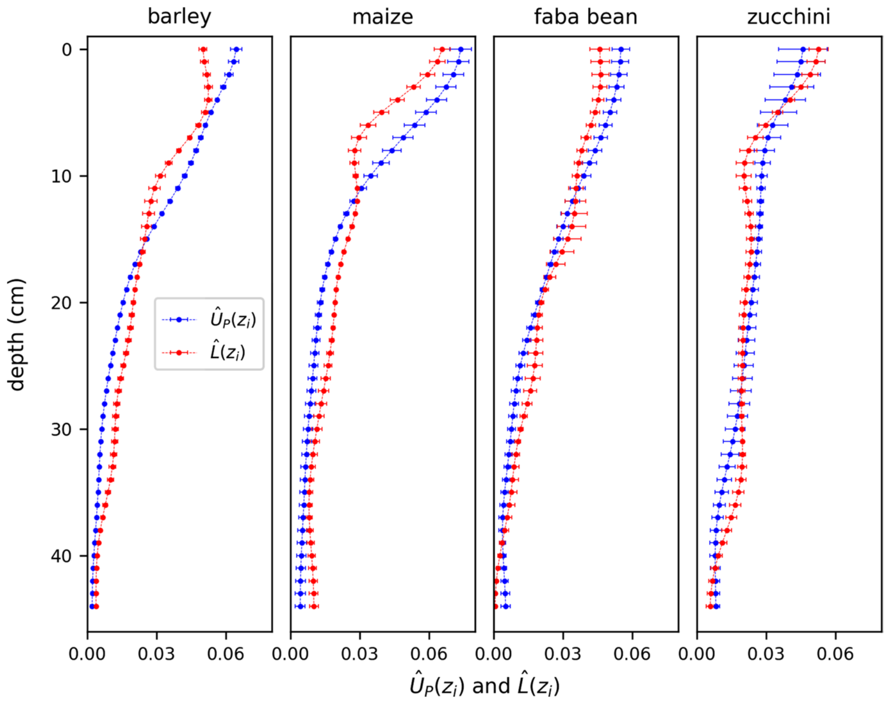

Fig. 4 $\hat{U}_P$ (blue) and $\hat{L}$ (red) as species averages ($n=4$). Horizontal error bars are standard errors of the mean in each layer. For total water uptake rate and total root length see Fig. 2

higher than $\hat{L}$ in the top layers but lower towards the bottom. $\hat{U}_P$ and $\hat{L}$ profiles of each individual plant are shown in Online resource 5. We evaluated to what extent variation in $U_P(z)$ is determined by variation in L(z) and A(z) respectively using Eqs. 9–11. This analysis was performed for each individual plant separately. Table 1 shows the results as species averages with standard errors of the mean. Between 61 and 71% of variation in $U_P(z)$ were explained by a variation in L(z), 29–39% were explained by a variation in A(z) without any significant differences among species.

Table 1 Relative importance of L and A in explaining variation in U_P with depth, determined as slopes of the linear fits between ln(L) and ln(U_P), and ln(A) and ln(U_P)

	$\hat{L}$	$\hat{A}$
barley	0.70 ± 0.01	0.30 ± 0.01
maize	0.61 ± 0.08	0.39 ± 0.08
faba bean	0.71 ± 0.12	0.29 ± 0.12
zucchini	0.67 ± 0.14	0.33 ± 0.14

Values shown are mean values with standard error of the mean among the four replicates of each species. There were no significant differences between species as tested by a one-way ANOVA

Shallow roots show significantly greater uptake rates per unit length than deeper roots

The findings reported in Table 1 indicate a variation of water uptake rates per root length over depth, which implies deviations from our null hypothesis, H_0, of constant uptake rates per unit root length with depth. In a next step, we analyzed whether these deviations in A(z) followed a spatial pattern (Fig. 5A). The vertical orange lines in Fig. 5A are the mean values over depth and represent H_0. In all four species, we observed that water uptake rates per root length in the top 15 cm (blue lines in Fig. 5A) were higher than in the bottom 30 cm (red lines), indicating a systematic deviation. Profiles of A(z) of each individual plant are shown in Online resource 6. To quantify this trend of higher uptake rates per unit root length in top layers, we compared A(z) between the top 15 cm and bottom 30 cm in each individual plant, and calculated the species averages (Fig. 5B). In barley, faba bean and maize, water uptake rates per root length were significantly higher in the top 15 cm compared to the bottom 30 cm. Except for one faba bean plant, this trend was found in each single plant (Online resource 6). In zucchini, there

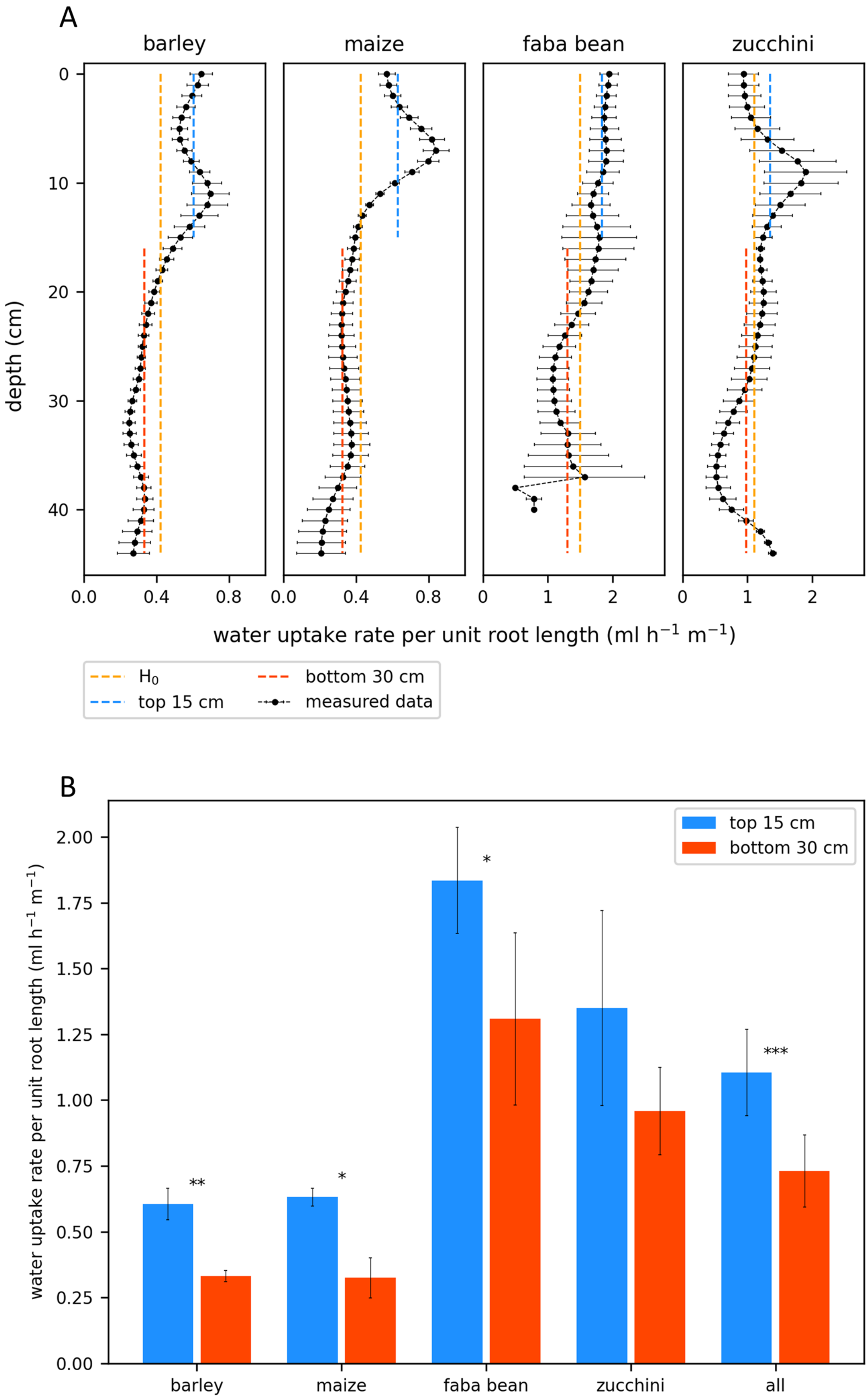
A
barley
maize
faba bean
zucchini
depth (cm)
0
10
20
30
40
0.0
0.4
0.8
0
1
2
water uptake rate per unit root length (ml h^{-1} m^{-1})
H_0
top 15 cm
bottom 30 cm
measured data
B
water uptake rate per unit root length (ml h^{-1} m^{-1})
0.00
0.25
0.50
0.75
1.00
1.25
1.50
1.75
2.00
top 15 cm
bottom 30 cm
**
*
*
***
barley
maize
faba bean
zucchini
all

◂**Fig. 5** Root water uptake rates per unit root length (A). **A** Complete A(z) profiles. Colored vertical lines are mean values over depth ($n=4$) for the whole pot (orange), top 15 cm only (blue), bottom 30 cm only (red). Note that the orange line represents the null hypothesis of constant water uptake rates per unit root length. Data points are averages among species, error bars are standard errors of the mean. Layers with a root length below 10 cm caused considerable scatter of uptake rates per root length and thus were dropped for this and the following figure. This only concerned the bottom 5 cm of faba bean. **B** A(z) separated into the top 15 cm and bottom 30 cm of the pot. Height of the error bars are mean values among species ($n=4$), error bars are standard deviations of the mean. For each species, and all replicates we tested for significant differences between the top 15 cm and bottom 30 cm using a Student's t-test. Significant differences with a p-value below 0.05, 0.01, or 0.001 are indicated by *, **, or *** respectively

was no significant difference, and two individual plants had higher, two had lower uptake rates per length in top layers (Online resource 6). Among all 16 plants from the four different species, shallow roots had a significantly higher water uptake rate per root length than deeper roots (Fig. 5B).

Does the distribution of root diameter explain the variation of water uptake per root length?

The observed deviations from the null hypothesis indicate a vertical gradient in root conductivity with higher conductivity in shallow roots and lower conductivity in deeper roots. In a next step, we analyzed whether this pattern is reflected by the distribution of root traits (Fig. 6). Figure 6A exemplary shows an image of a root system from each species, acquired with MRI. Barley and maize have a fibrous root system with thicker (yellowish and reddish pseudo colors) seminal and nodal roots from which thinner (blueish pseudo colors) lateral roots emerge. In both species, the seminal and nodal roots were thinner in deeper layers compared to shallower layers. Faba bean and zucchini both have a taproot system with one main root growing vertically and lateral roots emerging from it. In faba bean, laterals in the upper soil layers appear as thick as the taproot. The laterals preferably grew horizontally and started spiraling downwards when they reached the pot borders. In zucchini, there was a clear trend of generally thicker roots in deeper layers compared to shallower layers for both, the main root and laterals. Note that the MRI had a detection limit between 200 µm and 300 µm. The color-coded diameter in Fig. 6A suggests that, except for faba bean and deep layers of zucchini, a diameter of 0.5 mm is a reasonable threshold to distinguish between lateral roots and main roots. To quantify the distribution of laterals, we therefore analyzed the fraction of fine roots with a diameter below 0.5 mm over depth, using data from harvested and scanned roots (Fig. 6B). In barley, there was a continuous, significant decrease of this fine root fraction from 94% in the top soil layer to 69% in the bottom layer. In maize, the fine root fraction was greatest in the second layer (88% at a depth between 9 and 18 cm) and also decreased towards the bottom. In the deepest soil layer, it was significantly lower (66%) than in the second layer. In zucchini the decrease was even more pronounced, ranging from 92% in the top layer to only 30% in the bottom layer. Note, however that due to the general root thickening in the bottom layers of zucchini, a diameter-based distinction between laterals and main roots is difficult (Fig. 6A). In contrast to the other species, the fine root fraction in faba bean significantly increased from around 10% in the top 30 cm to 30% in the bottom layer. As mentioned above, the distinction based on root diameter in faba bean is questionable as laterals were comparably thick as the main root (Fig. 6A). Additionally, we analyzed the average root diameter over depth which revealed a similar picture (Online resource 7). For barley, maize and zucchini, the average diameter was almost constant in the top half of the pot and increased towards the bottom. Such a root thickening in deeper layers is typical for sandy soils (Lippold et al. 2021; Qin et al. 2005) and might be related to an increased ethylene concentration which reportedly induced root thickening in compacted soil layers (Pandey et al. 2021; Vanhees et al. 2022). For faba bean, however, average root diameter was lower in shallow than in deep soil layers.

Discussion

In the present study, we analyzed the common approximation of root water uptake profiles ($\hat{U}_P$) by the distribution of root length ($\hat{L}$) in 4 weeks old pot-grown crop plants. For that, we tested the hypothesis of a constant root water uptake rate per unit root length (A) with depth. We observed that only 61–71% of the variation in U_P with depth were explained by a variation of L with depth. 39–29% were explained

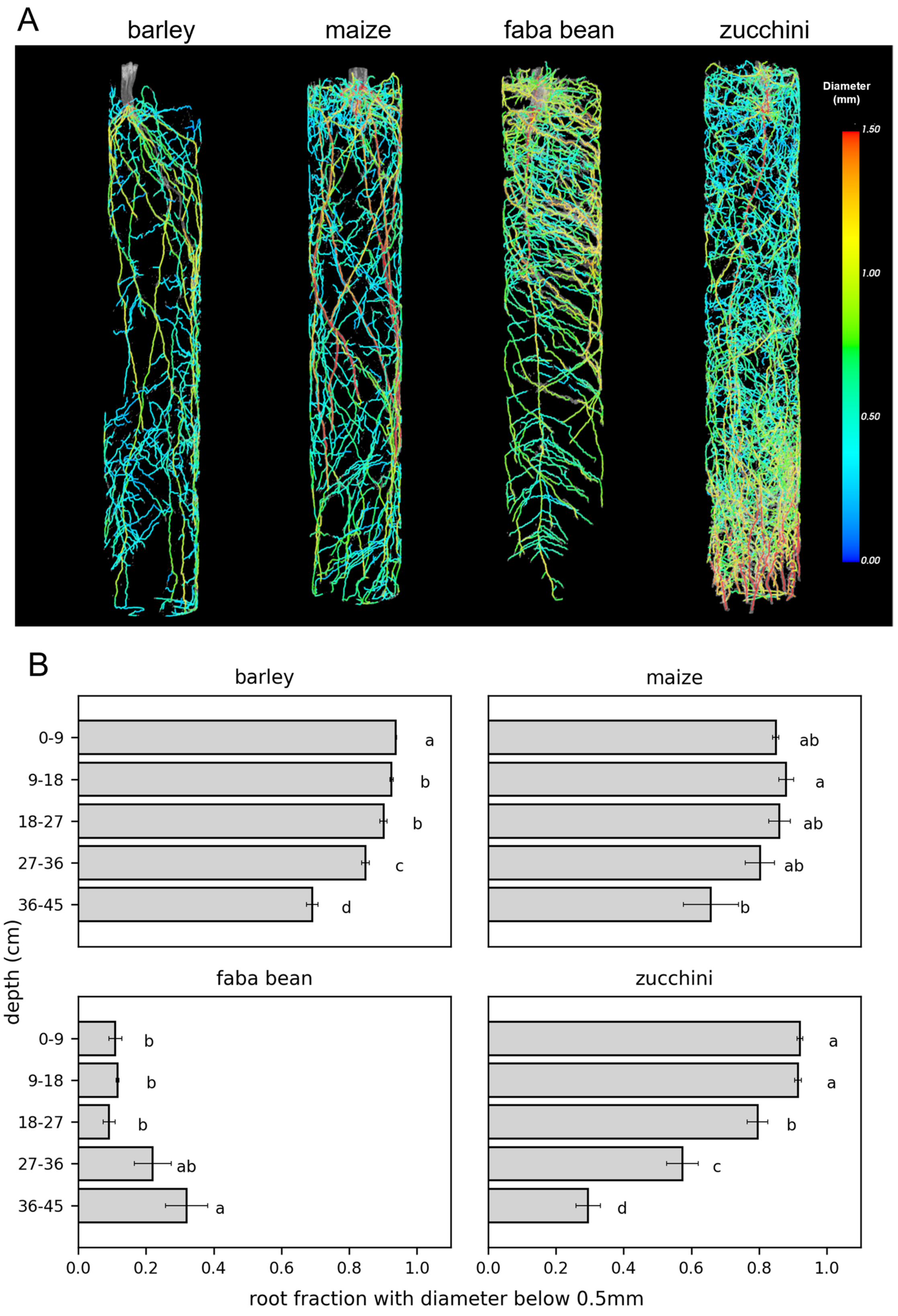
A
barley
maize
faba bean
zucchini
Diameter (mm)
1.50
1.00
0.50
0.00
B
barley
0-9
9-18
18-27
27-36
36-45
a
b
b
c
d
maize
ab
a
ab
ab
b
faba bean
b
b
b
ab
a
zucchini
a
a
b
c
d
depth (cm)
0.0
0.2
0.4
0.6
0.8
1.0
root fraction with diameter below 0.5mm

◂**Fig. 6** Distributions of characteristic root system traits measured with MRI and by scanning harvested roots. **A** Images of the different species' root systems and diameters acquired with MRI and analyzed with NMRooting. Exemplary, the image of one replicate per species is shown. Color code is root diameter ranging from blue (0 mm) to red (1.5 mm). Column size was 80.5 mm in diameter and 450 mm in height. **B** Fraction of fine roots with diameter below 0.5 mm over depth, derived by scanning of harvested roots. Horizontal bars are species averages, error bars are standard errors of the mean. Differences among depth were considered significant if p-values of a Student's t-test were <0.05. Significant differences between different layers are indicated by different letters, starting with 'a' for the greatest value

by a variation in A with depth. The hypothesis of a constant A(z) did not hold as we found significantly greater water uptake rates per unit root length in the top 15 cm than in the bottom 30 cm of the pots in barley, maize and faba bean. Also in these three species, the fraction of lateral roots appeared to decrease towards the bottom.

Since spatial data on root hydraulic traits are rarely available, the approximation of root water uptake profiles by root length distributions was established in macroscopic water uptake models (Coppola et al. 2015, 2019; Feddes et al. 2001; Wu et al. 1999). Our data suggest that this approximation comes with limitations as only 61–71% (without significant differences between species) of variation in U_P could be explained by a variation in L (Table 1). These values are generally lower than those reported by the few quantitative, empirical studies on this topic (70–100% in oat and faba bean (Ehlers et al. 1991), 91–100% in oat and horse bean (Shein and Pachepsky 1995)). One major difference between these studies and our approach is that we measure a component of the root water uptake profile, namely $\widehat{U}_P$, which reflects the distribution of root hydraulic conductance and is independent of the soil water potential distribution. This was realized by measuring the fast response of local water depletion rates to a changing light intensity. The change in light intensity induces a change in the root xylem suction while the soil water potential at first stays constant. Therefore, how strong a change in xylem suction affects the local water depletion rate only depends on the distribution of root hydraulic conductance (see Eq. 1), and thus $\widehat{U}_P$. Typically, as in our measurements (Fig. 3), the soil water potential is lower (more negative) in upper layers than in deeper layers. This causes a redistributive water flow from lower to upper soil layers through the roots. Therefore, U_S usually is in opposite direction to U_P in upper soil layers and in the same direction in deeper layers (Fig. 1A). According to Eq. 2 this results in RWU exceeding U_P in top layers and falling below it in bottom layers. Thus, if we had measured RWU instead of U_P the water uptake profiles (blue lines in Fig. 4) would have been closer to the root length profiles (red lines in Fig. 4). From this we conclude, that in studies measuring RWU instead of U_P, the predictive power of water uptake profiles by root length distributions is artificially increased by the impact of vertical soil water potential gradients on RWU. Approximating root water uptake profiles by root length distributions is equivalent to hypothesizing a constant water uptake rate per unit root length with depth. We observed that water uptake rates per root length were significantly greater in shallow roots compared to deeper roots (Fig. 5), emphasizing that the hypothesis does not hold. Two previous studies using neutron radiography to measure water fluxes into upper and lower parts of lupine root systems reported similar trends (Dara et al. 2015; Zarebanadkouki et al. 2013). Such a systematic deviation of water uptake rates per root length over depth is problematic for the common approximation of root water uptake profiles by root length distributions since it leads to a systematic underestimation of water uptake by roots in top layers and an overestimation in bottom layers. The trend of greater water uptake rates per root length in top layers was consistently observed for barley, maize and faba bean plants (Fig. 5 and Online resource 6). Note, that different physiological parameters, such as shoot size, root length, shoot–root ratio, and total water uptake rate per unit root length and leaf area (Fig. 2) varied, partly significantly, among these species. We therefore suggest that the trend of greater water uptake rates per root length in shallow roots is valid for a wider range of species and plants of different sizes and should be considered when water uptake profiles are approximated by root length distributions.

This leads us to the question of what caused the greater water uptake rates per root length in shallow roots. One potential reason is the impact of pot dimensions, which are known to constrain root growth (Poorter et al. 2012). However, since root length densities were greatest in shallow soil layers in our experiments (Figs. 4, 6A) we would also expect the strongest constrains in these layers. However, water uptake rates per root length were greater in upper soil layers compared to deeper layers (Fig. 5). This emphasizes that potential consequences of constrained pot dimensions, such as saturation effects or limited root functioning, did not result in measurable impairment of water uptake rates.

Mathematically, local root water uptake rates are the product of the local radial root conductance and the water potential difference between the root xylem and the soil (Eq. 1). The radial root conductance depends on the radial root conductivity, an intrinsic hydraulic property, and root length. Therefore, uniform soil water potential distribution, uniform radial conductivity, and sufficiently high axial conductance to provide uniform water potentials in the root xylem are requirements for constant uptake rates per unit root length throughout the root system (Javaux et al. 2013). Given that U_P is independent of the soil water potential distribution, the difference in A(z) between shallow and deep roots must be caused by differences in the hydraulic parameters (i.e. radial root conductivity and xylem water potential) between the top and bottom part of the root system. As summarized by (Vetterlein and Doussan 2016), root radial conductivity depends on several root anatomical traits changing with root age, such as apoplastic barriers, cortex thickness, or aquaporin density. Towards the root tip, there usually is a lower degree of suberization (Huang and Eissenstat 2000; Steudle 1994; Steudle and Peterson 1998), thinner cell walls (McCormack et al. 2015; Steudle and Peterson 1998) and higher aquaporin expression (Gambetta et al. 2013), all of which results in a greater radial conductivity. This contributes to the generally high radial conductivity in lateral roots (Ahmed et al. 2016) or roots with a low branching order (Rewald et al. 2012). Our analysis suggests a greater fraction of fine lateral roots with a diameter below 0.5 mm in shallower than in deeper soil layers for barley, maize, and zucchini (Fig. 6B). If this fine root fraction indeed had a relatively high radial conductivity, it might have contributed to the greater water uptake rates per unit root length in shallow soil layers. However, as argued above, the anatomical features causing greater radial root conductivity usually appear towards the root tip. Therefore, we would expect a greater radial conductivity in deeper layers, where roots are generally younger (Koebernick et al. 2014). We can only speculate here, whether the effect of an increased root diameter, and thus, a longer radial pathway outweighed the age-effect of a lower suberization and greater aquaporin expression in deeper roots. Note that for faba bean this quantitative analysis of root type distribution was not possible since lateral roots and main roots had a comparable diameter (Fig. 6A). Additionally, the general thickening of roots towards bottom layers (Online resource 7) could have obscured the distinction of lateral and main roots based on root diameter.

Another possibility is a less negative xylem water potential (less water suction) in deeper roots due to an insufficient axial conductance. The axial conductivity increases with increasing number and diameter of conducting xylem vessels. In addition, the axial conductance increases with increasing length of the hydraulic pathway (Frensch and Steudle 1989). In crops, both number and diameter of xylem vessels usually decrease towards the root tip, and thus with depth (Bramley et al. 2009; Clément et al. 2022; Frensch and Steudle 1989; Steudle and Peterson 1998; Watt et al. 2008). Note that in contrast, trees usually have a greater number and diameter of conducting root xylem in deeper layers (McElrone et al. 2004; Pate et al. 1995; Wang et al. 2015). For crops however, the root xylem anatomy, together with the long hydraulic pathway, lead to a decreasing axial conductance (Meunier et al. 2018; Zarebanadkouki et al. 2016), and finally to a less negative xylem water potential in deeper roots (Zarebanadkouki et al. 2016). In maize, the maturation of the late metaxylem in the main root was shown to occur around 25 cm from the root tip (Steudle and Peterson 1998) leading to increased axial conductance. This is spatially correlated to the rather sharp drop in A(z) that we observed within the top 15 cm in maize (Fig. 5A). In summary, the greater water uptake rates per unit root length in shallow roots in barley, maize and faba are most likely explained by a less restricted axial water transport as compared to deeper roots. This might be accompanied by the greater fraction of lateral roots, potentially leading to greater radial conductivity in shallow soil layers (Fig. 7).

In the field, greater water uptake efficiencies of shallow roots could be beneficial regarding the competition for rainwater in shallow soil layers. Our study, as well as those two studies reporting similar results (Dara et al. 2015; Zarebanadkouki et al. 2013), were performed with pot- or container-grown plants and, straightforwardly transferring the results

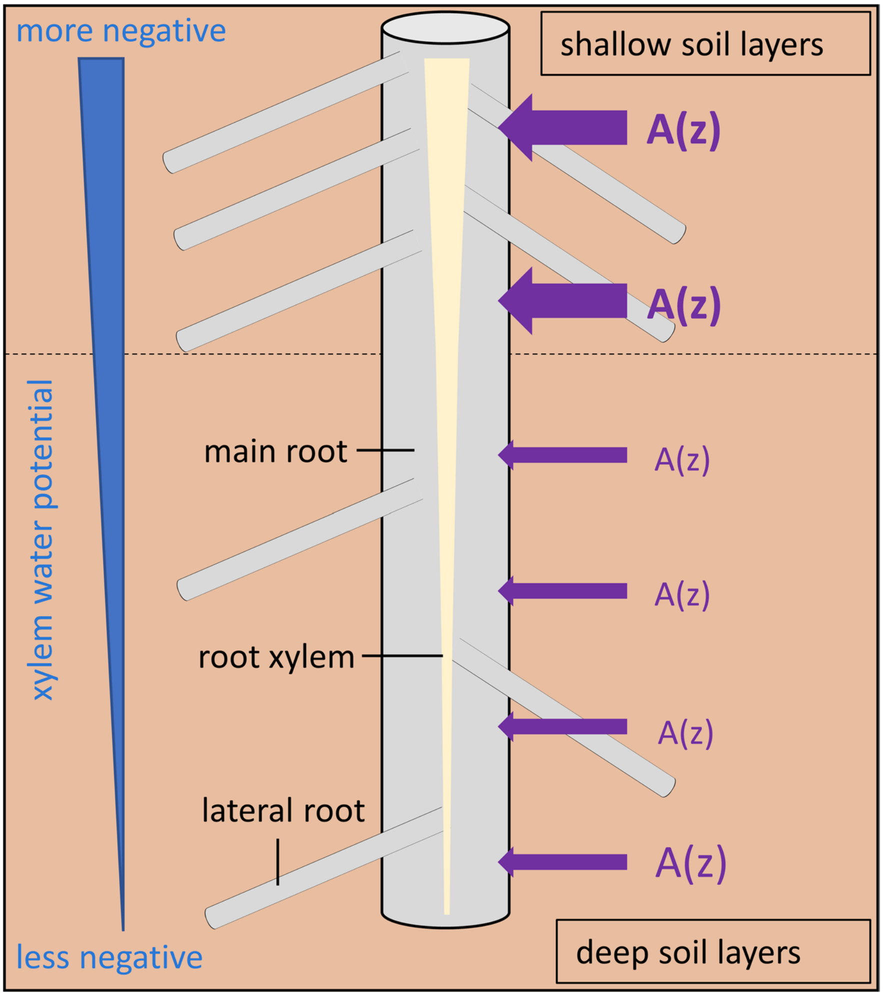

Fig. 7 Schematic evaluation of our hypothesis. Shallow roots generally have greater water uptake rates per unit root length (A(z)) than deeper roots. This is probably explained by a less negative xylem water potential in deeper layers due to an incomplete maturation of xylem vessels. Additionally, radial conductivity in shallow soil layers might be greater due to a higher fraction of fine lateral roots

to field-grown plants is difficult. Only limited data on water uptake rates per root length from field experiments are available in the literature, probably because soil water conditions are barely controllable in the field, making a reliable measurement of water uptake profiles even more challenging. Two recent field studies in wheat suggest that root length and water uptake rates are asymptotically related due to a saturation of water uptake in upper soil layers with great root length densities (Gao et al. 2022; Zhang et al. 2020), which is opposite to our findings. It is possible that the restricted horizontal root growth in our pots led to a stronger vertical gradient in root system traits compared to field conditions, which might have contributed to the reduced uptake per root length in deeper layers. Further experiments are required to determine the distribution of root hydraulic traits in field-grown plants, which is, however limited by the current technologies for measuring root water uptake patterns.

Concluding remarks

In the present study we tested the hypothesis of constant root water uptake rates per unit root length with depth to answer how reliably profiles of root water uptake rates can be approximated by root length distributions. We consistently found that in well-watered soil, water uptake rates per unit root length were significantly higher in shallower compared to deeper roots. Since this higher root activity in top soil layers was consistently observed among species which differed significantly in various physiological parameters, it seems to be an universal trend. We suggest that it is explained by a limiting axial conductance of deeper roots. The greater uptake rates per unit root lengths of shallow roots need to be taken into account when water uptake profiles are used to estimate root length distribution or vice versa.

Acknowledgements We gratefully acknowledge the group of Mathieu Javaux at the Université catholique de Louvain, Earth and Life Institute, for deriving the water retention curve of our soil. We would like to thank Andrea Schnepf, Kwabena Agyei, and Helena Bochmann, for internally reviewing and improving the manuscript.

Author contributions Conceptualization: Yannik Müllers, Dagmar van Dusschoten, Johannes Postma, Hendrik Poorter, Ulrich Schurr.

Formal Analysis: Yannik Müllers, Dagmar van Dusschoten Johannes Postma, Hendrik Poorter.

Funding Acquisition: Ulrich Schurr.

Investigation: Yannik Müllers, Dagmar van Dusschoten.

Methodology: Yannik Müllers, Dagmar van Dusschoten, Johannes Kochs, Daniel Pflugfelder.

Software: Yannik Müllers, Daniel Pflugfelder, Johannes Kochs.

Supervision: Dagmar van Dusschoten, Johannes Postma, Hendrik Poorter, Ulrich Schurr.

Validation: Yannik Müllers, Dagmar van Dusschoten.

Visualization: Yannik Müllers, Dagmar van Dusschoten.

Writing – Original Draft Preparation: Yannik Müllers, Dagmar van Dusschoten, Hendrik Poorter, Johannes Postma.

Writing – Review and Editing: Yannik Müllers, Dagmar van Dusschoten, Hendrik Poorter, Johannes Postma, Johannes Kochs, Daniel Pflugfelder, Ulrich Schurr.

Funding Open Access funding enabled and organized by Projekt DEAL. The authors declare that no funds, grants, or other support were received during the preparation of this manuscript.

Data availability The data supporting the findings of this study are available from the corresponding author, Dagmar van Dusschoten, upon request.

Declarations

Competing interests The authors have no relevant financial or non-financial interests to disclose.

Appendix 1

In the following, we will derive how root water uptake profiles can be separated into one part, solely determined by root conductance (U_P), and a second one, additionally determined by the soil water potential distribution (U_S). For this purpose, we will use a simplified form of the model introduced by Couvreur et al. (2012), together with the following assumptions and considerations: The soil columns used in the experiments consist of 45 stacked, cylindrical layers of 1 cm height and 8.1 cm. Each layer is indicated by i with i = 1,…, 45. The top of each layer is at depth z_i with $z_i = 0,\ldots, 44$ cm. RWU(z_i) denotes the root water uptake rate, $K_R(z_i)$ the radial conductance, $K_X(z_i)$ the axial conductance, and $\Psi_X(z_i)$ the water potential in the xylem of the bulk roots in each layer. The water potential of the bulk soil in each layer is $\Psi_{soil}(z_i)$. The hydraulic network used for the analysis is presented in Online Resource 1.

With this, the root water uptake rate in each layer can be described as follows:

$$RWU(z_i) = K_R(z_i) \cdot (\Psi_{soil}(z_i) - \Psi_X(z_i)) \tag{1}$$

The total root water uptake rate (U_{tot}) is the sum of the root water uptake rates of all layers:

$$U_{tot} = \sum_i RWU(z_i) \tag{2}$$

U_{tot} can be expressed using the water potential at the plant collar (Ψ_{collar}), the total conductance between soil and plant collar (K_{tot}), and the equivalent soil water potential (Ψ_{seq}):

$$U_{tot} = K_{tot} \cdot (\Psi_{seq} - \Psi_{collar}) \tag{3}$$

Ψ_{seq}, as used in Eq. 14, reflects the overall soil water potential sensed by the plant. This parameter is obtained by weighing the soil water potential distribution by the distribution of root conductance (Couvreur et al. 2012). Solving Eq. 14 for Ψ_{collar} gives:

$$\Psi_{collar} = \Psi_{seq} - \frac{U_{tot}}{K_{tot}} \tag{4}$$

At this point, we assume that $K_X(z_i)$ is much higher than $K_R(z_i)$ and therefore $\Psi_X(z_i)$ is well approximated by Ψ_{collar}. Note that this assumption is not required for the separation of RWU in U_P and U_S as shown by Couvreur et al. (2012), but used here to keep the derivation concise. With this, Eq. 12 writes:

$$RWU(z_i) = K_R(z_i) \cdot (\Psi_{soil}(z_i) - \Psi_{collar}) \tag{5}$$

Using Eq. 15 to replace Ψ_{collar} in Eq. 16 gives after rewriting:

$$RWU(z_i) = K_R(z_i) \cdot \frac{U_{tot}}{K_{tot}} + K_R(z_i) \cdot (\Psi_{soil}(z_i) - \Psi_{seq}) \tag{6}$$

In Eq. 17, RWU is expressed as sum of two terms, of which the first one is independent of the soil water potential distribution.

We define $U_P(z_i) = K_R(z_i) \cdot \frac{U_{tot}}{K_{tot}}$ and $U_S(z_i) = K_R(z_i) \cdot (\Psi_{soil}(z_i) - \Psi_{seq})$, and write Eq. 17 as:

$$RWU(z_i) = U_P(z_i) + U_S(z_i) \tag{7}$$

Note that under the assumption $K_X(z_i) >> K_R(z_i)$, K_{tot} simplifies to the sum of the radial conductance of all layers: $K_{tot} = \sum_i K_R(z_i)$. Therefore, U_P can be normalized by division by U_{tot}:

$$\widehat{U}_P(z_i) = \frac{U_P}{U_{tot}} = \frac{K_R(z_i)}{K_{tot}} = \frac{K_R(z_i)}{\sum_i K_R(z_i)} \tag{8}$$

Without the assumption $K_X(z_i) >> K_R(z_i)$, $\widehat{U}_P(z_i)$ would additionally depend on the axial and radial conductance of other layers and thus on the overall root hydraulic architecture. Nevertheless, it would still be independent of $\Psi_{soil}(z_i)$.

References

Ahmed MA, Zarebanadkouki M, Kaestner A, Carminati A (2016) Measurements of water uptake of maize roots: the key function of lateral roots. Plant Soil 398(1–2):59–77. https://doi.org/10.1007/s11104-015-2639-6

Ahmed MA, Zarebanadkouki M, Meunier F, Javaux M, Kaestner A, Carminati A (2018) Root type matters: Measurement of water uptake by seminal, crown, and lateral roots in maize. J Exp Bot 69(5):1199–1206. https://doi.org/10.1093/jxb/erx439

Bramley H, Turner NC, Turner DW, Tyerman SD (2009) Roles of morphology, anatomy, and aquaporins in determining contrasting hydraulic behavior of roots. Plant Physiol 150(1):348–364. https://doi.org/10.1104/pp.108.134098

Brooks RH, Corey AT (1964) Hydraulic properties of porous media. Hydrol Pap 27(3):293–296

Coppola A, Chaali N, Dragonetti G, Lamaddalena N, Comegna A (2015) Root uptake under non-uniform root-zone salinity. Ecohydrology 8(7):1363–1379. https://doi.org/10.1002/eco.1594

Couvreur V, Vanderborght J, Javaux M (2012) A simple three-dimensional macroscopic root water uptake model based on the hydraulic architecture approach. Hydrol Earth Syst Sci 16(8):2957–2971. https://doi.org/10.5194/hess-16-2957-2012

Dara A, Moradi BA, Vontobel P, Oswald SE (2015) Mapping compensating root water uptake in heterogeneous soil conditions via neutron radiography. Plant Soil 397(1–2):273–287. https://doi.org/10.1007/s11104-015-2613-3

Ehlers W, Hamblin AP, Tennant D, van der Ploeg RR (1991) Root system parameters determinig water uptake of field crops. Irrig Sci 12:115–124. https://doi.org/10.1007/BF00192282

Feddes RA, Hoff H, Bruen M, Dawson TE, de Rosnay P, Dyrmeyer P, Jackson RB, Kabat P, Kleidon A, Lilly A, Milly PCD, Pitman A (2001) Modeling root water uptake in hydrological and climat models. Bull Amer Meteorol Soc 82(12):2797–2809.https://doi.org/10.1175/1520-0477(2001)082<2797:MRWUIH>2.3.CO;2

Gambetta GA, Fei J, Rost TL, Knipfer T, Matthews MA, Shackel KA, Andrew Walker M, McElrone AJ (2013) Water uptake along the length of grapevine fine roots: Developmental anatomy, tissue-specific aquaporin expression, and pathways of water transport. Plant Physiol 163(3):1254–1265. https://doi.org/10.1104/pp.113.221283

Huang B, Eissenstat DM (2000) Linking hydraulic conductivity to anatomy in plants that vary in specific root length. J Am Soc Hortic Sci 125(2):260–264. https://doi.org/10.21273/JASHS.125.2.260

Lippold E, Phalempin M, Schlüter S, Vetterlein D (2021) Does the lack of root hairs alter root system architecture of Zea mays? Plant Soil 467(1–2):267–286. https://doi.org/10.1007/s11104-021-05084-8

McCormack ML, Dickie IA, Eissenstat DM, Fahey TJ, Fernandez CW, Guo D, Helmisaari HS, Hobbie EA, Iversen CM, Jackson RB, Leppälammi-Kujansuu J, Norby RJ, Phillips RP, Pregitzer KS, Pritchard SG, Rewald B, Zadworny M (2015) Redefining fine roots improves understanding of below-ground contributions to terrestrial biosphere processes. New Phytol 207(3):505–518. https://doi.org/10.1111/nph.13363

McElrone AJ, Pockman WT, Martínez-Vilalta J, Jackson RB (2004) Variation in xylem structure and function in stems and roots of trees to 20 m depth. New Phytol 163(3):507–517. https://doi.org/10.1111/j.1469-8137.2004.01127.x

Pandey BK, Huang G, Bhosale R, Hartman S, Sturrock CJ, Jose L, Martin OC, Karady M, Voesenek LACJ, Ljung K, Lynch JP, Brown KM, Whalley WR, Mooney SJ, Zhang D, Bennett MJ (2021) Plant roots sense soil compaction through restricted ethylene diffusion. Science

371(6526):276–280. https://doi.org/10.1126/science.abf3013

Pate JS, Jeschke WD, Aylward MJ (1995) Hydraulic architecture and xylem structure of the dimorphic root systems of south-west australian species of proteaceae. J Exp Bot 46(8):907–915. https://doi.org/10.1093/jxb/46.8.907

Peters A, Durner W (2008) Simplified evaporation method for determining soil hydraulic properties. J Hydrol 356:147–162. https://doi.org/10.1016/j.jhydrol.2008.04.016

Pflugfelder D, Metzner R, Dusschoten D, Reichel R, Jahnke S, Koller R (2017) Non-invasive imaging of plant roots in different soils using magnetic resonance imaging (MRI). Plant Methods 13(1):1–9. https://doi.org/10.1186/s13007-017-0252-9

Pohlmeier A, Haber-Pohlmeier S, Stapf S (2009) A fast field cycling nuclear magnetic resonance relaxometry study of natural soils. Vadose Zone J 8(3):735–742. https://doi.org/10.2136/vzj2008.0030

Poorter H, Nagel O (2000) The role of biomass allocation in the growth response of plants to different levels of light, CO2, nutrients and water: A quantitative review. Funct Plant Biol 27(6):595–607. https://doi.org/10.1071/pp99173_co

Poorter H, Bühler J, Van Dusschoten D, Climent J, Postma JA (2012) Pot size matters: A meta-analysis of the effects of rooting volume on plant growth. Funct Plant Biol 39(11):839–850. https://doi.org/10.1071/FP12049

Qin R, Stamp P, Richner W (2005) Impact of tillage and banded starter fertilizer on maize root growth in the top 25 centimeters of the soil. Agron J 97(3):674–683. https://doi.org/10.2134/agronj2004.0059

Rewald B, Raveh E, Gendler T, Ephrath JE, Rachmilevitch S (2012) Phenotypic plasticity and water flux rates of Citrus root orders under salinity. J Exp Bot 63(7):2717–2727. https://doi.org/10.1093/jxb/err457

Schneider HM, Wojciechowski T, Postma JA, Brown KM, Lücke A, Zeisler V, Schreiber L, Lynch JP (2017) Root cortical senescence decreases root respiration, nutrient content and radial water and nutrient transport in barley. Plant, Cell Environ 40(8):1392–1408. https://doi.org/10.1111/pce.12933

Schneider HM, Postma JA, Kochs J, Pflugfelder D, Lynch JP, van Dusschoten D (2020) Spatio-temporal variation in water uptake in seminal and nodal root systems of barley plants grown in soil. Front Plant Sci 11(August):1–13. https://doi.org/10.3389/fpls.2020.01247

Sharp RE, Davies WJ (1985) Root growth and water uptake by maize plants in drying soil. J Exp Bot 36(9):1441–1456. https://doi.org/10.1093/jxb/36.9.1441

Shein EV, Pachepsky YA (1995) Influence of root density on the critical soil water potential. Plant Soil 171(2):351–357. https://doi.org/10.1007/BF00010291

Steudle E (1994) Water transport across roots. Plant Soil 167(1):79–90. https://doi.org/10.1007/BF01587602

Steudle E, Peterson CA (1998) How does water get through roots? J Exp Bot 49(322):775–788. https://doi.org/10.1093/jexbot/49.322.775

van Dusschoten D, Kochs J, Kuppe CW, Sydoruk VA, Couvreur V, Pflugfelder D, Postma JA (2020) Spatially resolved root water uptake determination using a precise soil water sensor. Plant Physiol 184(3):1221–1235. https://doi.org/10.1104/pp.20.00488

Vanhees DJ, Schneider HM, Sidhu JS, Loades KW, Bengough AG, Bennett MJ, Pandey BK, Brown KM, Mooney SJ, Lynch JP (2022) Soil penetration by maize roots is negatively related to ethylene-induced thickening. Plant, Cell Environ 45(3):789–804. https://doi.org/10.1111/pce.14175

Vetterlein D, Doussan C (2016) Root age distribution: how does it matter in plant processes? A focus on water uptake. Plant Soil 407(1–2):145–160. https://doi.org/10.1007/s11104-016-2849-6

Wang Y, Dong X, Wang H, Wang Z, Gu J (2015) Root tip morphology, anatomy, chemistry and potential hydraulic conductivity vary with soil depth in three temperate hardwood species. Tree Physiol 36(1):99–108. https://doi.org/10.1093/treephys/tpv094

Watt M, Magee LJ, McCully ME (2008) Types, structure and potential for axial water flow in the deepest roots of field-grown cereals. New Phytol 178(3):690. https://doi.org/10.1111/j.1469-8137.2008.02434.x

Wu J, Zhang R, Gui S (1999) Modeling soil water movement with water uptake by roots. Plant Soil 215(1):7–17. https://doi.org/10.1023/A:1004702807951

Zarebanadkouki M, Kim YX, Carminati A (2013) Where do roots take up water? Neutron radiography of water flow into the roots of transpiring plants growing in soil. New Phytol 199(4):1034–1044. https://doi.org/10.1111/nph.12330

Zarebanadkouki M, Meunier F, Couvreur V, Cesar J, Javaux M, Carminati A (2016) Estimation of the hydraulic conductivities of lupine roots by inverse modelling of high-resolution measurements of root water uptake. Ann Bot 118(4):853–864. https://doi.org/10.1093/aob/mcw154

Zhang XX, Whalley PA, Ashton RW, Evans J, Hawkesford MJ, Griffiths S, Huang ZD, Zhou H, Mooney SJ, Whalley WR (2020) A comparison between water uptake and root length density in winter wheat: effects of root density and rhizosphere properties. Plant Soil 451(1–2):345–356. https://doi.org/10.1007/s11104-020-04530-3

Clément C, Schneider HM, Dresbøll DB, Lynch JP, Thorup-Kristensen K (2022) Root and xylem anatomy varies with root length, root order, soil depth and environment in intermediate wheatgrass (Kernza®) and alfalfa. Ann Bot 1–16. https://doi.org/10.1093/aob/mcac058

Coppola A, Dragonetti G, Sengouga A, Lamaddalena N, Comegna A, Basile A, Noviello N, Nardella L (2019) Identifying optimal irrigation water needs at district scale by using a physically based agro-hydrological model. Water (Switzerland) 11(4). https://doi.org/10.3390/w11040841

Frensch J, Steudle E (1989) Axial and radial hydraulic resistance to roots of maize (Zea mays L.). Plant Physiol 91(2):719–726. https://doi.org/10.1104/pp.91.2.719

Gao Y, Chen J, Wang G, Liu Z, Sun W, Zhang Y, Zhang X (2022) Different responses in root water uptake of summer maize to planting density and nitrogen fertilization. Front Plant Sci 13(June). https://doi.org/10.3389/fpls.2022.918043

Javaux M, Couvreur V, Vanderborght J, Vereecken H (2013) Root water uptake: from three-dimensional biophysical processes to macroscopic modeling approaches. Vadose Zone J 12(4):vzj2013.02.0042. https://doi.org/10.2136/vzj2013.02.0042

Koebernick N, Weller U, Huber K, Schlüter S, Vogel H, Jahn R, Vereecken H, Vetterlein D (2014) In situ visualization and quantiication of three- dimensional root system architecture and growth using x-ray computed tomography. Vadose Zone J 13(8). https://doi.org/10.2136/vzj2014.03.0024

Meunier F, Zarebanadkouki M, Ahmed MA, Carminati A, Couvreur V, Javaux M (2018) Hydraulic conductivity of soil-grown lupine and maize unbranched roots and maize root-shoot junctions. J Plant Physiol 227(December 2017):31–44. https://doi.org/10.1016/j.jplph.2017.12.019

van Dusschoten D, Metzner R, Kochs J, Postma JA, Pflugfelder D, Buehler J, Schurr U, Jahnke S (2016) Quantitative 3D analysis of plant roots growing in soil using magnetic resonance imaging. Plant Physiol 170(March):01388.2015. https://doi.org/10.1104/pp.15.01388

Supplementary Information

Online resource1: Model of the hydraulic network used in our study

Online resource 2: Calibration of the four SWaP sensors

Online Resource 3: Linear regression between $U_{tot}(t)$ and $\frac{\partial\theta(t)}{\partial t}$

Online Resource 4: Soil water characteristics at start and end of the SWaP measurement

Online Resource 5: Vertical profiles of soil water potential Ψ_{soil} (blue) and volumetric soil water content θ

Online Resource 6: Vertical profiles of $\widehat{U}_P$, and $\hat{L}$ of each individual barley, faba bean, maize and zucchini plant

Online Resource 7: Vertical profiles of root water uptake rates per unit root length of each individual barley, faba bean, maize and zucchini plant

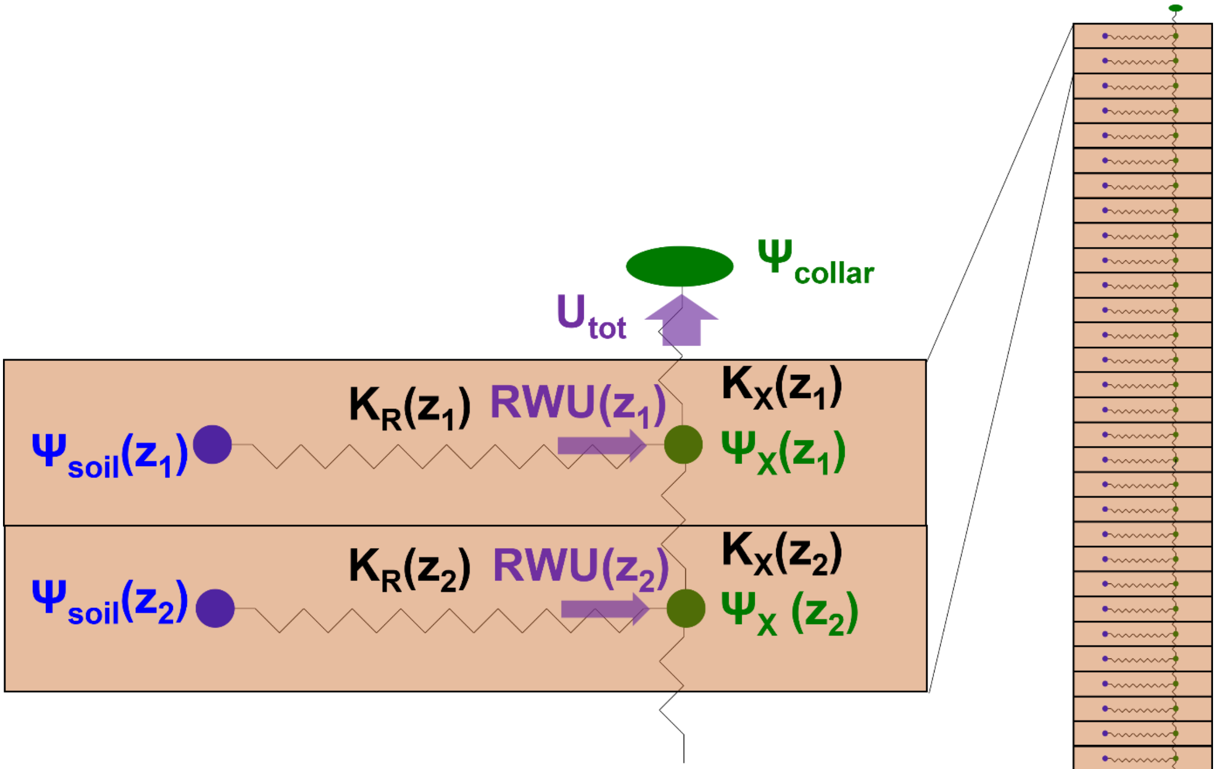

Online Resource 1 Model of the hydraulic network used in our study. The soil column is interpreted as 45 stacked soil layers of 1 cm height and 8.1 cm diameter. The top of each soil layer is located at depth z_i with z_1=0 cm,…, z_{45}=44 cm. The bulk roots in each layer are assigned a radial conductance ($K_R(z_i)$), an axial conductance ($K_X(z_i)$), and a water potential inside the xylem ($\Psi_X(z_i)$). The water potential in the bulk soil of each layer is denoted as $\Psi_{soil}(z_i)$. The local root water uptake rate is called $RWU(z_i)$. U_{tot} is the total root water uptake rate and Ψ_{collar} the water potential at the plant collar.

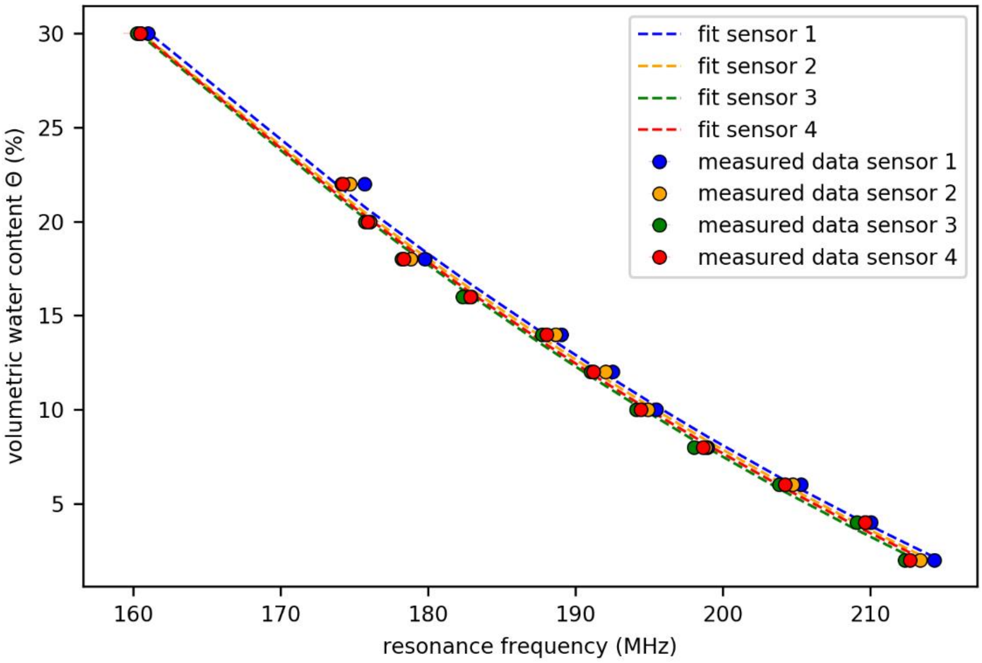

Online Resource 2 Calibration of the four SWaP sensors. 12 cm high pots with defined θ were measured four times in each sensor. In between the four measurements, the pots were turned by 90°. Dots are mean values of the four measurements, horizontal error bars are standard deviations. Dashed lines are fitting curves using a 2nd order polynomial

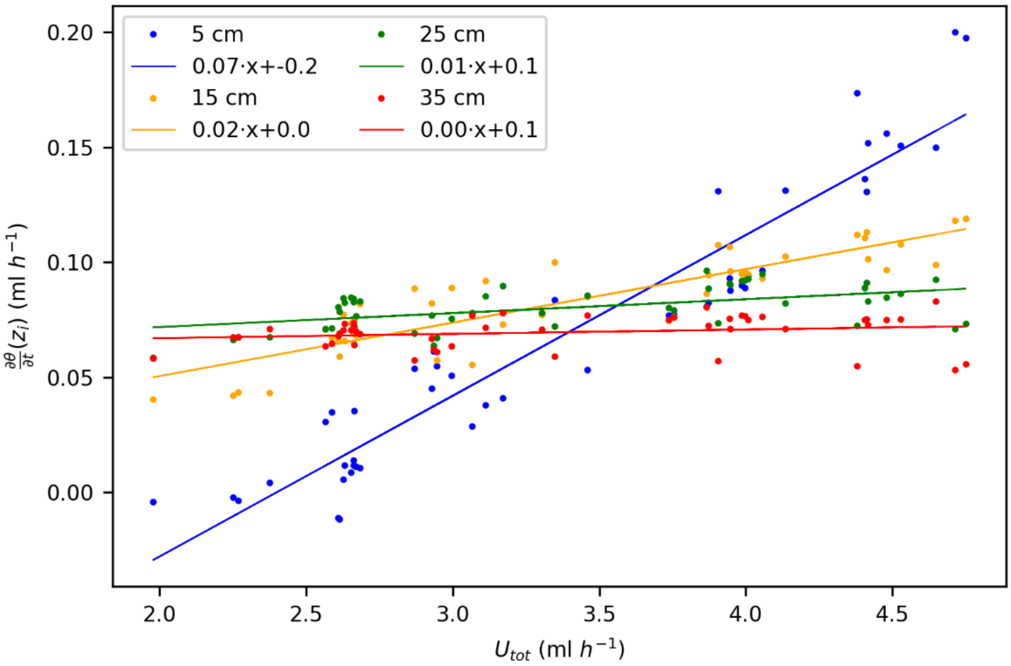

Online Resource 3 Linear regression between $U_{tot}(t)$ and $\frac{\partial\theta(t)}{\partial t}$. Different colors indicate soil layers from different depths. $\widehat{U}_P(z_i)$ is given as the slope of the linear regression from each layer. The exemplary shown data are from measurements of a maize plant

Online Resource 4 Soil water characteristics at start and end of the SWaP measurement. Values are species averages (n=4) ± standard deviation. Significant differences between species are indicated by different letters. Differences were considered significant if p-values of a Student's t-test were <0.05

species	$\bar{\theta}_{\mathrm{start}}$ (%)	$\bar{\theta}_{\mathrm{end}}$ (%)	$\bar{\Psi}_{\mathrm{start}}$ (kPa)	$\bar{\Psi}_{\mathrm{end}}$ (kPa)
barley	21 ± 1 a	19 ± 1 a	-11 ± 0 a	-13 ± 1 a
maize	20 ± 2 a	18 ± 3 ab	-11 ± 2 a	-14 ± 4 ab
faba bean	19 ± 1 a	18 ± 1 ab	-11 ± 1 a	-14 ± 2 a
zucchini	19 ±1 a	15 ± 2 b	-12 ± 1 a	-19 ± 3 b

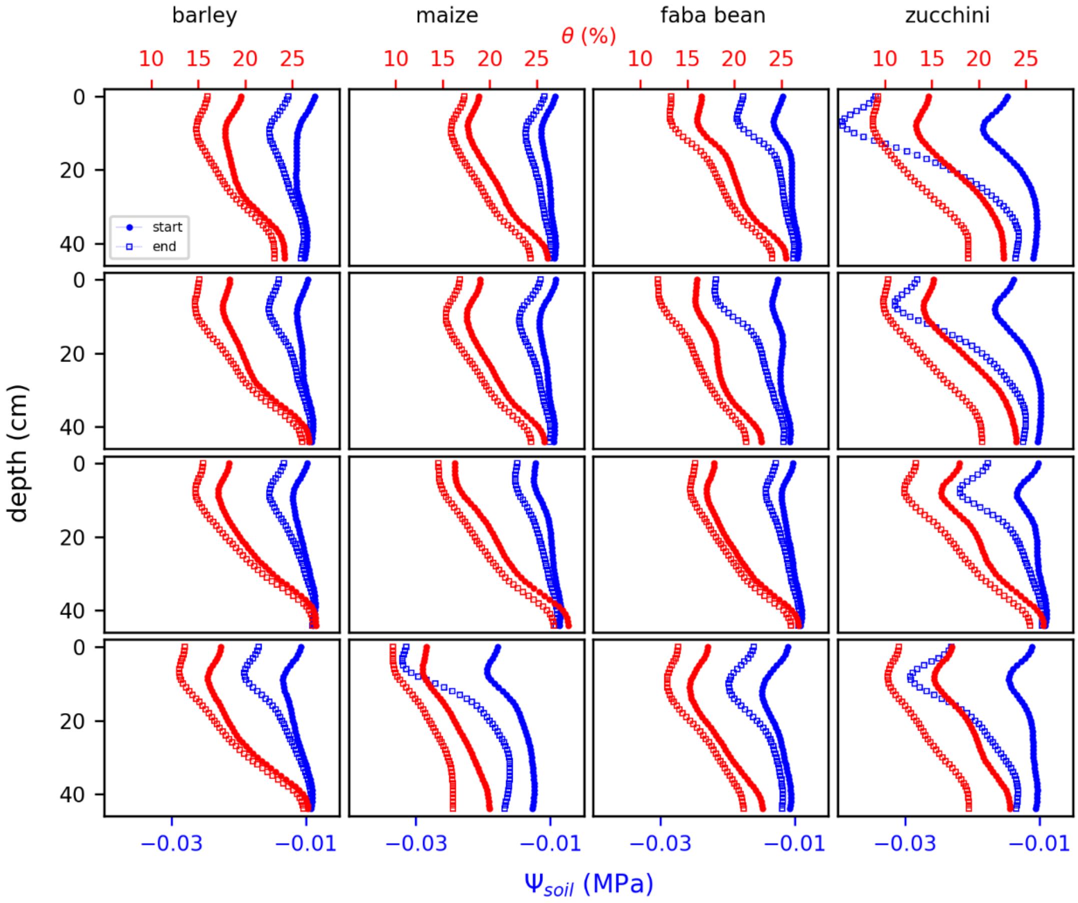

Online Resource 5 Vertical profiles of soil water potential Ψ$_{soil}$ (blue) and volumetric soil water content θ (red) at start (filled circles) and end (empty squares) of the SWaP measurements of each individual barley, faba bean, maize and zucchini plant

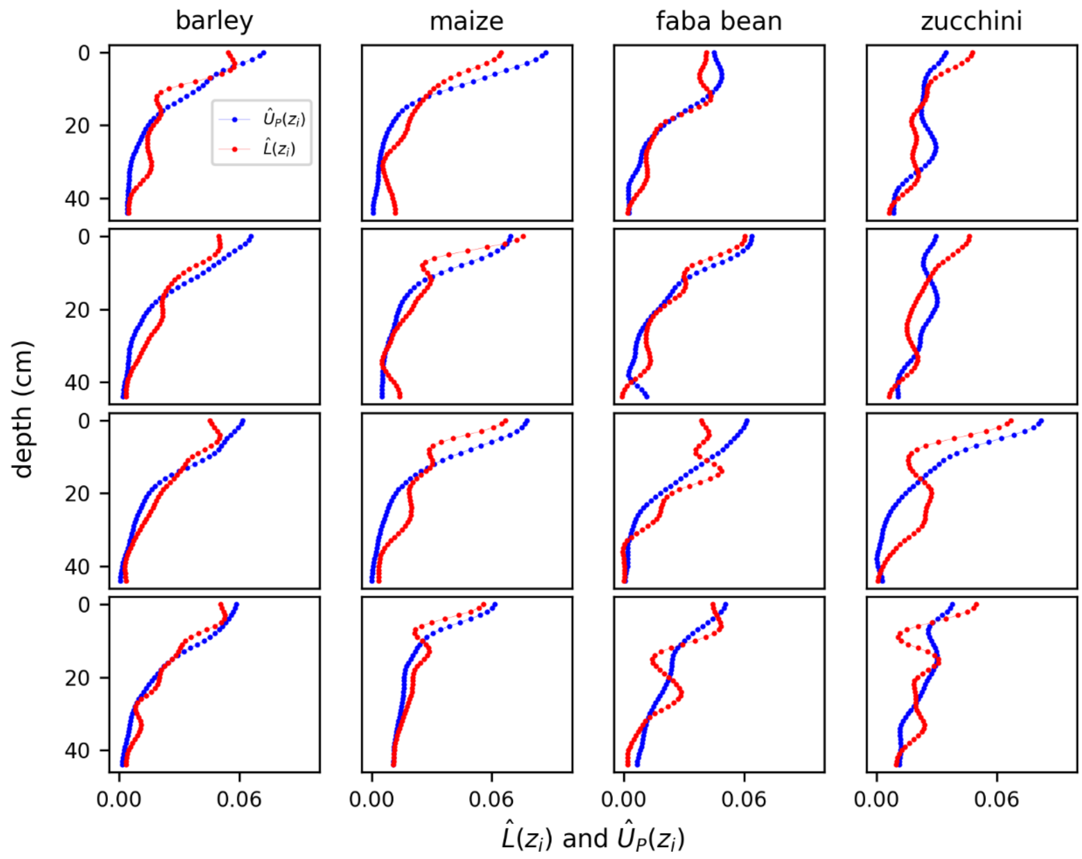

Online Resource 6 Vertical profiles of $\widehat{U}_P$, and $\hat{L}$ of each individual barley, faba bean, maize and zucchini plant

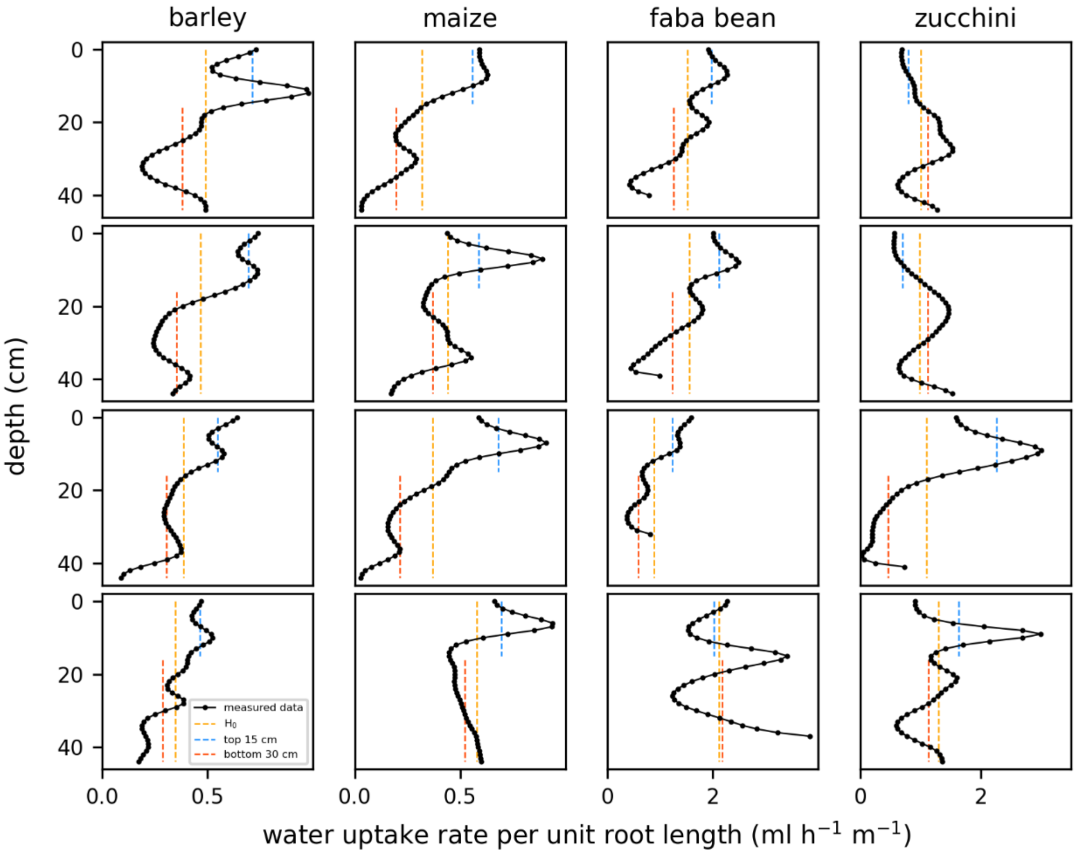

Online Resource 7 Vertical profiles of root water uptake rates per unit root length of each individual barley, faba bean, maize and zucchini plant. The orange vertical line is the average value over depth representing the hypothesis of constant water uptake rates per unit root length. The blue line is the average of the top 15 cm, the red line the average of the bottom 30 cm

Manuscript II

Yannik Müllers, Johannes A Postma, Hendrik Poorter, Dagmar van Dusschoten, Stomatal conductance tracks soil-to-leaf hydraulic conductance in faba bean and maize during soil drying, *Plant Physiology*, Volume 190, Issue 4, December 2022, Pages 2279–2294, https://doi.org/10.1093/plphys/kiac422

Own contribution: Design of the study (together with JP, HP, and DvD), Conductance of the experiments (with contributions from DvD), Data analysis, Drafting the manuscript, Revision and editing of the manuscript (with contributions from all authors)

https://doi.org/10.1093/plphys/kiac422 *PLANT PHYSIOLOGY* 2022: 190: 2279–2294

Plant Physiology®

Research Article

Stomatal conductance tracks soil-to-leaf hydraulic conductance in faba bean and maize during soil drying

Yannik Müllers,[1] **Johannes A. Postma**,[1] **Hendrik Poorter**[1,2] **and Dagmar van Dusschoten**[1,*]

1 Plant Sciences (IBG-2), Forschungszentrum Jülich GmbH, D-52425 Jülich, Germany
2 Department of Biological Sciences, Macquarie University, North Ryde, NSW, 2109 Australia

*Author for correspondence: d.van.dusschoten@fz-juelich.de

Y.M., J.A.P., H.P., and D.v.D. designed the research. Y.M. and D.v.D. performed the research. Y.M. analyzed the data and wrote the manuscript. All authors contributed to the discussion and revision of the manuscript.

The author responsible for distribution of materials integral to the findings presented in this article in accordance with the policy described in the Instructions for Authors (https://academic.oup.com/plphys/pages/general-instructions) is: Dagmar van Dusschoten (d.van.dusschoten@fz-juelich.de).

Abstract

Although regulation of stomatal conductance is widely assumed to be the most important plant response to soil drying, the picture is incomplete when hydraulic conductance from soil to the leaf, upstream of the stomata, is not considered. Here, we investigated to what extent soil drying reduces the conductance between soil and leaf, whether this reduction differs between species, how it affects stomatal regulation, and where in the hydraulic pathway it occurs. To this end, we noninvasively and continuously measured the total root water uptake rate, soil water potential, leaf water potential, and stomatal conductance of 4-week-old, pot-grown maize (*Zea mays*) and faba bean (*Vicia faba*) plants during 4 days of water restriction. In both species, the soil–plant conductance, excluding stomatal conductance, declined exponentially with soil drying and was reduced to 50% above a soil water potential of −0.1 MPa, which is far from the permanent wilting point. This loss of conductance has immediate consequences for leaf water potential and the associated stomatal regulation. Both stomatal conductance and soil–plant conductance declined at a higher rate in faba bean than in maize. Estimations of the water potential at the root surface and an incomplete recovery 22 h after rewatering indicate that the loss of conductance, at least partly, occurred inside the plants, for example, through root suberization or altered aquaporin gene expression. Our findings suggest that differences in the stomatal sensitivity among plant species are partly explained by the sensitivity of root hydraulic conductance to soil drying.

Introduction

To describe plant responses to soil drying, Feddes et al. (1978) proposed the concept of a water stress curve which still is the basis for most current root water uptake (RWU) models (Dos Santos et al., 2017). In this approach, a reduction factor of the transpiration rate is related to the soil water potential (Ψ_{soil}; see Table 1 for abbreviations). Within a specific range of reducing Ψ_{soil}, the transpiration rate is sustained implying a steadily reduced plant water potential to compensate for the reduced soil water potential. Below a critical Ψ_{soil}, the transpiration rate is linearly reduced due to a partial closure of stomata avoiding a too strong decrease of the plant water potential. At the permanent wilting point, usually assumed to be −1.5 MPa, transpiration ceases. The exact shape of such a water stress curve depends on the extent of stomatal closure at a given level of soil drying.

Received April 25, 2022. Accepted August 24, 2022. Advance access publication September 13, 2022

Table 1 Abbreviations used in the article

Term	Meaning	Unit
g_s	Stomatal conductance	mol H_2O m^{-2} s^{-1}
h	Soil matric potential	cm
K_{RL}	Hydraulic conductance between root and leaf	cm h^{-1} Mpa^{-1}
K_{sat}	Saturated soil hydraulic conductivity	cm s^{-1}
K_{SL}	Hydraulic conductance between soil and leaf	cm h^{-1} Mpa^{-1}
K_{SR}	Hydraulic conductance between bulk soil and root surface	cm h^{-1} Mpa^{-1}
K_{soil}	Soil hydraulic conductivity	cm d^{-1}
L	Root length	m
A	Leaf area	cm^2
r_0	Root radius	cm
r_b	Radial distance from the root center defining the start of the bulk soil	cm
RWU	RWU rate	mL h^{-1}
SWaP	Soil water profiler	
U_P	Plant-driven RWU distribution with depth	mL cm^{-3} h^{-1}
$\hat{U}_P$	Normalized plant-driven RWU distribution with depth	
U_S	Soil driven RWU redistribution	mL cm^{-3} h^{-1}
U_{tot}	Total RWU rate	mL h^{-1}
Z_i	Depth of soil layer i	cm
A	Inverse of the air entry pressure	cm^{-1}
θ	Volumetric soil water content	mL cm^{-3}
$\frac{\partial \theta}{\partial t}$	Soil water depletion rate	mL cm^{-3} h^{-1}
λ	Rate constant of the exponential relation between K_{SL} or g_s and Ψ_{seq}	Mpa^{-1}
λ_b	Dimensionless pore size index of the Brooks–Corey model	
τ	Brooks–Corey parameter with $\tau = -2-3\,\lambda_b$	
φ	Matrix flux potential	cm^2 s^{-1}
Ψ_{seq}	Equivalent water potential in the bulk soil	Mpa
Ψ_{seq_50}	Equivalent soil water potential at which the conductance (K_{SL} or g_s) was reduced to 50% of its initial value	Mpa
Ψ_{soil}	Water potential in the bulk soil	Mpa
Ψ_{sr}	Water potential at the soil–root interface	Mpa
$\Psi_{seq,\ sr}$	Equivalent water potential at the soil–root interface	Mpa

Variation of this stomatal sensitivity among species led to the classification in iso- and anisohydric species (Tardieu and Simmoneau, 1998), which is used to explain varying plant responses to soil drying (Pou et al., 2012; Sade et al., 2012; Hochberg et al., 2013; Attia et al., 2015). However, characterizing the hydraulic response of plants to soil drying by stomatal sensitivity only comes with limitations as stomatal control and leaf water potential regulation are not necessarily related when compared across various species (Martínez-Vilalta and Garcia-Forner, 2017).

One potential cause for these inconsistencies is that not only the stomatal conductance, but also the hydraulic conductance upstream toward the stomata, from soil to leaf (K_{SL}) can be affected by soil drying. For each part of this pathway, namely leaves (Cochard, 2002; Ryu et al., 2016), stems (Cochard, 2006; Li et al., 2009), and the soil root system (Saliendra and Meinzer, 1989; Nobel and Cui, 1992; Sperry and Saliendra, 1994; Cochard et al., 1996; Bourbia et al., 2021), a loss of conductance at a reduced soil water potential could be demonstrated. Potential reasons are air gaps between soil and root (North and Nobel, 1997), altered root aquaporin gene expression (Vandeleur et al., 2009; Grondin et al., 2016), suberization of the root epi-, endo-, and exodermis (North and Nobel, 1991; Cruz et al., 1992), or xylem embolisms (Cochard, 2006; Ryu et al., 2016). Assessing the importance of a declining K_{SL} for plant responses to soil drying requires data on characteristic parameters notably the decline rate, and the critical soil water potential at which the decline starts. Depending on these parameters a declining K_{SL} might contribute to varying plant responses to soil drying among species and thus account for the reduced validity of stomatal sensitivity in this context (Martínez-Vilalta et al., 2014; Martínez-Vilalta and Garcia-Forner, 2017).

Stomatal conductance and K_{SL}, act antagonistically on the plant water status, measured as leaf water potential (Ψ_{leaf}). This can be demonstrated by considering the equivalent soil water potential (Ψ_{seq}) to describe the water flow from soil to leaf. Ψ_{seq} reflects the distribution of soil water potential weighted by the distribution of root conductance (Couvreur et al., 2012). Especially during droughts, when the soil water potential usually becomes heterogeneous (Hillel et al., 1976) Ψ_{seq} has a more direct relation to Ψ_{leaf} than the commonly used average soil water potential. Using Ψ_{seq}, and the total RWU rate (U_{tot}), Ψ_{leaf} can be written as

$$\Psi_{leaf} = \Psi_{seq} - \frac{U_{tot}}{K_{SL}}. \tag{1}$$

During soil drying, Ψ_{seq}, which depends on the soil water content, is reduced. According to Equation (1), this would lead to a drop in Ψ_{leaf}. A reduction of the stomatal conductance, and thus U_{tot}, would dampen this drop whereas a reduction of K_{SL} would increase it. In other words, a declining

K_{SL} during soil drying potentially triggers stomatal closure by amplifying the drop in Ψ_{leaf}. Evidence for such a coupling comes from two recent studies reporting a parallel decline of the soil–plant hydraulic conductance and the stomatal conductance during soil drying (Rodriguez-Dominguez and Brodribb, 2020; Bourbia et al., 2021). Another study proposed a strong water depletion zone around the roots to directly trigger stomatal closure (Carminati and Javaux, 2020).

Based on these findings, our study aims at answering the following questions:

(1) Does soil drying cause a reduction in K_{SL}?
(2) Does the sensitivity of K_{SL} to soil drying vary among species?
(3) Does this variation partly account for the varying stomatal sensitivity among species?
(4) Does the variation in K_{SL} sensitivity occur in the soil or in the plant hydraulic pathway?

We hypothesize that the differences in the stomatal response to a reduced Ψ_{seq} between two species are associated with differences in the reduction of K_{SL}. We tested this hypothesis for two species, faba bean (*Vicia faba*), a dicot, and maize (*Zea mays*), a monocot, with different root systems and water uptake rates per unit root length. Using a highly precise soil water sensor, we continuously scanned soil water profiles during several days of progressive soil drying and derived Ψ_{seq} and U_{tot}. In combination with Ψ_{leaf}, which was measured with psychrometers, we could derive K_{SL} and compare it with measurements of the stomatal conductance (Figure 1). To evaluate whether the conductance between bulk soil and root surface (K_{SR}), or the conductance inside the plant, from root surface to leaf (K_{RL}), caused the decline in K_{SL}, we estimated the water potential at the root surface (Ψ_{sr}) using a model (van Lier et al., 2006, 2013; Carminati and Javaux, 2020).

Results

On the first day, maize plants were significantly larger than faba bean plants regarding both leaf area (A, 1.5-fold) and root length (L, four-fold) (Table 2). Compared with maize, the smaller faba bean plants had significantly greater water uptake rates per leaf area (two-fold) and root length (six-fold). The total water uptake rate was also slightly (1.2-fold), albeit not significantly greater in faba bean. The hydraulic conductance between soil and leaf (K_{SL} [mL h^{-1} MPa^{-1}]) was similar for faba bean and maize. Assuming that in wet soil most of the hydraulic resistance occurs in the radial pathway of the roots, the radial root conductivity can be approximated by the ratio of K_{SL} and L which was four times greater in faba bean compared with maize. As determined in a previous measurement, average root diameter was significantly greater in faba bean (0.04 cm) than in maize (0.02 cm).

Figure 2, A, C, and E, shows boxplots of Ψ_{seq}, U_{tot}, and Ψ_{leaf} at selected time points on each day during soil drying for faba bean and maize. For U_{tot} and Ψ_{leaf} each, one time point at low and one at high light were considered per day due to the strong light response of these two parameters. Figure 2, B, D, and F, shows the continuous time courses of the three parameters for one exemplary faba bean plant. The red vertical lines mark those time points selected for the boxplots. For faba bean, Ψ_{seq} decreased overall from −0.015 MPa on the first day to −0.12 MPa on the last day (Figure 2A). For maize, the reduction was lower, ranging from −0.015 to −0.06 MPa. The reduction of Ψ_{seq} mostly happened during the diurnal period, at a rate increasing from the first to the last day (Figure 2B). During the nights, Ψ_{seq} even increased slightly, resulting from a redistribution of soil water which Ψ_{seq} is sensitive to. U_{tot} decreased in faba bean from the first day on (Figure 2C) from 5.7 (high light) and 4.7 mL h^{-1} (low light) to 2.2 and 1.8 mL h^{-1} on the last day. In maize, U_{tot} was initially lower (4.7 mL h^{-1} at high light and 3.6 mL h^{-1} at low light) compared with faba bean and remained constant until the second day. From the third day on it also decreased to ultimately 3.4 and 2.8 mL h^{-1} and thus remained higher compared with faba bean. During the day, U_{tot} alternated between a higher and a lower level in response to the two different light levels. The differences in U_{tot} between the two light levels were lower in faba bean, especially during the last 2 days, indicating a reduced response to varying light (Figure 2D). During the night, U_{tot} remained constant at a low level but never zero. Also, note that U_{tot} at the first high light period of a day was similar to the last high light period of the previous day. This indicates that U_{tot} declined during the day and not at night, and thus followed the dynamics of Ψ_{seq}. Ψ_{leaf} decreased gradually in faba bean (Figure 2E) from −0.7 (high light) and −0.6 MPa (low light) on the first day to −1.1 MPa and −1.0 MPa on the last day. In maize, the initial values were slightly higher (−0.6 MPa at high light and −0.5 at low light) compared with faba bean. During the following 2 days, Ψ_{leaf} only decreased slightly but more pronounced until the last day to −1.1 and −0.9 MPa. Like U_{tot}, Ψ_{leaf} changed with the alternating light levels (Figure 2F). In contrast to U_{tot}, however, Ψ_{leaf} did not remain constant but steadily increased during the nights. This steady increase was faster during the first compared with the last night. The first light period of a day, Ψ_{leaf} was similar (second day) or even higher (third and fourth day) compared with the last light period from the previous day.

In a next step, we analyzed the effect of soil drying on Ψ_{seq} and the hydraulic conductance between soil and leaf, K_{SL}. K_{SL} was derived by rearranging Equation (1). Figure 3A shows an example K_{SL} (black dots) of a faba bean as a function of Ψ_{seq}. For the analysis, we considered four measurement points per light period (28 points per day) excluding data measured at night. After a short, initial phase of increase, we observed an exponential decrease of K_{SL}. Among all replicates, we found a Ψ_{seq} of −0.025 MPa as a consistent, critical point at which the exponential decline had started. For selected plants, we additionally measured the stomatal conductance g_s with a portable LiCor 6400 photosynthesis system. During the 4 days of soil drying, g_s (orange dots in

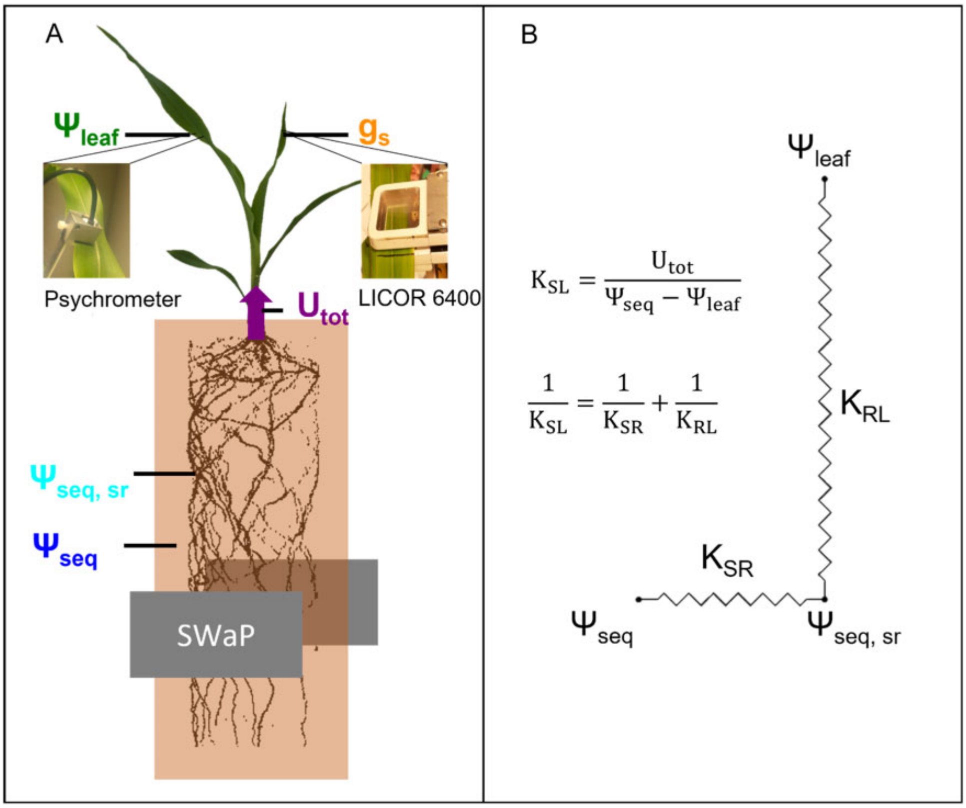

Figure 1 Experimental setup and hydraulic model used in this study. A, Scheme of the experimental setup and the different water potentials used for the data analysis. The equivalent water potential in the bulk soil (Ψ_{seq}), at the root surface ($\Psi_{seq,\ sr}$), and the total root water uptake rate (U_{tot}) were derived from the SWaP measurements. The leaf water potential (Ψ_{leaf}) was measured with psychrometers, the stomatal conductance with a LICOR 6400. Root length was determined with MRI. B, Scheme of the hydraulic network from the bulk soil to the leaf. The overall conductance from bulk soil to leaf (K_{SL}) can be separated into the conductance from bulk soil to the root surface (K_{SR}) and from root surface to the leaf (K_{RL}).

Table 2 Characteristic plant parameters at the beginning of the water restriction period as medians ± median absolute deviation among all measured replicates

Parameter	Faba bean	Maize
A (m^2)	$0.036 \pm 0.006^{***}$	0.063 ± 0.007
L (m)	$41 \pm 9^{***}$	162 ± 8
U_{tot} (mL h^{-1})	5.0 ± 0.7	4.1 ± 0.9
K_{SL} (mL h^{-1} MPa^{-1})	8.3 ± 1.2	7.8 ± 2.5
$U_{tot}\ A^{-1}$ (mL h^{-1} m^{-2})	$138 \pm 9^{***}$	64 ± 11
$U_{tot}\ L^{-1}$ (mL h^{-1} m^{-1})	$0.119 \pm 0.022^{***}$	0.022 ± 0.005
$K_{SL}\ L^{-1}$ (mL h^{-1} MPa^{-1} m^{-1})	$0.20 \pm 0.02^{***}$	0.05 ± 0.02

Leaf area (A) and root length (L) were determined before the start of the measurements. U_{tot} and K_{SL} were averaged across the first day of measurement (four data points per light period, excluding data from the night) for each plant. Asterisks indicate significant difference between faba bean and maize. P-values were derived with a Mann–Whitney U test. P-values < 0.05 are indicated as *, < 0.01 as ** and < 0.005 as ***.

Figure 3A) showed a similar dependence on Ψ_{seq} as K_{SL}: it decreased exponentially below a Ψ_{seq} of −0.025 MPa. Note that g_s was only measured once per light period, at least four times a day. We determined the rate constant λ of the decline by exponentially fitting the data starting from the critical Ψ_{seq} of −0.025 MPa: $K_{SL} = A \cdot e^{\lambda(\Psi_{seq}+0.025)}$ or $g_s = A \cdot e^{\lambda(\Psi_{seq}+0.025)}$. Note that Ψ_{seq} is negative and thus a positive λ implies a decline of K_{SL}. Measured data on K_{SL} and g_s together with the exponential fit and the resulting λ are shown in Supplemental Figures S1 and S2 for each replicate separately. Both, K_{SL} and g_s, declined at a higher rate in faba bean compared with maize (Figure 3B). One maize replicate (bottom left panel in Supplemental Figure S2) had a very low initial U_{tot} (2.5 mL h^{-1}) leading to only moderate soil water depletion and thus a narrow range of Ψ_{seq} along which K_{SL} and g_s were fitted. This caused the strong outlier in Figure 3B. Excluding this outlier, the differences in λ for K_{SL} between faba bean and maize were significant (P-value < 0.05, derived with a Mann–Whitney U test). Among faba bean replicates, λ was similar for K_{SL} (14.5 MPa^{-1}) and g_s (16.6 MPa^{-1}). Note that for K_{SL} the median shown in Figure 3B was calculated among all 12 replicates. Stomatal conductance, however, was only measured for six of these replicates. Considering those six replicates only, the median of λ for K_{SL} is 16.0 MPa^{-1}, which was not significantly different from the λ of g_s. In maize, λ for g_s (4.7 MPa^{-1}, Figure 3B) was lower than for K_{SL} (9.5 MPa^{-1}). Considering only replicates for which stomatal conductance was measured results in a λ of 7.8 MPa^{-1} for K_{SL}. This was significantly higher (P-value < 0.05) than λ of g_s when the outlier mentioned above was excluded.

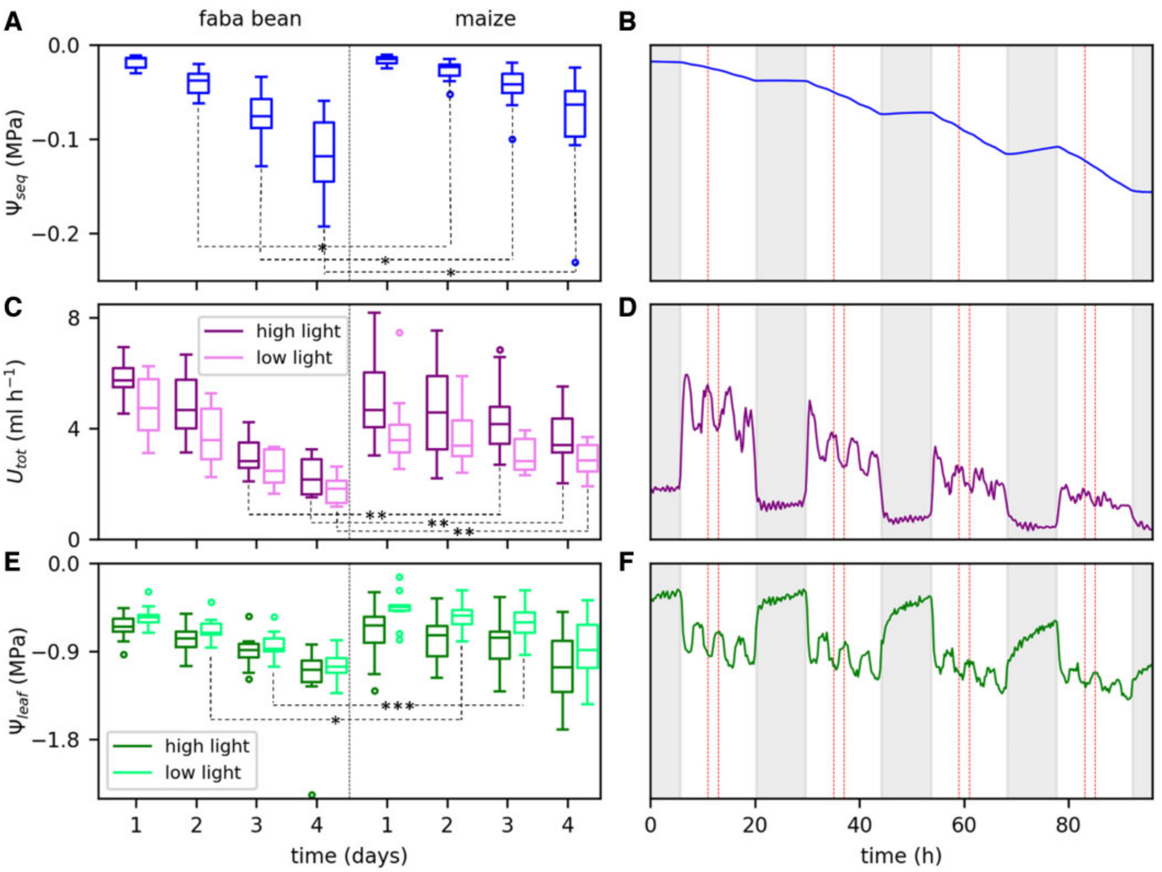

Figure 2 Reduction of the equivalent soil water potential (Ψ_{seq}), total root water uptake rate (U_{tot}), and leaf water potential (Ψ_{leaf}) during 4 days of soil drying. A, C, and E, Data of all replicates (faba bean $n = 12$, maize $n = 10$) as boxplots at selected time points. Different colors in (C) and (E) refer to the two different light levels. Horizontal lines are medians, boxes reach from the first to the third quartile. Whiskers mark the minimal (lower whisker) and maximal (upper whisker) data points within 1.5 times the interquartile range from the first and third quartile, respectively. Circles are outliers beyond the whiskers. We tested for significant differences in Ψ_{seq} U_{tot}, and Ψ_{leaf} between faba bean and maize at each selected time point. *P*-values were derived with a Mann–Whitney *U* test. *P*-values <0.05 are indicated by *, <0.01 by **, and <0.005 by ***. B, D, and F, The continuous time courses of the three parameters during the 4 days of soil drying for one example faba bean plant. Fluctuations of the observed parameters are caused by the fluctuating light intensity. Red dashed lines mark those points used for the boxplots. Shaded areas indicate the nonilluminated periods.

For an alternative interpretation of the decline rates λ, we calculated the equivalent soil water potential at which the initial conductance was reduced to 50% (Ψ_{seq_50}), as indicated by the vertical dotted lines in Figure 3A. Ψ_{seq_50} was calculated as

$$\Psi_{seq\_50} = -0.025\ \text{MPa} - \frac{\ln 2}{\lambda}.$$

For faba bean, K_{SL} and g_s were both reduced by 50% at a Ψ_{seq} of −0.07 MPa compared with the initial value at a Ψ_{seq} of −0.025 MPa (Table 3). Maize with generally lower λs, showed lower (more negative) values: Ψ_{seq_50} was −0.10 MPa for K_{SL} and −0.13 MPa for g_s.

To analyze how K_{SL} behaves on a daily scale, we determined K_{SL} as the slope of the relation between U_{tot} and Ψ_{leaf} at morning, afternoon, and evening separately (Supplemental Figure S3A). For faba bean, K_{SL} declined continuously during the day and was significantly lower in the evening compared with the morning on each day (Supplemental Figure S3B). However, each morning, K_{SL} tended to be greater than on the previous evening, consistent with the increasing Ψ_{seq} during the nights (Figure 2B). For maize, we also observed consistently lower K_{SL} in the evening compared with the morning of the same day, but on some days K_{SL} slightly increased from morning to afternoon or from afternoon to evening.

The hydraulic pathway from bulk soil to the leaf can be separated into a soil part (from bulk soil to the root surface) and a plant part (from root surface to the leaf). Here, we want to estimate whether the observed reduction in K_{SL} mostly happened in the soil or in the plant pathway. Deriving the hydraulic conductance of each part separately requires the water potential at the root surface $\Psi_{seq,\ sr}$ to be known. $\Psi_{seq,\ sr}$ can differ from Ψ_{seq} (referring to the bulk soil) due to a water depletion zone around the roots which can be estimated using a model (Carminati and

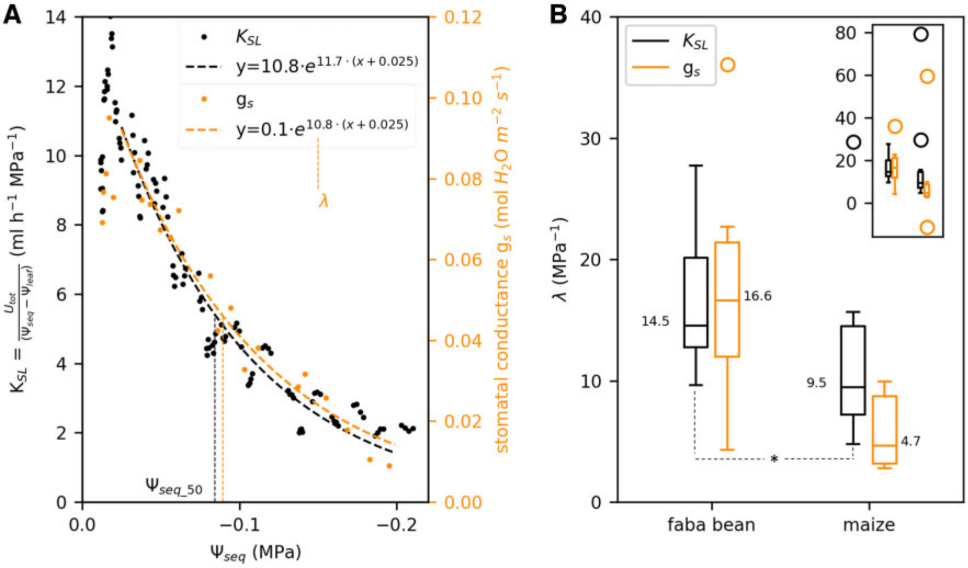

Figure 3 K_{SL} and g_s drop exponentially during soil drying at higher rates in faba bean than in maize. A, Example data of K_{SL} (black) and g_s (orange) at reducing Ψ_{seq} for one faba bean plant. Per light period we considered four measured data points of K_{SL} (black dots) and one measured data points of g_s (orange dots). Dashed lines follow an exponential fit of the form $K_{SL}(\Psi_{seq}) = A \cdot e^{\lambda(\Psi_{seq}+0.025)}$ or $g_s(\Psi_{seq}) = A \cdot e^{\lambda(\Psi_{seq}+0.025)}$ starting at a Ψ_{seq} of −0.025 MPa. Vertical dotted lines mark the values of Ψ_{seq} at which K_{SL} or g_s were reduced to 50% of their initial values at a Ψ_{seq} of −0.025 MPa. B, Variation of the rate constants λ obtained from the exponential fits of K_{SL} and g_s among faba bean and maize replicates. λ is a measure for the sensitivity of the conductance to soil drying. Characteristics of the boxplots are similar to Figure 2, A, C, and E. Numbers on the boxes indicate the median values. The inserted figure includes all outliers which are only partly shown in the main panel. g_s was only measured for six replicates while K_{SL} was measured for 12 (faba bean) and 10 (maize) replicates. Asterisks indicate significant differences (*P-value < 0.05, **P-value < 0.01, ***P-value < 0.005) between faba bean and maize, tested with a Mann–Whitney U test.

Table 3 Equivalent soil water potential at which K_{SL} and g_s were reduced to 50% of its initial value

Parameter	Faba bean	Maize
Ψ_{seq_50} (MPa) for K_{SL}	−0.07 ± 0.01	−0.10 ± 0.03
Ψ_{seq_50} (MPa) for g_s	−0.07 ± 0.02	−0.13 ± 0.08

Note that "initial" refers to the start of the exponential decay at a Ψ_{seq} of −0.025 MPa. Values are medians ± median absolute deviations.

Javaux, 2020). We estimated $\Psi_{seq,\ sr}$ for two different scenarios: (1) the full root length is actively involved in water uptake. (2) Only 50% of the root length takes up water. Figure 4 shows an example calculated $\Psi_{seq,\ sr}$ in comparison to Ψ_{seq} for one faba bean (Figure 4A) and one maize plant (Figure 4B). Generally, the difference between $\Psi_{seq,\ sr}$ and Ψ_{seq} increases with increasing water uptake rates per unit root length and decreasing Ψ_{seq}. For faba bean, considering 100% root length (cyan), there was only a marginal difference between $\Psi_{seq,\ sr}$ and Ψ_{seq} (black 1:1 line) (Figure 4A). Conservatively assuming that only 50% of the root length is active in water uptake led to a generally lower $\Psi_{seq,\ sr}$ (blue). In this scenario, $\Psi_{seq,\ sr}$ showed some fluctuations at the end of the measurement (Figure 4A) due to the dependency on the transpiration rate and thus the alternating light intensity. The difference between $\Psi_{seq,\ sr}$ and Ψ_{seq} was still low (<0.02 MPa) until a Ψ_{seq} of −0.10 MPa. At the end of the measurement, $\Psi_{seq,\ sr}$ was 0.05 MPa lower than Ψ_{seq}. For maize, in both scenarios, the differences between $\Psi_{seq,\ sr}$ and Ψ_{seq} were negligible.

Using the calculated $\Psi_{seq,\ sr}$, we could derive the conductance between bulk soil and root surface and between root surface and leaf (K_{RL}) separately. For this, we divided the total water uptake rate by the water potential difference between bulk soil and root surface and root surface and leaf, respectively. Since the estimation of $\Psi_{seq,\ sr}$ does not account for a loss of soil–root contact, the conductance of the interface between soil and root is included in K_{RL}. In the following, we compare K_{RL} to the overall conductance K_{SL}. For one faba bean replicate, Figure 5A shows an example K_{SL} (black, half-filled circles) and K_{RL} for 100% root length (cyan, half-filled circles) and 50% root length (blue, nonfilled circles). Over a broad range of Ψ_{seq}, K_{SL} and K_{RL} were almost identical, both showing the above-described exponential decay. Only below a Ψ_{seq} of −0.18 MPa, K_{RL} (50% root length) remained considerably higher than K_{SL} and even increased slightly. Note that at this point, K_{SL} was already reduced by 75%. Analogously to K_{SL} we quantified the decay of K_{RL} by determining the decay rate λ of an exponential fit. λ of K_{RL} was close to that of K_{SL} in all crops and simulated scenarios (Figure 5B).

These results suggest that the decline in K_{SL} is almost completely explained by a decline in K_{RL} and the effect of a reduced $\Psi_{seq,\ sr}$ was negligible. For further evidence, we created the hypothetical, opposite scenario and tested how

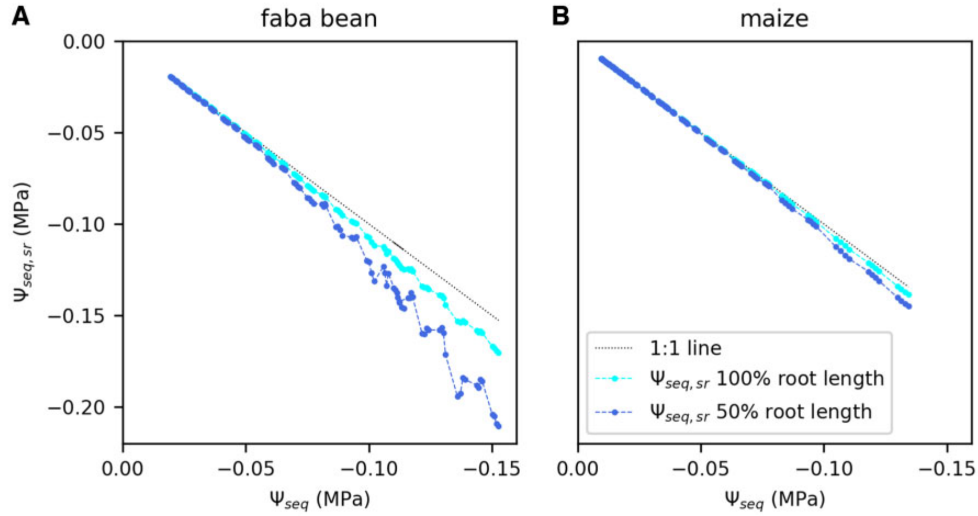

Figure 4 Estimated water potential at the root surface ($\Psi_{\text{seq, sr}}$) as a function of the bulk soil water potential (Ψ_{seq}). Data are an example shown for one faba bean (A) and one maize plant (B). Water potential at the root surface was calculated for the full measured root length and half of the measured root length. Dotted line is the 1:1 line.

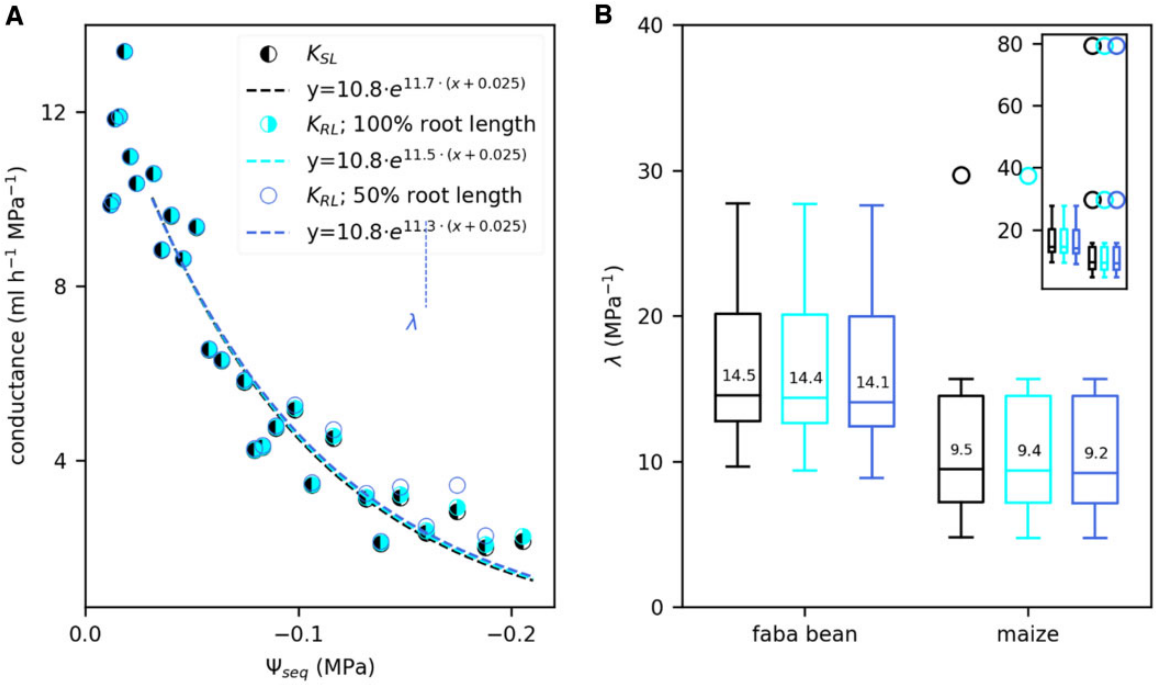

Figure 5 Comparison between the hydraulic conductance between root surface and leaf (K_{RL}) and K_{SL} throughout the soil drying period. A, K_{RL} compared with K_{SL}, as a function of Ψ_{seq}, example shown for one faba bean plant (same plant as in Figure 3A). K_{RL} was determined using the calculated water potential at the root surface for the full root length (cyan) or half of the root length (blue). We exponentially fitted the data (dashed lines) to determine the rate constants λ starting at a Ψ_{seq} of −0.025 MPa. For reasons of clarity, we plotted only one data point per light period here but derived the exponential fit using four data points per light period, analogously to Figure 3. B, Boxplots of the rate constants λ obtained from the exponential fits of K_{SL} (black, same data as in Figure 3B) and K_{RL} considering the full root length (cyan) or half of the full root length (blue) for faba bean (n = 12) and maize (n = 10). Characteristics of the boxplots are similar to Figure 2, A, C, and E. The main panel does not include all outliers which are shown in the inserted figure.

strong $\Psi_{\text{seq, sr}}$ would need to drop to fully explain the measured decline in K_{SL} (Supplemental Figure S4). The theoretical $\Psi_{\text{seq, sr}}$ was calculated using a variation of Equation (1) for the pathway between root surface and leaf:

$$\Psi_{\text{seq, sr}} = \Psi_{\text{leaf}} - \frac{U_{\text{tot}}}{K_{\text{RL}}}. \tag{2}$$

For this scenario, K_{RL} was assumed to be constant and approximated by the initial K_{SL} at Ψ_{seq} = −0.025 MPa. The

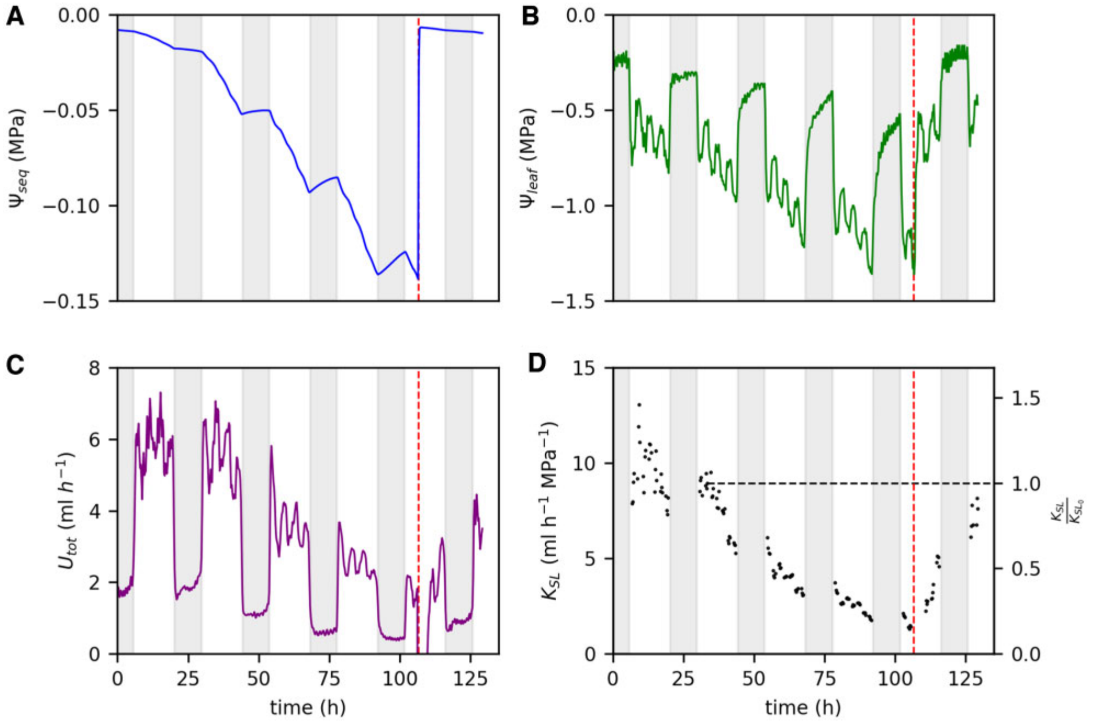

Figure 6 Recovery of different hydraulic parameters upon rewatering after 4 days of water restriction for one faba bean plant. Parameters are Ψ_{seq} (A), Ψ_{leaf} (B), U_{tot} (C), and K_{SL} (D). Vertical dashed lines mark the time point of rewatering. Horizontal dashed line in (D) marks the initial value of K_{SL} at a Ψ_{seq} of −0.025 MPa ($K_{SL,0}$). Nights are indicated by the shaded areas.

calculation shows that if K_{RL} was constant, $\Psi_{seq,\ sr}$ would need to decrease <-0.6 MPa at a Ψ_{seq} of −0.1 MPa and <-1.2 MPa at a Ψ_{seq} of −0.2 MPa to account for the reduction in K_{SL}. Then, we tested how close the estimated $\Psi_{seq,\ sr}$, using the water depletion model, could get to this hypothetical line by considering only a reduced fraction of root length or root diameter (Supplemental Figure S4). For none of the tested fractions, the estimated $\Psi_{seq,\ sr}$ was comparable to the theoretical one at constant K_{RL} either in terms of amplitude or shape of the decline. This analysis supports our conclusion that most of the decline in K_{SL} did not occur between bulk soil and root surface.

We compared the root architectures between faba bean and maize to further elucidate the different responses to soil drying between the species. As an example shown in Supplemental Figure S5A, faba bean had a greater fraction of root length in the top 10 cm while in maize the fraction <30 cm was greater. For quantification, we determined the depth D_{50}, at which 50% of the total root length was reached, which was significantly deeper in maize (20 cm, Supplemental Figure S5D) than in faba bean (12 cm). The resulting pattern of water uptake rates ($\hat{U}_P$) was initially contrasting, with a greater fraction of water uptake in shallow layers for maize compared with faba bean (Supplemental Figure S5B). This changed toward the last day of measurement when the fraction of $\hat{U}_P$ <30 cm was greater in maize than in faba bean (Supplemental Figure S5C). These observations were confirmed by the D_50 of $\hat{U}_P$, which was deeper in faba bean for the first day but shifted to a significantly deeper layer in maize for the last day (Supplemental Figure S5D).

After 4 days of soil drying, we rewatered four of the faba bean plants to analyze how the measured parameters would recover. The example in Figure 6 shows the data for one faba bean plant. Within 30 min after rewatering, Ψ_{seq} increased from −0.14 to −0.01 MPa (Figure 6A) which is comparable to the initial value on the first day. Within 1 h after rewatering, Ψ_{leaf} increased from −1.3 to −0.8 MPa (Figure 6B) which was only slightly lower compared with the initial Ψ_{leaf} of −0.7 MPa. During the next 20 h, Ψ_{leaf} further increased resulting in values of −0.6 MPa which is even lower compared with the start of the measurement. In contrast, the recovery of U_{tot} was slower (Figure 6C): 5 h after rewatering, U_{tot} at high light level was similar to the high light level before rewatering (around 1.9 mL h^{-1}). Four hours later, U_{tot} had increased to 3.1 mL h^{-1}. During the following night, U_{tot} further increased steadily and reached around 4.0 mL h^{-1} on the next morning (21 h after rewatering) which is around 40% lower compared with the initial values on the first day (6.5 mL h^{-1}). Compared with the value at a Ψ_{seq} of −0.025 (horizontal dotted line in Figure 6D), K_{SL} had declined to around 17% before rewatering (Figure 6D). Upon rewatering, K_{SL} steadily increased, up to 50% of the initial value after 8 h. The next morning, within 20 h after rewatering, K_{SL} had recovered to around 85%. For the other three rewatered faba bean plants, measurements were taken only up to 5.5 h after rewatering. Nevertheless, trends were similar (Supplemental Figure S6, A–F): Ψ_{leaf} reached the initial value within several hours after rewatering while U_{tot} recovered much slower. Data from a separate experiment on two 6-weeks-old faba bean plants indicate that full recovery of U_{tot} took 40 h after rewatering (Supplemental Figure S6, G–H).

Discussion

The hydraulic conductance between soil and leaf declined exponentially with reducing soil water potential. In faba bean, this decline occurred at a higher rate than in maize which partly explains that faba bean closed its stomata more quickly. Estimations of the water potential at the root surface suggest that not only the soil conductance but also the conductance between root surface and leaf dropped. This was supported by an incomplete recovery, 22 h after rewatering.

We analyzed to what extent the hydraulic conductance between soil and leaf (K_{SL}) is affected by soil drying. For that we continuously and noninvasively measured the total root water uptake rate (U_{tot}) and the equivalent water potential in the bulk soil (Ψ_{seq}) with the soil water profiler (SWaP) and the leaf water potential (Ψ_{leaf}) on faba bean and maize during 4 days of soil drying. The initial conductance at the beginning of soil drying was higher in faba bean (8.3 mL h^{-1} MPa^{-1}, or 3.5 mmol m^{-2} s^{-1} MPa^{-1} when normalized by leaf area) than in maize (7.8 mL h^{-1} MPa^{-1} or 1.9 mmol m^{-2} s^{-1} MPa^{-1}). These values fit in the range reported in the literature for lupine (*Lupinus albus* L.) (13.7 mL h^{-1} MPa^{-1}; Hayat et al., 2019) *Tanacetum cinerariifolium* and *Callitris rhomboidea* (both around 4.5 mmol m^{-2} s^{-1} MPa^{-1}; Bourbia et al., 2021) or olive (*Olea europaea* L. var. *arbequina*) (0.7 mmol m^{-2} s^{-1} MPa^{-1}; Rodriguez-Dominguez and Brodribb, 2020). Among replicates, K_{SL} consistently declined exponentially as a function of the equivalent soil water potential starting at a Ψ_{seq} of −0.025 MPa (Figure 3A). We determined the rate constant λ of this decline by exponentially fitting K_{SL} (Ψ_{seq}). The rate constant is a measure for how sensitive the conductance is to soil drying: A high λ reflects a fast decline of the conductance and thus high sensitivity to a reducing Ψ_{seq}. Among faba bean replicates we found a λ of 15 MPa^{-1}. This is equivalent to 50% reduction of K_{SL} within a range of Ψ_{seq} from −0.025 to −0.07 MPa. In maize, λ was lower (10 MPa^{-1}) and K_{SL} dropped to 50% only at a Ψ_{seq} of −0.10 MPa. These high decline rates are probably caused by the sandy soil substrate. Hayat et al. (2019) reported similar values for lupine plants in a sandy soil (90% loss of conductance at a Ψ_{seq} of −0.17 MPa). A study among different sugarcane (*Saccharum* spp. hybrid) cultivars reports an even faster decline, with an almost complete loss of conductance before Ψ_{soil} reached −0.1 MPa (Saliendra and Meinzer, 1989). On the other hand, slower declines have been observed as well, ranging from a 50% loss of conductance below a Ψ_{soil} of −1.0 MPa in *T. cinerariifolium* and *Callitris rhomboidei* (Bourbia et al., 2021) to a 30%–60% loss only below a Ψ_{soil} of −10 MPa in desert succulents (Nobel and Cui, 1992). The rate constants observed in our study highlight the impact of the K_{SL} decline on the plant response to soil drying: For faba bean, sustaining the initial transpiration rate, and thus stomatal opening, would lead to a drop in Ψ_{leaf} as little as −0.045 MPa to compensate the reduced Ψ_{seq} from −0.025 to −0.07 MPa. Due to the 50% reduction of K_{SL}, however, keeping the stomata open would result in a much greater drop in Ψ_{leaf} by −0.6 MPa (see Equation (1)). Given these values, it is highly likely that the drop of K_{SL} affects stomatal conductance. Note that for the considerations described above, we referred to the water potential in the bulk soil. Whether a drop of the water potential around the roots accounted for the observed drop in K_{SL} is discussed further below.

The stomatal conductance (g_s), measured with a portable LiCor 6400 photosynthesis system for selected plants, also declined exponentially starting at a Ψ_{seq} of −0.025 MPa (Figure 3A). Again, we quantified the exponential decay by determining the rate constant λ. In the case of g_s, λ is an estimate for how strong the stomata respond to soil drying. A higher λ indicates a higher reduction of the stomatal conductance at a given Ψ_{seq}, independent of how fast Ψ_{seq} was reduced. Like for K_{SL}, the decline rate for g_s was lower in maize compared with faba bean. This can be interpreted as follows: at a given level of soil drying, measured as Ψ_{seq}, faba bean experienced a stronger reduction of water availability than maize due to the stronger decline of the hydraulic conductance between bulk soil and leaf. This led to a stronger reduction of the stomatal conductance. The exact mechanism which couples K_{SL} and g_s is still unclear. Different, nonhydraulic signaling cascades such as enhanced abscisic acid biosynthesis (Liang et al., 1997), reduced cytokinin supply (Blackman and Davies, 1985), or suppressed stringolactone biosynthesis (Visentin et al., 2016) have been suggested to propagate from dehydrated roots to the shoot and initiate stomatal closure. In this case, K_{SL} and g_s would be linked. A recent review, however, concludes that most of the stomatal regulation happens hydraulically via the leaf water potential (Buckley, 2019). We, therefore, postulate that K_{SL} and g_s are indirectly linked by the balancing of Ψ_{leaf} and the transpiration rate (Equation (1)) although our data do not allow a clear distinction between transpiration rate and g_s. Both were closely linked since the VPD was kept constant by the climate chamber control and water-cooling of the LED panel. Irrespective of the above, our data suggest that the variation of stomatal sensitivity among species can partly be attributed to a variation of the K_{SL} sensitivity. Potential causes for the variation of the K_{SL} sensitivity among species are discussed below. However, while in faba bean, K_{SL} and g_s, in agreement with several recent studies (Rodriguez-Dominguez and Brodribb, 2020; Abdalla et al., 2021; Bourbia et al., 2021), declined almost in parallel, in maize g_s declined at a 50% lower rate than K_{SL} (Figure 3B). This indicates that in addition to its dependence on K_{SL}, stomatal sensitivity is partly a species-inherent trait as commonly assumed (Tardieu and Simmoneau, 1998; Klein, 2014).

We used Ψ_{seq} as a measure for the extent of soil drying that the plant is exposed to. Ψ_{seq} is the distribution of soil water potential weighted by the distribution of root conductance ($\hat{U}_P$) which is directly linked to the root distribution. During the 4 days of soil drying, Ψ_{seq} was generally lower in faba bean than in maize, especially on the last 2 days (Figure 1A). Since the total water uptake rates were comparable or, during the last 2 days even greater in maize (Figure 1C), the differences in Ψ_{seq} are most likely explained by the different root architectures between the two species: maize had a higher fraction of deep roots than faba bean (Supplemental Figure S5, A and D) and thus was able to acquire a higher fraction of water from deeper layers at the later stages of the experiment (Supplemental Figure S5, C and D). Since the soil water potential usually is less negative in those deeper layers, the weighted Ψ_{seq} was less negative in maize than in faba bean. Note that by using Ψ_{seq}, we account for the effect of root distribution on K_{SL} which is not case when the more common average soil water potential or soil water content are used as a measure for soil drying.

Explaining the different rate constants between faba bean and maize starts with determining which part of the hydraulic pathway between bulk soil and leaf caused the observed drop in K_{SL}. Recently, a water depletion zone around the roots has been proposed to account for a major loss of hydraulic conductance from soil to plant which could initiate stomatal closure (Carminati and Javaux, 2020). The water depletion zone would cause a much lower water potential at the root surface $\Psi_{seq,\ sr}$ than in the bulk soil Ψ_{seq}. Based on a model by Carminati and Javaux (2020), $\Psi_{seq,\ sr}$ can be calculated for given soil hydraulic properties. The difference between $\Psi_{seq,\ sr}$ and Ψ_{seq} increases with increasing water uptake rate per root length, decreasing root radius, and decreasing Ψ_{seq}. We observed a steeper decline of $\Psi_{seq,\ sr}$ with Ψ_{seq} in faba bean than in maize. Since the total water uptake rates were comparable between the two species, the differences in $\Psi_{seq,\ sr}$ are caused by differences in the total root length and the average root diameter. Faba bean had a greater average root radius but a smaller total root length than maize (Table 2) which is typical since dicots usually have a lower specific root length than monocots (Read et al., 2010). As demonstrated in Supplemental Figure S4, root length had a stronger impact on the estimated $\Psi_{seq,\ sr}$ than diameter. Therefore, the steeper decline of $\Psi_{seq,\ sr}$ in faba bean is explained by the much lower total root length compared with maize. Nevertheless, the calculated difference between $\Psi_{seq,\ sr}$ and Ψ_{seq} (Figure 4) and thus the impact on the decline of K_{SL} was marginal for both faba bean and maize (Figure 5). In another study, the drop of $\Psi_{seq,\ sr}$ could explain experimental data on the loss of soil–plant conductance when only 0.7%–2.5% of the measured root length was considered in the water uptake process (Hayat et al., 2020). From the magnetic resonance imaging (MRI) images, we know that parts of the root system were close to the pot borders in our experiment. This might have limited the access to soil water leading to a reduction of the active root length, however, not to such a drastic extent. Nevertheless, we tested the effect of halving the measured root length which resulted in a considerably lower $\Psi_{seq,\ sr}$ for faba bean at the end of the measurements (Figure 4) but had no remarkable impact on K_{SL} (Figure 5). This indicates that even though the soil conductivity around the roots drops sharply (Supplemental Figure S7) at the measured soil water regimes, it stays considerably greater than K_{RL}. Therefore, our data suggest that most of the K_{SL} decline did not occur in the soil zone close to the roots. Note that we used a total root length and average root radius for the estimation of $\Psi_{seq,\ sr}$ and did not consider the spatial root distributions. Nevertheless, our analysis shows that even though we probably overestimate local root length densities or root radius, the model estimations of $\Psi_{seq,\ sr}$ are far from explaining the decline in K_{SL} (Supplemental Figure S4).

To further clarify whether the drop of K_{SL} occurred inside or outside the plant, we need to consider a potential loss of the soil–root contact. Dehydration of root tissue in drying soils can lead to root shrinkage and thus enhance the reduction of the soil–root contact (Nobel and Cui, 1992; North and Nobel, 1997; Carminati et al., 2009). The estimation of $\Psi_{seq,\ sr}$ does not account for a reduced root soil contact. Therefore, the estimated decline of K_{RL} (Figure 5) includes the decreasing conductance resulting from a potential shrinkage of roots. Rodriguez-Dominguez and Brodribb (2020) observed a reduced conductance of the soil–root interface, attributed to root shrinkage, to mainly cause a 74% drop in the overall plant conductance during soil drying. Compared with our study, this drop is in the same order of magnitude but occurred at a much lower water potential (Ψ_{stem} between −1.0 and −4.0 MPa (Rodriguez-Dominguez and Brodribb, 2020) compared with Ψ_{leaf} between −0.6 and −1.1 MPa in our study (Figure 2)). However, X-ray CT studies on lupin (Carminati et al., 2013), faba bean (Koebernick et al., 2018), and maize (Duddek et al., 2022) revealed substantial root shrinkage leading to air gaps between soil and root starting already at a relatively high Ψ_{soil} of −0.01 to −0.02 MPa. This is comparable to the critical Ψ_{seq} of −0.025 MPa at which the decline of K_{SL} started in our study. Carminati et al. (2013) suggested that a slightly reduced soil conductivity led to the initial dehydration and shrinkage of the roots, which then, in a self-enhancing process, would cause an additional drop of the conductance and thus additional root shrinkage. In turn, the temporary recovery of K_{SL} that we observed during the night (Supplemental Figure S3) could result from root rehydration and thus a recovery of soil–root contact. This would fit the observation of a diurnal variation of root diameter with shrinkage during the day, and swelling during the night (Huck et al., 1970). However, in faba bean, root shrinkage was shown to be almost fully reversed within 3 h after rewatering (Koebernick et al., 2018). In our study, the K_{SL} of faba bean had not fully recovered within 20 h after rewatering (Figure 6D and Supplemental Figure S6) while Ψ_{seq} was almost fully recovered within 30 min (Figure 6A). This suggests that a reduction of the conductance between bulk soil and root surface was not the only reason for the reduced K_{SL}.

It is, therefore, likely that the drop of K_{SL} partly occurred inside the plant including the radial pathway from root surface into the root xylem and the axial pathway from root xylem into the leaf. Root aquaporin activity has been shown to modulate the loss of root hydraulic conductance during soil drying for various species (Martre et al., 2001; Aroca et al., 2006; Galmés et al., 2007; Perrone et al., 2012; Grondin et al., 2016; Rodríguez-Gamir et al., 2019). Other studies report a close linkage between a reduced radial root conductivity and suberization of the root endodermis (Cruz et al., 1992; Lo Gullo et al., 1998) or lacunae formation in the tissue of fine roots (Cuneo et al., 2016) or both (North and Nobel, 1991). Whereas the aquaporin contribution to root conductance was shown to fully recover within 5 h after rewatering (Rodríguez-Gamir et al., 2019), lacunae formation (Cuneo et al., 2016) and suberization (Lo Gullo et al., 1998) are permanent and require growth of new roots to restore K_{SL}. This could explain the incomplete recovery of K_{SL} 20 h after rewatering (Figure 6D) in our study. The extent of reduced conductance caused by changes in gene expression and root morphology varies among species. This is highlighted by two grapevine cultivars, for which differences in the reduction of root hydraulic conductance could be assigned to a difference in aquaporin expression during drought (Vandeleur et al., 2009). Another study on two different grapevine rootstocks revealed a stronger decline of root hydraulic conductance to correspond to a faster suberization (Barrios-Masias et al., 2015). If such variations occur even within the same species, it is likely that the different rate constants of K_{SL} between faba bean and maize in our study are partly caused by differences in root morphological changes upon soil drying.

Although xylem embolism is predominantly observed in trees below a stem water potential of −2.0 MPa (Cochard, 2006), some studies suggest that it also needs to be considered in crops: in maize, xylem embolism was shown to cause a 25% loss of conductance in leaves at a Ψ_{soil} of −0.25 MPa (Ryu et al., 2016) and 23% loss of conductance in stems at a Ψ_{stem} of −1.0 MPa (Li et al., 2009). Another study on maize leaves, however, shows that the conductance loss due to xylem embolism is less than 15% until a Ψ_{stem} of −1.5 MPa is reached (Cochard, 2002). Since in our experiments, Ψ_{leaf} mostly remained > -1.2 MPa (Figure 2E) and the decline of K_{SL} started at a Ψ_{seq} of −0.025 MPa, we conclude that a reduced xylem conductance due to embolism did not cause the decline in K_{SL}.

In summary, our estimations of $\Psi_{seq,\ sr}$ and the slow recovery after rewatering indicate that the decrease in K_{SL} partly occurred in the hydraulic pathway between root surface and leaf, and thus inside the plant. This should not obscure the fact that a reduction in the soil water potential around the roots with, however only a marginal effect on K_{SL}, is likely to be the initial cause leading to a decreasing plant hydraulic conductance. The greater extent of water depletion around faba bean roots compared with maize roots at a given Ψ_{seq} (Figure 4) could have led to a stronger response of K_{SL} in faba bean. From this perspective, the significant differences in root length densities (Table 2) might be the crucial factor to explain the differences of the decline in K_{SL}, and ultimately in g_s, between the two species. Additionally, faba bean generally had a greater initial stomatal conductance than maize (Supplemental Figures S1 and S2) which also contributed to the initially greater water uptake rates per unit root length (Table 2). The resulting dehydration of the root tissue could then have triggered a decrease of radial root conductance by alterations in the gene expression (aquaporins) or in root morphology (suberization) which amplifies the reduction of K_{SL}. But why would the plant initiate such a drastic decline of K_{SL} when the water supply toward the roots is only moderately constrained? As suggested by Carminati et al. (2020), stomatal closure at an early stage of water stress can prevent a severe drop of the water potential around the roots. Since leaf water status seems to be the principal factor regulating stomatal conductance (Buckley, 2019), we speculate that the decrease in K_{SL} is a mechanism to force stomatal closure by enhancing the drop in Ψ_{leaf}. Such a strategy would amplify the initial water stress but could be beneficial in the long-term by avoiding a steep water potential gradient toward the root surface. In addition, the decrease of K_{SL} in roots in drier soil layers could be accompanied by root growth in wetter soil layers. This would lead to lower water uptake rates per unit root length and thus help to avoid excessive rhizosphere drying. However, it should be kept in mind that due to the potential loss of soil–root contact, it remains difficult to evaluate to what extent the plant is in control of the K_{SL} decline. Despite this speculative aspect, our study clearly highlights that how a plant responds to water stress, strongly depends on how sensitive K_{SL} is to soil drying. This has different implications on the widely used Feddes model (Feddes et al., 1978; Feddes et al., 2001), at least when plants grow in a loamy sand:

(1) The range of Ψ_{seq} at which the transpiration rate is sustained is very narrow because K_{SL} starts already declining at $\Psi_{seq} = -0.025$ MPa.
(2) The slope of the declining part of the water stress curve is not expected to be constant anymore since it depends on K_{SL} (Couvreur et al., 2015).
(3) The point at which transpiration reaches zero is much higher (less negative) than the permanent wilting point of −1.5 MPa.
(4) The extent of reduced water availability at a given Ψ_{seq} is not constant anymore but varies among species due to a varying K_{SL} sensitivity to soil drying.

To obtain a more precise description of plant responses to soil drying, the reduction of K_{SL} should be taken into account when calculating water stress curves. This could be realized by the rate constant λ of the declining $K_{SL}(\Psi_{seq})$ which, however, varies among species.

Conclusion

We observed a strong reduction of the hydraulic conductance between soil and leaf, K_{SL}, at even moderately low soil water potentials. This implies that the main hydraulic impairment during soil drying does not only result from the reduced soil water potential but from the reduced hydraulic conductance between soil and leaves. Therefore, how plants respond to a gradually reduced soil water potential strongly depends on the extent of the K_{SL} reduction. Here, we show that between two species, faba bean and maize the sensitivity of K_{SL} differs as quantified by the rate constant of the exponential decline. In faba bean, this rate constant is higher than in maize implying a faster reduction of the water availability at a given soil water potential and thus a stronger impulse for stomatal closure. In agreement with that, also the stomatal conductance declined at a higher rate in faba bean than in maize suggesting that varying stomatal sensitivity among species partly arises from a varying susceptibility of K_{SL}. A potential origin for the differences in the K_{SL} susceptibility could be the initial water uptake rate per root length which was six times higher in faba bean than in maize. Our data suggest that the K_{SL} decline partly occurs inside the plant which could be a strategy to avoid a severe water depletion zone around the roots and thus improve plant performance during a longer drought. However, additional studies are needed to further disentangle the role of the soil and plant in response to drought. This could be realized by comparing the K_{SL} decline among plants grown in different soils with varying hydraulic properties.

Materials and methods

Plant growing conditions and experimental design

Faba bean (*V. faba*, $n = 12$) and maize (*Z. mays*, $n = 10$) plants were grown in PVC pipes (50 cm high, inner diameter: 8.1 cm) filled with a sandy loam containing 73.3% sand, 23.1% silt, 3.6% clay, as reported by Pohlmeier et al. (2009), mixed with 20% (v) coarse sand (0.7–1.4 mm). The water retention curve of the substrate is shown in Supplemental Figure S7. A total substrate volume of 2.32 L was filled into the pots to a height of 45 cm resulting in a bulk density of 1.47 kg/L. Plants were grown in a climate chamber at the Research Centre Jülich under a constant temperature of 21.5°C ± 0.2°C and a VPD_{air} of 1.49 kPa. Until the start of the measurements, plants were regularly watered to maintain an average volumetric soil water content (θ) of around 20%. Once a week, plants were fertilized using an NPK nutrient salt (Hakaphos Red; Compo Expert; 8% N, 12% P, 24% K), diluted in water at 0.3% (v/v). Plants were illuminated using a water-cooled LED panel (3200K, 5 × 5 LEDs 20W each) for 14 h during the day. Within these 14 h, light intensity was regulated to alternate in 2-h periods of a high (PPFD of 1,000 μmol m^{-2} s^{-1}) and a low light intensity (PPFD of 500 μmol m^{-2} s^{-1}) resulting in a daily light integral of 39.6 mol m^{-2} d^{-1}. The alternating light pattern enabled us to derive water uptake profiles with the SWaP as described below. At an age between 4 and 5 weeks after sowing, selected according to a preferably similar water uptake rate among replicates, root system of the plants were imaged with MRI. Then, water supply was withheld for 4 days. During these 4 days U_{tot} and Ψ_{seq} were determined with the SWaP. Simultaneously, Ψ_{leaf} and the leaf gas exchange were measured with a psychrometer and a LiCor 6400, respectively. After the 4 days of soil drying, some of the plants were rewatered to observe if U_{tot}, Ψ_{seq}, and Ψ_{leaf} recovered.

Root length measurement with MRI

Right before the start of the soil drying experiment, root length distributions of the plants were determined using noninvasive imaging with MRI. A 4.7T vertical wide bore (310 mm) magnet (Magnex, Oxford, UK) and a gradient coil (ID 205 mm [MR Solutions]) generating gradients up to 400 mT/m were used in our setup. An MR Solutions (Guildford, UK) console was used to control the measurements. MRI data were analyzed with NMRooting software (van Dusschoten et al., 2016) yielding the total root length and root length distributions at a 1-cm vertical resolution. For a similar MRI setup, roots with a diameter <200–300 μm were below the detection limit (van Dusschoten et al., 2016). In an earlier experiment with 4-weeks-old faba bean and maize plants, grown under the same conditions, we compared a destructive measurement (harvest and scanning roots) of the total root length to the noninvasive measurement with MRI and NMRooting. For faba bean, 70.5% of the destructively determined root length was detected with MRI. For maize with generally thinner roots, 18.0% were detected. To correct for that, we multiplied the total root length measured with MRI in this study by the respective correction factors (1.4 for faba bean and 5.6 for maize). Additionally, we obtained the average root radius (r_0) of both species from the scanning of harvested roots in the earlier experiment.

SWaP measurements of U_{tot} and Ψ_{seq}

We used the recently developed SWaP (van Dusschoten et al., 2020) to continuously scan the profile of the volumetric soil water content (θ) which enabled us to derive both U_{tot} and Ψ_{seq}. In principle, the SWaP measurement is based on integrating the pots with the soil columns into a resonator circuit and then determining the resonance frequency which largely depends on θ. To this end, a sensor with two opposing copper plates (7 × 5 cm^2) coupled to a coil partially encloses the pots with soil. The resonance frequency is determined by applying a frequency sweep between 150 and 220 MHz using a virtual network analyzer (DG8SAQ, VNWA3, SDR-Kits, UK). The sensor moves upward the pots in 1-cm steps and determines the resonance frequency at each step. This yields a vertical profile of the resonance frequency consisting of 45 values. The profiles were measured every 15 min which, for four pots simultaneously, took around 11 min. The sensors were calibrated using soil samples with a defined θ ranging from 2% to 30% in 2% steps which enabled us to transfer the resonance frequency profiles into θ profiles. Since the sensors have a height of 12 cm and measurements were taken in 1-cm steps, the measured θ value in each layer is a convolution of the sensors' field strength distribution and the θ values from the adjacent layers. We, therefore, applied a deconvolution of the measured θ profiles. To avoid an error amplification by the deconvolution, we used a regularization term to constrain the deconvolved profiles.

For the following analysis, we treat the 45-cm high soil column as consisting of 45 stacked soil layers of 1 cm height, each with a uniform θ. Since both evaporation from the topsoil, which was covered with plastic, and water drainage at the bottom of the pots were negligible we could derive U_{tot} as the sum of water depletion rates in each layer:

$$U_{\mathrm{tot}}(t) = \sum_{i=1}^{45} \frac{\partial\theta(z_i,t)}{\partial t}, \tag{3}$$

with time t and depth of each layer z_i, ranging from 0 to 44 cm.

The equivalent soil water potential (Ψ_{seq}) as proposed by Couvreur et al. (2012) is the distribution of soil water potential (Ψ_{soil}) weighted by the plant-driven RWU distribution ($\hat{U}_{\mathrm{P}}$) which is the distribution of root hydraulic conductance:

$$\Psi_{\mathrm{seq}}(t) = \sum_{i=1}^{45} \Psi_{\mathrm{soil}}(z_i,t) \cdot \hat{U}_{\mathrm{P}}(z_i,t). \tag{4}$$

Note that Ψ_{seq} is defined for the pot as a whole and does not depend on z. $\hat{U}_{\mathrm{P}}$ in Equation (4) is equivalent to the standard sink fraction used by Couvreur et al. (2012) which is the profile of RWU rates under conditions of uniformly distributed soil water potential. Note that $\hat{U}_{\mathrm{P}}$ is normalized and thus $\sum_{i=1}^{45} \hat{U}_{\mathrm{P}}(z_i,t) = 1$. From Equation (4), we see that the Ψ_{soil} in layers with a higher root conductance (roughly corresponding to a higher root length) contributes more to Ψ_{seq} than the Ψ_{soil} in layers with a lower root conductance. In the case of a uniform Ψ_{soil} distribution, Ψ_{seq} and Ψ_{soil} are equal. In the following paragraphs, we explain how we obtained Ψ_{soil} and $\hat{U}_{\mathrm{P}}$ to calculate Ψ_{seq}.

The water retention curve of the soil substrate (Supplemental Figure S7) used in our experiments was measured with an evaporation method (Peters and Durner, 2008) and the HYPROP setup (METER Group, Munich, Germany). We used the Brooks–Corey parameters determined by fitting the soil water retention curve to derive the soil matric potential (h) and the soil conductivity (K_{Soil}) in each layer:

$$h(\theta,\ z_i) = \alpha^{-1}\left(\frac{\theta(z_i)-\theta_r}{\theta_s-\theta_r}\right)^{-\frac{1}{\lambda_b}} \tag{5}$$

$$K_{\mathrm{soil}}(\theta,\ z_i) = K_{\mathrm{sat}} \cdot (\alpha \cdot h(\theta,\ z_i))^{\tau}. \tag{6}$$

The Brooks–Corey parameters are saturated water content θ_s, residual water content θ_r, air entry pressure head α^{-1} (cm) which depends on the soil pore sizes, a dimensionless pore size index λ_b, the saturated soil conductivity K_{sat} and τ which is derived from λ_b with $\tau = -2 - 3 \cdot \lambda_b$. The values of all Brooks–Corey parameters of our soil substrate are given in Table 4. The local Ψ_{soil} was obtained by adding a gravity component to h:

Table 4 Brooks–Corey parameters of our soil substrate derived from the water retention curve

Parameter	Value
θ_s	0.4 mL cm^{-3}
θ_r	0.0 mL cm^{-3}
α	0.072 cm^{-1}
λ_b	0.43
K_{sat}	113.7 cm d^{-1}
τ	−3.29

$$\Psi_{\mathrm{soil}}(\theta,\ z_i) = (h(\theta,\ z_i) - z_i) \cdot 9.8 \cdot 10^{-5}\,\frac{\mathrm{MPa}}{\mathrm{cm}}. \tag{7}$$

A detailed description on deriving $\hat{U}_{\mathrm{P}}$ from SWaP measurements is provided by van Dusschoten et al. (2020) which we will summarize here. The soil water depletion rate $\frac{\partial\theta}{\partial t}$ in each layer is the sum of the RWU rate (RWU)and redistributive soil water flow (rSWF) between adjacent layers:

$$\frac{\partial\theta(z_i,t)}{\partial t} = \mathrm{RWU}(z_i,\ t) + \mathrm{rSWF}(z_i,\ t). \tag{8}$$

Analogously to the model of Couvreur et al. (2012), we write RWU as the sum of U_{P} and a second term which corrects U_{P} for vertical gradients in the soil water potential. We call this second term soil-driven RWU redistribution (U_{S}):

$$\mathrm{RWU}(z_i,\ t) = U_{\mathrm{P}}(z_i,\ t) + U_{\mathrm{S}}(z_i,\ t), \tag{9}$$

with $U_{\mathrm{P}}(z_i,\ t) = \frac{\hat{U}_{\mathrm{P}}(z_i)\cdot\ U_{\mathrm{tot}}(t)}{V}$, total pot volume V, and $U_{\mathrm{tot}}(t) = \sum_{i=1}^{45}\frac{\partial\theta(z_i,t)}{\partial t}$. Note that U_{S} is negative in layers with $\Psi_{\mathrm{soil}} < \Psi_{\mathrm{seq}}$ (lower water uptake rates compared with conditions of uniform Ψ_{soil}) and positive in layers with $\Psi_{\mathrm{soil}} > \Psi_{\mathrm{seq}}$ (higher water uptake rates compared with conditions of uniform Ψ_{soil}). In total, the negative corrections just compensate the positive ones and thus $\sum_{i=1}^{45} U_{\mathrm{S}}(z_i,t) = 0$. Similarly, also rSWF sums up to zero: $\sum_{i=1}^{45}\mathrm{rSWF}(z_i,t) = 0$. We summarize U_{S} and rSWF as soil water redistribution through soil and roots (S_r) and reformulate Equation (8):

$$\frac{\partial\theta(z_i,t)}{\partial t} = \hat{U}_{\mathrm{P}}(z_i)\cdot\frac{U_{\mathrm{tot}}(t)}{V} + S_r(z_i,t), \tag{10}$$

$\frac{\partial\theta(z_i,t)}{\partial t}$ and U_{tot} (t) can be directly derived from the SWaP measurements of θ $(z_i,\ t)$. The two terms in Equation (10) react differently to a change in light intensity. While U_{tot}, and thus the first term, responds within minutes, the response of the soil-driven water flow, S_{R}, is much slower. Therefore, the variation of $\frac{\partial\theta(z_i,t)}{\partial t}$, induced by the fluctuating light intensity, can be solely attributed to a variation of the first term in Equation (10). Given these considerations, we can derive $\hat{U}_{\mathrm{P}}(z_i)$ as slope of the linear relation between $\frac{\partial\theta(z_i,t)}{\partial t}$ and U_{tot} (t) in each layer. SWaP data from 7.00 a.m. (midpoint of first daily high light level) to 7.00 p.m. (midpoint of last daily high light level) were used for the regression. The entire process of deriving $\hat{U}_P(z_i)$ from the SWaP measurements is exemplified by one faba bean plant in Supplemental Figure S8. This analysis was performed for each day of the soil drying experiment separately, resulting in one $\hat{U}_P$ profile per day. In contrast, Ψ_{soil} was determined every 15 min. For the calculation of Ψ_{seq}, we therefore linearly interpolated the $\hat{U}_P$ profiles with the measured profiles fixed at the center of the regression period at 12.00 a.m. each day. Given both, Ψ_{soil} and $\hat{U}_P$ in each layer and point in time, we derived Ψ_{seq} according to Equation (4).

Measurements of Ψ_{leaf} and stomatal conductance

We continuously measured Ψ_{leaf} on the youngest fully developed leaf using a thermocouple leaf psychrometer (ICT International, Armidale, Australia). Before attaching the psychrometer, the leaf cuticle was carefully removed with abrasive paper. For synchronization with SWaP measurements, Ψ_{leaf} was recorded every 15 min. Stomatal conductance (g_s) was measured using a portable LiCor 6400 photosynthesis system (LiCOR Inc., Lincoln, Nebraska, USA) with a transparent cuvette head. The cuvette was attached to a leaf adjacent to the leaf used for the psychrometer measurements. Since we measured multiple plants at once with only one LiCor 6400, measurements of g_s were not performed continuously but only once per light period at least 45 min after a change in light intensity to allow g_s to reach steady state. Stomatal conductance was measured at least during four light periods a day and for six replicates per species only.

Calculating the water potential at the root surface

Carminati and Javaux (2020) recently suggested that with proceeding soil drying strong water depletion zones around the roots occur leading to a drop of the soil water potential at the root surface. This local drop of the soil water potential was claimed to drive stomatal closure during drought. The Ψ_{soil} that we derived here with the SWaP is based on a measure of the average water content in a soil layer. Thus, Ψ_{soil} better approximates the water potential in the bulk soil than at the root surface. To estimate how strong K_{SL} is affected by the hydraulic pathway from bulk soil to root surface, the water potential at the root surface, Ψ_{sr} needs to be known. To calculate Ψ_{sr}, we followed the approach described Carminati and Javaux (2020) which is summarized in Supplemental Methods S1 and derived in more detail by Abdalla et al. (2022):

$$\psi_{sr} = \left[\frac{\Phi_{sr} \cdot (\tau + 1) \cdot \alpha^{-\tau}}{K_{sat}}\right]^{\frac{1}{\tau+1}}, \tag{11}$$

Φ_{sr} is the matrix flux potential at the root surface which is given by

$$\Phi_{sr} = \Phi_{bulk} - \frac{U_{tot}}{2\pi r_0 L}\left(\frac{r_0}{2} - r_0 r_b^2 \frac{\ln(r_b/r_0)}{r_b^2 - r_0{}^2}\right), \tag{12}$$

where L is the root length, r_0 is root radius, and r_b is the radius defining the start of the bulk soil which is approximated by $r_b = \sqrt{\frac{V}{\pi L}}$ with the soil volume V. Φ_{bulk} is the matrix flux potential in the bulk soil which can be derived from Ψ_{soil} analogously to Equation (11):

$$\Phi_{bulk} = \frac{\alpha^{\tau}}{(\tau + 1)} \cdot K_{sat} \cdot \psi_{soil}{}^{\tau+1}. \tag{13}$$

According to Equation (12), the difference between Φ_{sr} and Φ_{bulk} and thus the difference between Ψ_{sr} and Ψ_{soil} increases with increasing water uptake rate per unit root length. For our analysis, we calculated the equivalent water potential at the root surface ($\Psi_{seq,\ sr}$) by using Ψ_{seq} in Equation (13) instead of Ψ_{soil}. With the calculated $\Psi_{seq,\ sr}$, we could derive the hydraulic conductance from bulk soil to the root surface (K_{SR}) and from the root surface to the leaf (K_{RL}) separately:

$$K_{SR} = \frac{U_{tot}}{\psi_{seq} - \psi_{seq,\ sr}} \tag{14}$$

and

$$K_{RL} = \frac{U_{tot}}{\psi_{seq,\ sr} - \psi_{leaf}}. \tag{15}$$

K_{SR} and K_{RL} are related to K_{SL} as follows:

$$\frac{1}{K_{SL}} = \frac{1}{K_{SR}} + \frac{1}{K_{RL}}. \tag{16}$$

Statistical analyses

We used Mann–Whitney U tests (Mann and Whitney, 1947) to test for statistical differences in several parameters between faba bean and maize. The Mann–Whitney U test is a nonparametric test for two independent samples, testing the null hypothesis that each of two randomly selected values from two different samples have the same probability of being greater than the other value. Mann–Whitney U test were performed using the SciPy package (Virtanen et al., 2020) in Python.

Supplemental data

The following materials are available in the online version of this article.

Supplemental Methods S1.

Supplemental Figure S1. Relation between K_{SL} (black) and Ψ_{seq} and g_s (orange) and Ψ_{seq} for all measured faba bean plants separately.

Supplemental Figure S2. Relation between K_{SL} (black) and Ψ_{seq} and g_s (orange) and Ψ_{seq} for all measured maize plants separately.

Supplemental Figure S3. Daily trend of K_{SL}.

Supplemental Figure S4. Water potential at the root surface ($\Psi_{seq,\ sr}$) as a function of the bulk soil water potential (Ψ_{seq}) for different scenarios.

Supplemental Figure S5. Distribution of root length (L) and RWU rates ($\hat{U}_P$).

Supplemental Figure S6. Recovery of U_{tot} and Ψ_{leaf} upon rewatering for different faba bean plants.

Supplemental Figure S7. Water retention curve of the soil substrate used in the experiments.

Supplemental Figure S8. Determination of $\hat{U}_P$ profiles from the SWaP data on the local soil water depletion rate $\frac{\partial\theta(z_i,t)}{\partial t}$ and the total root water uptake rate $U_{tot}\ (t)$.

Acknowledgments

We thank Johannes Kochs for setting up the LED panel which was required for the light modulation in our measurements. Additionally, we would like to thank Dr. Carel Windt and Congcong Zheng for commenting on the manuscript. We gratefully acknowledge the group of Mathieu Javaux at the Université catholique de Louvain, Earth and Life Institute, for deriving the water retention curve of our soil.

Funding

This study was institutionally funded by the Helmholtz Association, Germany—POF4-899.

Conflict of interest statement. The authors declare no conflict of interests.

References

Abdalla M, Ahmed MA, Cai G, Wankmüller F, Schwartz N, Litig O, Javaux M, Carminati A (2022) Stomatal closure during water deficit is controlled by below-ground hydraulics. Ann Bot **129**: 161–170

Abdalla M, Carminati A, Cai G, Javaux M, Ahmed MA (2021) Stomatal closure of tomato under drought is driven by an increase in soil–root hydraulic resistance. Plant Cell Environ **44**: 425–431

Aroca R, Ferrante A, Vernieri P, Chrispeels MJ (2006) Drought, abscisic acid and transpiration rate effects on the regulation of PIP aquaporin gene expression and abundance in *Phaseolus vulgaris* plants. Ann Bot **98**: 1301–1310

Attia Z, Domec JC, Oren R, Way DA, Moshelion M (2015) Growth and physiological responses of isohydric and anisohydric poplars to drought. J Exp Bot **66**: 4373–4381

Barrios-Masias FH, Knipfer T, McElrone AJ (2015) Differential responses of grapevine rootstocks to water stress are associated with adjustments in fine root hydraulic physiology and suberization. J Exp Bot **66**: 6069–6078

Blackman PG, Davies WJ (1985) Root to shoot communication in maize plants of the effects of soil drying. J Exp Bot **36**: 39–48

Bourbia I, Pritzkow C, Brodribb TJ (2021) Herb and conifer roots show similar high sensitivity to water deficit. Plant Physiol **186**: 1908–1918

Buckley TN (2019) How do stomata respond to water status? New Phytol **224**: 21–36

Carminati A, Ahmed MA, Zarebanadkouki M, Cai G, Lovric G, Javaux M (2020) Stomatal closure prevents the drop in soil water potential around roots. New Phytol **226**: 1541–1543

Carminati A, Javaux M (2020) Soil rather than xylem vulnerability controls stomatal response to drought. Trends Plant Sci **25**: 868–880

Carminati A, Vetterlein D, Koebernick N, Blaser S, Weller U, Vogel HJ (2013) Do roots mind the gap? Plant Soil **367**: 651–661

Carminati A, Vetterlein D, Weller U, Vogel HJ, Oswald SE (2009) When roots lose contact. Vadose Zone J **8**: 805–809

Cochard H (2002) Xylem embolism and drought-induced stomatal closure in maize. Planta **215**: 466–471

Cochard H (2006) Cavitation in trees. Compt Rendus Phys **7**: 1018–1026

Cochard H, Bréda N, Granier A (1996) Whole tree hydraulic conductance and water loss regulation in Quercus during drought: evidence for stomatal control of embolism? Ann Sci For **53**: 197–206

Couvreur V, Vanderborght J, Draye X, Javaux1 M (2015) Dynamic aspects of soil water availability for isohydric plants: focus on root hydraulic resistances. Water Resources Res **51**: 2707–2723

Couvreur V, Vanderborght J, Javaux M (2012) A simple three-dimensional macroscopic root water uptake model based on the hydraulic architecture approach. Hydrol Earth Syst Sci **16**: 2957–2971

Cruz RT, Jordan WR, Drew MC (1992) Structural changes and associated reduction of hydraulic conductance in roots of *Sorghum bicolor* L. following exposure to water deficit. Plant Physiol **99**: 203–212

Cuneo IF, Knipfer T, Brodersen CR, McElrone AJ (2016) Mechanical failure of fine root cortical cells initiates plant hydraulic decline during drought. Plant Physiol **172**: 1669–1678

Dos Santos MA, De Jong Van Lier Q, Van Dam JC, Bezerra AHF (2017) Benchmarking test of empirical root water uptake models. Hydrol Earth Syst Sci **21**: 473–493

Duddek P, Carminati A, Koebernick N, Ohmann L, Lovric G, Delzon S, Rodriguez-Dominguez CM, King A, Ahmed MA (2022) The impact of drought-induced root and root hair shrinkage on root–soil contact. Plant Physiol **189**: 1232–1236

Feddes RA, Kowalik PJ, Zaradny H, (1978) Simulation of Field Water Use and Crop Yield. Centre for Agricultural Publishing and Documentation, Wageningen, The Netherlands

Feddes RA, Hoff H, Bruen M, Dawson TE, de Rosnay P, Dyrmeyer P, Jackson RB, Kabat P, Kleidon A, Lilly A, et al. (2001) Modeling root water uptake in hydrological and climat models. Bull Am Meteorol Soc **82**: 2797–2809

Galmés J, Pou A, Alsina MM, Tomàs M, Medrano H, Flexas J (2007) Aquaporin expression in response to different water stress intensities and recovery in Richter-110 (*Vitis* sp.): relationship with ecophysiological status. Planta **226**: 671–681

Grondin A, Mauleon R, Vadez V, Henry A (2016) Root aquaporins contribute to whole plant water fluxes under drought stress in rice (*Oryza sativa* L.) Plant Cell Environ **39**: 347–365

Hayat F, Ahmed MA, Zarebanadkouki M, Cai G, Carminati A (2019) Measurements and simulation of leaf xylem water potential and root water uptake in heterogeneous soil water contents. Adv Water Resource **124**: 96–105

Hayat F, Ahmed MA, Zarebanadkouki M, Javaux M, Cai G, Carminati A (2020) Transpiration reduction in maize (*Zea mays* L.) in response to soil drying. Front Plant Sci **10**: 1–8

Hillel D, Talpaz H, van keulen H (1976) A macroscopic-scale model of water uptake by a nonuniform root system and of water and salt movement in the soil profile. Soil Sci **121**: 242–255

Hochberg U, Degu A, Fait A, Rachmilevitch S (2013) Near isohydric grapevine cultivar displays higher photosynthetic efficiency and photorespiration rates under drought stress as compared with near anisohydric grapevine cultivar. Physiol Plant **147**: 443–452

Huck MG, Klepper B, Taylor HM (1970) Diurnal variations in root diameter. Plant Physiol **45**: 529–530

Klein T (2014) The variability of stomatal sensitivity to leaf water potential across tree species indicates a continuum between isohydric and anisohydric behaviours. Funct Ecol **28**: 1313–1320

Koebernick N, Schlüter S, Blaser SRGA, Vetterlein D (2018) Root-soil contact dynamics of *Vicia faba* in sand. Plant Soil Soil **431**: 417–431

Li Y, Sperry JS, Shao M (2009) Hydraulic conductance and vulnerability to cavitation in corn (*Zea mays* L.) hybrids of differing drought resistance. Environ Exp Bot **66**: 341–346

Liang J, Zhang J, Wong MH (1997) How do roots control xylem sap ABA concentration in response to soil drying? Plant Cell Physiol **38**: 10–16

Lo Gullo MA, Nardini A, Salleo S, Tyree MT (1998) Changes in root hydraulic conductance (K(R)) of Olea oleaster seedlings following drought stress and irrigation. New Phytol **140**: 25–31

Mann HB, Whitney DR (1947) On a test of whether one of two random variables is stochastically larger than the other. Ann Math Statist **18**: 50–60

Martínez-Vilalta J, Garcia-Forner N (2017) Water potential regulation, stomatal behaviour and hydraulic transport under drought: deconstructing the iso/anisohydric concept. Plant Cell Environ **40**: 962–976

Martínez-Vilalta J, Poyatos R, Aguadé D, Retana J, Mencuccini M (2014) A new look at water transport regulation in plants. New Phytol **204**: 105–115

Martre P, North GB, Nobel PS (2001) Hydraulic conductance and mercury-sensitive water transport for roots of *Opuntia acanthocarpa* in relation to soil drying and rewetting. Plant Physiol **126**: 352–362

Nobel PS, Cui M (1992) Shrinkage of attached roots of opuntia ficus-indica in response to lowered water potentials—predicted consequences for water uptake or loss to soil. Ann Bot **70**: 485–491

North GB, Nobel PS (1991) Changes in hydraulic conductivity and anatomy caused by drying and rewetting roots of agave deserti (agavaceae). Am J Bot **78**: 906–915

North GB, Nobel PS (1997) Drought-induced changes in soil contact and hydraulic conductivity for roots of *Opuntia ficus-indica* with and without rhizosheaths. Plant Soil **191**: 249–258

Perrone I, Gambino G, Chitarra W, Vitali M, Pagliarani C, Riccomagno N, Balestrini R, Kaldenhoff R, Uehlein N, Gribaudo I, et al. (2012) The grapevine root-specific aquaporin VvPIP2;4N controls root hydraulic conductance and leaf gas exchange under well-watered conditions but not under water stress. Plant Physiol **160**: 965–977

Peters A, Durner W (2008) Simplified evaporation method for determining soil hydraulic properties. J Hydrol **356**: 147–162

Pohlmeier A, Haber-Pohlmeier S, Stapf S (2009) A fast field cycling nuclear magnetic resonance relaxometry study of natural soils. Vadose Zone J **8**: 735–742

Pou A, Medrano H, Tomàs M, Martorell S, Ribas-Carbó M, Flexas J (2012) Anisohydric behaviour in grapevines results in better performance under moderate water stress and recovery than isohydric behaviour. Plant Soil **359**: 335–349

Read J, Fletcher TD, Wevill T, Deletic A (2010) Plant traits that enhance pollutant removal from stormwater in biofiltration systems. Int J Phytoremed **12**: 34–53

Rodriguez-Dominguez CM, Brodribb TJ (2020) Declining root water transport drives stomatal closure in olive under moderate water stress. New Phytol **225**: 126–134

Rodríguez-Gamir J, Xue J, Clearwater MJ, Meason DF, Clinton PW, Domec JC (2019) Aquaporin regulation in roots controls plant hydraulic conductance, stomatal conductance, and leaf water potential in *Pinus radiata* under water stress. Plant Cell Environ **42**: 717–729

Ryu J, Hwang BG, Kim YX, Lee SJ (2016) Direct observation of local xylem embolisms induced by soil drying in intact *Zea mays* leaves. J Exp Bot **67**: 2617–2626

Sade N, Gebremedhin A, Moshelion M (2012) Risk-taking plants: anisohydric behavior as a stress-resistance trait. Plant Signal Behav **7**: 767–770

Saliendra NZ, Meinzer FC (1989) Relationship between root/soil hydraulic properties and stomatal behavior in sugarcane. Austral J Plant Physiol **16**: 241–250

Sperry JS, Saliendra NZ (1994) Intra- and inter-plant variation in xylem cavitation in Betula occidentalis. Plant Cell Environ **17**: 1233–1241

Tardieu F, Simmoneau T (1998) Variability among species of stomatal control under fluctuating soil water status and evaporative demand: modelling isohydric and anisohydric behaviours. J Exp Bot **49**: 443–452

van Dusschoten D, Kochs J, Kuppe CW, Sydoruk VA, Couvreur V, Pflugfelder D, Postma JA (2020) Spatially resolved root water uptake determination using a precise soil water sensor. Plant Physiol **184**: 1221–1235

van Dusschoten D, Metzner R, Kochs J, Postma JA, Pflugfelder D, Buehler J, Schurr U, Jahnke S (2016) Quantitative 3D analysis of plant roots growing in soil using magnetic resonance imaging. Plant Physiol **170**: https://doi.org/10.1104/pp.15.01388

van Lier Q de J, Metselaar K, van Dam JC (2006) Root water extraction and limiting soil hydraulic conditions estimated by numerical simulation. Vadose Zone J **5**: 1264–1277

van Lier Q de J, van Dam JC, Durigon A, dos Santos MA, Metselaar K (2013) Modeling water potentials and flows in the soil–plant system comparing hydraulic resistances and transpiration reduction functions. Vadose Zone J **12**: https://doi.org/10.2136/vzj2013.02.0039

Vandeleur RK, Mayo G, Shelden MC, Gilliham M, Kaiser BN, Tyerman SD (2009) The role of plasma membrane intrinsic protein aquaporins in water transport through roots: diurnal and drought stress responses reveal different strategies between isohydric and anisohydric cultivars of grapevine. Plant Physiol **149**: 445–460

Virtanen P, Gommers R, Oliphant TE, Haberland M, Reddy T, Cournapeau D, Burovski E, Peterson P, Weckesser W, Bright J, et al. (2020) SciPy 1.0: fundamental algorithms for scientific computing in Python. Nat Methods **17**: 261–272

Visentin I, Vitali M, Ferrero M, Zhang Y, Ruyter-Spira C, Novák O, Strnad M, Lovisolo C, Schubert A, Cardinale F (2016) Low levels of strigolactones in roots as a component of the systemic signal of drought stress in tomato. New Phytol **212**: 954–963

Supplemental figures

Supplemental Figure S1: Relation between K_{SL} (black) and Ψ_{seq} and g_s (orange) and Ψ_{seq} for all measured faba bean plants separately.

Supplemental Figure S2: Relation between K_{SL} (black) and Ψ_{seq} and g_s (orange) and Ψ_{seq} for all measured maize plants separately.

Supplemental Figure S3: Daily trend of K_{SL}.

Supplemental Figure S4: Water potential at the root surface ($\Psi_{seq, sr}$) as a function of the bulk soil water potential (Ψ_{seq}) for different scenarios.

Supplemental Figure S5: Distribution of root length (L) and RWU rates ($\widehat{U}_P$).

Supplemental Figure S6: Recovery of U_{tot} and Ψ_{leaf} upon rewatering for different faba bean plants.

Supplemental Figure S7: Water retention curve of the soil substrate used in the experiments.

Supplemental Figure S8: Determination of $\widehat{U}_P$ profiles from the SWaP data on the local soil water depletion rate and the total root water uptake rate U_{tot} (t).

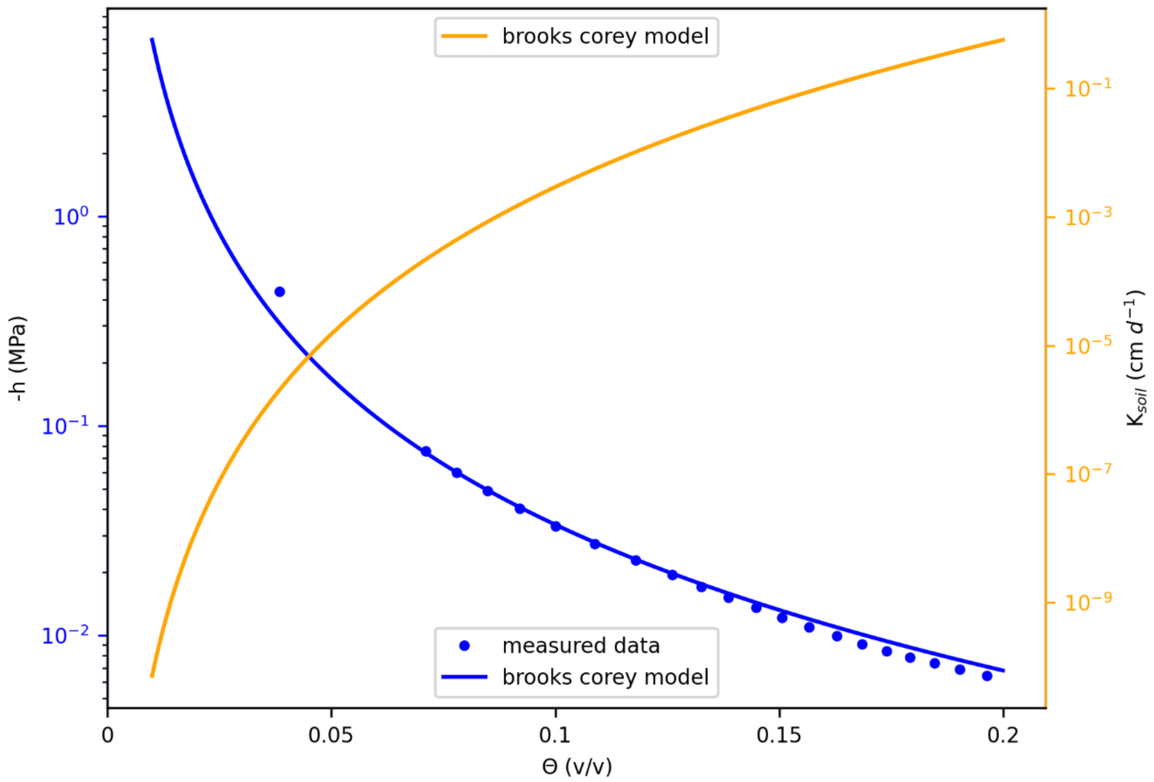

Supplemental Fig. 1 Water retention curve of the soil substrate used in the experiments. Blue data points are the measured, negative matric potentials h (left y-axis). Blue line is the fitted matric potential using the Brooks-Corey model (eq. 5). Orange line is the Brooks-Corey model of the soil hydraulic conductivity (K_{soil}, eq. 6) (right y-axis). The obtained values of the Brooks-Corey parameters are given in Table 4. X-axis is the relevant range of volumetric soil water content Θ in our study.

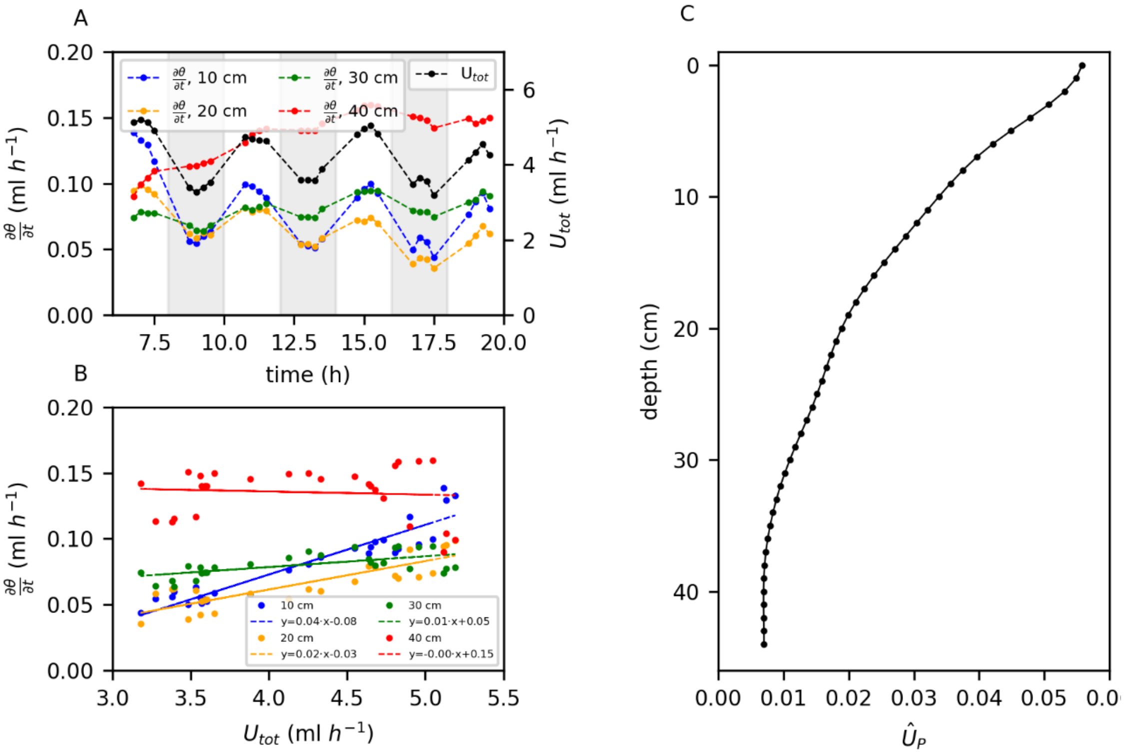

Supplemental Fig. 2 Determination of $\widehat{U}_P$ profiles from the SWaP data on the local soil water depletion rate $\frac{\partial\theta(z_i,t)}{\partial t}$ and the total root water uptake rate U_{tot} (t). A) Response of $\frac{\partial\theta(z_i,t)}{\partial t}$ in different depths (different colors, left y-axis) and U_{tot} (black, right y-axis) to the fluctuating light intensity. White areas indicate a high light period, grey areas a low light period. B) Determination of $\widehat{U}_P$ in each soil layer as slope of the linear relation between $\frac{\partial\theta(z_i,t)}{\partial t}$ and U_{tot} according to eq. 8. C) Resulting $\widehat{U}_P$ profile of one exemplary faba bean plant at the first day of measurement. Note that this entire process was necessary to ultimately derive Ψ_{seq} as a precise measure for the level of soil drying sensed by the plant.

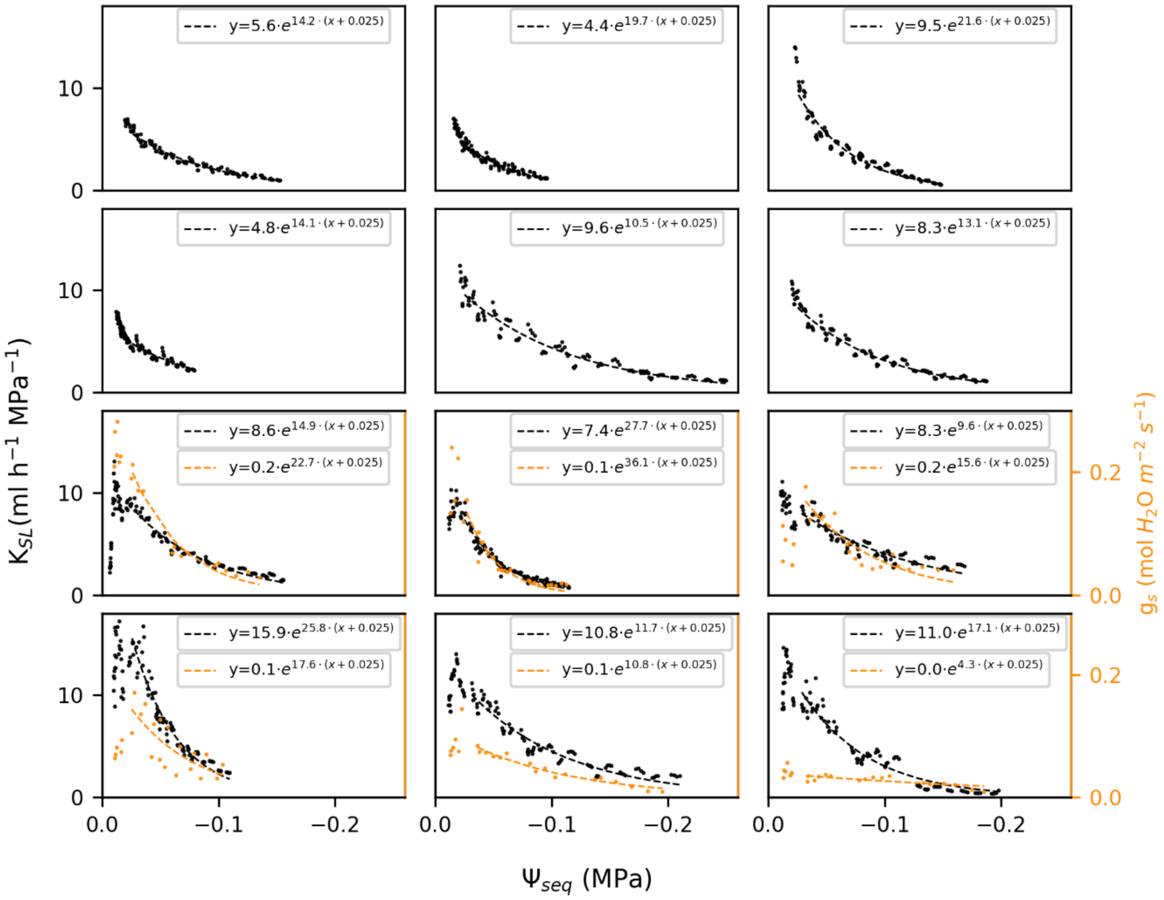

Supplemental Fig. 3 Relation between K_{SL} (black) and Ψ_{seq} and g_s (orange) and Ψ_{seq} for all measured faba bean plants separately. Dashed lines show an exponential fit of the data starting at a Ψ_{seq} of -0.025 MPa.

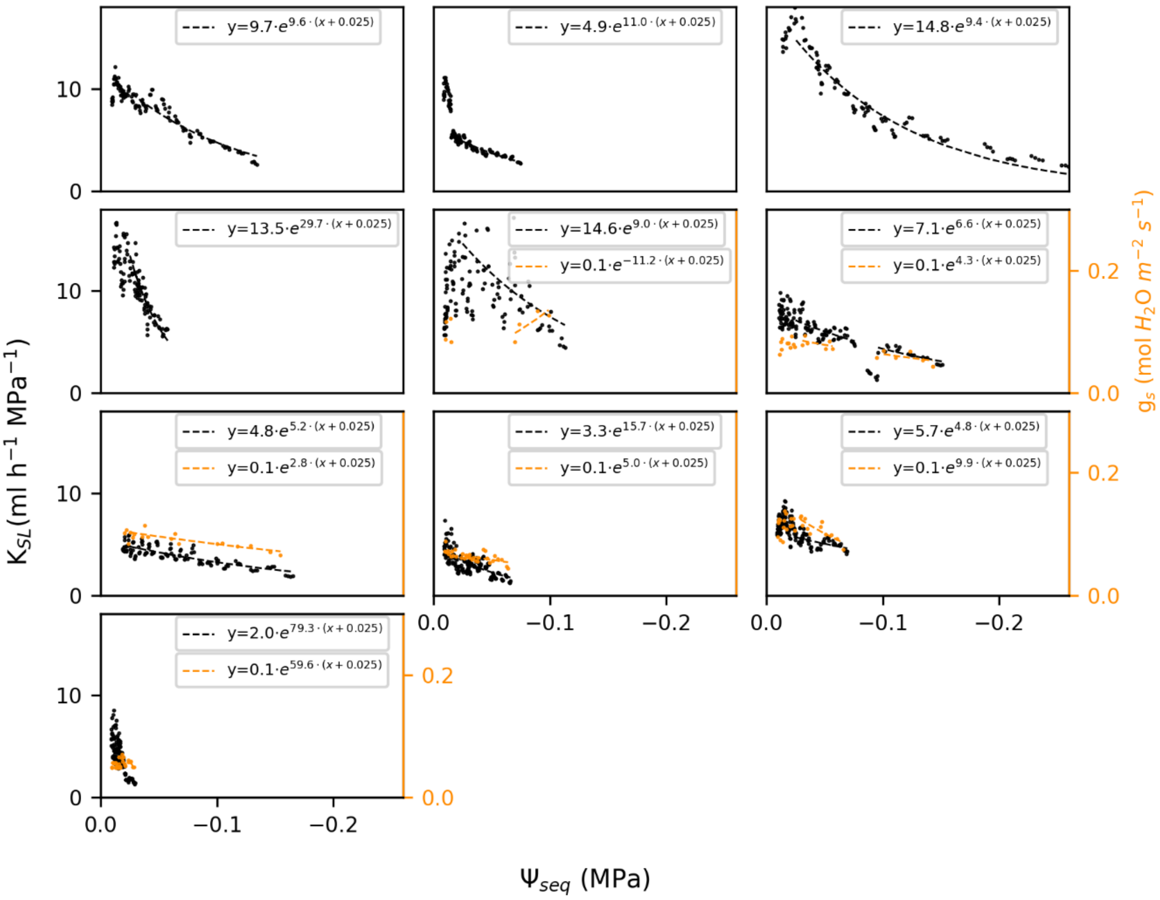

Supplemental Fig. 4 Relation between K_{SL} (black) and Ψ_{seq} and g_s (orange) and Ψ_{seq} for all measured maize plants separately. Dashed lines show an exponential fit of the data starting at a Ψ_{seq} of -0.025 MPa.

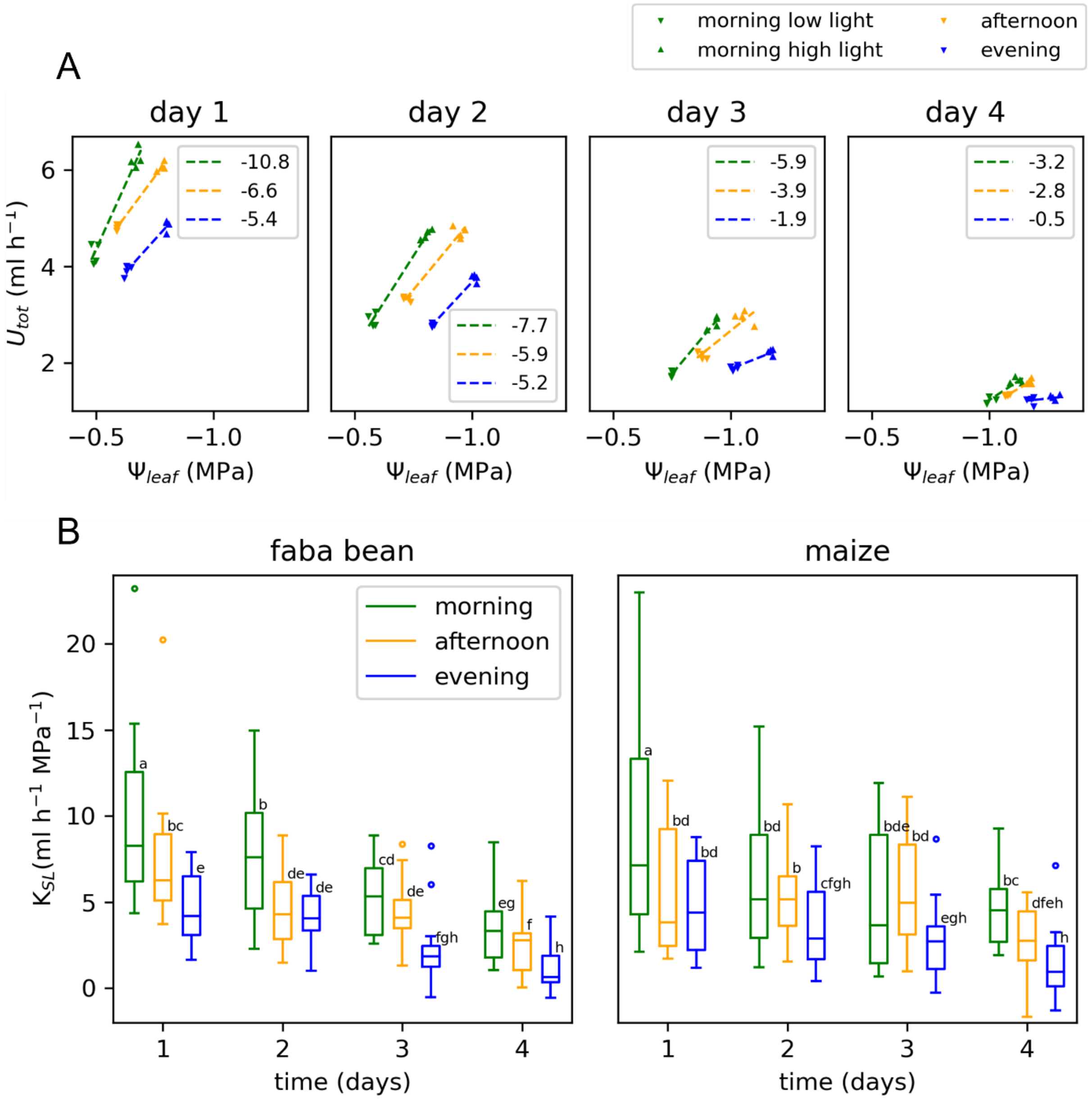

Supplemental Fig. 5 Daily trend of K_{SL}. A) Relation between U_{tot} and Ψ_{leaf} at three different time intervals each day, exemplary shown for one faba bean plant. Four data points per low light period (downward triangles) and high light period (upward triangles) in the morning (green), afternoon (orange) and evening (blue) are shown. K_{SL} is given as slope of the relation between U_{tot} and Ψ_{leaf} which we derived by linearly fitting the data from each time interval separately (values in ml h^{-1} MPa^{-1} in the figure legends). B) Boxplots of K_{SL} derived as shown in A) for all replicates. Characteristics of the boxplots are similar to Fig. 2 A, C, E. Significant differences (P-value of a paired Student's t-test <0.05) between the different time points are denoted by different letters.

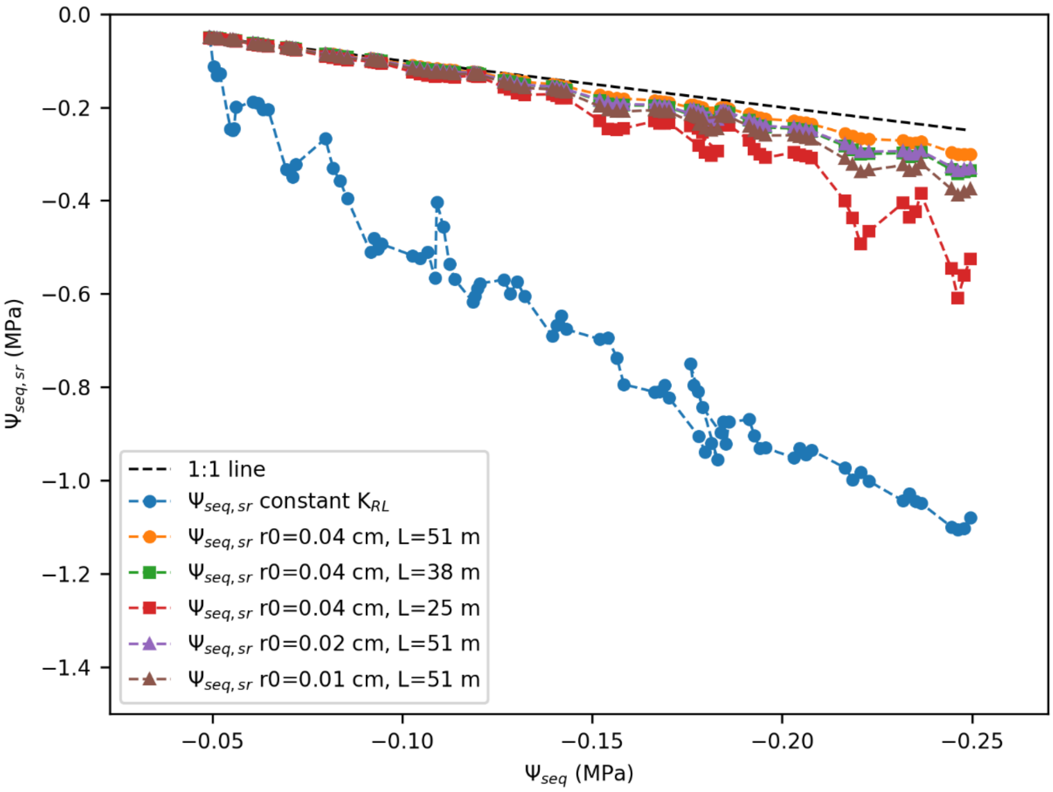

Supplemental Fig. 6 Water potential at the root surface ($\Psi_{seq, sr}$) as a function of the bulk soil water potential (Ψ_{seq}) for different scenarios. Data are from one exemplary faba bean plant. The blue curve is the theoretical $\Psi_{seq, sr}$ for the scenario of a constant K_{RL}, meaning that the measured decline in K_{SL} had solely occurred in the soil. It was calculated using eq. 1 with a constant, initial K_{SL}. The orange curve is the estimated $\Psi_{seq, sr}$ using the model and 100% of both, the measured total root length (L) and the measured average root radius (r0). The other curves are the model estimations of $\Psi_{seq, sr}$ if only a reduced fraction of either L (green and red) or r0 (purple and brown) are considered. The green and purple curves are very similar making the green curve hardly visible.

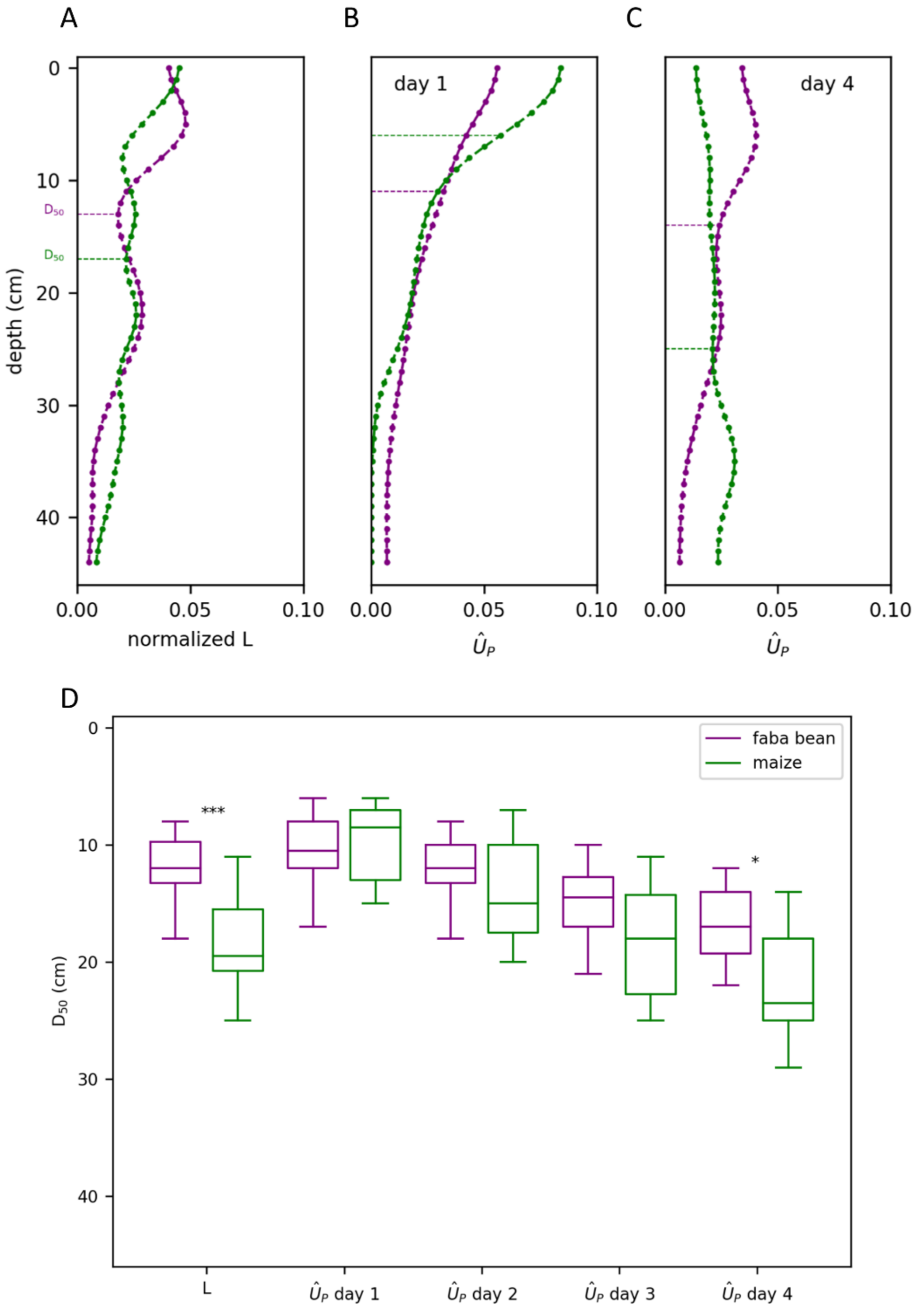

Supplemental Fig. 7 Distribution of root length (L) and root water uptake rates ($\widehat{U}_P$). Exemplary data of L (A), and $\widehat{U}_P$ at the first (B) and last day (C) of measurement for one faba bean and one maize plant. Horizontal dashed lines in A-C indicate the depth (D_50) at which 50% of L or $\widehat{U}_P$ were reached. D) Boxplots of D_50 for L and $\widehat{U}_P$ during the four days of measurement. Asterisks indicates significant differences between faba bean and maize, determined with a Mann-Whitney U test. P-values below 0.05 are indicated by *, below 0.01 by ** and below 0.005 by ***. Characteristics of the boxplots are similar to Fig. 2 A, C, E.

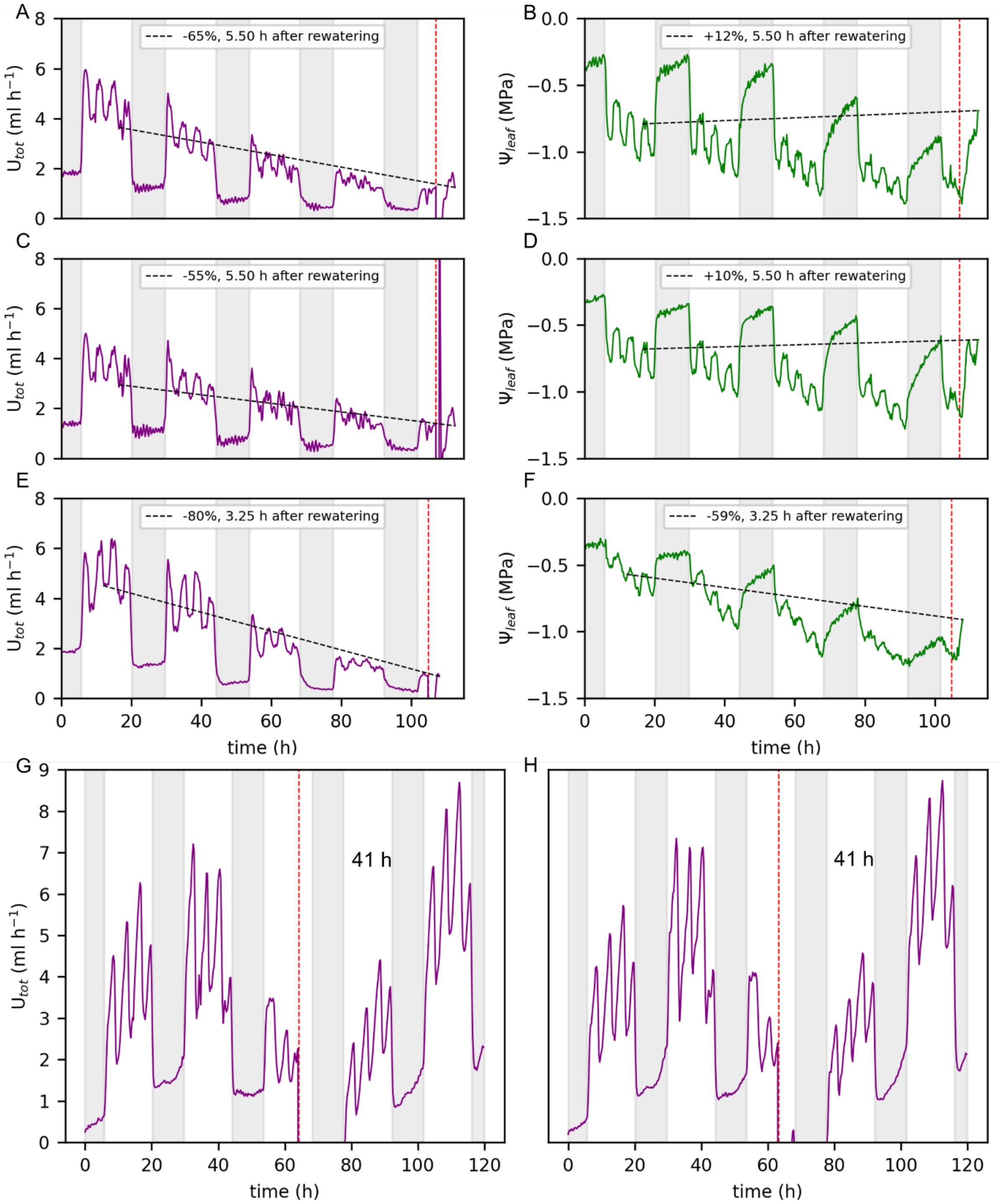

Supplemental Fig. 8 Recovery of U_{tot} (A, C, E) and Ψ_{leaf} (B, D, F) for three faba bean plants upon rewatering after four days of water restriction. Black dashed lines connect the last measured point after rewatering with the corresponding point (same time of day) at the first day of measurement. The percentage difference between these two points is shown in the figure legends together with the time passed between rewatering and the last measured point. (G and H) Longer recovery period of U_{tot} after rewatering for two six weeks old faba bean plants from a separate experiment without measurements of Ψ_{leaf}. In both plants it took around 41 hours of recovery for U_{tot} to reach the maximum values from before rewatering. Nights are indicated by the shaded areas.

Supplemental Methods

Supplemental Method S1: Estimation of the water potential at the root surface

A Kirchhoff transformation of the soil hydraulic conductivity (K_{Soil}) yields the matrix flux potential (ϕ) at a certain location x:

$$\Phi_x = \int_{-\infty}^{\psi_x} K_{soil}(\psi) d\psi \qquad [1]$$

For a Brooks-Corey soil, this writes:

$$\Phi_x = \int_{-\infty}^{\psi_x} K_{sat} \cdot (\alpha \cdot \psi)^{\tau} d\psi \quad [2]$$

with the saturated soil hydraulic conductivity K_{sat}, the air entry pressure head α^{-1} and a fitting parameter τ. Solving eq 2 results in a relation between the matrix flux potential and the water potential.

$$\Phi_x = \frac{\alpha^{\tau}}{(\tau+1)} \cdot K_{soil} \cdot {\psi_x}^{\tau+1} \qquad [3]$$

Solving eq 3 for Ψ at the root surface gives

$$\psi_{\mathrm{sr}} = \left[\frac{\Phi_{sr} \cdot (\tau+1) \cdot \alpha^{-\tau}}{K_{sat}}\right]^{\frac{1}{\tau+1}} \qquad [4]$$

Additionally, the Kirchhoff transformation can be used to solve the radial 1D Richards equation for water flow from bulk soil towards the root surface which yields a relation between the matrix flux potential at the root surface (ϕ_{sr}) and in the bulk soil (ϕ_{bulk}):

$$\Phi_{sr} = \Phi_{bulk} - \frac{\mathrm{U}_{tot}}{2\pi r_0 L}\left(\frac{r_0}{2} - r_0 r_b^2 \frac{ln(r_b/r_0)}{r_b^2 - {r_0}^2}\right) \qquad [5]$$

with root length L, root radius r_0 and the radius defining the start of the bulk soil r_b which is approximated by $r_b = \sqrt{\frac{V}{\pi L}}$ with the soil volume V. Given eq. 3-5, Ψ_{sr} was derived as follows:

1. Calculating ϕ_{bulk} using eq. 3 and the measured bulk soil water potential together with the Brooks-Corey parameters of our soil
2. Calculating ϕ_{sr} with the derived ϕ_{bulk} according to eq. 5
3. Calculating Ψ_{sr} with the derived ϕ_{sr} and the Brooks-Corey parameters according to eq. 3.

Manuscript III

Yannik Müllers, Johannes A Postma, Hendrik Poorter, Dagmar van Dusschoten, Deep-water uptake under drought improved due to locally increased root conductivity in maize, but not in faba bean, *Plant Cell & Environment*, Volume 46, Issue 7, July 2023, Pages 2046-2060, https://doi.org/10.1111/pce.14587

Own contribution: Design of the study (together with JP, HP, and DvD), Conductance of the experiments (with contributions from DvD), Data analysis, Drafting the manuscript, Revision and editing of the manuscript (with contributions from all authors)

Received: 22 December 2022 | Revised: 16 March 2023 | Accepted: 19 March 2023

DOI: 10.1111/pce.14587

ORIGINAL ARTICLE

Plant, Cell & Environment WILEY

Deep-water uptake under drought improved due to locally increased root conductivity in maize, but not in faba bean

Yannik Müllers[1] | **Johannes A. Postma**[1] | **Hendrik Poorter**[1,2] | **Dagmar van Dusschoten**[1]

[1]IBG-2, Plant Sciences, Forschungszentrum Jülich, Jülich, Germany

[2]Department of Natural Sciences, Macquarie University, Sydney, Australia

Correspondence
Dagmar van Dusschoten, IBG-2, Plant Sciences, Forschungszentrum Jülich, Jülich, Germany.
Email: d.van.dusschoten@fz-juelich.de

Funding information
Helmholtz Association, Germany, Grant/Award Number: POF4-899; Deutsche Forschungsgemeinschaft (DFG, German Research Foundation), Grant/Award Number: 491111487

Abstract

Moderate soil drying can cause a strong decrease in the soil-root system conductance. The resulting impact on root water uptake depends on the spatial distribution of the altered conductance relatively to remaining soil water resources, which is largely unknown. Here, we analyzed the vertical distribution of conductance across root systems using a novel, noninvasive sensor technology on pot-grown faba bean and maize plants. Withholding water for 4 days strongly enhanced the vertical gradient in soil water potential. Therefore, roots in upper and deeper soil layers were affected differently: In drier, upper layers, root conductance decreased by 66%–72%, causing an amplification of the drop in leaf water potential. In wetter, deeper layers, root conductance increased in maize but not in faba bean. The consequently facilitated deep-water uptake in maize contributed up to 21% of total water uptake at the end of the measurement. Analysis of root length distributions with MRI indicated that the locally increased conductance was mainly caused by an increased intrinsic conductivity and not by additional root growth. Our findings show that plants can partly compensate for a reduced root conductance in upper, drier soil layers by locally increasing root conductivity in wetter layers, thereby improving deep-water uptake.

KEYWORDS

MRI, plant water stress, root conductance, root hydraulic architecture, root water uptake, soil drying, soil water profiler, water uptake compensation

1 | INTRODUCTION

Terrestrial plants exposed to drying soils suffer from a reduced water potential which can lead to cell turgor loss (Bartlett et al., 2012), hydraulic failure of xylem vessels (Urli et al., 2013) and impaired phloem transport (Thompson, 2006). To mitigate this, plants close stomata at the cost of reduced CO_2 gain, up to carbon starvation (McDowell, 2011). In the first place, the reduced plant water potential is caused by the drop in soil water potential. However, the plant water potential additionally depends on how the hydraulic conductance of the root system is affected by soil drying (Bourbia et al., 2021; Nobel & Cui, 1992; Rodriguez-Dominguez & Brodribb, 2020; Saliendra & Meinzer, 1989). In a recent study, we showed that even moderate soil drying can induce an exponential

---

decline of the total root system conductance (Müllers, Postma, Poorter, & van Dusschoten, 2022). Considering the distribution along the root system of such a net decline is crucial to understand its impact on the plant water balance.

Soil drying is a highly nonuniform process and usually results in a pronounced vertical gradient with relatively dry shallow soil layers and relatively wet deep soil layers (Hillel et al., 1976; Kondo et al., 2000; Markesteijn et al., 2010). Under such conditions, water in deeper layers is much easier to extract, that is, a deep root requires a less negative xylem water potential to realize a certain water uptake rate compared with an otherwise identical shallow root. Following this rationale, effectively using deep water resources is a key to withstand droughts (Wasson et al., 2012). However, several studies emphasize that plants often fail to do so and experience severe drought stress despite a relatively high water availability in deeper root zones (Gessler et al., 2022; Passioura, 1983; Prechsl et al., 2015; Rasmussen et al., 2020). A major reason is that the root conductance (K_{root}, see Table 1 for abbreviations) in deeper layers usually is low since roots are less abundant (Haberle & Svoboda, 2015; Kemper et al., 2020; Righes, 1980) and less conductive compared with shallow roots (Dara et al., 2015; Müllers, Postma, Poorter, Kochs, et al., 2022; Zarebanadkouki et al., 2013). Therefore, a more effective acquisition of deep water would require to locally increase root conductance over time. This can be achieved by increasing root length via additional root growth in deeper layers, which has been often observed upon soil drying (Alsina et al., 2011; Asseng et al., 1998; Dubrovsky et al., 1998; Rodrigues et al., 1995; Sharp & Davies, 1985). Nevertheless, as root hydraulic traits vary among individual roots and entire root systems (Ahmed et al., 2016, 2018; Clément et al., 2022; Müllers, Postma, Poorter, Kochs, et al., 2022; Rewald et al., 2012; Steudle & Peterson, 1998), local root length only partly determines a plant's ability to use deep water. Additionally, plants can increase the intrinsic root conductivity (conductance per length) by, for example, increasing the amount of active aquaporins (Johnson et al., 2014; McLean et al., 2011).

While in deeper, wetter layers, increasing the root conductance is a reasonable strategy for an effective water usage, it might be the other way around in upper, drier soil layers. Unregulated water uptake from drying soil can result in a severe water depletion zone around the roots, strongly reduce the local soil conductivity, and thus restrict water flow from the bulk soil towards the roots (Carminati & Javaux, 2020). The drop of the local soil conductivity scales with the water potential of the bulk soil and the water uptake rate per unit root length. Therefore, locally decreasing root conductance, and thus water uptake rates, in drier soil layers might be beneficial to avoid an interruption of the hydraulic pathway between remaining water in the bulk soil and the root surface. Mechanisms like enhanced root suberization (Barrios-Masias et al., 2015; Cruz et al., 1992; Lo Gullo et al., 1998; North & Nobel, 1991), or reducing the amount of open aquaporins (Martre et al., 2001; Rodríguez-Gamir et al., 2019) enable plants to reduce root hydraulic conductance during droughts.

Following these considerations, we analyzed how previously measured changes in the total root system conductance (Müllers, Postma, Poorter, & van Dusschoten, 2022) are distributed over depth.

TABLE 1 Abbreviations as used in the article.

Term	Meaning	Unit
h	Soil matric potential	cm H_2O
K_{comp}	Compensatory root water uptake conductance	mL h^{-1} MPa^{-1}
k_h	Soil hydraulic conductivity	cm h^{-1}
K_{root}	Radial root conductance	mL h^{-1} MPa^{-1}
k_{root}	Radial root conductivity	mL h^{-1} MPa^{-1} m^{-1}
K_{sat}	Soil hydraulic conductivity at water saturation	cm h^{-1}
K_{SL}	Hydraulic conductance between soil and leaf	mL h^{-1} MPa^{-1}
K_{soil}	Soil hydraulic conductance	mL h^{-1} MPa^{-1}
K_{SR}	Local soil-root conductance	mL h^{-1} MPa^{-1}
$K_{SR,\ tot}$	Total conductance of the soil-root system	mL h^{-1} MPa^{-1}
L	Root length	m
r_0	Root radius	cm
r_b	Radial distance from the root centre defining the start of the bulk soil	cm
RWU	Root water uptake rate	mL h^{-1}
SWaP	Soil water profiler	
U_P	Plant-driven root water uptake distribution with depth	mL cm^{-3} h^{-1}
$\hat{U}_P$	Normalized plant-driven root water uptake distribution with depth	
U_S	Soil driven root water uptake redistribution	mL cm^{-3} h^{-1}
U_S'	Hypothetical U_S for assuming no local increases in K_{root}	mL cm^{-3} h^{-1}
U_{tot}	Total root water uptake rate	mL h^{-1}
V	Soil volume	cm^3
z_i	Depth of soil layer i	cm
α	Inverse of the air entry pressure	cm H_2O $^{-1}$
θ	Volumetric soil water content	%
$\frac{\partial\theta}{\partial t}$	Soil water depletion rate	mL cm^{-3} h^{-1}
λ_b	Dimensionless pore size index of the Brooks–Corey model	
τ	Brooks–Corey parameter with $\tau = -2-3\,\lambda_b$	
φ	Matrix flux potential	cm^2 h^{-1}
Ψ_{collar}	Water potential at the plant collar	MPa
Ψ_{leaf}	Leaf water potential	MPa
Ψ_{soil}	Water potential in the bulk soil	MPa
Ψ_{seq}	Equivalent soil water potential	MPa
Ψ_{sr}	Water potential at the soil-root interface	MPa

Although this spatial aspect is highly relevant for the plant water balance, it has been poorly investigated. The few studies measuring a spatial component of soil drying-induced alterations of root hydraulic traits used single roots, sampled at different depths (Johnson et al., 2014; Wan et al., 1994). Additional information comes from studies on partial root zone drying in which root hydraulic traits were either measured on single, sampled roots (McLean et al., 2011) or entire root systems divided into halves (Hu et al., 2011). These studies generally suggest that the conductance of roots in rather wet soil increases relatively to that of roots in rather dry soil. However, how the full vertical distributions of root hydraulic conductance change in response to soil drying is unknown, probably due to limitations in the available measurement technologies. Here, we used a recently developed, highly precise soil water sensor, called soil water profiler (SWaP; van Dusschoten et al., 2020), to noninvasively measure root water uptake profiles which reflect the distribution of root hydraulic conductance. We hypothesize that the root conductance decreases in upper soil layers while it increases in deeper layers as an early response to soil drying by means of active regulation by the plant. Such a response would reduce water stress by facilitating deep water usage and sustaining a hydraulic connection to remaining water resources in drier layers. In Figure 1, the hypothesized effect of soil drying on the spatial distribution of root conductance is summarized. The hypothesis was tested on pot-grown faba bean and maize plants during 4 days of soil drying. These two species were chosen because they differ in root system architecture, and water uptake rates per unit root length. Faba bean has a taproot system with comparably great water uptake rates per unit root length, whereas maize has a fibrous root system with comparably low water uptake rates per unit root length. Both factors potentially affect the distribution of remaining soil water under drought, and thus the resulting alterations of the local root conductance.

2 | MATERIALS AND METHODS

Data used in this study were obtained during an experiment described previously in Müllers, Postma, Poorter, and van Dusschoten (2022). Below, we shortly summarize the experimental design and explain the determination of the distribution of root conductance and root length in more detail.

2.1 | Experimental design

We germinated seeds of faba bean (*Vicia faba*, *n* = 10) and maize (*Zea mays*, *n* = 10), and transferred them into soil-filled PVC pipes (80% of a loamy sand collected in Kaldenkirchen, Germany (Pohlmeier et al., 2009), mixed with 20% coarse sand). PVC pipes had an inner diameter of 8.1 cm and were filled to a height of 45 cm resulting in 2.32 L of soil substrate at a bulk dry density of 1.47 kg L^{-1}. Plants

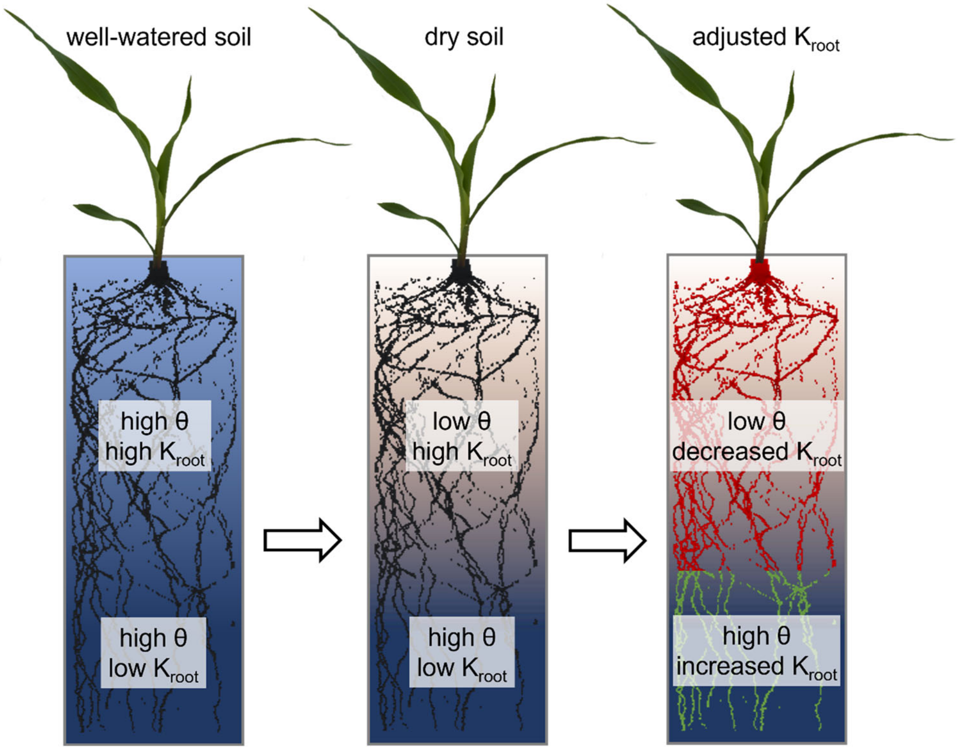

FIGURE 1 Hypothesized alterations of the spatial distribution of root hydraulic conductance (K_{root}) in response to soil drying. Usually, soil water content (θ) is reduced faster in upper than in deeper soil layers. Increasing the root conductance in deeper layers could facilitate deep water uptake while a decreasing root conductance in upper layers might prevent an interruption of water flow from the bulk soil towards the root surface.

were grown in a climate chamber at a constant temperature of 21.5 ± 0.2°C and a $\mathrm{VPD_{air}}$ of 1.49 kPa. We used a water-cooled LED panel (3200 K, 5 × 5 LEDs á 20 W) for controlled illumination of the plants. Light intensity alternated between a higher (1000 μmol $\mathrm{m^{-2}\,s^{-1}}$) and lower level (500 μmol $\mathrm{m^{-2}\,s^{-1}}$) in periods of 2 h. Each day, four high and three low light periods were applied resulting in a total of 14 h illumination and a daily light integral of 39.6 mol $\mathrm{m^{-2}\,day^{-1}}$. The alternating light levels were required to determine root water uptake profiles as described below. Plants were regularly watered from the top to keep the average volumetric soil water content around 20%. For fertilization, once a week an NPK nutrient salt (Hakaphos Red; Compo Expert; 8% N, 12% P, 24% K), was diluted in water at 0.3% (v/v) and used for watering. At an age between 4 and 5 weeks (thereby selecting for similar total plant water uptake rates), plants were imaged with MRI and then placed into the SWaP for continuous measurement of soil water profiles. From that moment onwards, plants were not watered anymore. Simultaneously, leaf water potential was continuously measured with a psychrometer (ICT International). After 4 days, plants were imaged with MRI again.

2.2 | Determining the normalized distribution of plant-driven root water uptake rates

For the following analysis, we interpret the 45 cm high soil columns with roots as 45 vertically stacked layers of 1 cm height. Layers are numbered with $i = 1, \ldots, 45$ from top to bottom. Upper boundary of each layer is at depth $z_i = 0, \ldots, 44$ cm. The volumetric soil water content ($\theta(z_i)$) in each layer was measured with the so-called SWaP (van Dusschoten et al., 2020). The SWaP is sensitive for the permittivity of the soil which is determined by θ. Using a calibration curve, values measured with the SWaP were converted to the local $\theta(z_i)$. Sensors of the SWaP were automatically moved along the pots with soil columns, which allowed for measuring θ-profiles in equidistant vertical steps of 1 cm every 15 min. The SWaP measurements and required data processing, is explained in more detail by van Dusschoten et al. (2020), and Müllers, Postma, Poorter, Kochs, et al. (2022).

Using this methodology, we could derive the soil water depletion rate $\left(\frac{\partial\theta(z_i,t)}{\partial t}\right)$ for each individual soil layer. $\frac{\partial\theta(z_i,t)}{\partial t}$ is determined by local root water uptake rates ($\mathrm{RWU}(z_i,t)$) and redistributive soil water flow ($\mathrm{rSWF}(z_i,t)$) between adjacent layers:

$$\frac{\partial\theta(z_i,t)}{\partial t} = \mathrm{RWU}(z_i,t) + \mathrm{rSWF}(z_i,t). \tag{1}$$

Following the hydraulic model developed by Couvreur et al. (2012), the distribution of RWU is determined by one term, solely depending on the distribution of root hydraulic conductance, and a second term additionally depending on vertical soil water gradients. We call the first term plant-driven root water uptake distributions (U_P), and the latter term soil-driven root water uptake redistribution (U_S):

$$RWU(z_i) = U_\mathrm{P}(z_i) + U_\mathrm{S}(z_i). \tag{2}$$

Under the hypothetical conditions of a uniform soil water potential over depth, U_P is equal to RWU. Across the whole pot, U_P integrates to the total root water uptake rate (U_tot). U_S is a correction term which is negative in relatively dry soil layers (local soil water potential below pot average) and positive in relatively wet soil layers (local soil water potential above pot average). Across the whole pot, U_S integrates to zero. Using these definitions and summarizing U_S and rSWF as soil water redistribution through soil and roots (S_R), Equation (1) writes:

$$\frac{\partial\theta(z_i,t)}{\partial t} = \hat{U}_\mathrm{P}(z_i)\cdot\frac{U_\mathrm{tot}(t)}{V} + S_\mathrm{R}(z_i,t). \tag{3}$$

In Equation (3) we used the normalized plant-driven root water uptake distribution ($\hat{U}_\mathrm{P}$) with $\hat{U}_\mathrm{P}(z_i) = \frac{U_{\mathrm{P}(z_i)}}{U_\mathrm{tot}}$ and the total pot volume V. Given a data set with varying U_tot, $\hat{U}_\mathrm{P}$, according to Equation (3), can be derived by a linear regression between $\frac{\partial\theta(z_i,t)}{\partial t}$ and U_tot if variations in U_tot and S_R are independent. Decoupling of variation in U_tot and S_R is achieved by the fluctuating light intensity in periods of 2 h. Assuming that changes in the soil water distribution are negligible on short time scales, a change in light intensity causes a rapid response in U_tot without affecting S_R. Thus, for data measured during a fluctuating light intensity, the slope of $\frac{\partial\theta(z_i,t)}{\partial t}$ (U_tot) is $\hat{U}_\mathrm{P}$. Since $\hat{U}_\mathrm{P}$ is determined by the distribution of root conductance, this can be understood as follows: The greater the root conductance in a specific soil layer, the greater the change in the local soil water depletion rate induced by a change in transpiration rate. The linear regression, and thus determination of $\hat{U}_\mathrm{P}$, was performed at each day separately, covering data from 12 h of alternating light. Supporting Information: Figure 1 shows the process of deriving $\hat{U}_\mathrm{P}$ profiles from the SWaP data for an exemplary maize plant at Day 1 and Day 4 of the soil drying period.

2.3 | Determining the distribution of soil water potential

The soil matric potential (h) was calculated from θ values measured with the SWaP, using a water retention curve, fitted with a Brooks–Corey model. This water retention curve has been reported in Müllers, Postma, Poorter, and van Dusschoten (2022). To obtain the distribution of soil water potential (Ψ_soil), h was corrected for gravity.

2.4 | Determining the distribution of root hydraulic conductance

To derive the spatial distribution of root hydraulic conductance (K_root), the normalized $\hat{U}_\mathrm{P}$, containing the spatial component of K_root, needs to be multiplied by the total conductance of the root system. Table 2 shows data on U_tot, leaf water potential (Ψ_leaf), the equivalent soil water potential (Ψ_seq), and the resulting total conductance between soil and leaf (K_SL) separately averaged across each day of the measurement. A detailed

TABLE 2 Total root water uptake rate (U_{tot}), leaf water potential (Ψ_{leaf}), equivalent soil water potential (Ψ_{seq}), and the resulting, total conductance between soil and leaf (K_{SL}), averaged for each day of soil drying.

	Faba bean		Maize	
Day	U_{tot} (mL h^{-1})	Ψ_{leaf} (MPa)	U_{tot} (mL h^{-1})	Ψ_{leaf} (MPa)
1	4.85 ± 0.41^{a}	−0.62 ± 0.05^{a}	4.09 ± 0.58^{a}	−0.55 ± 0.05^{a}
2	3.75 ± 0.70^{a}	−0.76 ± 0.04^{b}	3.94 ± 0.77^{a}	−0.64 ± 0.14^{a}
3	2.47 ± 0.42^{b}	−0.93 ± 0.07^{b}	3.51 ± 0.54^{ab}	−0.71 ± 0.17^{a}
4	1.64 ± 0.31^{c}	−1.11 ± 0.09^{c}	3.10 ± 0.43^{b}	−1.05 ± 0.19^{b}

	Faba bean		Maize	
Day	Ψ_{seq} (MPa)	K_{SL} (mL h^{-1} MPa^{-1})	Ψ_{seq} (MPa)	K_{SL} (mL h^{-1} MPa^{-1})
1	−0.02 ± 0.01^{a}	8.27 ± 1.12^{a}	−0.02 ± 0.00^{a}	8.73 ± 4.07^{a}
2	−0.04 ± 0.01^{b}	5.15 ± 1.30^{b}	−0.03 ± 0.01^{b}	6.55 ± 2.43^{a}
3	−0.08 ± 0.02^{c}	2.87 ± 0.56^{c}	−0.05 ± 0.01^{c}	5.67 ± 2.21^{ab}
4	−0.12 ± 0.03^{d}	1.57 ± 0.37^{d}	−0.07 ± 0.03^{c}	3.34 ± 1.45^{b}

Note: Values are species medians with median absolute deviations.

analysis of these data, especially of the exponential decline in K_{SL} in response to soil drying, is provided by Müllers, Postma, Poorter, and van Dusschoten (2022). In the present study, the data on K_{SL} were used to approximate the total conductance of the root system. For this, we assumed that the axial conductance of the shoot between root system and leaf is much greater than the total conductance of the soil-root system ($K_{SR,\ tot}$). This assumption is justified in wet soil, where radial root conductance is usually limiting water uptake (Frensch & Steudle, 1989; Reid & Hutchison, 1986; Steudle & Peterson, 1998). During soil drying, the axial shoot conductance can be reduced due to xylem embolism, and thus become an important determinant of K_{SL}. However, considerable reduction of the axial conductance due to xylem embolism in maize were measured at a soil water potential of −0.25 MPa (Ryu et al., 2016), stem water potential of −1.0 MPa (Li et al., 2009) and leaf water potential of −1.5 MPa (Cochard, 2002). Comparable values of Ψ_{leaf} were not reached in our measurements (Table 2), indicating that axial shoot conductance was not limiting for a large part of the measurement, similar to the findings of two recent studies (Corso et al., 2020; Rodríguez-Gamir et al., 2019). Therefore, we can approximate K_{SL} by $K_{SR,\ tot}$, and derive the local soil-root conductance (K_{SR}) in each layer:

$$K_{SR}(z_i) = K_{SL} \cdot \hat{U}_P(z_i). \tag{4}$$

For an overview of the hydraulic network model and the terminology used here, see Supporting Information: Figure 2. K_{SR} is composed of the local soil hydraulic conductance (K_{soil}), and the local root conductance (K_{root}), connected in series. In Supporting Information: Appendix 1, we explain two different methods to estimate the hydraulic conductance of K_{soil}. These estimations indicated that for a large part of the measurement, K_{soil} in each layer was much greater than K_{SR} (Supporting Information: Figure 3), and K_{SR} was largely determined by K_{root}. Thus, K_{root} can be reliably approximated by K_{SR}, as determined in Equation (4):

$$K_{root}(z_i) = K_{SL} \cdot \hat{U}_P(z_i). \tag{5}$$

Supporting Information: Appendix 1 also provides a more detailed discussion in Supporting Information: Figure 3 and the resulting conclusions.

2.5 | Determining the distribution of root length and root conductivity

Before and after the SWaP measurement, root length profiles of the plants were determined noninvasively using MRI. The MRI setup consisted of a 4.7 T vertical wide bore (310 mm) magnet (Magnex) and a gradient coil (ID 205 mm; MR Solutions) generating gradients up to 400 mT/m, controlled with an MR Solutions console. We used NMRooting software (van Dusschoten et al., 2016) to derive root length profiles at a vertical stepped-down resolution of 1 cm from the MRI data. To estimate the root length distribution at each intermediate day between the two MRI measurements, we applied an exponential interpolation in each layer separately, assuming exponential root growth during the 4 days. Since the MRI setup has a detection limit of roots with diameter around 200–300 µm we used correction factors to account for the distribution of fine roots. These correction factors were derived in a previous experiment comparing root length profiles measured with MRI and with scanning of harvested roots (Müllers, Postma, Poorter, Kochs, et al., 2022). Plants in that study and the present study were of the same age and grown under similar conditions until the onset of water stress. Root length profiles ($L(z_i)$) were used to determine how the intrinsic root hydraulic conductivity (conductance per root length, k_{root}) was distributed along the root system:

$$k_{root}(z_i) = \frac{K_{root}(z_i)}{L(z_i)}. \tag{6}$$

In layers with both, small conductance and small root length this calculation can lead to erratic results. Therefore, for determination of k_{root}, we neglected soil layers with few roots (root length <1 cm) or root conductance <0.001 $\mathrm{mL^{-1}\,h\,MPa^{-1}}$.

2.6 | Statistical analysis

Generally, for data analysis of a certain parameter X, we considered its median value ($\tilde{X}$) among replicates of each species. Variability within the data set is given as median absolute deviation (MAD):

$$MAD = \mathrm{median}(|X_i - \tilde{X}|), \tag{7}$$

with X_i being the measured values from each individual replicate. For each species separately, we used Wilcoxon sign tests (matched pairs) to test for statistically significant differences in each soil layer among the 4 different days. The tested null-hypothesis was that there are no significant differences among the 4 days. If not stated differently, significant differences refer to a p value of 0.05. To test for significant differences between species, we used Mann–Whitney U tests. Both, Wilcoxon tests and Mann–Whitney U tests were performed using the SciPy-package (Virtanen et al., 2020) in Python.

We used a log transformation of Equation (6) to quantify to what extent measured changes in K_{root} over time were associated with a change in root length and to what extent with a change in root conductivity:

$$\ln\,(K_{\mathrm{root}}) = \ln\,(L) + \ln\,(k_{\mathrm{root}}). \tag{8}$$

Following the approach described by Poorter and Nagel (2000), the relative contribution of a change in L to a change in K_{root} (C_L) was calculated as:

$$C_L = \frac{\Delta \ln\,(K_{\mathrm{root}})}{\Delta \ln\,(L)}. \tag{9}$$

In Equation (9), the difference Δ refers to the measured differences between two points in time. The relative contribution of a change in k_{root} (C_k) is then given as:

$$C_k = 1 - C_L. \tag{10}$$

3 | RESULTS

Withholding water for 4 days resulted in a progressive, significant reduction in both the soil water content ($\bar{\theta}$) and soil water potential ($\bar{\Psi}_{\mathrm{soil}}$) averaged over depth (Table 3). For both species, $\bar{\theta}$ decreased from 16 $\mathrm{mL\,cm^{-3}}$ at Day 1 to 8 $\mathrm{mL\,cm^{-3}}$ at Day 4. $\bar{\Psi}_{\mathrm{soil}}$ decreased from −0.01 MPa at Day 1 to −0.09 MPa (faba bean), and −0.07 MPa (maize) respectively, at Day 4.

Figure 2 shows how these reductions were distributed over depth. At Day 1 after withholding water, for both species, there was a vertical gradient in θ with drier soil layers in the top and wetter layers in the bottom (Figure 2a,c). θ ranged from 12 $\mathrm{mL\,cm^{-3}}$ (at 5 cm depth) to 20 $\mathrm{mL\,cm^{-3}}$ (44 cm) for faba bean and from 12 $\mathrm{mL\,cm^{-3}}$ (6 cm) to 23 $\mathrm{mL\,cm^{-3}}$ (44 cm) for maize (Table 4). In each individual soil layer, θ was significantly ($p < 0.01$) reduced from each day towards the next one for both species. At Day 4, θ ranged from 5 $\mathrm{mL\,cm^{-3}}$ (7 cm) to 11 $\mathrm{mL\,cm^{-3}}$ (38) cm for faba bean and from 5 $\mathrm{mL\,cm^{-3}}$ (5 cm) to 10 $\mathrm{mL\,cm^{-3}}$ (38 cm) for maize. Like θ, Ψ_{soil} in each individual soil layer decreased significantly ($p < 0.01$) from each to the next day for both species (Figure 2b,d). At Day 1, Ψ_{soil} was almost uniformly distributed, with only a slight vertical gradient (around −0.02 MPa in the upper half of the pot, and −0.01 MPa in the lower half for both species). However, proceeding soil drying led to an increase in the vertical gradient: At Day 4, Ψ_{soil} ranged from −0.23 MPa (at 7 cm depth) to −0.03 MPa (38 cm) for faba bean, and from −0.14 MPa (5 cm) to −0.04 MPa (38 cm) for maize. In conclusion, although the vertical gradient in θ even decreased during soil drying, the gradient in Ψ_{soil} increased strongly. This is due to the nonlinear character of the water retention curve: in the dry regime, a small reduction in θ causes a strong reduction in Ψ_{soil}.

TABLE 3 Volumetric soil water content and soil water potential averaged over depth and across each day of the experiment.

Day	Faba bean $\bar{\theta}$ (%)	 $\bar{\Psi}_{soil}$ (MPa)	Maize $\bar{\theta}$ (%)	 $\bar{\Psi}_{soil}$ (MPa)
1	16.1 ± 2.0^{a}	-0.01 ± 0.00^{a}	16.0 ± 2.0^{a}	-0.01 ± 0.00^{a}
2	12.9 ± 1.2^{b}	-0.03 ± 0.01^{b}	13.4 ± 2.5^{b}	-0.02 ± 0.01^{b}
3	9.9 ± 1.2^{c}	-0.06 ± 0.01^{c}	10.7 ± 2.0^{c}	-0.04 ± 0.01^{c}
4	8.0 ± 1.2^{d}	-0.09 ± 0.03^{d}	7.8 ± 1.9^{d}	-0.07 ± 0.03^{d}

Note: Values are species medians with median absolute deviation. For each species separately, we tested for significant changes of each parameter among the 4 days using Wilcoxon rank tests. Different letters indicate significantly different values ($p < 0.05$).

In the next step, we analyzed how the changes in Ψ_{soil} affected root water uptake patterns measured as the normalized plant-driven root water uptake distributions ($\hat{U}_P$), using the SWaP. At Day 1, for both species there was a vertical gradient in $\hat{U}_P$ with greater values in upper soil layers and lower values in deeper layers (Figure 3). $\hat{U}_P$ was not constant over time: Generally, $\hat{U}_P$ decreased in the drier, upper soil layers, while it increased in relatively wetter, deeper layers. For the parameters described below, in deeper layers we observed a consistent trend from Days 1 to 3, reversing from Days 3 to 4. Therefore, we primarily tested for significant differences between Days 1 and 3. As indicated by a different background colour in Figure 3, we observed the following significant changes: For faba bean, $\hat{U}_P$ decreased in the top 8 cm ($p < 0.01$) and increased between 11 and 38 cm depth ($p < 0.05$ at 11–13 cm depth, <0.01 at 13–38 cm depth). For maize, $\hat{U}_P$ decreased in the top 10 cm ($p < 0.05$ at 10 cm depth, <0.001 else) and increased below 20 cm depth ($p < 0.05$ at 20–23 cm depth, <0.01 below).

Alterations of $\hat{U}_P$ are caused by a shift in the distribution of root hydraulic conductance (K_{root}). To derive the distribution of K_{root} over depth, we multiplied the daily average of the total conductance, as determined in a previous study (Müllers, Postma, Poorter, & van Dusschoten, 2022) (Table 2), with the daily $\hat{U}_P(z)$, according to

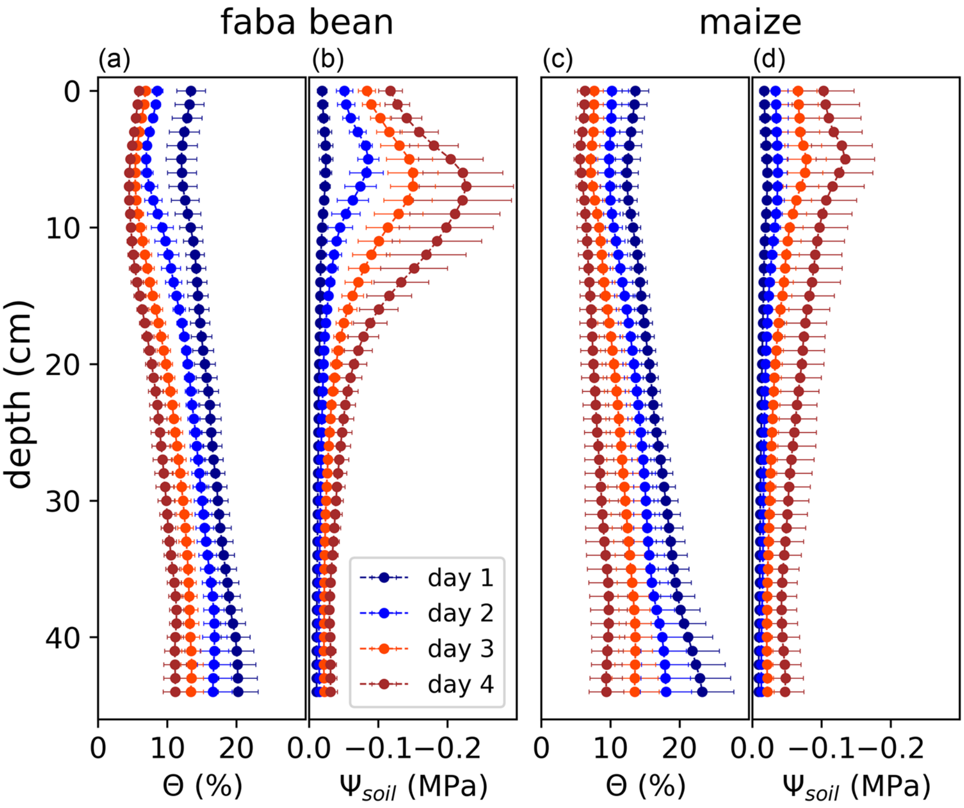

FIGURE 2 Distribution of soil moisture parameters over depth during 4 days of soil drying. (a and c) Show volumetric soil water content (θ), (b and d) show soil water potential (Ψ_{soil}). Data points are median values among all faba bean (a and c) and maize (b and d) replicates ($N = 10$). Error bars are median absolute deviations. A Wilcoxon rank test was used to test for significant differences among the 4 days of soil drying at each depth separately. In each soil layer, both, θ and Ψ_{soil}, decreased significantly between each of the 4 days.

TABLE 4 Maximal and minimal values of soil water content and soil water potential over depth, at each day of the measurement.

Day	Faba bean $\theta_{\min}$ (%)	Faba bean $\theta_{\max}$ (%)	Maize $\theta_{\min}$ (%)	Maize $\theta_{\max}$ (%)
1	12.0 ± 3.1^a	20.3 ± 4.0^a	12.4 ± 2.1^a	23.3 ± 6.8^a
2	6.9 ± 1.2^b	16.8 ± 3.2^b	9.7 ± 2.9^b	18.0 ± 5.1^b
3	5.4 ± 0.7^c	13.9 ± 1.7^c	6.8 ± 1.9^c	13.7 ± 4.3^c
4	4.5 ± 0.7^d	11.4 ± 2.0^d	5.4 ± 1.6^d	9.8 ± 3.1^d
Day	**Faba bean $\Psi_{\text{soil, min}}$ (MPa)**	**Faba bean $\Psi_{\text{soil, max}}$ (MPa)**	**Maize $\Psi_{\text{soil, min}}$ (MPa)**	**Maize $\Psi_{\text{soil, max}}$ (MPa)**
1	-0.02 ± 0.01^a	-0.01 ± 0.00^a	-0.02 ± 0.01^a	-0.01 ± 0.00^a
2	-0.09 ± 0.03^b	-0.01 ± 0.00^b	-0.04 ± 0.02^b	-0.01 ± 0.01^b
3	-0.15 ± 0.05^c	-0.02 ± 0.00^c	-0.09 ± 0.05^c	-0.02 ± 0.01^c
4	-0.23 ± 0.08^d	-0.03 ± 0.01^d	-0.14 ± 0.10^d	-0.04 ± 0.03^d

Note: Values are species medians with median absolute deviation. For each species separately, we tested for significant changes of each parameter among the 4 days using Wilcoxon rank tests. Different letters indicate significantly different values ($p < 0.05$).

Equation (5). The total conductance at the 1st day was similar for faba bean and maize (8–9 mL h^{-1} MPa^{-1} Table 2). At Day 1, for both species, there was a vertical gradient in K_{root} with greater values in upper soil layers (54% in the upper 10 cm for faba bean, 47% for maize) and lower values in the bottom (13% in the bottom half for faba bean, 21% for maize) (Figure 4). Withholding water for 4 days resulted in a strong reduction of K_{root} in upper soil layers with more negative Ψ_{soil}: For faba bean, K_{root} significantly decreased from

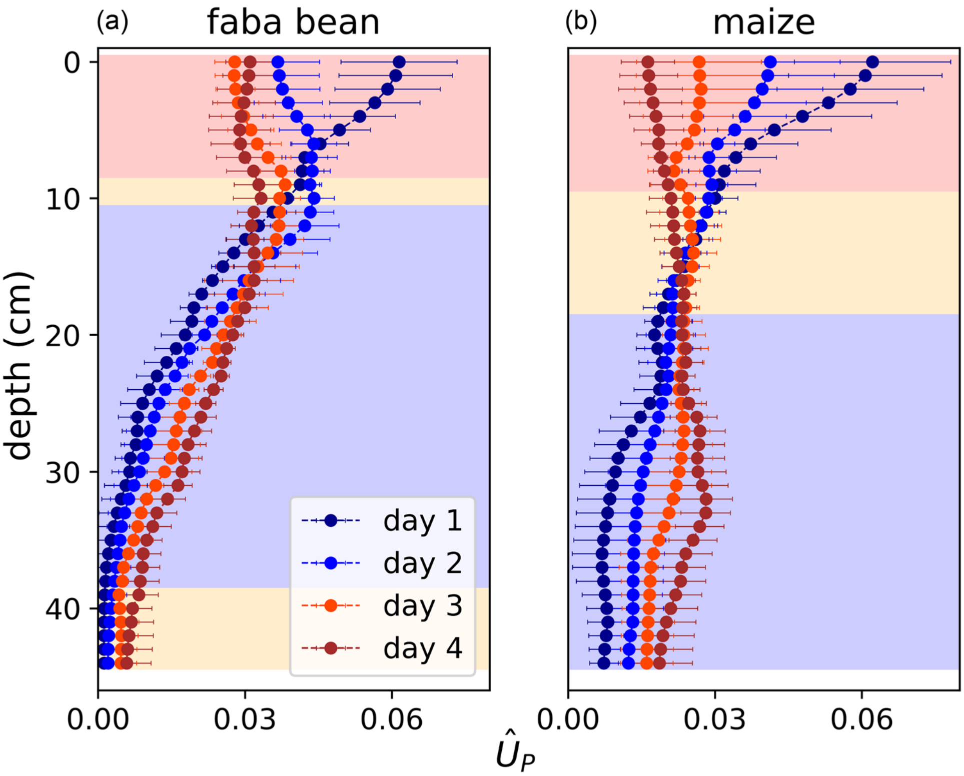

FIGURE 3 Normalized plant-driven root water uptake distribution ($\hat{U}_P$) over depth during 4 days of soil drying. Data points are median values among all faba bean (a) and maize (b) replicates ($N = 10$). Error bars are median absolute deviations. Background colour in each layer indicates a significant decrease (pink), increase (blue), or no significant change (yellow) between Days 1 and 3, tested with a Wilcoxon rank test. Days 1 and 3 were chosen as reference points, because the parameters analyzed below showed a consistent trend within this period.

Days 1 to 3 in the entire upper half of the pot ($p < 0.01$) by, on average, 72% (Figure 4a). In the lower half, K_{root} did not change significantly. For maize, K_{root} significantly decreased from Days 1 to 3 in the upper 16 cm of the pot ($p < 0.01$ above 12 cm depth, <0.05 else) by, on average, 66% (Figure 4b). However, between a depth of 31 and 41 cm, K_{root} increased significantly ($p < 0.01$ at 35–37 cm depth, <0.05 else) by, on average, 107% (Figure 4c). With proceeding soil drying from Days 3 to 4, K_{root} decreased again in these layers, such that it was not significantly different compared with Day 1.

The temporarily increased K_{root} in deeper parts of the maize root systems supports the uptake of deep soil water resources. We estimated the relevance of this facilitated deep water uptake by calculating how much it contributed to the total root water uptake (Figure 5). For maize, the measured increases in K_{root} contributed 5% to the total root water uptake rate at Day 2, 11% at Day 3, and 21% at Day 4. In different words, without the enhanced K_{root}, only 80% of the measured water uptake rate might have been realized at Day 4. Note that the hypothetical uptake rates (grey bars in Figure 5) were calculated by setting all measured increases in K_{root} to zero and assuming that this would not affect the leaf water potential, implying a strict stomatal control of the plant water status. More realistically, a lack of the increases in K_{root} would not be fully reflected in a reduction in total water uptake rate, but also partially in leaf water potential. However, mitigation of both, the drop in total root water uptake rate and in leaf water potential comes with reduced plant water stress. For faba bean, measured increases in K_{root} at each day contributed significantly less to the total root water uptake rate compared with maize ($p < 0.05$).

The determination of K_{root}, along with the associated increases in deeper layers for maize (Figures 4 and 5), are based on a correct separation of U_P and U_S by the SWaP measurements (Equations 1–3). Otherwise, the local increases might also be explained by an altered soil water distribution and the resulting compensated root water uptake. Although theoretically, U_P and U_S were separated using the fluctuating light intensity, we evaluated the potential effect of compensated root water uptake on U_P by comparing the changes in U_P and U_S between Days 1 and 3 in deeper layers for maize (Supporting Information: Appendix 2 and Figure 4). Below 20 cm depth, the measured U_P increased between Days 1 and 3 (Supporting Information: Figure 4A,D). Below 30 cm depth, this increase was of the order of 0.2 mL h^{-1} (Supporting Information: Figure 4C,F). At the same time, the estimated U_S also increased in these layers (Supporting Information: Figure 4B,E) indicating enhanced compensated root water uptake. However, U_S at Day 3 was only of the order of 0.02 m h^{-1}, and thus a factor 10 smaller than the increase in U_P. Calculation of U_S assuming no local increases in K_{root} (U_S', see Supporting Information: Appendix 2) gave even smaller values (Supporting Information: Figure 4B,E). In conclusion, even if U_P and

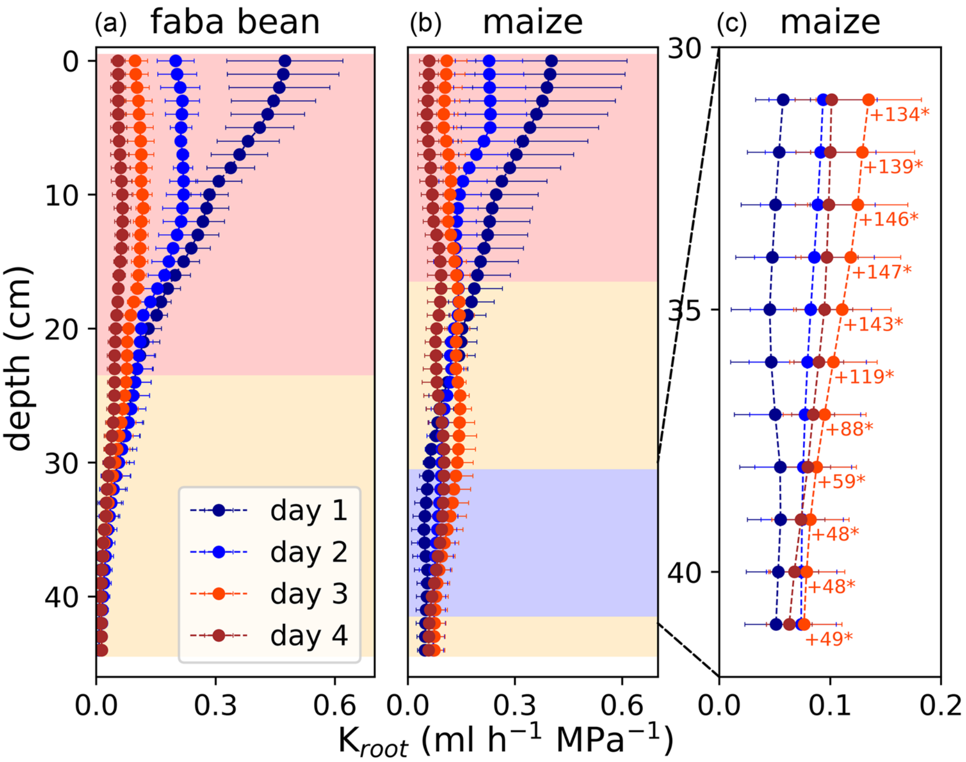

FIGURE 4 Distribution of root conductance (K_{root}) over depth during 4 days of soil drying. Data points are median values among all faba bean (a) and maize (b) replicates ($N = 10$). Error bars are median absolute deviations. Significant differences between Days 1 and 3 in each layer are indicated by the background colour, analogue to Figure 3. (c) Shows a magnification of (b) for layers with a significantly increasing K_{root} between Days 1 and 3. Values next to data points are percentage increases compared with Day 1.

U_S were not separated correctly by our approach, contribution of U_S to the increased U_P in deeper layers was marginal, such that the increase in K_{root} (Figures 4 and 5) remained.

We analyzed whether the locally enhanced K_{root} in maize was caused by additional root growth or an increase in root conductivity (conductance per length, k_{root}). Root length distributions at each day were derived from MRI images before and after the 4 days, making use of exponentially interpolating the data (Figure 6a–c). Then we derived k_{root} profiles at each day by dividing K_{root} by the root length distributions (Figure 6d–f). Initially, faba bean roots had a much greater conductivity (0.19 mL h^{-1} MPa^{-1} m^{-1} on average over depth) than maize roots (0.05 mL h^{-1} MPa^{-1} m^{-1} on average over depth). Like for the other parameters analyzed above, at Day 1, there was a vertical gradient in k_{root}. Shallow roots of both species had a greater conductivity than deeper roots. Withholding water for 4 days resulted in a decreasing k_{root} of shallow roots, in the faster drying, upper soil layers. In faba bean, k_{root} decreased significantly from Days 1 to 3 in the upper 29 cm of the pot ($p < 0.01$) by, on average, 76% (Figure 6d). Below 30 cm, k_{root} remained mostly constant. In maize, k_{root} decreased significantly from Days 1 to 3 in the upper 15 cm of the pot ($p < 0.01$ above 12 cm depth, <0.05 else) by, on average, 66% (Figure 6e). Between a depth of 27 and 35 cm, however, k_{root} increased significantly ($p < 0.05$) by up to 81% (Figure 6f). Like K_{root}, k_{root} from Days 3 to 4 decreased again in these layers. Distributions of k_{root} for each individual maize plant during the 4 days are shown in Supporting Information: Figure 5. For each plant, there were local increases in k_{root}, indicated by green dots, during the 4 days. The depth and day at which these increases occurred, however, varied strongly among the different replicates, causing the limited significance observed in Figure 6e. Using Equations (8–10), we calculated how much changes in root length, and k_{root} contributed to the significantly increased K_{root} at 31–41 cm depth for maize (Table 5). In each of these soil layers, the increase in K_{root} was primarily caused by an increase in k_{root} (relative contribution >0.75 in 8 out of 10 layers). Note that in some layers, root length even decreased slightly, causing the negative values for the contribution of root length and values >1 for the contribution of root conductivity in Table 5.

4 | DISCUSSION

The spatial distributions of root hydraulic traits and how they are affected by soil drying has important implications for the plant water balance. The strong reduction of soil water potential in upper soil layers led to a significant reduction of the local root hydraulic conductance. In maize, this was partly compensated by an increased conductivity (conductance per length) in deep roots. This enabled plants to maintain an estimated 20% greater total water uptake rate compared with a scenario without local increases in root conductance.

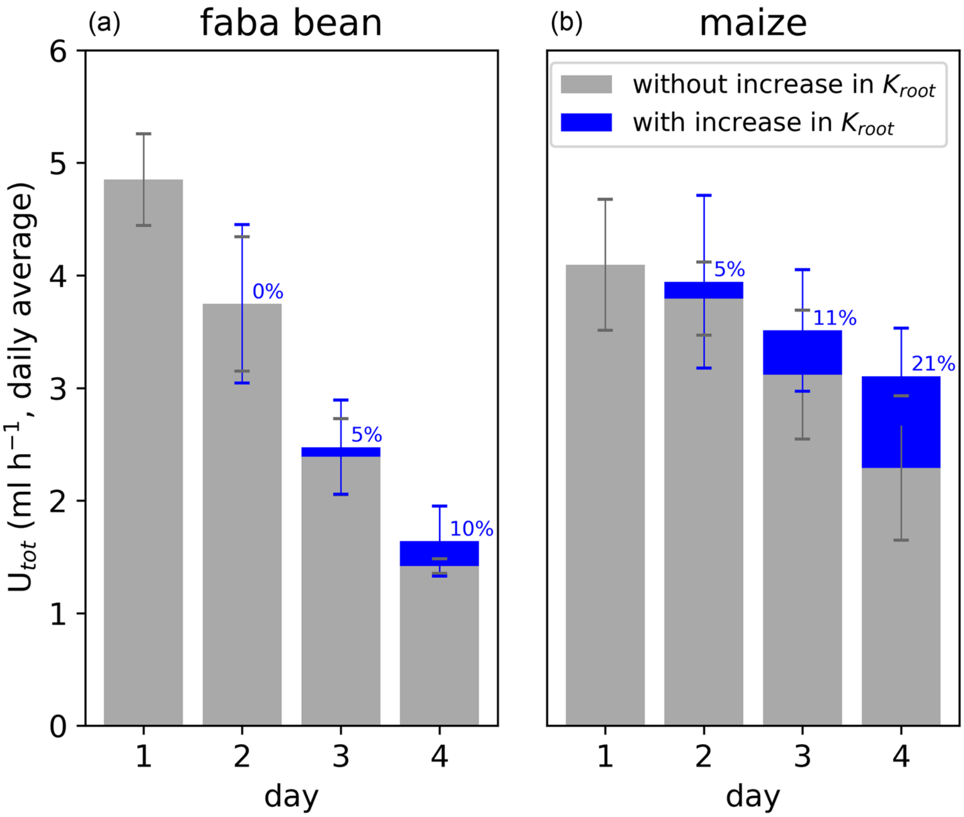

FIGURE 5 Effect of increases in root conductance on the total root water uptake rate (U_{tot}) during 4 days of soil drying. Grey bars are hypothetical uptake rates, calculated by setting all measured local increases in K_{root} to zero. Blue parts of the bars are the fractions of total water uptake rates attributed to the measured increases in K_{root}. Blue values give the relative contribution of these fractions to the measured uptake rates. Total water uptake rates are the temporal averages across the illuminated period at each day. Height of the error bars are medians among faba bean (a) and maize (b) replicates, error bars are median absolute deviations ($N = 10$).

Initially, root conductance in upper soil layers was much greater (87% in upper half of the pot for faba bean, 79% for maize) than in deeper soil layers (Figure 4). This is typical for well-watered conditions since shallow roots are usually more abundant (Haberle & Svoboda, 2015; Kemper et al., 2020; Righes, 1980) and more conductive than deeper roots (Dara et al., 2015; Müllers, Postma, Poorter, Kochs, et al., 2022; Zarebanadkouki et al., 2013). Consequently, withholding water resulted in a considerable vertical gradient in soil water potential with more negative values in the top and less negative values in the bottom (Figure 2). In response to soil drying, we observed a significant decrease in K_{root} in upper, relatively dry soil layers for both species (Figure 4). One plausible reason for this decrease is a partial loss of soil root contact due to root shrinkage, which was shown to be initiated at a soil water potential of around −0.02 MPa for faba bean (Koebernick et al., 2018) and maize (Duddek et al., 2022). Therefore, in upper soil layers, the relatively low (more negative) Ψ_{soil} might have induced root shrinkage in our study, resulting in the observed reduction in K_{root}, whereas in deeper layers, Ψ_{soil} was still sufficiently high (less negative). Nevertheless, the critical Ψ_{soil} at which we observed significant reductions in K_{root} was around −0.04 MPa (compare Figures 2 and 4), and thus slightly more negative than reported by the two studies mentioned above. Besides a loss of soil-root contact, K_{root} can also decrease due to enhanced root suberization and reducing the amount of active aquaporins, two mechanisms which are under biological control of the plant. Soil drying reportedly led to a decreased expression of aquaporin genes in shallow roots (Johnson et al., 2014), and an enhanced suberization of, especially, basal root parts (Kreszies et al., 2019) which predominantly reside in the top soil. Both processes might have contributed to the observed reduction in K_{root} in upper soil layers (Figure 4).

We assumed that the soil conductance was much greater than the root conductance to approximate K_{root} by K_{SL} (Equations 4 and 5). Estimations of K_{soil} (Supporting Information: Appendix 1) showed that this approximation was justified for a large part of the measurement (Supporting Information: Figure 3). Only in upper soil layers for faba bean at Day 4, K_{soil} was of the same order of magnitude as K_{root} (Supporting Information: Figure 3I). There, up to 8% of the decline in K_{root} from Days 3 to 4 as shown in Figure 4 were caused by a reduction in K_{soil}. Nevertheless, this effect was of minor importance, as K_{root} was already reduced by 72% on average between Days 1 and 3 in the upper half of the pot.

Theoretically, unregulated water uptake from drying soils can lead to steep water potential gradients in the soil around roots and

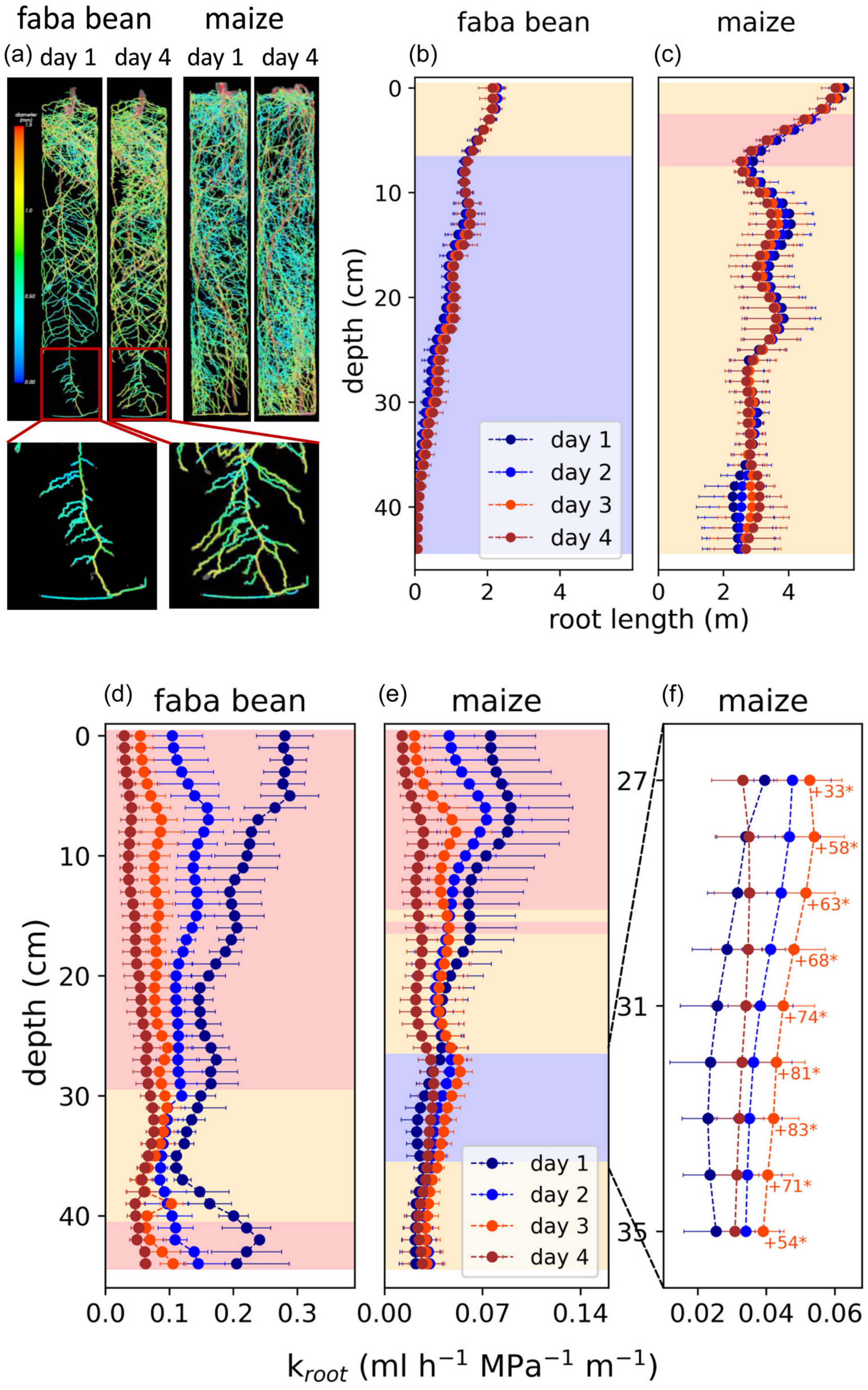

FIGURE 6 Distribution of root length and root conductivity (conductance per root length, k_{root}) over depth during 4 days of soil drying. Example, MRI images show the root system of a faba bean and maize plant at the first and last day of the measurement (a). Pseudo colours indicate root diameter with the colour bar ranging from 0 mm (blue) to 1.5 mm (red). Root length distribution over depth for faba bean (b) and maize (c) were derived from the MRI images. Data points are median values, error bars are median absolute deviations. Significant differences between Days 1 and 4 in each layer are indicated by the background colour, analogue to Figure 3. The distributions of k_{root} over depth (d and e) were derived by dividing K_{root} as shown in Figure 4 by the root length distributions. (f) Shows a magnification of (e) for layers with a significantly increasing k_{root} between Days 1 and 3. Values next to data points are percentage changes compared with Day 1.

TABLE 5 Contribution of changes in root length and conductivity to the significant increase in maize root conductance between Days 1 and 3 at 31–41 cm depth as shown in Figure 4c.

Depth (cm)	Relative contribution root length	Relative contribution conductivity
31	−0.09 ± 0.31	1.09 ± 0.31
32	−0.05 ± 0.39	1.05 ± 0.39
33	−0.02 ± 0.48	1.02 ± 0.48
34	−0.00 ± 0.49	1.00 ± 0.49
35	0.08 ± 0.45	0.92 ± 0.45
36	0.38 ± 0.40	0.62 ± 0.40
37	0.41 ± 0.44	0.59 ± 0.44
38	0.22 ± 0.40	0.78 ± 0.40
39	0.15 ± 0.50	0.85 ± 0.50
40	0.20 ± 0.54	0.80 ± 0.54
41	0.24 ± 0.56	0.76 ± 0.56

Note: Data were calculated using the log-transformed differences between Days 1 and 3. Values are median values with median absolute deviations. Values <0 for the contribution of root length (and >1 for the contribution of conductivity) are caused by a decrease in root length between the two points in time.

thus interrupt the hydraulic pathway from the bulk soil towards the roots, and force stomatal closure (Carminati & Javaux, 2020). Our estimations of the water potential at the root surface (Supporting Information: Figure 3A,C) emphasize that such a severe water depletion zone did not occur during the measurements presented here. Most likely, the early local reduction in K_{root}, due to the mechanisms discussed above, and the resulting stomatal closure, could prevent an incisive drop in the local K_{soil}. These conclusions on the effect of K_{soil} initially apply only to the soil type used in this study, a loamy sand. In this context, a recent study showed that the total conductance between soil and plant decreased at a less negative Ψ_{soil} in a sandy soil compared with loamy soil, probably because the loamy soil sustained a greater conductivity at a given Ψ_{soil} (Cai et al., 2022). Additionally, the effect of a reduced soil-root contact depends on soil texture, and might be more pronounced in the loamy sand used here, compared with a sandy soil (Carminati et al., 2009).

Despite the potential benefit of preventing a severe water depletion zone around the roots, the strong reduction in K_{root} in upper soil layers (76% reduction in faba bean, 66% reduction in maize [Figure 4]) comes with different impairments for the plant: A reduction in K_{root} hampers the hydraulic redistribution of soil water from relatively wetter towards relatively drier soil layers through the roots (Neumann & Cardon, 2012). Moreover, as demonstrated in a previous study, the reduction in K_{root} amplifies the drop in plant water potential (Müllers, Postma, Poorter, & van Dusschoten, 2022). One possibility to partly compensate for this is deep-water uptake. Up until Day 3, water in the bottom third of the pots was much easier to access (Ψ_{soil} less negative than −0.03 MPa) than water in shallow soil layers (Ψ_{soil} locally as low as −0.15 MPa [faba bean] and −0.08 MPa [maize] [Figure 2]). However, in agreement with other studies (Clément et al., 2022; Dara et al., 2015; Zarebanadkouki et al., 2013), effectively taking up deep water was initially limited by a low local K_{root} (Figure 4). With proceeding soil drying, maize, but not faba bean was able to significantly increase K_{root} in deeper, comparably wet soil layers. The deep-water uptake, facilitated in this way, contributed up to 20% to the total root water uptake rate in maize (Figure 5) and thus, at least temporarily, alleviated the drop in plant water potential.

Deep-water uptake under drought can increase due to a local increase in root conductance, but also due to compensated root water uptake, quantified as U_S. This happens when the local Ψ_{soil} drops less than the global Ψ_{seq} which was the case in deeper soil layers in our study (compare Figure 2 and Table 2). Theoretically, we had separated U_P and U_S using the fluctuating light intensity which, on short time scales, only changes U_P but not U_S. To not fully rely on the success of this separation, we additionally estimated which impact it had for our conclusions on K_{root} if compensated water uptake had influenced the measured U_P (Supporting Information: Appendix 2). Since the estimated U_S at Day 3 in deeper layers in maize was a factor 10 smaller than the measured increase in U_P (Supporting Information: Figure 4), we conclude that the measured local increases in K_{root} largely remained, even if the separation of U_P and U_S had failed.

Normalization by root length indicated that the increase in K_{root} was mainly caused by a significantly increased root conductivity (conductance per length) (Figure 6). One potential reason for this phenomenon is directed, enhanced aquaporin gene expression, as observed by Johnson et al. (2014) or McLean et al. (2011). By relating empirical data on Ψ_{soil}, ABA concentration in roots, and its impact on aquaporin expression, Couvreur et al. (2015) estimated a 250% increase in k_{root} between a local Ψ_{soil} of −0.005 and −0.1 MPa. This effect would lead to a net increase in k_{root} as long as it is not outweighed by a reduced soil-root contact and other forementioned processes reducing k_{root}. The fact that increases in k_{root} only occurred above a Ψ_{soil} of −0.04 MPa in our study (compare Figures 2 and 6e,f) fits these considerations. Furthermore, the different abilities of faba bean and maize to increase K_{root} might be explained by root aquaporin regulation as well: Under nonstressed conditions, radial water uptake in bean occurs predominantly via the cell-to-cell pathway, mediated by aquaporins, whereas in maize, the apoplastic pathway contributes considerably (Javot & Maurel, 2002; Steudle & Brinckmann, 1989; Steudle & Frensch, 1989). This fits the initially greater conductivity of faba bean roots compared to maize roots (Figure 6a,b at Day 1). To compensate this, maize had a greater root length (Figure 6b,c), thus achieving a similar initial conductance (compare Figure 4a and 4b at Day 1) with a greater flexibility and potential for local increases via a facilitated cell-to-cell water transport.

However, the observed increase in k_{root} could have also been caused by xylem maturation. As summarized by M. McCully (1995), maturation of the late metaxylem can occur far behind the root tip (up to 10–50 cm) for various species, including maize (St. Aubin et al., 1986) and soybean (M.E. McCully, 1994). Since maturation of the metaxylem results in an increase in axial conductivity, the measured increase in k_{root} in maize possibly reflects the development of xylem vessels. This would imply that the axial conductivity had initially limited root water uptake in deeper soil layers, as suggested by previous studies (Clément et al., 2022; Sanderson et al., 1988; Strock et al., 2021). However, the strong increase in local k_{root} (up to 82%) indicates a simultaneous response of all roots of various growth stages within the respective soil layers, rather than a continuous developmental process. Additionally, Steudle & Peterson (1998) reported for maize that even though the late metaxylem is not fully developed within 25 cm from the root tip, axial conductance is orders of magnitude greater than radial conductance, except for a small apical region without developed early metaxylem. We conclude that an increased amount of active aquaporins is a plausible explanation for the measured local increases in k_{root}, which could have been enhanced by other mechanisms, such as xylem development.

5 | CONCLUSION

We analyzed the effect of soil drying on vertical profiles of root hydraulic conductance in faba bean and maize. Withholding water for 4 days resulted in a pronounced vertical gradient in soil water potential with drier layers in the top and wetter layers in the bottom. In drier, shallow soil layers, the reduced soil water potential caused a strong decrease in root conductance, which on the one hand prevented a severe drop in soil hydraulic conductivity around the roots, on the other hand amplified water stress and forced stomatal closure. To partly compensate for this, maize, in contrast to faba bean, was able to facilitate deep water uptake by locally increasing its root conductivity. This increase improved the overall water uptake rate, and thus is an effective plant strategy to reduce water stress during soil drying.

ACKNOWLEDGEMENTS

This study was institutionally funded by the Helmholtz Association, Germany – POF4-899. Open access was partly funded by the Deutsche Forschungsgemeinschaft (DFG, German Research Foundation) – 491111487. Open Access funding enabled and organized by Projekt DEAL.

DATA AVAILABILITY STATEMENT

The data are available on request from the corresponding author, Dagmar van Dusschoten.

ORCID

Yannik Müllers http://orcid.org/0000-0002-0475-3734
Johannes A. Postma http://orcid.org/0000-0002-5222-6648

REFERENCES

Ahmed, M.A., Zarebanadkouki, M., Kaestner, A. & Carminati, A. (2016) Measurements of water uptake of maize roots: the key function of lateral roots. *Plant and Soil*, 398(1–2), 59–77. Available at: https://doi.org/10.1007/s11104-015-2639-6

Ahmed, M.A., Zarebanadkouki, M., Meunier, F., Javaux, M., Kaestner, A. & Carminati, A. (2018) Root type matters: measurement of water uptake by seminal, crown, and lateral roots in maize. *Journal of Experimental Botany*, 69(5), 1199–1206. https://doi.org/10.1093/jxb/erx439

Alsina, M.M., Smart, D.R., Bauerle, T., De Herralde, F., Biel, C., Stockert, C. et al. (2011) Seasonal changes of whole root system conductance by a drought-tolerant grape root system. *Journal of Experimental Botany*, 62(1), 99–109. https://doi.org/10.1093/jxb/erq247

Asseng, S., Ritchie, J.T., Smucker, A.J.M. & Robertson, M.J. (1998) Root growth and water uptake during water deficit and recovering in wheat. *Plant and Soil*, 201(2), 265–273. https://doi.org/10.1023/A:1004317523264

Barrios-Masias, F.H., Knipfer, T. & McElrone, A.J. (2015) Differential responses of grapevine rootstocks to water stress are associated with adjustments in fine root hydraulic physiology and suberization. *Journal of Experimental Botany*, 66(19), 6069–6078. https://doi.org/10.1093/jxb/erv324

Bartlett, M.K., Scoffoni, C. & Sack, L. (2012) The determinants of leaf turgor loss point and prediction of drought tolerance of species and biomes: a global meta-analysis. *Ecology Letters*, 15(5), 393–405. https://doi.org/10.1111/j.1461-0248.2012.01751.x

Bourbia, I., Pritzkow, C. & Brodribb, T.J. (2021) Herb and conifer roots show similar high sensitivity to water deficit. *Plant Physiology*, 186(4), 1908–1918. https://doi.org/10.1093/PLPHYS/KIAB207

Cai, G., König, M., Carminati, A., Abdalla, M., Javaux, M. & Wankmüller, F. et al. (2022) Transpiration response to soil drying and vapor pressure deficit is soil texture specific. *Plant and Soil* 17. https://doi.org/10.1007/s11104-022-05818-2

Carminati, A. & Javaux, M. (2020) Soil rather than xylem vulnerability controls stomatal response to drought. *Trends in Plant Science*, 25(9), 868–880. https://doi.org/10.1016/j.tplants.2020.04.003

Carminati, A., Vetterlein, D., Weller, U., Vogel, H.-J. & Oswald, S.E. (2009) When roots lose contact. *Vadose Zone Journal*, 8(3), 805–809. https://doi.org/10.2136/vzj2008.0147

Clément, C., Schneider, H.M., Dresbøll, D.B., Lynch, J.P. & Thorup-Kristensen, K. (2022) Root and xylem anatomy varies with root length, root order, soil depth and environment in intermediate wheatgrass (Kernza®) and alfalfa. *Annals of Botany*, 130, 367–382. https://doi.org/10.1093/aob/mcac058

Cochard, H. (2002) Xylem embolism and drought-induced stomatal closure in maize. *Planta*, 215(3), 466–471. https://doi.org/10.1007/s00425-002-0766-9

Corso, D., Delzon, S., Lamarque, L.J., Cochard, H., Torres-Ruiz, J.M., King, A. et al. (2020) Neither xylem collapse, cavitation, or changing leaf conductance drive stomatal closure in wheat. *Plant, Cell & Environment*, 43(4), 854–865. https://doi.org/10.1111/pce.13722

Couvreur, V., Vanderborght, J., Draye, X. & Javaux1, M. (2015) Dynamic aspects of soil water availability for isohydric plants: focus on root hydraulic resistances. *Water Resources Research*, 51, 2707–2723. https://doi.org/10.1002/2014WR015608.Received

Couvreur, V., Vanderborght, J. & Javaux, M. (2012) A simple three-dimensional macroscopic root water uptake model based on the hydraulic architecture approach. *Hydrology and Earth System Sciences*, 16(8), 2957–2971. https://doi.org/10.5194/hess-16-2957-2012

Cruz, R.T., Jordan, W.R. & Drew, M.C. (1992) Structural changes and associated reduction of hydraulic conductance in roots of *Sorghum bicolor* L. following exposure to water deficit. *Plant Physiology*, 99(1), 203–212. https://doi.org/10.1104/pp.99.1.203

Dara, A., Moradi, B.A., Vontobel, P. & Oswald, S.E. (2015) Mapping compensating root water uptake in heterogeneous soil conditions via neutron radiography. *Plant and Soil*, 397(1–2), 273–287. https://doi.org/10.1007/s11104-015-2613-3

Dubrovsky, J.G., North, G.B. & Nobel, P.S. (1998) Root growth, developmental changes in the apex, and hydraulic conductivity for Opuntia ficus-indica during drought. *New Phytologist*, 138(1), 75–82. https://doi.org/10.1046/j.1469-8137.1998.00884.x

Duddek, P., Carminati, A., Koebernick, N., Ohmann, L., Lovric, G., Delzon, S. et al. (2022) The impact of drought-induced root and root hair shrinkage on root–soil contact. *Plant Physiology*, 189, 1232–1236. https://doi.org/10.1093/plphys/kiac144

van Dusschoten, D., Kochs, J., Kuppe, C.W., Sydoruk, V.A., Couvreur, V., Pflugfelder, D. et al. (2020) Spatially resolved root water uptake determination using a precise soil water sensor. *Plant Physiology*, 184(3), 1221–1235. https://doi.org/10.1104/pp.20.00488

van Dusschoten, D., Metzner, R., Kochs, J., Postma, J.A., Pflugfelder, D. & Buehler, J. et al. (2016) Quantitative 3D analysis of plant roots growing in soil using magnetic resonance imaging. *Plant Physiology*, 170(3), 1176–1188. https://doi.org/10.1104/pp.15.01388

Frensch, J. & Steudle, E. (1989). Axial and radial hydraulic resistance to roots of maize (*Zea mays* L.). *Plant Physiology*, 91(2), 719–726. https://doi.org/10.1104/pp.91.2.719

Gessler, A., Bächli, L., Rouholahnejad Freund, E., Treydte, K., Schaub, M., Haeni, M. et al. (2022) Drought reduces water uptake in beech from the drying topsoil, but no compensatory uptake occurs from deeper soil layers. *New Phytologist*, 233, 194–206. https://doi.org/10.1111/nph.17767

Haberle, J. & Svoboda, P. (2015) Calculation of available water supply in crop root zone and the water balance of crops. *Contributions to Geophysics and Geodesy*, 45(4), 285–298. https://doi.org/10.1515/congeo-2015-0025

Hillel, D., Talpaz, H. & Keulen, H.V. (1976) A macroscopic-scale model of water uptake by a nonuniform root system and of water and salt movement in the soil profile. *Soil Science*, 121(4), 242–255.

Hu, T., Kang, S., Li, F. & Zhang, J. (2011) Effects of partial root-zone irrigation on hydraulic conductivity in the soil-root system of maize plants. *Journal of Experimental Botany*, 62(12), 4163–4172. https://doi.org/10.1093/jxb/err110

Javot, H. (2002) The role of aquaporins in root water uptake. *Annals of Botany*, 90(3), 301–313. https://doi.org/10.1093/aob/mcf199

Johnson, D.M., Sherrard, M.E., Domec, J.C. & Jackson, R.B. (2014) Role of aquaporin activity in regulating deep and shallow root hydraulic conductance during extreme drought. *Trees*, 28(5), 1323–1331. https://doi.org/10.1007/s00468-014-1036-8

Kemper, R., Bublitz, T.A., Müller, P., Kautz, T., Döring, T.F. & Athmann, M. (2020) Vertical root distribution of different cover crops determined with the profile wall method. *Agriculture*, 10(11), 503. https://doi.org/10.3390/agriculture10110503

Koebernick, N., Schlüter, S., Blaser, S.R.G.A. & Vetterlein, D. (2018) Root-soil contact dynamics of *Vicia faba* in sand. *Plant and Soil*, 431, 417–431.

Kondo, M., Murty, M.V.R. & Aragones, D.V. (2000) Characteristics of root growth and water uptake from soil in upland rice and maize under water stress. *Soil Science and Plant Nutrition*, 46(3), 721–732. https://doi.org/10.1080/00380768.2000.10409137

Kreszies, T., Shellakkutti, N., Osthoff, A., Yu, P., Baldauf, J.A., Zeisler-Diehl, V.V. et al. (2019) Osmotic stress enhances suberization of apoplastic barriers in barley seminal roots: analysis of chemical, transcriptomic and physiological responses. *New Phytologist*, 221(1), 180–194. https://doi.org/10.1111/nph.15351

Li, Y., Sperry, J.S. & Shao, M. (2009) Hydraulic conductance and vulnerability to cavitation in corn (*Zea mays* L.) hybrids of differing drought resistance. *Environmental and Experimental Botany*, 66(2), 341–346. https://doi.org/10.1016/j.envexpbot.2009.02.001

Lo Gullo, M.A., Nardini, A., Salleo, S. & Tyree, M.T. (1998) Changes in root hydraulic conductance (K(R)) of Olea oleaster seedlings following drought stress and irrigation. *New Phytologist*, 140(1), 25–31. https://doi.org/10.1046/j.1469-8137.1998.00258.x

Markesteijn, L., Iraipi, J., Bongers, F. & Poorter, L. (2010) Seasonal variation in soil and plant water potentials in a Bolivian tropical moist and dry forest. *Journal of Tropical Ecology*, 26(5), 497–508. https://doi.org/10.1017/S0266467410000271

Martre, P., North, G.B. & Nobel, P.S. (2001) Hydraulic conductance and mercury-sensitive water transport for roots of Opuntia acanthocarpa in relation to soil drying and rewetting. *Plant Physiology*, 126(1), 352–362. https://doi.org/10.1104/pp.126.1.352

McCully, M. (1995) How do real roots work? (Some new views of root structure). *Plant Physiology*, 109, 1–6. https://doi.org/10.1104/pp.109.1.1

McCully, M.E. (1994) Accumulation of high levels of potassium in the developing xylem elements in roots of soybean and some other dicotyledons. *Protoplasma*, 183(1–4), 116–125. https://doi.org/10.1007/BF01276819

McDowell, N.G. (2011) Mechanisms linking drought, hydraulics, carbon metabolism, and vegetation mortality. *Plant Physiology*, 155(3), 1051–1059. https://doi.org/10.1104/pp.110.170704

McLean, E.H., Ludwig, M. & Grierson, P.F. (2011) Root hydraulic conductance and aquaporin abundance respond rapidly to partial root-zone drying events in a riparian Melaleuca species. *New Phytologist*, 192(3), 664–675. https://doi.org/10.1111/j.1469-8137.2011.03834.x

Müllers, Y., Postma, J.A., Poorter, H. & van Dusschoten, D. (2022) Stomatal conductance tracks soil-to-leaf hydraulic conductance in faba bean and maize during soil drying. *Plant Physiology*, 190, 2279–2294. https://doi.org/10.1093/plphys/kiac422

Müllers, Y., Postma, J.A., Poorter, H., Kochs, J., Pflugfelder, D. & Schurr, U. et al. (2022) Shallow roots of different crops have greater water uptake rates per unit length than deep roots in well-watered soil. *Plant and Soil*, 481, 475–493. https://doi.org/10.1007/s11104-022-05650-8

Neumann, R.B. & Cardon, Z.G. (2012) The magnitude of hydraulic redistribution by plant roots: a review and synthesis of empirical and modeling studies. *New Phytologist*, 194(2), 337–352. https://doi.org/10.1111/j.1469-8137.2012.04088.x

Nobel, P.S. & Cui, M. (1992) Shrinkage of attached roots of opuntia ficus-indica in response to lowered water potentials—predicted consequences for water uptake or loss to soil. *Annals of Botany*, 70(6), 485–491. https://doi.org/10.1093/oxfordjournals.aob.a088508

North, G.B. & Nobel, P.S. (1991) Changes in hydraulic conductivity and anatomy caused by drying and rewetting roots of *Agave deserti* (Agavaceae). *American Journal of Botany*, 78(7), 906–915.

Passioura, J.B. (1983) Roots and drought resistance. *Agricultural Water Management*, 7(1–3), 265–280. https://doi.org/10.1016/0378-3774(83)90089-6

Pohlmeier, A., Haber-Pohlmeier, S. & Stapf, S. (2009) A fast field cycling nuclear magnetic resonance relaxometry study of natural soils. *Vadose Zone Journal*, 8(3), 735–742. https://doi.org/10.2136/vzj2008.0030

Poorter, H. & Nagel, O. (2000) The role of biomass allocation in the growth response of plants to different levels of light, CO_2, nutrients and water: a quantitative review. *Functional Plant Biology*, 27(6), 595–607. https://doi.org/10.1071/pp99173_co

Prechsl, U.E., Burri, S., Gilgen, A.K., Kahmen, A. & Buchmann, N. (2015) No shift to a deeper water uptake depth in response to summer drought of two lowland and sub-alpine C_3-grasslands in Switzerland. *Oecologia*, 177(1), 97–111. https://doi.org/10.1007/s00442-014-3092-6

Rasmussen, C.R., Thorup-Kristensen, K. & Dresbøll, D.B. (2020). Uptake of subsoil water below 2 m fails to alleviate drought response in deep-rooted Chicory (*Cichorium intybus* L.). *Plant and Soil*, 446(1–2), 275–290. https://doi.org/10.1007/s11104-019-04349-7

Reid, J.B. & Hutchison, B. (1986) Soil and plant resistances to water uptake by *Vicia faba* L. *Plant and Soil*, 92(3), 431–441. https://doi.org/10.1007/BF02372491

Rewald, B., Raveh, E., Gendler, T., Ephrath, J.E. & Rachmilevitch, S. (2012) Phenotypic plasticity and water flux rates of *Citrus* root orders under salinity. *Journal of Experimental Botany*, 63(7), 2717–2727. https://doi.org/10.1093/jxb/err457

Righes, A.A. (1980) Water uptake and root distribution of soybeans, grain sorghum and corn. *Retrospective Theses and Dissertations*. 134. https://lib.dr.iastate.edu/rtd/7122/

Rodrigues, M.L., Pacheco, C.M.A. & Chaves, M.M. (1995) Soil-plant water relations, root distribution and biomass partitioning in *Lupinus albus* L. under drought conditions. *Journal of Experimental Botany*, 46(8), 947–956. https://doi.org/10.1093/jxb/46.8.947

Rodriguez-Dominguez, C.M. & Brodribb, T.J. (2020) Declining root water transport drives stomatal closure in olive under moderate water stress. *New Phytologist*, 225(1), 126–134. https://doi.org/10.1111/nph.16177

Rodríguez-Gamir, J., Xue, J., Clearwater, M.J., Meason, D.F., Clinton, P.W. & Domec, J.C. (2019) Aquaporin regulation in roots controls plant hydraulic conductance, stomatal conductance, and leaf water potential in *Pinus radiata* under water stress. *Plant, Cell & Environment*, 42(2), 717–729. https://doi.org/10.1111/pce.13460

Ryu, J., Hwang, B.G., Kim, Y.X. & Lee, S.J. (2016) Direct observation of local xylem embolisms induced by soil drying in intact *Zea mays* leaves. *Journal of Experimental Botany*, 67(9), 2617–2626. https://doi.org/10.1093/jxb/erw087

Saliendra, N.Z. & Meinzer, F.C. (1989) Relationship between root/soil hydraulic properties and stomatal behavior in sugarcane. *Australian Journal of Plant Physiology*, 16(3), 241–250. https://doi.org/10.1071/PP9890241

Sanderson, J., Whitbread, F.C. & Clarkson, D.T. (1988) Persistent xylem cross-walls reduce the axial hydraulic conductivity in the apical 20 cm of barley seminal root axes: implications for the driving force for water movement. *Plant, Cell & Environment*, 11(4), 247–256. https://doi.org/10.1111/j.1365-3040.1988.tb01143.x

Sharp, R.E. & Davies, W.J. (1985) Root growth and water uptake by maize plants in drying soil. *Journal of Experimental Botany*, 36(9), 1441–1456. https://doi.org/10.1093/jxb/36.9.1441

St. Aubin, G., Canny, M.J. & Mccully, M.E. (1986) Living vessel elements in the late metaxylem of sheathed maize roots. *Annals of Botany*, 58(4), 577–588. https://doi.org/10.1093/annbot/58.4.577

Steudle, E. & Brinckmann, E. (1989) The osmometer model of the root: water and solute relations of roots of *Phaseolus coccineus*. *Botanica Acta*, 102(1), 85–95. https://doi.org/10.1111/j.1438-8677.1989.tb00071.x

Steudle, E. & Frensch, J. (1989) Osmotic responses of maize roots: water and solute relations. *Planta*, 177(3), 281–295. https://doi.org/10.1007/BF00403585

Steudle, E. & Peterson, C.A. (1998) How does water get through roots? *Journal of Experimental Botany*, 49(322), 775–788. https://doi.org/10.1093/jexbot/49.322.775

Strock, C.F., Burridge, J.D., Niemiec, M.D., Brown, K.M. & Lynch, J.P. (2021) Root metaxylem and architecture phenotypes integrate to regulate water use under drought stress. *Plant, Cell & Environment*, 44(1), 49–67. https://doi.org/10.1111/pce.13875

Thompson, M.V. (2006) Phloem: the long and the short of it. *Trends in Plant Science*, 11(1), 26–32. https://doi.org/10.1016/j.tplants.2005.11.009

Urli, M., Porte, A.J., Cochard, H., Guengant, Y., Burlett, R. & Delzon, S. (2013) Xylem embolism threshold for catastrophic hydraulic failure in angiosperm trees. *Tree Physiology*, 33(7), 672–683. https://doi.org/10.1093/treephys/tpt030

Virtanen, P., Gommers, R., Oliphant, T.E., Haberland, M., Reddy, T., Cournapeau, D. et al. (2020) SciPy 1.0: fundamental algorithms for scientific computing in Python. *Nature Methods*, 17(3), 261–272. https://doi.org/10.1038/s41592-019-0686-2

Wan, C., Sosebee, R.E. & McMichael, B.L. (1994) Hydraulic properties of shallow vs. deep lateral roots in a semiarid shrub, *Gutierrezia sarothrae*. *American Midland Naturalist*, 131(1), 120–127.

Wasson, A.P., Richards, R.A., Chatrath, R., Misra, S.C., Prasad, S.V.S., Rebetzke, G.J. et al. (2012) Traits and selection strategies to improve root systems and water uptake in water-limited wheat crops. *Journal of Experimental Botany*, 63(9), 3485–3498. https://doi.org/10.1093/jxb/ers111

Zarebanadkouki, M., Kim, Y.X. & Carminati, A. (2013) Where do roots take up water? Neutron radiography of water flow into the roots of transpiring plants growing in soil. *New Phytologist*, 199(4), 1034–1044. https://doi.org/10.1111/nph.12330

SUPPORTING INFORMATION

Additional supporting information can be found online in the Supporting Information section at the end of this article.

How to cite this article: Müllers, Y., Postma, J.A., Poorter, H. & Dusschoten, D. (2023) Deep-water uptake under drought improved due to locally increased root conductivity in maize, but not in faba bean. *Plant, Cell & Environment*, 46, 2046–2060. https://doi.org/10.1111/pce.14587

Supporting information

Appendix 1 Estimating the influence of soil hydraulic conductance on root water uptake.

Appendix 2 Estimating the impact of compensated root water uptake on measured water flow profiles.

Suppl. Fig. 1 Determination of $\widehat{U_P}$ using data measured with the SWaP at day 1 and day 4 of the drying period for an example maize plant.

Suppl. Fig. 2: Scheme of the hydraulic model used in this study.

Suppl. Fig. 3: Comparison between the soil conductance (K_{soil}), estimated by two different methods, and the root conductance (K_{root})

Suppl. Fig. 4: Comparison of the changes in plant-driven root water uptake distribution (U_P) and soil-driven root water uptake redistribution (U_S) between day 1 and day 3 for maize.

Suppl. Fig. 5: Distribution of root conductivity (conductance per root length, k_{root}) over depth during four days of soil drying for each single maize plant.

Appendix 1: Estimating the influence of soil hydraulic conductance on root water uptake

Assuming a much greater axial conductance between root system and leaf, multiplication of the normalized plant-driven root water uptake distribution ($\widehat{U}_P$) by the total hydraulic conductance between soil and leaf (K_{SL}) yields the local hydraulic conductance between bulk soil and root xylem (K_{SR}).

$$K_{SR}(z_i) = K_{SL} \cdot \widehat{U}_P(z_i) \qquad (1)$$

Table 1 in the main article shows the used terminology, their abbreviations, and units. K_{SR} is composed of the local soil conductance (K_{soil}) between bulk soil and root surface, and of the local root conductance between root surface and root xylem (K_{root}) (Suppl. Fig. 2). Since K_{soil} and K_{root} are connected in series, the sum of their reciprocals gives the reciprocal of K_{SR}:

$$K_{SR}{}^{-1} = K_{soil}{}^{-1} + K_{root}{}^{-1} \qquad (2)$$

To separate the contribution of the soil and the root to K_{SR}, we used two different methods to estimate K_{soil}.

Method 1: Estimation of the water potential at the soil-root interface (Ψ_{sr})

As suggested by Carminati and Javaux (2020), soil drying can lead to a severe water depletion zone around the roots, and thus a strong difference between the water potential in the bulk soil (Ψ_{soil}) and at the root surface (Ψ_{sr}). The difference between Ψ_{soil} and Ψ_{sr} is directly proportional to the hydraulic conductance between bulk soil and root surface, and thus K_{soil}. Therefore, estimation of Ψ_{sr}, together with data on Ψ_{soil} (measured with the SWaP) can be used to determine K_{soil}. Estimating Ψ_{sr} requires the soil hydraulic parameters derived with the water retention curve, root water uptake rates (RWU), root length, and root diameter to be known. Generally, Ψ_{sr} decreases with increasing water uptake rates per unit root length and decreasing Ψ_{soil}. Below, we show the basic equations used for the estimation of Ψ_{sr}, following the approach described in more detail by Carminati & Javaux (2020) or Abdalla et al. (2022).

First, the matrix flux potential at the root surface (ϕ_{sr}) is calculated as:

$$\Phi_{sr}(z_i) = \Phi_{bulk}(z_i) - \frac{RWU(z_i)}{2\pi r_0(z_i)L(z_i)}\left(\frac{r_0}{2} - r_0 r_b^2 \frac{ln(r_b(z_i)/r_0(z_i))}{r_b^2(z_i) - r_0(z_i)^2}\right) \qquad (3)$$

with root length L, root radius r_0 and the radius defining the start of the bulk soil r_b. r_b is approximated by $\sqrt{\frac{V}{\pi L(z_i)}}$ with the soil volume V in each layer. ϕ_{bulk} is the matrix flux potential in the bulk soil which, for a Brooks-Corey soil, is given by:

$$\Phi_{bulk} = \frac{\alpha^{\tau}}{(\tau+1)} \cdot K_{sat} \cdot \Psi_{soil}(z_i)^{\tau+1} \qquad (4)$$

with the Brooks-Corey parameters derived from the water retention curve: inverse of the air entry pressure α, saturated soil conductivity K_{sat}, and a dimensionless parameter based on the pore size index τ. Using eq. 3 and 4, we calculated Φ_{sr} for each soil layer separately using the locally measured Ψ_{soil} and L. The local RWU in eq. 3 was estimated by $\widehat{U_P} \cdot U_{tot}$. Note that this comes with an overestimation of RWU in drier soil layers and an underestimation in wetter layers. Therefore, the difference between Ψ_{sr} and Ψ_{soil} is overestimated in drier soil layers. We considered average values of r_0 for the entire root system with r_0=0.04 cm for faba bean and r_0=0.02 cm for maize as determined by (Müllers et al., 2022). Given the calculated ϕ_{sr}, Ψ_{sr} could be derived in each soil layer. For a Brooks-Corey soil, the relation between ϕ_{sr}, Ψ_{sr} is given by:

$$\Psi_{sr}(z_i) = \left[\frac{\Phi_{sr}(z_i) \cdot (\tau+1) \cdot \alpha^{-\tau}}{K_{sat}}\right]^{\frac{1}{\tau+1}} \qquad (5)$$

Suppl. Fig. 3 A and C show the estimated Ψ_{sr} profiles (filled circles), compared to the Ψ_{soil} profiles (non-filled squares) measured with the SWaP. In general, throughout the four days of measurement, Ψ_{sr} and Ψ_{soil} were very similar. Only at day 4 in upper soil layers in faba bean, Ψ_{sr} was notably more negative than Ψ_{soil} (around 0.1 MPa difference). The difference between Ψ_{sr} and Ψ_{soil} is directly related to K_{soil}, and can be calculated as follows: The local root water uptake rate is the product of the soil-root conductance, and the water potential gradient between soil and root xylem (Ψ_{root}) (Landsberg & Fowkes, 1978):

$$RWU(z_i) = K_{SR}(z_i) \cdot (\Psi_{soil}(z_i) - \Psi_{root}(z_i)) \qquad (6)$$

Assuming steady state water flow, the flow rate across the whole pathway from bulk soil into the root is constant (Alm et al., 1992). Under these conditions, the water flow rate in eq. 6 is equal to the water flow rate from bulk soil towards root surface:

$$K_{SR}(z_i) \cdot (\Psi_{soil}(z_i) - \Psi_{root}(z_i)) = K_{soil}(z_i) \cdot (\Psi_{soil}(z_i) - \Psi_{sr}(z_i)) \qquad (7)$$

After rewriting, eq. 7 gives an expression for the soil hydraulic conductance:

$$K_{soil}(z_i) = \frac{K_{SR}(z_i)\cdot(\Psi_{soil}(z_i)-\Psi_{root})}{(\Psi_{soil}(z_i)-\Psi_{sr}(z_i))} \quad (8)$$

In eq. 8, Ψ_{soil} is a measured parameter, K_{SR} was calculated using the measured $\widehat{U}_P$ and K_{SL} according to eq. 1, and Ψ_{sr} was estimated using the model described above. Ψ_{root} was approximated by the measured leaf water potential (Ψ_{leaf}) under the assumption of much greater axial than radial root conductance. This assumption is discussed in the discussion of the main article. With this, data on K_{soil} as shown in Suppl. Fig. 3 B and D could be calculated. According to these data, K_{soil} was of the order of 10^3 ml h^{-1} MPa^{-1} and 10^4 ml h^{-1} MPa^{-1}, for faba bean and maize respectively, at day 1. During the four days of withholding water, K_{soil} was strongly reduced, especially in the upper soil layers. At day 4, the minimum K_{soil} over depth was as low as 0.9 ml h^{-1} MPa^{-1} in faba bean and 14 ml h^{-1} MPa^{-1} in maize. Before evaluating the resulting effect on K_{RS}, we first describe an alternative method to estimate K_{soil}.

Method 2: Estimating an effective soil conductance

Following the approach from Nobel & Cui (1992), K_{soil} can be calculated as an effective soil conductance, based on Darcy's law of water flow from bulk soil towards the root surface. For water flow through a cylindrical root surface, K_{soil} writes:

$$K_{soil}(z_i) = \frac{2\pi L(z_i)}{r_0 \log\left(\frac{r_{b(z_i)}}{r_0}\right)} k_h(z_i) \quad (9)$$

In eq. 9, k_h is the soil hydraulic conductivity, and the other parameters are equivalent to those used in eq. 3. For a Brooks-Corey soil, k_h is given as:

$$k_h(z_i) = K_{sat}\cdot(\alpha\cdot\Psi_{soil}(z_i))^{\tau} \quad (10)$$

with the Brooks-Corey parameters as described above. Using this method, K_{soil} as shown in Suppl. Fig. 3 E-F was calculated. The data were similar to those obtained by method 1 (Suppl. Fig. 3 B and D): While at the first day, K_{soil} was of the order of 10^3 – 10^4 ml h^{-1} MPa^{-1} it dropped by more than a factor 100 towards the last day of the measurement in upper soil layers.

Determining the influence of K_{soil} on K_{SR}

To quantify the impact of K_{soil} on K_{SR}, we calculated the ratio $\frac{K_{SR}}{K_{soil}}$. This ratio is equivalent to the contribution of the soil resistance (reciprocal of conductance) to the total resistance between soil and root xylem. The greater this contribution, the greater is the impact of K_{soil} on K_{SR}, in relation to the impact of K_{root} on K_{SR}. Suppl. Fig. 3 G and I shows for faba bean, that up until day 3, the local soil resistance only contributed up to 5% (method 1), or 10% (method 2) respectively, to the total resistance between bulk soil and root xylem. This means that K_{soil} was 19 times, or 9 times respectively, greater than K_{root}. For this period, even in the driest zones deviations between K_{SR} and K_{root} were negligible, which justifies the approximation used for eq. 5 in the main article. At day 4, however, the local soil resistance contributed up to 20% according to method 2, meaning that K_{soil} was only 4 times greater than K_{root}, and thus becomes an important determinant of K_{SR}. We therefore discuss the contribution of K_{soil} to the observed changes at day 4 in the discussion of the main article. For maize, Suppl. Fig. 3 H and I show that by either method, the estimated contribution of the soil resistance remained below 4% during the four days, and thus the impact on K_{SR} was negligible.

References

Abdalla, M., Ahmed, M. A., Cai, G., Wankmüller, F., Schwartz, N., Litig, O., Javaux, M., & Carminati, A. (2022). Stomatal closure during water deficit is controlled by below-ground hydraulics. *Annals of Botany*, *129*(2), 161–170. https://doi.org/10.1093/aob/mcab141

Alm, D. J., Cavelier, J., & Nobel, P. S. (1992). A finite-element model of radial and axial conductivities for individual roots: Development and validation for two desert succulents. *Annals of Botany*, *69*(1), 87–92.

Carminati, A., & Javaux, M. (2020). Soil Rather Than Xylem Vulnerability Controls Stomatal Response to Drought. *Trends in Plant Science*, *xx*(xx), 1–13. https://doi.org/10.1016/j.tplants.2020.04.003

Landsberg, J. J., & Fowkes, N. D. (1978). Water Movement Through Plant Roots. *Ann. Botany*, *42*(August), 493–508. https://doi.org/10.1093/oxfordjournals.aob.a085488

Müllers, Y., Postma, J. A., Poorter, H., Kochs, J., Pflugfelder, D., Schurr, U., & Dusschoten, D. Van. (2022). Shallow roots of different crops have greater water uptake rates per unit length than deep roots in well - watered soil. *Plant and Soil*, *0123456789*. https://doi.org/10.1007/s11104-022-05650-8

Nobel, P. S., & Cui, M. (1992). Hydraulic conductances of the soil, the root-soil air gap, and the root: Changes for desert succulents in drying soil. *Journal of Experimental Botany*, *43*(3), 319–326. https://doi.org/10.1093/jxb/43.3.319

Appendix 2: Estimating the impact of compensated root water uptake on measured water flow profiles

In the present study, we analyzed how the distribution of root conductance changes during soil drying by measuring root water uptake patterns with the soil water profiler (SWaP). A key for this approach is separating the distribution of root water uptake rates (RWU) into one part which is solely determined by the distribution of root conductance (plant-driven root water uptake distribution, U_P) and a second part which additionally depends on the distribution of soil water potential (soil-driven root water uptake redistribution, U_S). As described in the main article, this was achieved by a fluctuating light intensity which induces a rapid change in plant water potential, and thus changes U_P but not U_S on short time scales. Using this separation, and a measure for the total conductance of the root system (approximated here by the total conductance between soil and leaf, K_{SL}), we could determine the distribution of root conductance. The reported increase in the local root conductance in deeper layers in maize (Fig. 4) is based on the measured increase in the local U_P and thus relies on a correct separation of U_P and U_S. Although this is theoretically achieved by the fluctuating light pattern, we want to clear up doubts, and estimated which effect it had if U_P and U_S would have not been separated correctly. As explained below, this was done by estimating U_S and comparing it to the measured increase in U_P.

Following the approach derived by (Couvreur et al., 2012), the local U_S, using our terminology, is given as:

$$U_S(z_i) = K_{comp} \cdot (\Psi_{soil}(z_i) - \Psi_{seq}) \cdot \widehat{U}_P(z_i) \qquad (1)$$

with the compensatory RWU conductance (K_{comp}), local soil water potential (Ψ_{soil}), equivalent soil water potential (Ψ_{seq}), and the normalized U_P ($\widehat{U}_P = \frac{U_P}{U_{tot}}$). Ψ_{seq} is the distribution of soil water potential weighted by $\widehat{U}_P$:

$$\Psi_{seq} = \sum_z \Psi_{soil}(z_i) \cdot \widehat{U}_P(z_i) \qquad (2)$$

Eq. 2 shows, that the local U_S, and thus the local RWU, increases when the difference between the local soil water potential and the equivalent soil water potential increases. This usually happens in deeper soil layers, where Ψ_{soil} drops less than Ψ_{seq}. In upper, relatively drier layers, it is the other way around, causing a decrease in the local RWU. This process, usually referred to as compensated root water uptake is quantified by U_S. If we had not correctly separated U_P and U_S by our method, part of the measured increase in U_P in deeper layers in maize between day 1 and day 3 (Fig. 4) could have been caused by an increased difference between the local Ψ_{soil} and Ψ_{seq}.

To test this, we estimated U_S for day 1 and day 3 using eq. 2. Since the total root system conductance reliably predicts K_{comp} (Meunier et al., 2017), K_{SL} was used here to approximate K_{comp}. The resulting U_S profiles are shown in Suppl. Fig. 4.

Calculation of U_S is based on the measured $\widehat{U}_P$, which could be problematic since $\widehat{U}_P$ is the parameter to evaluate by this procedure. What are the consequences of this dependency? If indeed U_S had influenced the measured $\widehat{U}_P$, $\widehat{U}_P$ would be overestimated in deeper layers. Then, the multiplication of $\widehat{U}_P$ in eq. 1 would contribute to an overestimation of U_S in deeper layers. However, it also causes an overestimation of Ψ_{seq} (greater $\widehat{U}_P$ in deeper, wetter layers results in a less negative Ψ_{seq} (eq. 2)), and thus underestimation of the local difference between Ψ_{soil} and Ψ_{seq}. This would contribute to an underestimation of U_S in deeper layers. The overall effect of an overestimation of $\widehat{U}_P$ on U_S is therefore difficult to predict. To address this uncertainty, we additionally calculated U_S using a hypothetical $\widehat{U}_P$ for which all measured increases in the local root conductance were set to zero. The resulting profiles, called U_S', are also shown in Suppl. Fig. 4 B.

References

Couvreur, V., Vanderborght, J., & Javaux, M. (2012). A simple three-dimensional macroscopic root water uptake model based on the hydraulic architecture approach. *Hydrology and Earth System Sciences*, *16*(8), 2957–2971. https://doi.org/10.5194/hess-16-2957-2012

Meunier, F., Couvreur, V., Draye, X., Vanderborght, J., & Javaux, M. (2017). Towards quantitative root hydraulic phenotyping: novel mathematical functions to calculate plant-scale hydraulic parameters from root system functional and structural traits. *Journal of Mathematical Biology*, *75*(5), 1133–1170. https://doi.org/10.1007/s00285-017-1111-z

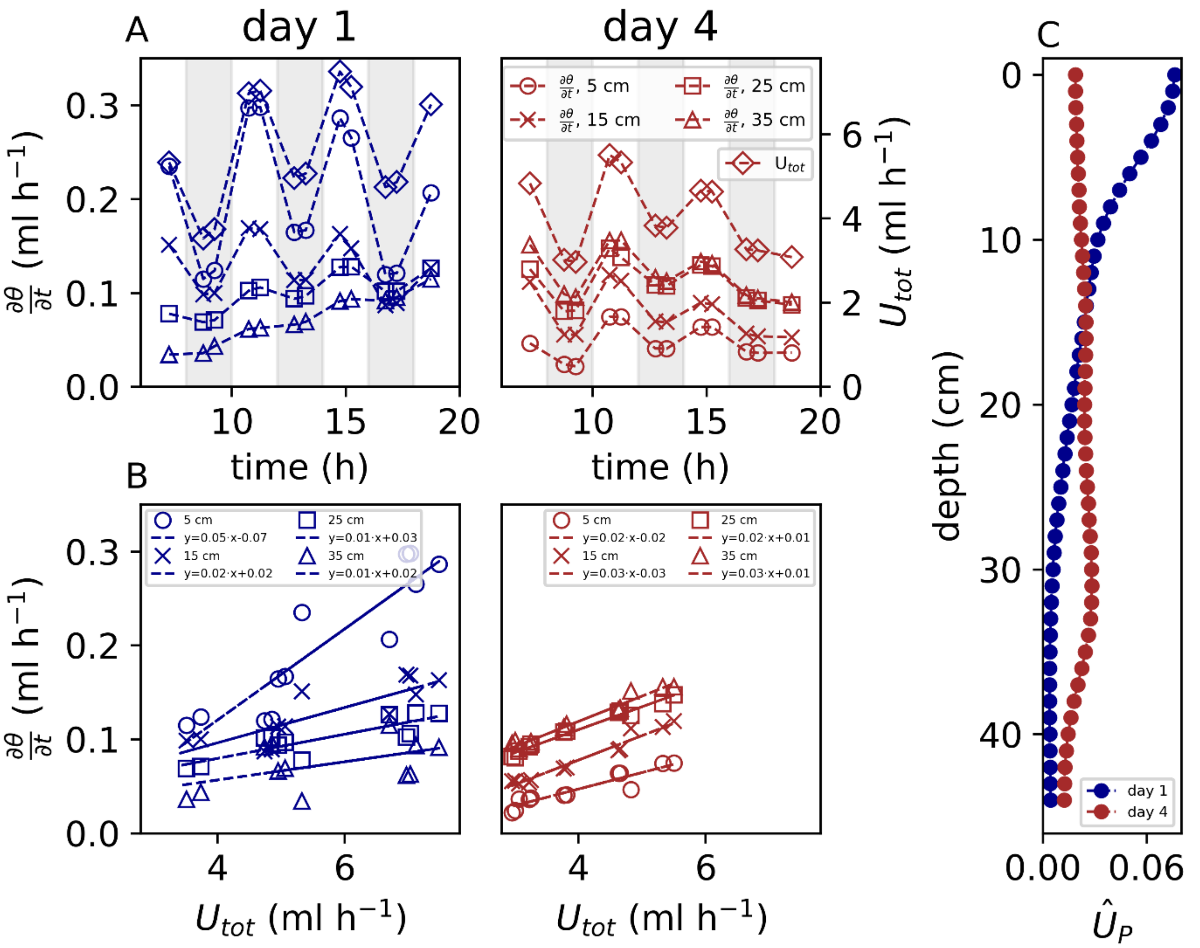

Suppl. Fig. 1 Determination of $\widehat{U}_P$ using data measured with the SWaP at day 1 and day 4 of the drying period for an example maize plant. (A) shows the local soil water depletion rates ($\frac{\partial\theta}{\partial t}$) at different depths (left y-axis) and the total root water uptake rate over time (U$_{tot}$, right y-axis). Shaded areas indicate a low-light intensity period, non-shaded areas a high light intensity period. (B) linear regression between $\frac{\partial\theta}{\partial t}$ and U$_{tot}$ at different depths, using the data shown in (A). The slope of the linear regression in each layer is the local $\widehat{U}_P$(z). (C) Complete $\widehat{U}_P$ profiles at day 1 and day 4, determined by a linear regression in each layer as shown in (B).

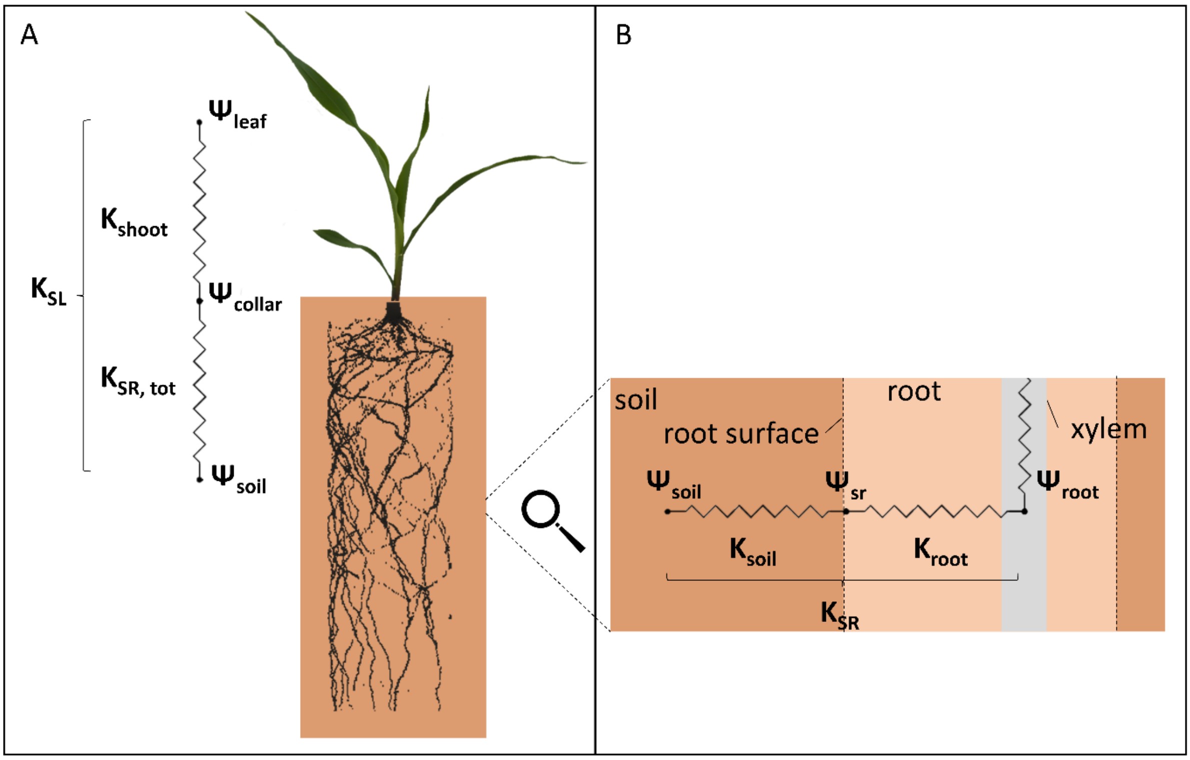

Suppl. Fig. 2: Scheme of the hydraulic model used in this study. (A) The total conductance between soil and leaf (K_{SL}) is composed of the shoot conductance (K_{shoot}), and the total conductance of the soil-root system ($K_{SR, tot}$). (B) The local soil-root conductance (K_{SR}) in each layer is composed of the local soil conductance (K_{soil}) and the local root conductance (K_{root}).

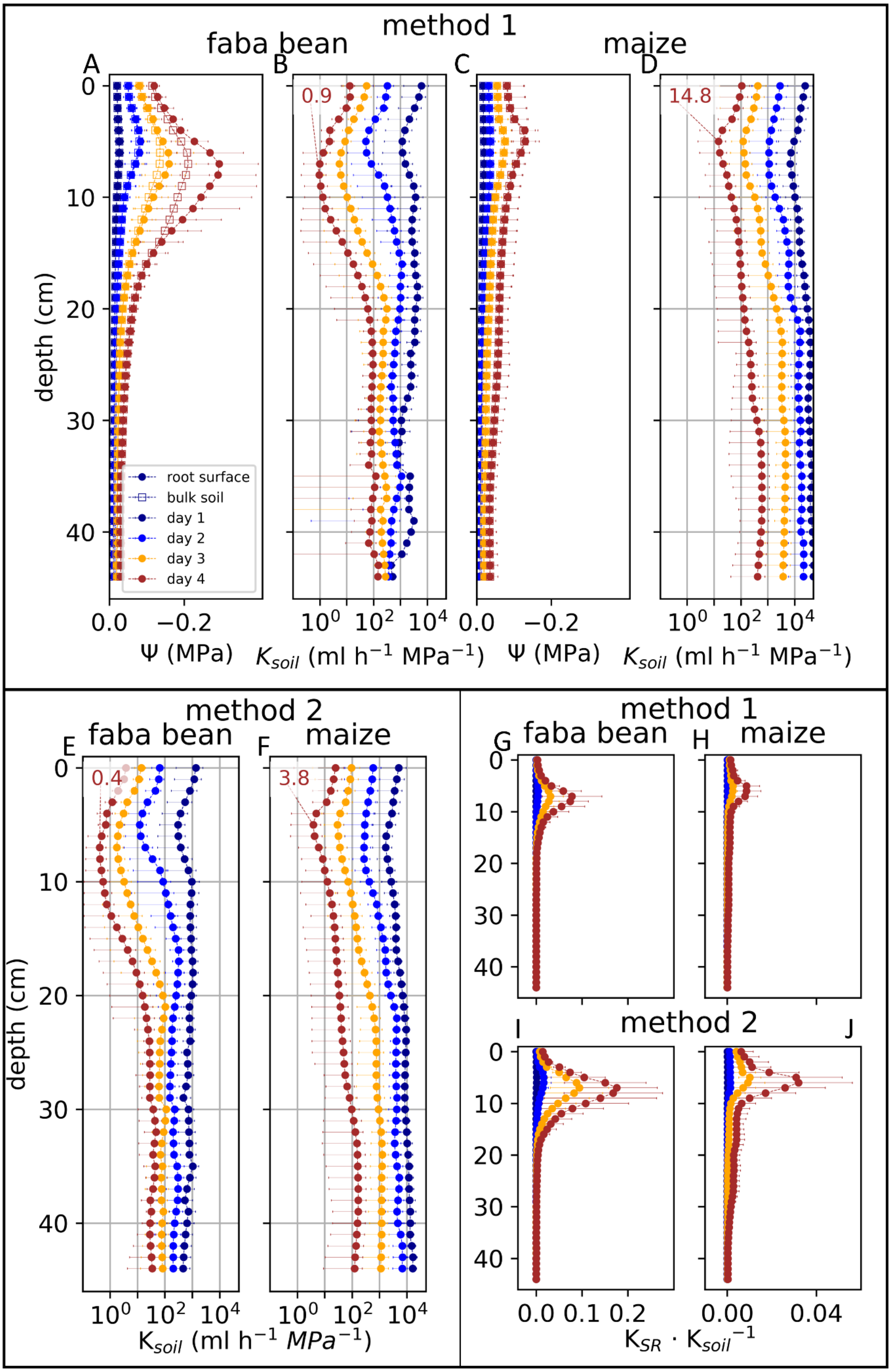
method 1
faba bean
maize
A
B
C
D
0
10
20
30
40
depth (cm)
0.9
14.8
root surface
bulk soil
day 1
day 2
day 3
day 4
0.0
−0.2
Ψ (MPa)
10^0
10^2
10^4
K_{soil} (ml h^{-1} MPa^{-1})
method 2
E
F
0.4
3.8
K_{soil} (ml h^{-1} MPa^{-1})
G
H
I
J
0.0
0.1
0.2
0.00
0.04
$K_{SR} \cdot K_{soil}^{-1}$

Suppl. Fig. 3: Comparison between the soil conductance (K_{soil}), estimated by two different methods, and the root conductance (K_{root}). K_{soil} was determined by estimating the water potential at the soil root interface using a steady state model (method 1, A-D) and estimating an effective soil conductance (method 2, E-F). Both methods are explained in Appendix 1. Data points are median values, error bars are median absolute deviations among replicates per species. For each, one faba bean, and maize replicate with very low local soil water content at day 4, estimations of K_{soil} partly yielded negative values. Only data from the other nine replicates were used for this figure. A and C show the estimated water potential at the root surface (filled circles) and the water potential in the bulk soil (non-filled squares, similar to Fig. 2B and D). Differences between the water potential at the root surface and in the bulk soil were used to calculate K_{soil} as shown in B and D. Additionally, K_{soil} was estimated as effective soil conductance according to eq. 9 in Appendix 1 (E-F). In B, D, E, F, X-axes are scaled logarithmically. Values in the top left corners in B, D, E, F are minimum values over depth at day 4. To quantify the effect of soil conductance on K_{SR}, K_{SR} was divided by the estimated data on K_{soil}, using both methods (G-J). The resulting values give the contribution of the soil hydraulic resistance to the total resistance between soil and root xylem. In G-J, faba bean and maize have different X-axes scaling.

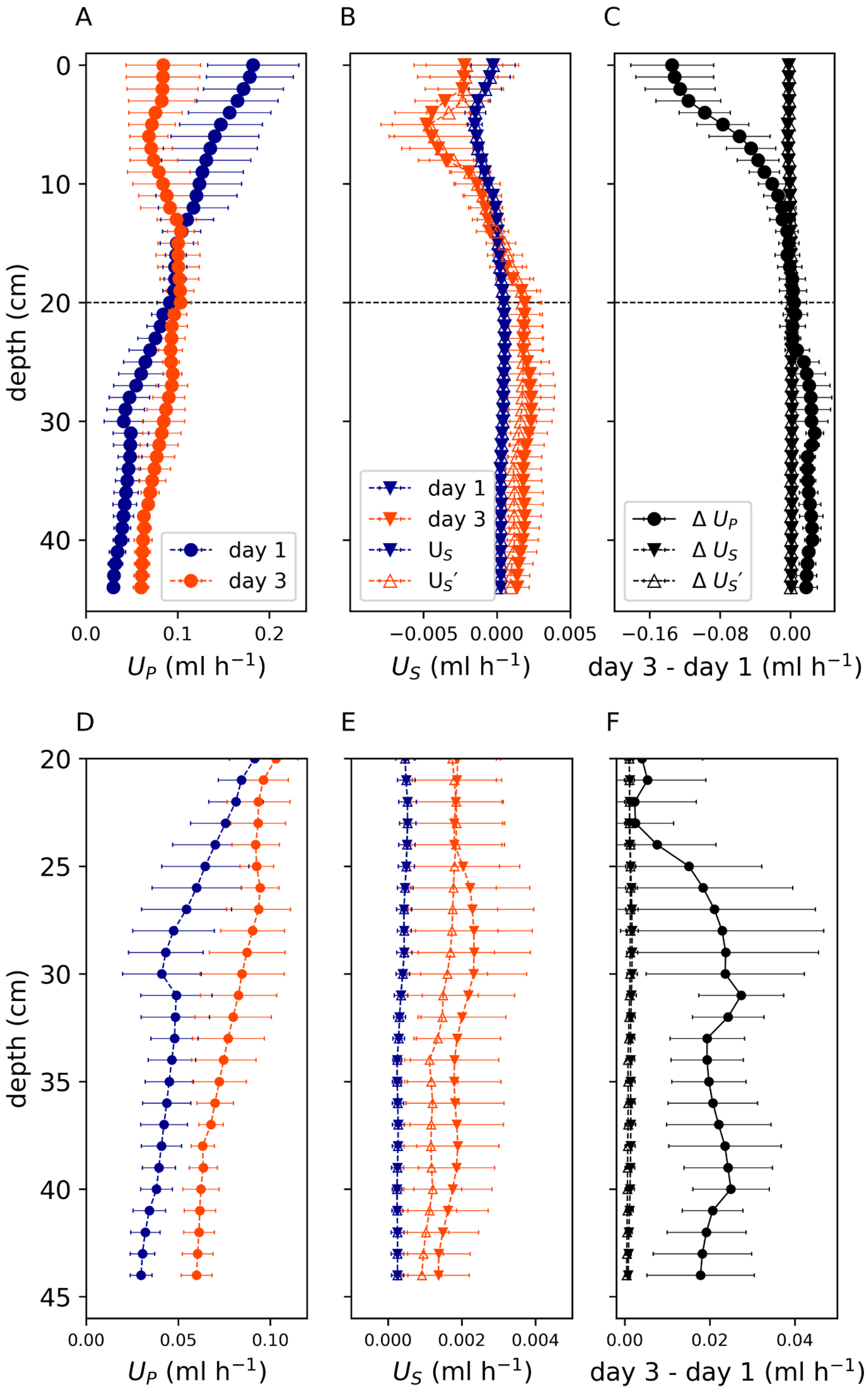
A
B
C
depth (cm)
0
10
20
30
40
day 1
day 3
0.0
0.1
0.2
U_P (ml h^{-1})
day 1
day 3
U_S
U_S'
−0.005
0.000
0.005
U_S (ml h^{-1})
Δ U_P
Δ U_S
Δ U_S'
−0.16
−0.08
0.00
day 3 - day 1 (ml h^{-1})
D
E
F
depth (cm)
20
25
30
35
40
45
0.00
0.05
0.10
U_P (ml h^{-1})
0.000
0.002
0.004
U_S (ml h^{-1})
0.00
0.02
0.04
day 3 - day 1 (ml h^{-1})

Suppl. Fig. 4: Comparison of the changes in plant-driven root water uptake distribution (U_P) and soil-driven root water uptake redistribution (U_S) between day 1 and day 3 for maize. (A) U_P was derived by multiplying the normalized plant-driven root water uptake distribution (Fig. 3) by the daily averaged total root water uptake rate (Table 2). (B) U_S was estimated using the distribution of soil water potential and the distribution of root conductance as described in Appendix 2. U_S' was calculated under the assumption that the local root conductance had not increased in deeper layers between day 1 and day 3. (C) Changes in U_P (filled circles) and U_S (non-filled circles) over time, calculated as differences between day 3 and day 1. Data points are median values among all maize replicates (N=10). Error bars are median absolute deviations. D, E, and F show a magnification of A, B, and C respectively, below a depth of 20 cm.

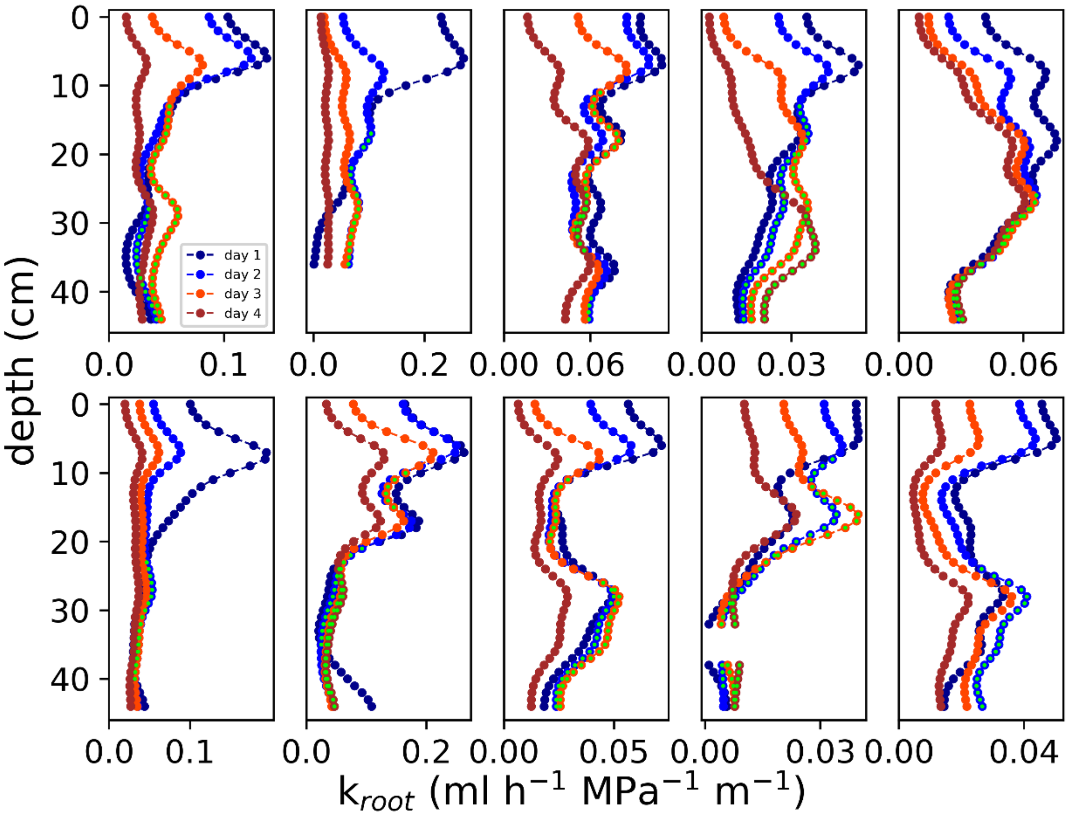

Suppl. Fig. 5: Distribution of root conductivity (conductance per root length, k_{root}) over depth during four days of soil drying for each single maize plant. Layers with a greater, k_{root} as compared to the previous day are indicated by green dots. Missing values were not considered due to too small root length or $\widehat{U}_P$ as described in the methods section.

Conclusions and outlook

The goal of this thesis was to analyze the effect of soil drying on the hydraulic conductance of the root system, its spatial distribution relatively to remaining soil water resources, and the resulting consequences for the plant water balance. To perform such an analysis, I established an experimental setup, based on spatially resolved root water uptake measurements using the recently developed soil water profiler (SWaP, (van Dusschoten et al., 2020)). This involved some methodological adaptations and combining SWaP measurements with leaf water potential measurements using psychrometers, and leaf gas exchange measurements using a portable photosynthesis system. Additionally, MRI measurements of root length distributions were included which I corrected for the missing fine root distribution. This unique experimental setup allowed for analyzing how soil drying affects the hydraulic conductance of the root system, its distribution over depth relatively to remaining water resources, the underlying distributions of root length, and intrinsic root conductivity, and how all these changes impact water flow regulation in the leaves.

The results I have presented here emphasize that alterations of the hydraulic conductance between soil and leaf (K_{SL}) play a key role for plant responses to water stress: Starting in moderately dry soil, K_{SL} declined exponentially which was the main cause for plant water stress in form of a reduced plant water potential and stomatal closure. Therefore, the rate constant (λ) of this exponential decline, which significantly differed between the two species tested, faba bean and maize, is a principal factor determining the extent of water stress. This parameter λ might explain differences in the drought robustness among different soil-plant systems and should be considered in future studies on plant water stress. Here, plants with a greater λ tended to have a greater decline rate in stomatal conductance. Probably, there is a general relation between the decline in K_{SL} and a plant's ability to sustain a high transpiration rate and CO_2 uptake rate at a given soil water deficit. This hypothesis needs to be tested among a wider range of species. Variation in λ might also account for the lack of correlation between leaf water potential and stomatal regulation that has been observed across different species (Martínez-Vilalta & Garcia-Forner, 2017). More generally, the potential correlation between stomatal regulation and λ raises the question whether λ affects crop production under water deficit: Are crop lines, previously found to be comparably high-yielding under drought (Cabello et al., 2013; Carvalho et al., 2014; Denčić et al., 2000; Khalili et al., 2013; Menezes et al., 2014; Oya et al., 2004), characterized by a comparably low decline rate of the soil-leaf hydraulic conductance?

Analysis of the spatial distribution of root water uptake rates and the underlying conductance revealed that most of the decline in K_{SL} occurred within the upper 10 cm of the soil-root system, where roots were exposed to much drier soil compared to deeper layers. Consequently, the remaining soil water in these upper soil layers was difficult to extract. Since estimations of the water potential at the root surface indicated that the loss of conductance did not occur between bulk soil and root surface, it must have been caused by a reduction in soil root contact, or by a molecularly modified root conductivity. Since the full recovery of K_{SL} upon rewatering took more than 24 hours it is likely that not only a reduced soil-root contact, but additional, plant-controlled mechanisms, such as downregulation of active aquaporins or root suberization, were involved. To what extent these different mechanisms contributed needs to be clarified in future studies: The contribution of aquaporins can be quantified using inhibitors like mercury (Martre, 2001), NaN_3 (Grondin et al., 2016), or hydroxyl radicals (Rodríguez-Gamir et al., 2019), and measuring K_{SL} in inhibited and control plants, before and after exposure to drought stress. Furthermore, the decline rate in K_{SL} could be compared between control plants and mutants with an aquaporin isoform knocked out (Ding et al., 2020). The level of suberization before and after drought stress can be analyzed using fluorescence microscopy of harvested, stained root samples (Cruz et al., 1992; Kreszies et al., 2019; North & Nobel, 1991), but a quantitative analysis is challenging. One approach to evaluate the contribution of altered soil hydraulic properties is testing the effect of different soil types on drought-induced changes in K_{SL}. Alternatively, the experiments described above could be combined with quantitative measurements of the soil-root contact. For this purpose, NMR micro-coils, enclosing single roots, were tested as part of this project. A more established method used in this context is X-ray tomography (Carminati et al., 2013; Duddek et al., 2022; Koebernick et al., 2018).

In their theoretical work, Couvreur et al. (2012) point out that at the root system level, plants exposed to drought stress have two different options to maintain relatively high water uptake rates 1) increasing the total root system conductance 2) shifting its distribution more towards relatively wet soil layers. Since the total conductance of the root system decreased in the experiments presented here, the second option becomes even more important. While the conductance strongly decreased in upper layers, it simultaneously increased in deeper layers for maize, but not for faba bean. This increase partly compensated the decrease in upper soil layers, and contributed to the lower decline rate of K_{SL}, and thus greater drought robustness in maize compared to faba bean. The local increase in conductance would not have been detected when the total conductance of the system was analyzed, which highlights the need for spatially resolved data on water uptake rates. Since the local soil water content also decreased in the respective deeper layers, although much less compared to upper layers, the increase in conductance must have occurred in the roots, due to a plant-controlled mechanism. Although, xylem maturation could have contributed, it is likely that regulation of aquaporin gene expression and their posttranslational modifications was involved. To clarify this, aquaporin activity before and after drought needs to be analyzed. However, such an analysis must be performed locally, since an average across the entire root system would be dominated by mechanisms that caused the reduced conductance in upper soil layers. A local analysis would require harvesting roots from the identified area (between 30 and 40 cm depths for the setup used here) under controlled and drought-stressed conditions, and either comparing the contribution of aquaporins to the hydraulic conductance by aquaporin inhibition (Johnson et al., 2014) or comparing the abundance of aquaporins using immunoassays (McLean et al., 2011).

The findings discussed above show that the response of the root system conductance depends on both, the global water balance of the plant, and the local soil water status. Therefore, the vertical gradient in soil water potential influences the response of the plant to soil drying. The extent of this gradient depends on the initial root hydraulic architecture in well-watered soil: Among all species tested, shallow roots were more abundant and had a greater intrinsic conductivity compared to deeper roots, resulting in a much stronger water depletion in upper soil layers. Upon water restriction, this strongly enhanced the vertical gradient in soil water potential. The observed alterations in root system conductance suggest that the plant tries to adapt the distribution of root conductance to the altered soil water conditions: In non-stressed conditions, greater root conductance in upper layers might be beneficial to compete for nutrients and rainwater. In water limited conditions, a greater conductance in deeper layers is required to better access the easily extractable deep water, while in upper layers, reducing the root conductance could prevent a hydraulic interruption between remaining bulk soil water and the root surface.

References

Cabello, R., Monneveux, P., De Mendiburu, F., & Bonierbale, M. (2013). Comparison of yield based drought tolerance indices in improved varieties, genetic stocks and landraces of potato (Solanum tuberosum L.). *Euphytica*, *193*(2), 147–156. https://doi.org/10.1007/s10681-013-0887-1

Carminati, A., Vetterlein, D., Koebernick, N., Blaser, S., Weller, U., & Vogel, H. J. (2013). Do roots mind the gap? *Plant and Soil*, *367*(1–2), 651–661. https://doi.org/10.1007/s11104-012-1496-9

Carvalho, P., Azam-Ali, S., & Foulkes, M. J. (2014). Quantifying relationships between rooting traits and water uptake under drought in Mediterranean barley and durum wheat. *Journal of Integrative Plant Biology*, *56*(5), 455–469. https://doi.org/10.1111/jipb.12109

Couvreur, V., Vanderborght, J., & Javaux, M. (2012). A simple three-dimensional macroscopic root water uptake model based on the hydraulic architecture approach. *Hydrology and Earth System Sciences*, *16*(8), 2957–2971. https://doi.org/10.5194/hess-16-2957-2012

Cruz, R. T., Jordan, W. R., & Drew, M. C. (1992). Structural changes and associated reduction of hydraulic conductance in roots of Sorghum bicolor L. following exposure to water deficit. *Plant Physiology*, *99*(1), 203–212. https://doi.org/10.1104/pp.99.1.203

Denčić, S., Kastori, R., Kobiljski, B., & Duggan, B. (2000). Evaluation of grain yield and its components in wheat cultivars and landraces under near optimal and drought conditions. *Euphytica*, *113*(1), 43–52. https://doi.org/10.1023/A:1003997700865

Ding, L., Milhiet, T., Couvreur, V., Nelissen, H., Meziane, A., Parent, B., Aesaert, S., Van Lijsebettens, M., Inzé, D., Tardieu, F., Draye, X., & Chaumont, F. (2020). Modification of the expression of the aquaporin ZmPIP2;5 affects water relations and plant growth. *Plant Physiology*, *182*(4), 2154–2165. https://doi.org/10.1104/PP.19.01183

Duddek, P., Carminati, A., Koebernick, N., Ohmann, L., Lovric, G., Delzon, S., Rodriguez-Dominguez, C. M., King, A., & Ahmed, M. A. (2022). The impact of drought-induced root and root hair shrinkage on root–soil contact. *Plant Physiology*, 1232–1236. https://doi.org/10.1093/plphys/kiac144

Grondin, A., Mauleon, R., Vadez, V., & Henry, A. (2016). Root aquaporins contribute to whole plant water fluxes under drought stress in rice (Oryza sativa L.). *Plant Cell and Environment*, *39*(2), 347–365. https://doi.org/10.1111/pce.12616

Johnson, D. M., Sherrard, M. E., Domec, J. C., & Jackson, R. B. (2014). Role of aquaporin activity in regulating deep and shallow root hydraulic conductance during extreme drought. *Trees - Structure and Function*, *28*(5), 1323–1331. https://doi.org/10.1007/s00468-014-1036-8

Khalili, M., Naghavi, M. R., Aboughadareh, A. P., & Rad, H. N. (2013). Effects of Drought Stress on Yield and Yield Components in Maize cultivars (Zea mays L .). *International Journal of Agronomy and Plant Production*, *4*(4), 809–812.

Koebernick, N., Schlüter, S., Blaser, S. R. G. A., & Vetterlein, D. (2018). Root-soil contact dynamics of Vicia faba in sand. *Plant and Soil Soil*, *431*, 417–431.

Kreszies, T., Shellakkutti, N., Osthoff, A., Yu, P., Baldauf, J. A., Zeisler-Diehl, V. V., Ranathunge, K., Hochholdinger, F., & Schreiber, L. (2019). Osmotic stress enhances suberization of apoplastic barriers in barley seminal roots: analysis of chemical, transcriptomic and physiological responses. *New Phytologist*, *221*(1), 180–194. https://doi.org/10.1111/nph.15351

Martínez-Vilalta, J., & Garcia-Forner, N. (2017). Water potential regulation, stomatal behaviour and hydraulic transport under drought: deconstructing the iso/anisohydric concept. *Plant Cell and Environment*, *40*(6), 962–976. https://doi.org/10.1111/pce.12846

Martre, P. (2001). Hydraulic Conductance and Mercury-Sensitive Water Transport for Roots of Opuntia acanthocarpa in Relation to Soil Drying and Rewetting. *Plant Physiology*, *126*(1), 352–362. https://doi.org/10.1104/pp.126.1.352

McLean, E. H., Ludwig, M., & Grierson, P. F. (2011). Root hydraulic conductance and aquaporin abundance respond rapidly to partial root-zone drying events in a riparian Melaleuca species. *New Phytologist*, *192*(3), 664–675. https://doi.org/10.1111/j.1469-8137.2011.03834.x

Menezes, C. B., Ticona-Benavente, C. A., Tardin, F. D., Cardoso, M. J., Bastos, E. A., Nogueira, D. W., Portugal, A. F., Santos, C. V., & Schaffert, R. E. (2014). Selection indices to identify drought-tolerant grain sorghum cultivars. *Genetics and Molecular Research*, *13*(4), 9817–9827. https://doi.org/10.4238/2014.November.27.9

North, G. B., & Nobel, P. S. (1991). CHANGES IN HYDRAULIC CONDUCTIVITY AND ANATOMY CAUSED BY DRYING AND REWETTING ROOTS OF AGAVE DESERTI (AGAVACEAE). *American Journal of Botany*, *78*(7), 906–915.

Oya, T., Nepomuceno, A. L., Neumaier, N., Farias, J. R. B., Tobita, S., & Ito, O. (2004). Drought tolerance characteristics of Brazilian soybean cultivars - Evaluation and characterization of drought tolerance of various Brazilian soybean cultivars in the field. *Plant Production Science*, *7*(2), 129–137. https://doi.org/10.1626/pps.7.129

Rodríguez-Gamir, J., Xue, J., Clearwater, M. J., Meason, D. F., Clinton, P. W., & Domec, J. C. (2019). Aquaporin regulation in roots controls plant hydraulic conductance, stomatal conductance, and leaf water potential in Pinus radiata under water stress. *Plant Cell and Environment*, *42*(2), 717–729. https://doi.org/10.1111/pce.13460

van Dusschoten, D., Kochs, J., Kuppe, C. W., Sydoruk, V. A., Couvreur, V., Pflugfelder, D., & Postma, J. A. (2020). Spatially resolved root water uptake determination using a precise soil water sensor. *Plant Physiology*, *184*(3), 1221–1235. https://doi.org/10.1104/pp.20.00488

Abbreviations

term	meaning	unit
K_{SL}	hydraulic conductance between soil and leaf	$ml\ h^{-1}\ MPa^{-1}$
SWaP	soil water profiler	
λ	rate constant of the exponential decline in K_{SL} with reducing soil water potential	MPa^{-1}

Acknowledgements

First of all, I want to thank Prof. Ulrich Schurr for giving me the opportunity to pursue my PhD at the IBG-2, his contribution to conceptualizing this project, and providing scientific feedback.

I would also like to thank Prof. Georg Groth for taking over the co-supervision of this project.

My special thanks go to Dagmar van Dusschoten. Not only for all the scientific, experimental, and personal support, but also for his creativity and enthusiasm which have inspired me and contributed crucially to the success of this project.

Another big thank you goes to Johannes Postma and Hendrik Poorter. I really appreciate how much time they invested into pushing this project forward by discussing results, planning further steps, and helping to revise manuscripts.

Johannes Kochs supported me on several occasions with technical advice and setting up measurement hardware. Daniel Pflugfelder helped me to develop and improve algorithms for data processing and analysis. Many thanks to both of you!

Additionally, I want to acknowledge Prof. Ingar Janzik and Robert Koller for their guidance throughout the project and always being available to give advice.

I would like to thank Kwabena Agyei, Helena Bochmann, Prof. Andrea Schnepf, Carel Windt and Congcong Zheng for commenting on our manuscripts.

Lastly, I am grateful for the company I had during my time as a PhD student at the IBG-2. All the lunch breaks and after-work activities we shared were a lot of fun, and sometimes even promoted scientific progress. Many thanks to all of you.